Optimization of Structures Considering Environmental Sustainability

by

Vahid Shobeiri

Thesis submitted for the degree of Doctor of Philosophy at The University of Adelaide (The School of Civil, Environmental and Mining Engineering) Australia

-March 2023-

TABLES OF CONTENTS

ABSTRACT

Concrete which is the most commonly used construction material on earth needs a large amount of cement and natural aggregates and approximately 0.85 to 0.92 tonne of carbon dioxide ($CO_{2\text{-}eq}$) are emitted for every tonne of cement produced. Therefore, to alleviate the effects of climate change we need sustainable solutions that can not only reduce greenhouse gas emissions from concrete but also introduce environmentally friendly alternative materials for conventional concrete materials. This thesis focuses on overcoming this obstacle by integrating multi-objective optimization techniques into the comprehensive environmental life-cycle assessment tools with a focus on global warming potential (GWP) for optimization of concrete containing alternative waste materials for cement and natural aggregates. From this thesis, it is possible to find the optimal mix designs of low emission waste-based concretes with desired mechanical properties based on transport distance and mode of concrete materials, source of supplementary cementitious materials, and optimum type of waste-based aggregates which benefit not only environment but also help conserve natural resources.

This thesis presents a series of journal articles outlining a generic framework for optimization of environmental impacts of concrete materials which are responsible for about 8% of the total greenhouse gas emissions. This generic framework applies a cradle-to- gate life-cycle assessment tool (LCA), artificial neural networks (ANNs) and multi-objective genetic algorithm (GA) optimization to reduce the global warming potential and mix cost of a range of concrete types while maintaining its mechanical properties (compressive strength and slump) at desired levels. This framework is developed for both concrete with supplementary cementitious materials (SCMs) and geopolymer concrete, which is important as these two types of concrete contain alternative binders as a partial or complete replacement for cement. Further, because of its efficiency and flexibility, this framework is also applied for optimization of concrete containing alternative fillers without modification by simply adding the production and transport emissions of alternative fillers.

The first part of this thesis is devoted to quantifying the global warming potential of concrete ingredients through conducting a cradle-to-gate life-cycle assessment (LCA) associated with all life stages of concrete production from raw material extraction through to production, manufacture, and transportation. A significant part of this research is to account for allocation and transport emissions as well as renewable energy sources for the electricity grid mix when quantifying greenhouse gas emissions from a range of concrete types. The development of this model is important as it allows for specifying optimal concrete types for reducing carbon dioxide emissions considering the intended use of the concrete.

Having investigated a detailed life-cycle assessment of concrete production, an artificial neural network (ANNs) based on a large database for concrete mixes is developed to predict properties (compressive strength and slump) of concrete with alternative binders with high accuracy ($R^2 > 0.90$). The prediction model is developed to allow for the impact of chemical makeup of cement and SCMs and is validated using different statistical indicators. The developed ANN model is then integrated with a multi-objective genetic algorithm (GA) optimization, life-cycle assessment and financial models to find optimum mix designs with desired properties in terms of compressive strength and slump to minimize carbon dioxide emissions and cost for a range of concrete types with alternative binders based on several case studies.

Finally, the developed framework is applied to investigate optimum mix designs of concrete with alternative fillers. Analysing a large database of concrete with a wide range of waste-based aggregates and SCMs, the influence of waste-based aggregate type and replacement ratio on the mechanical properties of concrete containing them are first investigated and the relationship between the mechanical properties of concrete with waste-based aggregate is then developed and validated by existing models in the codes of practice. The development of this part of study was important as it allows for identifying the optimum waste-based aggregate type based on the intended use of the concrete. This is followed by the application of an ANN model to predict fresh and hardened properties of concrete with alternative fillers. Having the prediction models, the developed framework without fundamental modification is applied to minimize carbon dioxide emissions and natural resource utilization from concrete with different types of waste-based aggregate. It is important because it shows the difficulty in minimising both natural resource utilisation and GWP because they are competing as the addition of waste-based aggregates leads to poorer mechanical performance which is recovered via an increase in binder.

Possible extensions of this work include developing a generic framework considering a broader set of concrete properties. Another possible extension of this work is to develop a framework to reduce emissions and cost at the structural level by developing structural optimization techniques to design material-efficient and carbon- and cost- effective structural frames (e.g., concrete, timber and steel frames) with optimal decking and foundation types at early-stage design decisions.

STATEMENT OF ORIGINALITY

I certify that this work contains no material which has been accepted for the award of any other degree or diploma in my name, in any university or other tertiary institution and, to the best of my knowledge and belief, contains no material previously published or written by another person, except where due reference has been made in the text. In addition, I certify that no part of this work will, in the future, be used in a submission in my name, for any other degree or diploma in any university or other tertiary institution without the prior approval of the University of Adelaide and where applicable, any partner institution responsible for the joint-award of this degree.

I acknowledge that copyright of published works contained within this thesis resides with the copyright holder(s) of those works.

I also give permission for the digital version of my thesis to be made available on the web, via the University's digital research repository, the Library Search and also through web search engines, unless permission has been granted by the University to restrict access for a period of time.

I acknowledge the support I have received for my research through the provision of an Australian Government Research Training Program Scholarship.

16/03/2023

Vahid Shobeiri — Date

LIST OF PUBLICATIONS

Journal Papers

Shobeiri, V., Bennett, B., Xie, T., & Visintin, P. (2023). "Mix Design Optimization of Waste-based Aggregate Concrete for Natural Resource Utilization and Global Warming Potential". For Submission to *Journal of Cleaner Production*

Shobeiri, V., Bennett, B., Xie, T., & Visintin, P. (2023). "A Comprehensive Data Driven Study of Mechanical Properties of Concrete with Waste-Based Aggregates: Plastic, Rubber, Slag, Glass and Concrete". For Submission to *Journal of Sustainable Cement-Based Materials*

Shobeiri, V., Bennett, B., Xie, T., & Visintin, P. (2023). "Mix Design Optimization of Concrete Containing Fly Ash and Slag for Global Warming Potential and Cost Reduction". *Case Studies in Construction Materials*, e01832.

Shobeiri, V., Bennett, B., Xie, T., & Visintin, P. (2022). "A generic framework for augmented concrete mix design: Optimisation of geopolymer concrete considering environmental, financial and mechanical properties". *Journal of Cleaner Production*, 369, 133382.

Shobeiri, V., Bennett, B., Xie, T., & Visintin, P. (2021). "A comprehensive assessment of the global warming potential of geopolymer concrete". *Journal of Cleaner Production*, 297, 126669.

AKNOWLEDGEMENTS

I wish to extend my sincere gratitude to Prof. Phillip Visintin, Dr. Bree Bennett and Prof. Tianyu Xie for their excellent supervision over the duration of my doctoral studies. I also wish to acknowledge the Australian Government Research Training Program for providing the cost of tuition fee and living expenses for the duration of my PhD.

Finally, I wish to express my gratitude to my wife, Elnaz. This thesis is dedicated to her.

INTRODUCTION & GENERAL OVERVIEW

This thesis outlines a generic framework for the mix design optimization of a range of concrete types with alternative binders including geopolymer concrete and concrete with supplementary cementitious materials (SCMs) as well as a range of concrete with alternative fillers including plastic, rubber, slag, glass and concrete aggregates. The approach is based on application of a cradle-to-gate life-cycle assessment tool, artificial neural networks and multi-objective genetic algorithm optimization to reduce the global warming potential, mix cost and natural resource utilization of concrete while maintaining its physiomechanical and durability-related properties at desired levels. The direct application of the proposed generic concrete mix design framework is important as it can be tailored to any local application via modification of the input parameters allowing the user to make their own choice regarding what local values are suited for their application for the purpose of reducing emissions, cost and natural resource usage.

The goal of the first chapter is to quantify the global warming potential of concrete ingredients through conducting a cradle-to-gate life-cycle assessment associated with all life stages of concrete materials from raw material extraction through to production and use that are required for the concrete mix design optimization framework presented in the subsequent chapters. This is important because the global warming potential of concrete is highly dependent on the system boundary for life-cycle assessment analysis, type of allocation scenario and material transport distances and mode. The paper presented in this chapter quantifies carbon dioxide equivalent emissions ($CO_{2\text{-}eq}$) associated with the production of a large number of developed mix designs investigating the impacts of curing, allocation, transportation and energy grid sources. A series of case studies were then performed to obtain the influence of transport emissions and allocation type (no allocation, economic allocation and mass allocation) on the relative carbon dioxide emissions of geopolymer and traditional concretes. The emissions factors developed in this paper are used later in the thesis to quantify global warming potential on the basis of a unit volume of concrete for the developed mix design optimization framework.

The second chapter presents two papers on the mix design optimization of concrete with alternative binders. The first paper of this chapter presents the developed generic framework for mix design optimisation of geopolymer concrete considering environmental, financial and mechanical properties. The framework was implemented within a single and multi-objective optimisation procedure using a genetic algorithm to minimize carbon dioxide emissions and mix cost by examining the impact of regional scale transportation scenarios and the chemical composition of binders and alkali activators on the optimum mix designs. The second paper in this chapter investigates the optimum mix designs for concrete with supplementary cementitious materials (SCMs). The optimum mixes of concrete with SCMs are investigated through five case studies investigating the impact of chemical composition of cement and SCMs, minimum cement content, regional transportation, emissions allocation, and binder type on global warming potential and concrete mix cost.

The third chapter presents a further application of the developed generic concrete mix design framework to explore the optimum mixes of concrete with alternative fillers. The first paper investigates the properties (compressive strength, splitting tensile strength, flexural strength, elastic modulus, water absorption and slump) of concrete containing recycled plastic, rubber, slag, glass and concrete aggregates by analysing a large database of waste aggregate based concrete mixes. A performance indicator is utilized to quantify the interaction between

minimizing natural resource utilization by using waste-based aggregates and mechanical properties of concrete containing them. A series of regression analyses is then undertaken to find the empirical models that link the elastic modulus, splitting tensile and flexural tensile strength to the compressive strength of the concrete. These empirical models are then validated by comparing with existing models in various codes of practice globally. The second paper in this chapter first utilizes an ANN model to predict different properties of concrete with waste-based aggregates including slump, compressive strength, splitting tensile strength, flexural strength, elastic modulus and water absorption, and then integrates the generic concrete mix design optimization framework to minimize carbon dioxide emissions and natural resource utilization from concrete with different types of waste-based aggregates.

The final chapter then summarises the research contribution, and presents concluding remarks as well as possible avenues for future research. The possible extensions that are explored include using the structural optimization techniques to design material-efficient and carbon- and cost- effective structures at early-stage design decisions.

CHAPTER 1

Background

In this chapter, a detailed life-cycle assessment of concrete ingredients with an emphasis on global warming potential is explored to provide the inputs used in the subsequent chapters.

The publication *"A comprehensive assessment of the global warming potential of geopolymer concrete"* quantifies carbon dioxide emissions from concrete ingredients through conducting a cradle-to-gate life-cycle assessment associated with all life stages of concrete materials. The main parameters that are explored are the emissions factors from concrete ingredients and the effect of several parameters including curing, allocation, transportation and energy grid sources on the global warming potential of geopolymer and traditional concretes.

List of manuscripts

Shobeiri, V., Bennett, B., Xie, T., & Visintin, P. (2021). "A comprehensive assessment of the global warming potential of geopolymer concrete". *Journal of Cleaner Production*, 297, 126669.

STATEMENT OF AUTHORSHIP

"A comprehensive assessment of the global warming potential of geopolymer concrete"
Journal of Cleaner Production, 297, 126669

Shobeiri, V. (Candidate)

Prepared manuscript, performed all analyses, and developed model and theory (70%)

This paper reports on original research I conducted during the period of my Higher Degree by Research candidature and is not subject to any obligations or contractual agreements with a third party that would constrain its inclusion in this thesis. I am the primary author of this paper.

Signed… Date16/03/2023

Bennett, B.

Supervised and contributed to research (10%)

I certify that the candidate's stated contribution to the publication is accurate (as detailed above); permission is granted for the candidate in include the publication in the thesis; and the sum of all co-author contributions is equal to 100% less the candidate's stated contribution.

Signed… Date 17/04/2023

Xie, T.

Supervised and contributed to research (10%)

I certify that the candidate's stated contribution to the publication is accurate (as detailed above); permission is granted for the candidate in include the publication in the thesis; and the sum of all co-author contributions is equal to 100% less the candidate's stated contribution.

Signed… Date 17/04/2023

Visintin, P.

Supervised and contributed to research, and acted as corresponding author (10%)

I certify that the candidate's stated contribution to the publication is accurate (as detailed above); permission is granted for the candidate in include the publication in the thesis; and the sum of all co-author contributions is equal to 100% less the candidate's stated contribution.

Signed… Date 04/04/2023

A Comprehensive Assessment of the Global Warming Potential of Geopolymer Concrete

Vahid Shobeiri, Bree Bennett, Tianyu Xie and Phillip Visintin

Abstract

Approximately 5%-7% of global Carbon Dioxide (CO_2) emissions can be attributed to Ordinary Portland Cement (OPC), which has traditionally been used as the primary binder in concrete. Geopolymer concrete has been widely claimed to have lower global warming potential than OPC concrete, and this claim has formed the basis of many studies examining mix designs and mechanical properties of geopolymer concretes. A major limitation with the vast majority of existing studies is a lack of the direct quantification of the global warming potential of the materials developed. That is, the underlying assumption in the majority of these studies is that geopolymer concrete is more sustainable than OPC based concretes. The aim of this paper is to quantify the CO_2 equivalent ($CO_{2\text{-eq}}$) emissions associated with production of a large number of previously developed mix designs (1404 mix designs from 110 studies) including the impacts of curing, allocation and transportation and allowing for variation in energy grid source and the production of the activator solution. When considering the impact of transportation, a case study based on five major capital cities in Australia is presented and the critical transport distances at which the manufacture of geopolymers becomes more emissions intensive than conventional concrete is identified. The results show that the relative $CO_{2\text{-eq}}$ emissions of geopolymer and OPC based concretes of the same strength, are highly dependent on the system boundary for analysis, the type of allocation scenario and material transportation distances and mode, and further, that depending on these factors geopolymer concretes can either have significantly lower, or significantly higher $CO_{2\text{-eq}}$ emissions than OPC concretes of the same strength. It is expected that the findings of this work can aid in specifying the optimal concrete types for reducing $CO_{2\text{-eq}}$ emissions considering the intended use of the concrete.

Keywords: Geopolymer concrete manufacturing; Ordinary Portland Cement;

sustainability; global warming potential; carbon dioxide emissions

1. Introduction

Concrete manufactured with an Ordinary Portland Cement (OPC) binder is the most commonly used construction material by mass globally (Naik 2008; Gautam et al. 2014). This is significant because OPC manufacture is energy intensive due to pyroprocessing, and as a result approximately 0.85 to 0.92 tonnes of CO_2 is emitted for every tonne of OPC manufactured (Turner & Collins 2013; Prakasan 2020). In an attempt to reduce the environmental impact of concrete, substitution of cement with a more environmentally friendly binder has been of significant research and practical interest during the past two decades. Geopolymer binders (GP) which are produced by the reaction of aluminosilicate precursors such as fly ash, slag and metakaolin with alkaline solutions have been suggested as an environmentally friendly and sustainable alternative to OPC binders. Based on this viewpoint, many studies have been conducted to develop mix designs and to quantify the mechanical properties of GP concretes (Hardjito et al. 2004; Bakharev 2005; Nuruddin et al. 2011; Mohamed et al. 2011; Pan et al. 2011; Bernal et al. 2013; Ryu et al. 2013; Vora and Dave 2013; Song et al. 2014; Chindaprasirt & Chalee 2014; Bernal et al. 2015; Law et al. 2015; Pasupathy et al. 2016; Assi et al. 2016;

Ramujee and PothaRaju 2017; Khan et al. 2017; Pasupathy et al. 2017; Albitar et al. 2017; Zhuguo and Sha 2018; Chithambaram et al. 2018; Shahmansouri et al. 2020; Bellum et al. 2020).

While many studies have shown that it is possible to manufacture GP concretes with similar material properties to OPC concretes, far fewer have explicitly quantified the environmental impact of the materials developed (McLellan et al. 2011; Turner and Collins 2013; Yang et al. 2013; Heath et al. 2014; Passuello et al. 2017; Salas et al. 2018; Asadollahfardi et al. 2019; Hassan et al. 2019a; Hassan et al. 2020a). That is, in the vast majority of studies, it has been assumed that GP concretes developed are more environmentally friendly than conventional concrete without modelling the expected emissions (Hassan et al. 2019b; Hassan et al. 2020b). This is important because recent works such as those of Vinothkumar et al. (2019) and Alyousef et al. (2020) have shown that the range of reported CO_2 equivalent ($CO_{2\text{-eq}}$) emissions emitted when producing a unit volume of GP concrete range from 9% to 80% of that arising from an OPC concrete with similar material properties. The considerable differences in $CO_{2\text{-eq}}$ emissions can be attributed to several factors including: (i) the small-scale study of GP concretes, in which a very small number of mix designs are considered, thus making the results highly dependent on the efficiency of the individual mix designs; (ii) the system boundaries of the analysis, particularly, the inclusion of emissions allocation; (iii) the consideration of the impact of heat curing; (iv) energy consumption during the production of alkali activators; and (v) the transportation of raw materials.

Of the above factors, the definition of a system boundary to include the role of emissions allocation is of particular importance. This is because, ground granulated blast furnace slag (GGBFS) and fly ash (FA) are no longer regarded as waste products because they meet all the conditions set by the European Union Directive (EU 2008) to be considered as industrial by-products. As a result of classification as a by-product, it is necessary to allocate a proportion of the emissions associated with their manufacture to the emissions of the products in which they are later used. Despite this requirement, relatively few studies have considered allocation scenarios when quantifying the emissions from GP concrete (Chen et al. 2010; Habert et al. 2011; Seto et al. 2017; Van den Heede and De Belie 2012; Abbas et al. 2020) – see Table 1 for examples specific to geopolymer concrete.

Table 1 System boundaries adopted in the literature on GP based concrete

Source	**Allocation**	**Regional scale transportation**	**Curing**	**Renewable energy sources**	**Alkali activator type**
O'Brien et al. (2009)	✗	✓	✗	✗	✗
Weil et al. (2009)	✗	✗	✓	✗	✗
McLellan et al. (2011)	✗	✓	✗	✗	✗
Habert et al. (2011)	✓	✗	✗	✗	✗
Turner & Collins (2013)	✗	✗	✓	✗	✗
Yang et al. (2013)	✗	✓	✗	✗	✗
Passuello et al. (2017)	✗	✗	✓	✗	✗
Salas et al. (2018)	✗	✗	✓	✓	✓

Dal Pozzo et al. (2019)	✓	✗	✗	✗	✗
Asadollahfardi et al. (2019)	✗	✗	✓	✗	✗
Bajpai et al. (2020)	✗	✓	✗	✗	✗
This study	✓	✓	✓	✓	✓

In addition, few studies (see Table 1) have considered the emissions associated with the curing of GP concrete despite the fact that GP concretes generally require high curing temperatures to achieve good strength development (Turner and Collins 2013; Yang et al. 2013; Salas et al. 2018; Hassan et al. 2019c). Likewise, the influences of factors relating to transportation on the emissions of GP concretes in a regional context are often ignored (O'Brien et al. 2009; McLellan et al. 2011; Van den Heede and De Belie 2012; Di Maria and Van Acker 2018; Bajpai et al. 2020), which is important because unlike cement which is often manufactured locally, GGBFS and FA are often transported at the regional scale depending on local industry.

A summary of the scope of existing life-cycle assessments of geopolymer concretes is presented in Table 1, where it can be seen that although several studies consider one or two of the factors that have been defined as important to predict the overall global warming potential (GWP) of GP concretes, there is no existing study that considers them all. In order to fill this gap, in this paper we conduct a large-scale study to quantify the GWP of GP concretes considering the impacts of: emissions allocation, heat curing and regional scale transportation.

When investigating emissions allocation, the influence of allocation type (none, economic or mass allocation) is investigated and it is demonstrated that classifying FA and GGBFS as a waste product rather than a by-product results in a significant underestimation of GWP. Based on a region scale transportation case study incorporating five Australian capital cities with different local availabilities of source materials, it is shown that the transportation distances and mode play a crucial role in the final GWP of GP concretes, largely because of the need to transport large volumes of precursor materials. A combination of different allocation scenarios and transportation cases for GP and OPC concretes are then analysed and relationships between compressive strength and $CO_{2\text{-eq}}$ emissions of GP and OPC concretes are discussed. Further, it is shown through a sensitivity analysis that alkali activator type significantly contributes to the sustainability of GP concretes as different chemical processes with different energy inputs exist for the production of these high-energy consumption materials. To further investigate the sensitivity of this result, the impacts of electricity grid mix and curing energy on the $CO_{2\text{-eq}}$ emissions from GP concretes are further discussed.

2. Life cycle assessment model

Previous studies applying life-cycle assessment (LCA) to geopolymer concretes have typically shown that GP concrete has a larger impact in categories such as human toxicity, ozone layer depletion, and abiotic depletion than OPC concretes. This is because the emissions arising from sodium silicate production all influence these categories, while the emissions arising from OPC production do not (Weil et al. 2009; Habert et al. 2011; Petrillo et al. 2016; Zain et al. 2017; Dal Pozzo et al. 2019; Asadollahfardi et al. 2019; Abbas et al. 2020; Dontriros et al. 2020; Bajpai et al. 2020). Similarly, previous studies have reported that GP concretes have lower $CO_{2\text{-eq}}$ emissions than OPC concretes (Duxson et al. 2007; Weil et al. 2009; van Deventer et. al 2010; McLellan et al. 2011; Turner and Collins 2013; Yang et al. 2013; Heath et al. 2014; ; Petrillo et al. 2016; Zain et al. 2017; Passuello et al. 2017; Teh et al. 2017; Salas et al. 2018; Dal Pozzo et al. 2019; Dal Pozzo et al. 2019; Asadollahfardi et al. 2019; Abbas et al. 2020;

Dontriros et al. 2020; Bajpai et al. 2020), but this finding is less straight forward because of the range of assumption parameters applied (see Table 1) and the small range of mix designs considered. This is problematic because GP concretes have been developed largely on the basis of reducing the GWP of concrete and hence it is necessary to have a thorough understanding of the circumstances when the application of GP concretes is beneficial over OPC concretes and vice versa. Hence in this study we consider a detailed analysis of GWP and refer the reader to previous broader scale studies for a discussion of the broader impact of GP concrete production (Weil et al. 2009; Habert et al. 2011; Petrillo et al. 2016; Zain et al. 2017; Dal Pozzo et al. 2019; Asadollahfardi et al. 2019; Abbas et al. 2020; Dontriros et al. 2020; Bajpai et al. 2020).

To achieve this goal, in this study the GWP of a broad range of GP concrete mix designs are quantified and compared with the GWP of OPC concretes with the same compressive strength. Hence the functional unit for analysis is defined as 1 m^3 of GP concrete which is compared to 1 m^3 of OPC concrete with equal strength. The LCA is performed considering a cradle to gate system boundary as shown in Fig. 1. To assess the variability of the results, sensitivity analyses are carried out based on the volumetric functional unit to assess the influence of:

- Alkali activator manufacture technique,
- Electricity grid mix,
- Curing energy,
- Transportation distance and mode, and
- Allocation of emissions associated with alternative binders.

A sensitivity analysis of transportation is performed based on a case study to quantify the influence of the transport distance and type for batching plants in the major capital cities of Australia. In this analysis, road, rail and sea transportations are considered to take into account all the possible transportation scenarios. Further, three different allocation scenarios: no allocation, economic allocation with future trends in the price of FA and GGBFS, and mass allocation scenarios are considered for sensitivity analysis of allocation. Throughout the analysis, emissions released from four major processes including fuel pre-combustion, fuel combustion, electricity generation and transportation taking place within the system boundary are calculated for global warming potential assessment of OPC and GP concretes. The system boundary for OPC concrete, which have been implemented based on the Green Concrete LCA Tool developed by Gursel (2014) and includes:

- Quarrying: this process involves emissions arising from fuel pre-combustion, fuel combustion and electricity use for mining, crushing and drilling of cement raw materials.
- Cement raw material preparation: including emissions generated from electricity usage for blending and grinding of raw materials.
- Cement pyroprocessing: including emissions associated with the use of fossil fuels (pre-combustion and combustion) and electricity generation for clinkering of raw materials.
- Cement clinker cooling process: including emissions from electricity usage for rapid cooling of clinkers.
- Cement finish milling and grinding process: including emissions generated from the electricity usage for milling and grinding of clinkers.
- Cement conveying: this process involves emissions arisen from the electricity use for conveying all cement materials within the cement plant.
- Non-process related electricity and fuel usage for cement plant: including emissions

generated from lighting, onsite transportation and other facilities in a cement plant.

- Aggregates production: emissions from fuel pre-combustion, fuel combustion and electricity usage for mining, crushing and screening of fine and coarse aggregates.
- Admixture manufacture: emissions generation from the production of chemical admixtures which is taken from the European Federation of Concrete Admixture Association (EFCA).
- Concrete batching: including emissions associated with electricity generation, fuel pre-combustion and fuel combustion for loading and mixing of concrete materials.

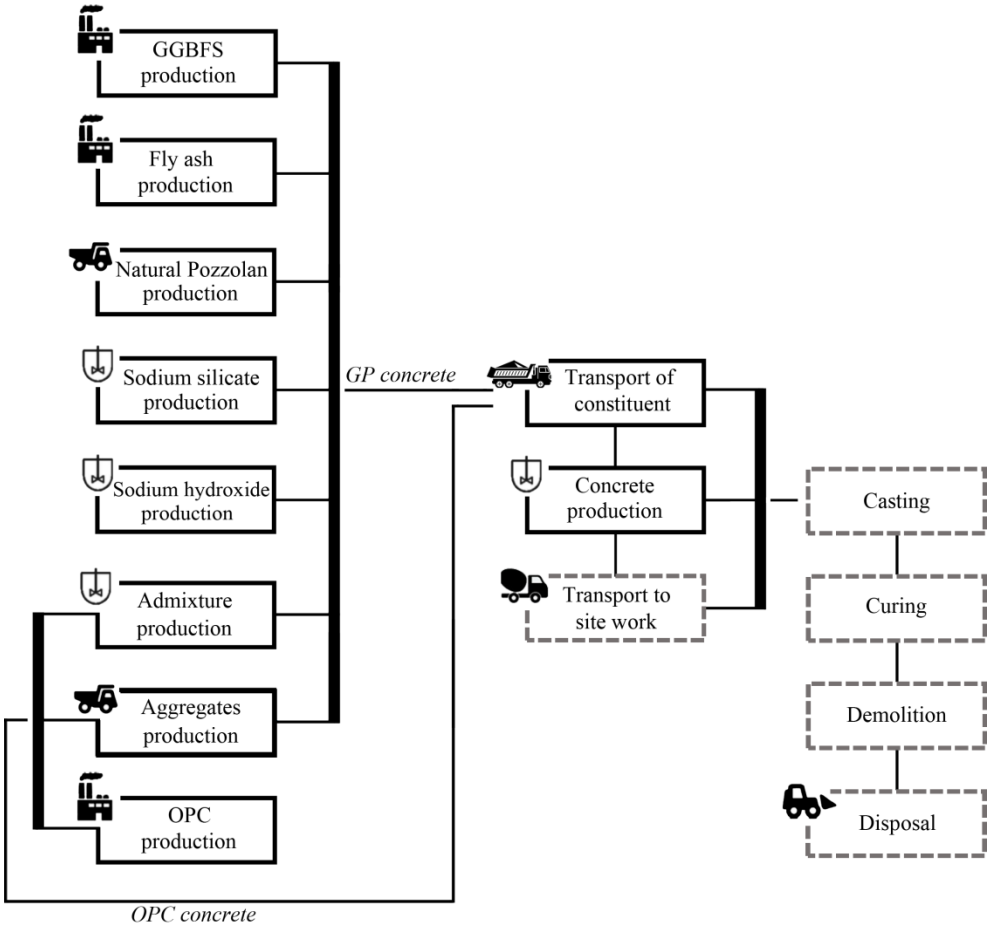

Fig.1 Scope of system boundary and life cycle assessment (LCA) (dashed boxes represent processes that are not considered in the LCA)

In addition to aggregate production, admixture manufacture and concrete batching, the system boundary for GP concrete also includes fuel pre-combustion, fuel combustion and electricity generation for the production of FA, GGBFS, natural pozzolans (NP) (type F pozzolan according to ASTM), alkali manufacture and curing. Emission factors for alkali activator production were taken from Wernet et al. (2016) and Fawer (1999) and for all other components from Gursel (2014). A detailed of the inventory data sources can be found in Supplementary Material A.

Table 2 shows the material type and technologies used in the LCA of cement and concrete production. For the production of OPC the technologies have been selected as those which result in average emissions (Gursel 2014). Similarly, while there are many options for transport distance, an average transport distance within Australia as suggested by Grant (2015) was

assumed for the base-case analysis and these transport distances are further investigated in the sensitivity analysis to follow (Section 4.2).

Table 2 Assumptions and technologies for OPC and GP concretes

User-input data	Material type for base case analysis					
Type of cement	Portland cement type 1					
Type of Admixture	Superplasticiser					
Type of sodium silicates	Sodium silicate 3.3 WR furnace lumps (Fawer 1999)					
Power of electric heater (PEH)	600 Watt					
Electricity grid mix	Australian average (Stuart 2017)					
Fuel type	Bitumous coal	Natural gas	Hydro	Biomass	Solar	Wind
Contribution (%)	34.75	37.35	17.53	0.68	0.35	8.29
Transportation details	Mode			Distance (km)		
Cement raw materials to cement plant	Class 8b truck			55		
Gypsum to cement plant	Class 8b truck			55		
Cement to concrete plant	Class 8b truck			62		
Fine aggregates to concrete plant	Class 8b truck			50		
Coarse aggregates to concrete plant	Class 8b truck			50		
Admixture to concrete plant	Class 8b truck			200		
Alkali activators to concrete plant	Class 8b truck			200		
FA to concrete plant	Class 8b truck			200		
GGBFS to concrete plant	Class 8b truck			200		
Natural pozzolans to concrete plant	Class 8b truck			200		
Technology options	Type of technology					
Cement raw materials prehomogenization	Dry, raw storing, non-preblending					
Cement raw materials grinding	Dry, raw grinding, vertical roller mill					
Cement raw meal blending/homogenization	Raw meal homogenization, blending, and storage					
Clinker pyroprocessing	Long dry kiln with average US kiln					
Clinker cooling	Vertical gravity cooler with planetary cooler					
Kiln fuel	US average					
Cement finish milling/grinding/blending	Horizontal roller mill					
Cement PM control technology	Fabric filter (FF)					
Conveying within the cement plant	Screw pump (20 meters between all processes)					
Concrete batching plant loading/mixing	Mixer loading (central mix)					
Concrete batching plant PM control	Fabric filter (FF)					

3. Methodology

In this section, geopolymer concrete mix designs, determination of equivalent OPC and curing energy are reviewed in details.

3.1. Geopolymer concrete mix designs

To establish the variation in emissions arising from a broad range of GP concretes, the LCA considers 1404 GP concrete mix designs developed in 110 previously published studies which

were previously collated and reviewed by (Xie et al. 2020). In establishing this original database the following conditions were imposed:

(a) A detailed description of the chemical composition of all the source materials (aluminosilicate precursors and alkali activators) must have been provided
(b) A complete mix design must have been reported
(c) Only mixes containing natural aggregates were included
(d) Mixes containing nano-scale materials were excluded because of the difficulty in quantifying the impact of these materials.
(e) Only mixes containing sodium silicate and sodium hydroxide activators were included
(f) Compressive strength must have been reported from tests on cylindrical or cubic specimens.

While the terms geopolymer and inorganic polymer refer to fundamentally different materials, they have often been used interchangeably in the concrete technology community. As a result, in the compilation of Xie's original test database, and also in this study, we are considering both geopolymer and inorganic polymer concretes using the single term geopolymer because it has most commonly been applied by the research community.

For this analysis the database was further refined from its original size of 1756 mix designs to the final 1404 mix designs analyzed by imposing the following additional criteria:

(a) Only mix designs containing FA, GGBFS, blended FA and GGBFS (FA-GGBFS) and natural pozzolans (NP) were considered, mixes containing other cementitious materials have been excluded from this study because of the difficulty in quantifying emissions associated with their processing.
(b) Geopolymer mixes containing cement as a secondary binder were excluded.
(c) Geopolymers with strength of less than 10 MPa were ignored as their application in civil engineering is limited.

The reader is referred to Supplementary Material B for the complete mix designs of all GP concretes analyzed in this study.

Importantly, in this paper we consider a functional unit of 1 m^3 of GP concrete compared to 1 m^3 of OPC concrete with the same compressive strength. While ideally a functional unit that considers volume, strength and durability would be used for comparison, at present no broadly applicable model could be identified to quantify the durability of GP concretes and hence a functional unit based only on volume and strength is chosen. It is therefore suggested that further research is needed in this area such that the mix design can be compared on the basis of strength and durability in the future.

The distribution of concrete compressive strength (f_c) for four different types of GP concretes (FA, GGBFS, FA-GGBFS, NP) considered in the database are shown in Fig. 2(a), in which the compressive strength of cubic specimens has been converted to an equivalent compressive strength of cylindrical specimens. Conversion factors given in UNESCO (1971) were used to convert the compressive strength of 100 × 200 mm cylinder specimens to 150 × 300 mm cylinder specimens (Table A1) and conversion factors specified in BS EN 206-1 and Wong (2013) were used to convert compressive strength of 100 and 150 mm cube specimens to 150 × 300 mm cylinder specimens (Table A2).

From Fig.2(a) it can be seen that most studies developed FA based GP concretes with compressive strengths of between 30 MPa and 50 MPa (52% of all mixes), and less than 12% of mixes are for concretes with a strength greater than 60 MPa and 26% of mixes have a strength of between 20 MPa and 30 MPa. Fig. 2(b) illustrates the mass range of GP concrete mix designs along with corresponding curing temperature and time in the database. From this

breakdown it can be seen that the GP concretes analyzed cover a broad range of expected mix performance, with the mass of coarse and fine aggregates ranging from between [525-1591] kg and [277-1110] kg respectively, while the dried mass of sodium silicates and sodium hydroxide are ranged respectively between [12-160] kg and [3-130] kg respectively. The maximum mass of FA and GGBFS is respectively 640 kg and 560 kg and the minimum and maximum curing temperature is 25°C and 120°C respectively. When interpreting Fig. 2(b) and all of the remaining box plots in this paper, it should be noted that outliers have been identified based on the interquartile range (IQR) criterion, which defines any point that is more than 1.5 times the interquartile range above or below the third and first quartile as an outlier.

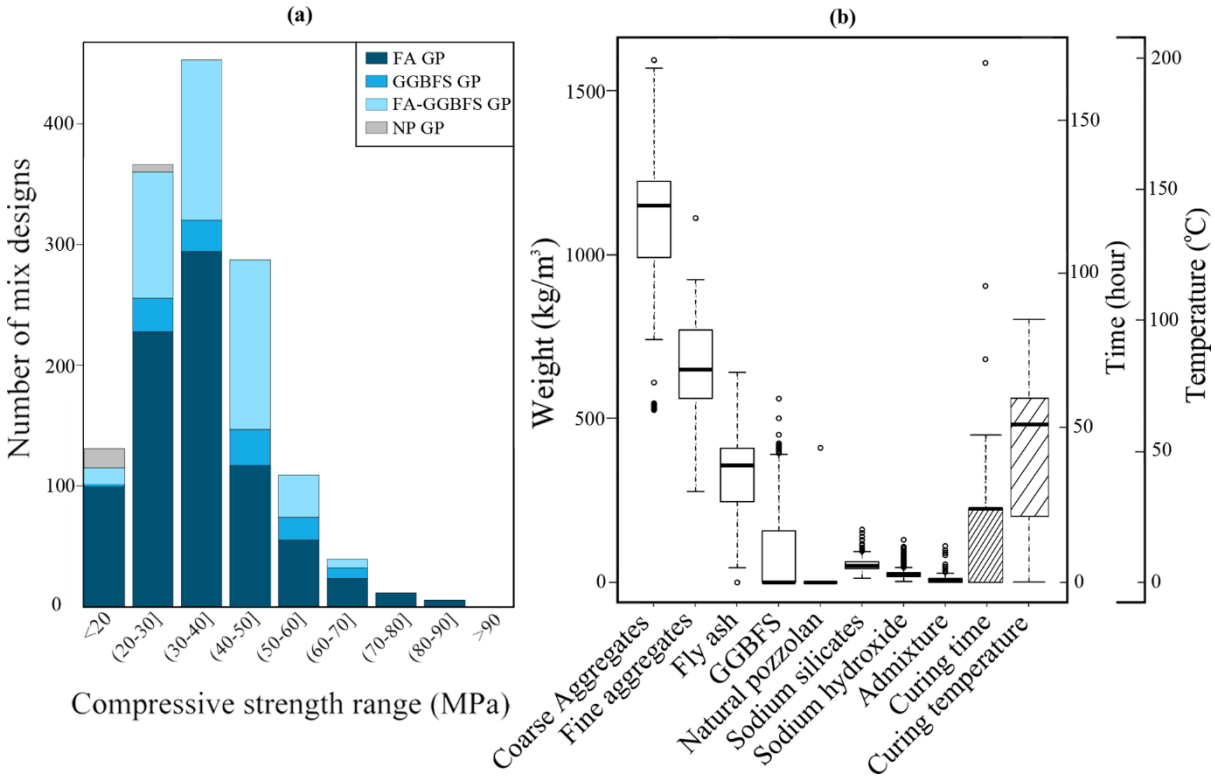

Fig.2 Distribution of: (a) compressive strength; (b) GP concrete mix designs in the database.

3.2. Equivalent OPC concrete

To provide a meaningful comparison between GP concrete and OPC concrete they should be evaluated with the same compressive strength and binder paste content. In this study, a technique based on the Feret equation (De Larrard 1999) is used to define an OPC concrete mix design with the same compressive strength (f_c) as the GP concrete as follows:

$$f_c \approx Z.S_c\left(\frac{V_c}{V_c+V_w+V_a}\right)^2 \quad (1)$$

where V_c, V_w and V_a are respectively the volume of cement, water and air used in 1 m^3 of concrete; S_c is the specific strength of cement and Z is the aggregates factor which is quantified as:

$$Z = \frac{1}{S_c} f_c \left(\frac{W_c}{W_c+W_w+W_a}\right)^{-2} \quad (2)$$

In Eq. 2, S_c is taken to be 52.5 MPa; and W_c, W_w and W_a are the weight of cement, water and air which are calculated based on the ACI concrete mix design approach (ACI 2011), where

the weight of equivalent OPC ($W_{c_{eq}}$) is given by:

$$W_{c_{eq}} = \left[\left(1 - \frac{W_{fine_{agg}}}{\rho_{fine_{agg}}} + \frac{W_{coarse_{agg}}}{\rho_{coarse_{agg}}}\right)\left(\frac{f_c}{ZS_c}\right)^{\frac{1}{2}}\right]\rho_c \quad (3)$$

where $W_{fine_{agg}}$, $W_{coarse_{agg}}$, $\rho_{fine_{agg}}$ and $\rho_{coarse_{agg}}$ are respectively weight and specific density of fine and coarse aggregates in GP concrete; and ρ_c is the specific gravity of cement which is assumed to be 3.15 (Butler 1906; Struble 2006; Helsel et al. 2016).

For analysis, Eqns. 1-3 are applied to quantify the mass of cement required in an OPC concrete with the same mass of coarse and fine aggregates as the reference GP concrete. The following assumptions were also applied for all mix designs in the database:

a) Cylinders with an aspect ratio of 2 were taken as the reference compressive strength test. The compressive strength of all GP concretes in the database was converted to the reference compressive strength using conversion factors in Elwell and Fu (1995).
b) The compressive strength of GP concretes in its hardened stage was taken for the LCA calculations, that is, for ambient cured specimens the strength was taken at 28-days, and for heat-cured specimens, the strength was taken on the test day.
c) If the information for the density of fine and coarse aggregates was not available for a typical GP concrete, it is assumed to be 2590 and 2620 kg/m^3 respectively.

3.3. Curing energy estimation

To obtain a desired degree of geopolymerisation and therefore compressive strength, it is often necessary to heat cure GP concretes, particularly if they use low-calcium fly ash as the aluminosilicate source. Few studies have included the energy required for heat curing when quantifying the emissions associated with the manufacture of GP concretes. Of the studies that do consider emissions arising from heat curing (Turner and Collins 2013; Salas et al. 2018), the emissions are determined based on the application of a constant curing time and temperature, this approach is limited because it is not easy to quantify how the emissions would change if the method for applying the heat were to change. To address this limitation, in this study, heat curing is modelled to consider different curing times and temperatures as follows. According to the heat transfer theory (Bergman et al. 2017), the curing energy per functional unit of concrete can be quantified as:

$$Energy_{curing} = P.t_{curing} + m.c.\left(T_{curing} - 25\right);\ T_{curing} > 25℃ \quad (4)$$

where P and m are respectively the power of oven or furnace (J/s) and the mass of GP concrete (kg); and T_{curing} and t_{curing} are respectively curing temperature (^oC) and time (s). In Eq. (4), c is the specific heat capacity of GP concrete which is assumed to be 700 ($J/kg\ ^oC$) according to Snell et al. (2017). Equation 4 is intended to only be applied to specimens that have been heat-cured at temperatures greater than ambient (defined as 25℃). Further, it should also be noted that a limitation of this approach is that heat loss and energy efficiency are not taken into account and this approximation is made because of the difficulty in quantifying these parameters.

4. Results and discussion

Figure 3 compares the CO_2 equivalent ($CO_{2\text{-eq}}$) emissions calculated using the TRACI lifecycle impact assessment approach (Bare 2002) released from the production of 1 m^3 of each of the

GP concrete mix designs in the database and their equivalent OPC concretes. In this plot the results are presented as a function of compressive strength using the base-case scenario outlined in Table 2. It can be seen from Fig. 3 that the $CO_{2\text{-eq}}$ emissions arising from GP concretes are lower than those arising from OPC concretes of an equivalent strength in almost all cases. However, it should be emphasized here that this analysis does not consider any emissions allocation, considers the average Australian transport distances defined by Grant (2015) and for mixes requiring heat curing, it assumes heating using a 600-Watt element.

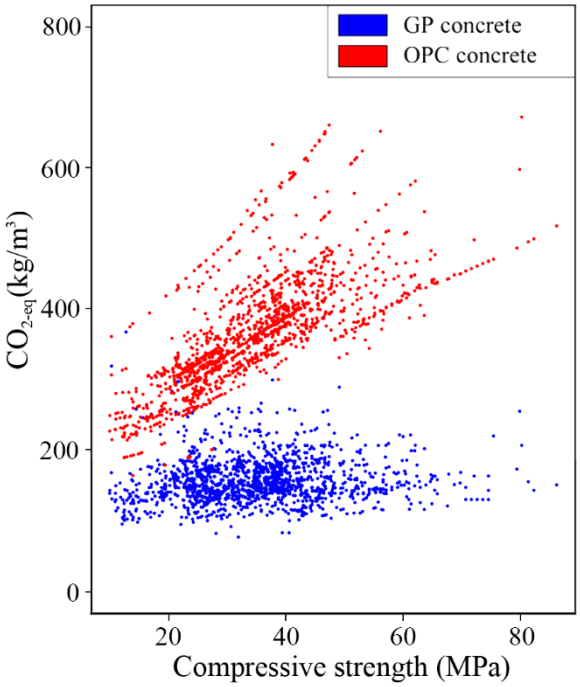

Fig.3 Distribution of $CO_{2\text{-eq}}$ emissions related to GP and OPC concretes.

It can also be seen from Fig. 3 that $CO_{2\text{-eq}}$ emissions from OPC concretes increase with increasing compressive strength. However, this relationship is not observed to the same extent for GP concretes. This is because the compressive strength of OPC concretes is most strongly related to the cement content, which is responsible for more than 90% of the $CO_{2\text{-eq}}$ emissions from OPC concrete. However, the compressive strength of GP concretes is dependent on several parameters (e.g. binder to activator ratio, activator molarity, heat curing) with the $CO_{2\text{-eq}}$ contribution of each of these factors generally being less than 30% of the total emissions. This observation is not in agreement with the results of previous studies (Yang et al. 2013; Salas et al. 2018) and it is suggested that this is because only a few concrete mix designs were analysed such that the variation arising from chemical composition (and therefore reactivity) of the different aluminosilicate sources, or from sub-optimal mix design could not be detected (Xie et al. 2020).

To better understand the source of $CO_{2\text{-eq}}$ emissions arising from the production of the four types of GP concretes and the comparison of OPC concretes, in Fig. 4, the emissions arising from each process are shown separately.

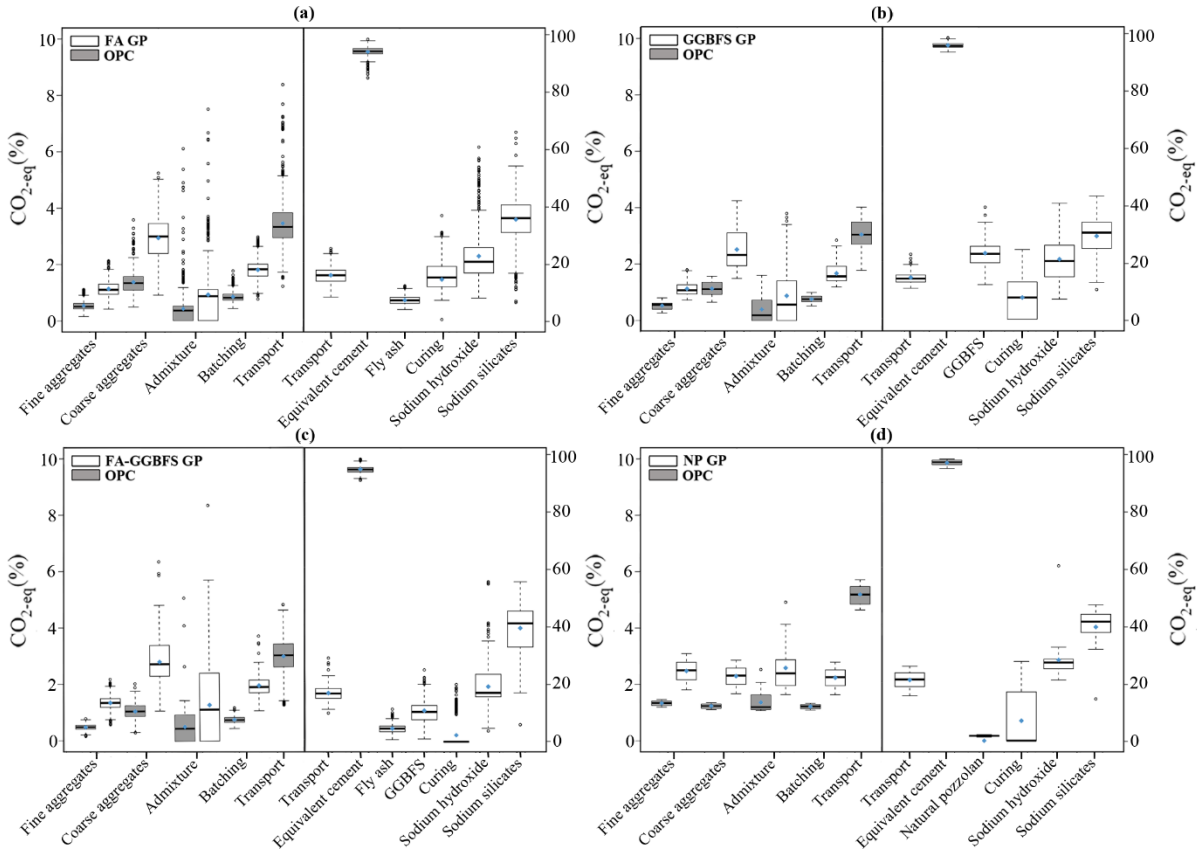

Fig.4 Percentage contribution of GP concrete ingredients and equivalent OPC to total $CO_{2\text{-eq}}$ emissions: (a) FA GP concrete; (b) GGBFS GP concrete; (c) FA-GGBFS GP concrete; (d) NP GP concrete

In Fig. 4, boxplots are used to show the range of $CO_{2\text{-eq}}$ emissions allocated to each process for all 1404 GP mix designs separated by type, along with the $CO_{2\text{-eq}}$ emissions for the corresponding OPC mix designs. For each boxplot a diamond marker is used to show the mean emissions for each process. Firstly considering the equivalent OPC mix designs (which are comprised of only the fine aggregate, coarse aggregate, admixture, batching, OPC mix design related transport and equivalent cement components), it can be seen that cement manufacture is responsible for more than 90% of the $CO_{2\text{-eq}}/m^3$ of OPC concrete produced, and this can be explained by the energy and emissions intensive pyroprocessing stage of cement manufacture.

Now considering the GP concretes, sodium silicates and sodium hydroxide are shown to have the greatest contribution to the overall $CO_{2\text{-eq}}$ emissions (between ~50% and ~65%), while batching, admixtures and aggregates have the smallest contributions (between ~1% and ~3%). The reason for this finding is that the manufacture of the alkali activators is energy intensive in nature and the chemical reactions that produce the activators themselves result in carbon dioxide emissions. This base-case analysis (using the properties outlined in Table 2) also shows that for all types of GP concretes except GGBFS based GP concretes, transportation has the greatest contribution to $CO_{2\text{-eq}}$ emissions (more than 15%) after the alkali activators. It should be noted that this finding does not fully capture the range of $CO_{2\text{-eq}}$ emissions arising from transportation, and this is further investigated through a sensitivity analysis based on real scenarios in Section 4.2.

Comparing the results in Fig. 4, it can also be confirmed that curing has a lower contribution to the $CO_{2\text{-eq}}$ emissions arising from GGBFS GP concrete and blended FA-GGBFS GP concrete than the two other types of GP concretes. The reason for this is that GGBFS based GP concretes generally need lower curing temperatures due to the self-cementing capacity of GGBFS (Yang et al. 2013), conversely, fly ash and natural pozzolans weakly self-cement and do not properly polycondense under ambient temperatures, and therefore high temperature is commonly required to achieve strengths suitable for civil engineering applications. The impact of changing the heat curing energy source (away from the 600 Watt assumed here) is further investigated in the sensitivity analysis (Section 4.1).

Finally, Fig. 4 shows that the preparation of GGBFS based GP concrete results in higher $CO_{2\text{-eq}}$ emissions from the binders because, regardless of binder type, similar mix proportions are used and the preparation of GGBFS is more energy intensive than fly ash and natural pozzolans (between 3 and 15 times respectively). This is because of the significant energy consumption associated with the preparation, quenching, dewatering, drying and grinding of slags after their production in the steel factories (Gursel 2014).

To examine the environmental efficiency of GP concretes in the case of the 'no allocation' scenario, an efficiency indicator is used to evaluate the environmental performance of all four types of GP concretes and their equivalent OPC concretes, namely $CO_{2\text{-eq}}$ intensity (C_i). As reported in Damineli et al. (2010), a concrete efficiency indicator can be defined as the environmental load of delivering one unit of functional performance. Considering the compressive strength as the functional performance, efficiency C_i can be defined as:

$$C_i = \frac{C_t}{f_c} \tag{5}$$

where C_t is the total $CO_{2\text{-eq}}$ emissions associated with the production of 1 m^3 of concrete and f_c is the concrete compressive strength. The $CO_{2\text{-eq}}$ intensity (C_i) associated with four different types of GP concrete (FA, GGBFS, FA-GGBFS and NP GP concrete) and their equivalent OPC concretes with respect to concrete compressive strength is shown in Fig. 5.

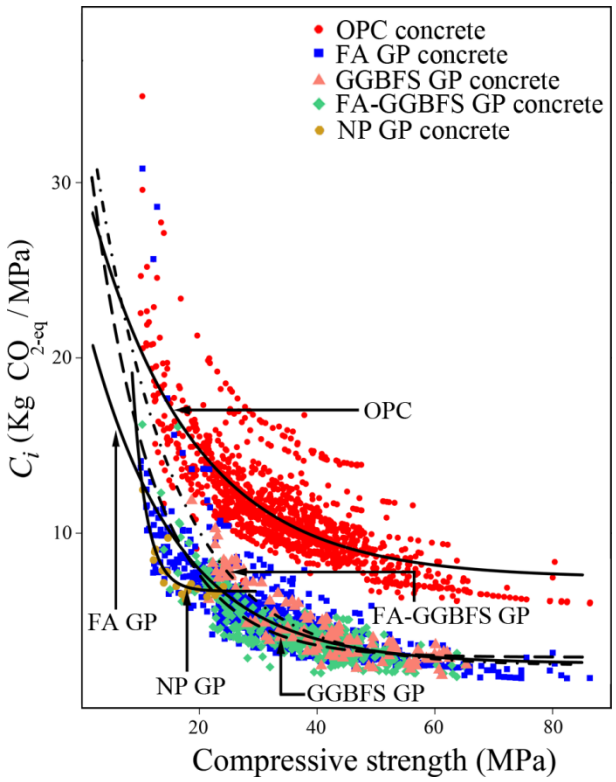

Fig.5 Relationship between $CO_{2\text{-eq}}$ intensity (C_i) and compressive strength for four different types of GP concretes

Based on the trendlines of the sub-populations shown in Fig. 5, it is seen that for all types of concretes, $CO_{2\text{-eq}}$ intensity tends to reduce with an increase in the compressive strength. This indicates that high-strength concretes tend to have better efficiency in terms of the amount of the $CO_{2\text{-eq}}$ emitted for delivering a unit of mechanical strength (Habert and Roussel 2009; Damineli et al. 2010). In general, $CO_{2\text{-eq}}$ intensities calculated for the four types of GP concretes are lower than that of OPC concretes with equivalent compressive strength. The $CO_{2\text{-eq}}$ intensity for FA GP concrete is around 2.3 times lower than that calculated for OPC concrete with the same concrete compressive strength and the $CO_{2\text{-eq}}$ intensity for GGBFS GP concrete is slightly lower again. It should be noted that the compressive strength range of NP GP concretes is less than that of the other binder types because of a lack of availability of mix designs that obtain a higher strength. It is suggested that this may be a focus of future materials research. The results of this analysis also show that FA-GGBFS GP concrete and NP GP concrete possess $CO_{2\text{-eq}}$ intensities that are respectively around 2.7 and 1.9 times lower than those of their OPC concrete counterparts with the same compressive strength. This demonstrates that, if ignoring allocation, replacing OPC concrete with an appropriate geopolymer binder appears to be a sustainable option. This is particularly the case if an appropriate blend of GGBFS and FA is obtained such that the transport distances and curing temperatures can be minimized. This is because the addition of GGBFS in FA GP concrete will, in general, improve compressive strength and reduce the need for heat curing, but at the same time also minimize the use of GGBFS, which is more energy intensive to produce than fly ash (Smith and Osborne 1997; Shi and Day 1999; Puertas et al. 2000; Nath and Sarker 2014).

4.1. Sensitivity analysis of electricity grid mix, sodium silicate type and curing energy

In the previous section, the $CO_{2\text{-eq}}$ emissions associated with the production of 1 m^3 of GP concrete were based on the base-case scenario as set out in Table 2. To investigate the influence that a variation in curing energy can have on $CO_{2\text{-eq}}$ emissions, a change in the power of the heating unit is considered for the sensitivity analysis. This is done by establishing the energy input during the experimentally reported heat curing process using Eq. 4, for each given element power, P, the new curing time, t, is quantified by ensuring the total curing energy is the same as recorded in the original experimental work. The results of this analysis are shown in Fig. 6(a) which demonstrates that there is a little variation in the $CO_{2\text{-eq}}$ emissions released from the production of 1 m^3 of GP concrete when the power of heating unit is less than 1500 Watt. However, an increase in the power of heating unit from 1500 Watt to 3000 Watt and 6000 Watt can lead to 10% and 30% increases respectively in the $CO_{2\text{-eq}}$ emissions per functional unit of GP concrete. This can be attributed to the fact that the energy consumed by machine operation generally dominates the energy absorbed by concrete during curing.

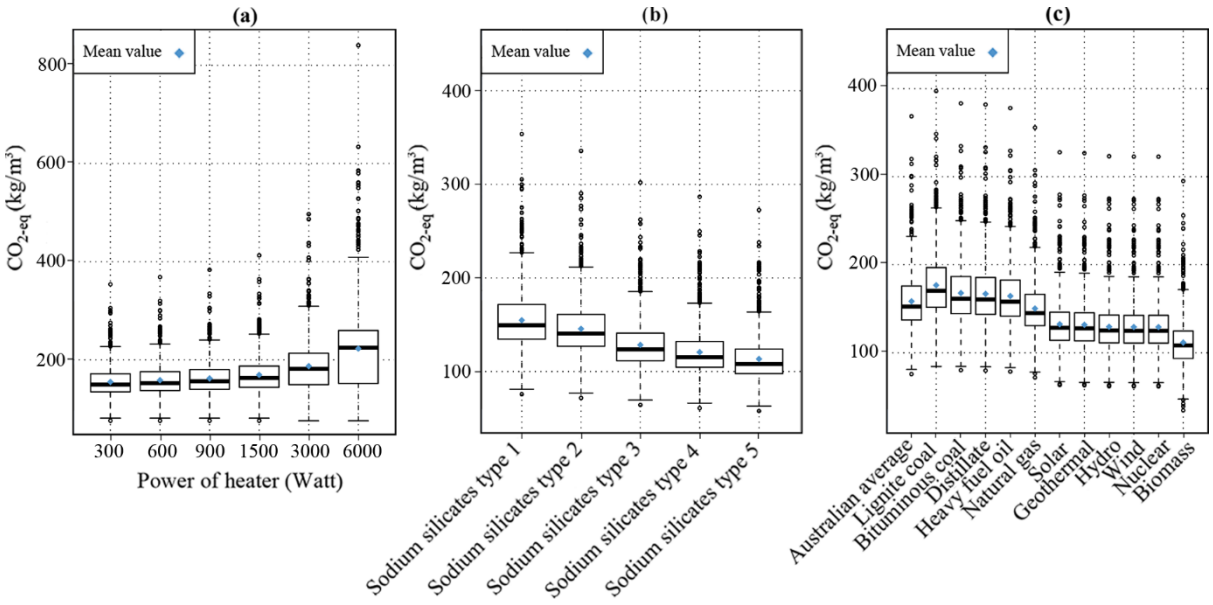

Fig.6 Sensitivity analysis for different: (a) power of heating unit; (b) alkali activator types; (c) electricity grid mix.

Now consider the effects of various manufacturing processes of sodium silicate on the $CO_{2\text{-eq}}$ emissions in Fig. 6(b). Here we are considering sodium silicate production because it is the most significant contributor to the overall $CO_{2\text{-eq}}$ emissions from GP concretes (between 30% and 40%) and because there are several different manufacturing processes that are driven by different chemical reactions. For the purpose of this sensitivity analysis, the LCI of five different types of sodium silicate including 'sodium silicate 3.3 WR furnace lumps (100%)', 'sodium silicate 2.0 WR spray powder (80% solid)', 'sodium metasilicate pentahydrate 1.0WR (58% dry matter)', 'sodium silicate 3.3 WR furnace liquor (37% solid)', 'sodium silicate 2.0WR hydrothermal liquor (48% solid)' are taken from Fawer et al. (1999) and renamed respectively as the sodium silicate type 1 to 5 as shown in Fig. 6(b). The results of analysis demonstrate that the type of sodium silicate used generally plays an important role in the

$CO_{2\text{-eq}}$ emissions per functional unit of GP concrete. However, its effects on the mechanical properties of GP concrete need further investigation since each soluble silica source can have different solubility. It can be seen that by replacing sodium silicate type 1 with type 3, $CO_{2\text{-eq}}$ emissions per unit volume of GP concrete can decrease up to 30%. It also appears that the $CO_{2\text{-eq}}$ emissions generally increase with an increase in the ratio of solid sodium silicate. However, the sodium silicate type 2 with a lower ratio of solid (37%) has more $CO_{2\text{-eq}}$ emissions (7%) than the sodium silicate type 3 with a higher ratio of solid (48%). This can be attributed to the different manufacturing processes of these two different types of sodium silicate.

The impact of different electricity grid mixes on the $CO_{2\text{-eq}}$ emissions released from the manufacture of 1 m^3 of GP concrete is shown in Fig. 6(c). It can be seen that there is a little variation (around 5%) in the $CO_{2\text{-eq}}$ emissions by a shift from the Australian average energy grid mix to non-renewable energy sources with the exception of using lignite coal as the electricity energy source (11%), this is because of its intensive carbon content of coal. It can also be seen that the use of natural gas is preferable as it produces less $CO_{2\text{-eq}}$ emissions than the Australian average energy grid mix. It also appears that a reduction in the $CO_{2\text{-eq}}$ emissions of between 15% and 30% is possible when the Australian average energy grid mix is entirely replaced with renewable energy sources such as solar, wind and biomass. This shows that optimization of electricity grid mix has obvious advantages in terms of the $CO_{2\text{-eq}}$ emissions because it can significantly reduce $CO_{2\text{-eq}}$ emissions from the production of GP concretes without any impact on their mechanical properties. To investigate which manufacturing process of GP concrete is most affected by a shift from the Australian average energy grid mix to renewable energy sources, the distribution of the $CO_{2\text{-eq}}$ emissions arisen

from each manufacturing process of GP concrete involving electricity usage is shown in Fig. 7. It can be seen from Fig. 7 that while $CO_{2\text{-eq}}$ emissions from the curing and batching reduced by more than 90%, the $CO_{2\text{-eq}}$ emissions from the production of FA, aggregates and GGBFS have experienced a reduction of up to 15%, 55% and 65% respectively. The reason why different $CO_{2\text{-eq}}$ reductions can be seen for each manufacturing process of GP concrete when the energy grid mix is replaced by renewable energy sources is that different amounts of electricity are used for the preparation and production of each material. For instance, the electricity use factor for the preparation of fly ash is 6.82 kWh/tonne, while it is 94.7 kWh/tonne for the preparation of GGBFS (see Supplementary Material A for further details).

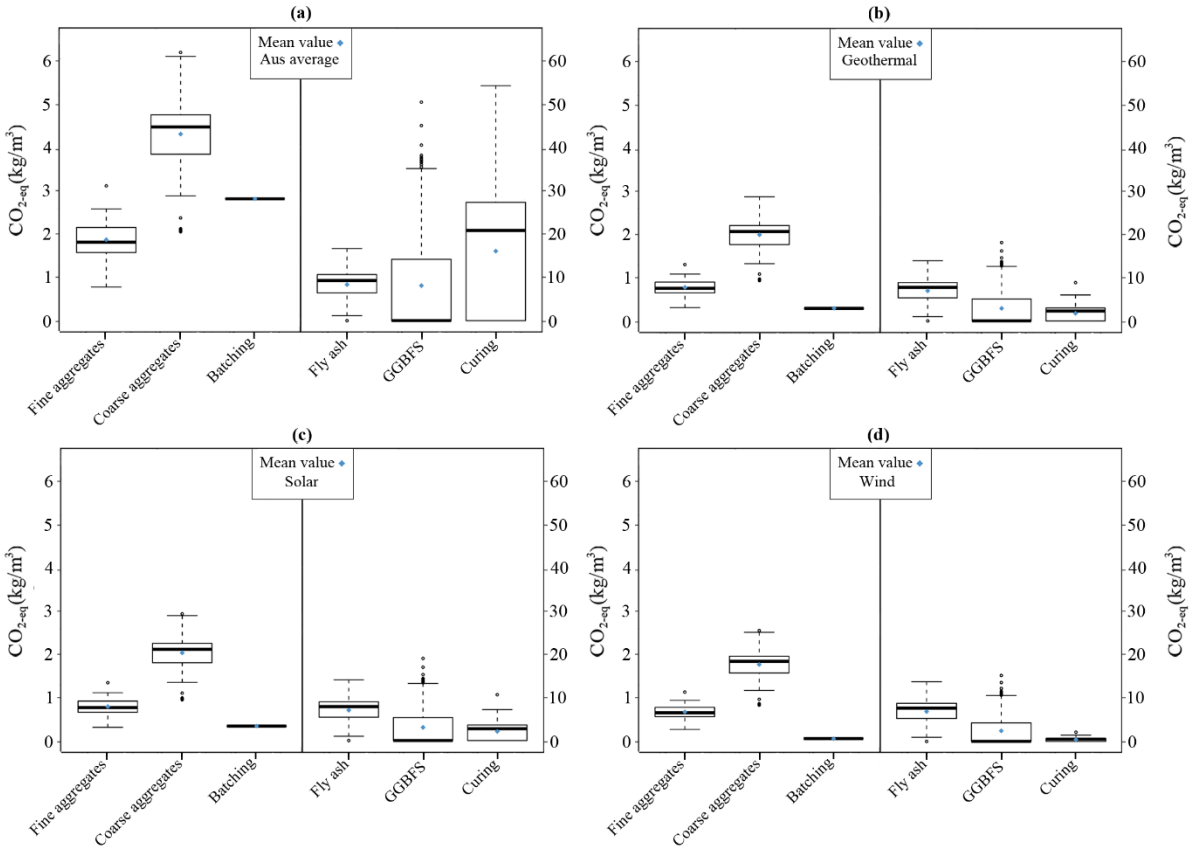

Fig.7 Contribution of each process of GP concrete production involving electricity usage to $CO_{2\text{-eq}}$ emissions for different electricity energy sources: (a) Australian average electricity grid mix; (b) geothermal energy source; (c) solar energy sources; and (d) wind energy sources.

4.2. Sensitivity analysis of transportation

For the base-case analysis outlined in Table 2, transportation distances were assumed to be the average distances in Australia previously determined by Grant (2015). Let us now consider the importance of accurately modelling transportation distances based on a case study in a specific regional context. The following assumptions are made to implement the sensitivity analysis of transportation for an Australian context:

a) Chemical products including alkali activators and superplasticizers are provided from the same providers.
b) GGBFS can be provided locally by steel factories in Port Kembla or imported from Japan (Port Yokohama) (see Fig. 8).
c) FA can be provided by coal power stations in Australia including Eraring Power Station, Collie Power Station, Mt Piper Power Station and Bayswater Power Station (see Fig. 8).
d) Only quarries within a state are considered in the sensitivity analysis, that is, no transport of quarry material occurs between states.
e) Rail transportation was considered for bulky materials such as FA and GGBFS. The reason for this is that, unlike aggregates that are widely available around Australia, materials such as FA and GGBFS are not necessarily available locally and therefore high volumes are transported long distances.
f) Batching plants are assumed to be in the suburbs of five major Australian cities including Sydney, Melbourne, Adelaide, Perth and Brisbane (see Fig. 8).

g) All five cities have ports capable of unloading GGBFS.
h) Since transportation emissions factors are a function of transportation distance, the minimum and maximum transportation distances between batching plants and material sources are considered across Australia to capture the full range of expected outcomes.

The locations of batching plants and material sources for OPC and GP based concretes in Australia are shown in Fig. 8. Table 3 details the maximum and minimum distances between material sources and batching plants in the five different cities studied and Table 4 outlines the scenarios for the sensitivity analysis of transportation.

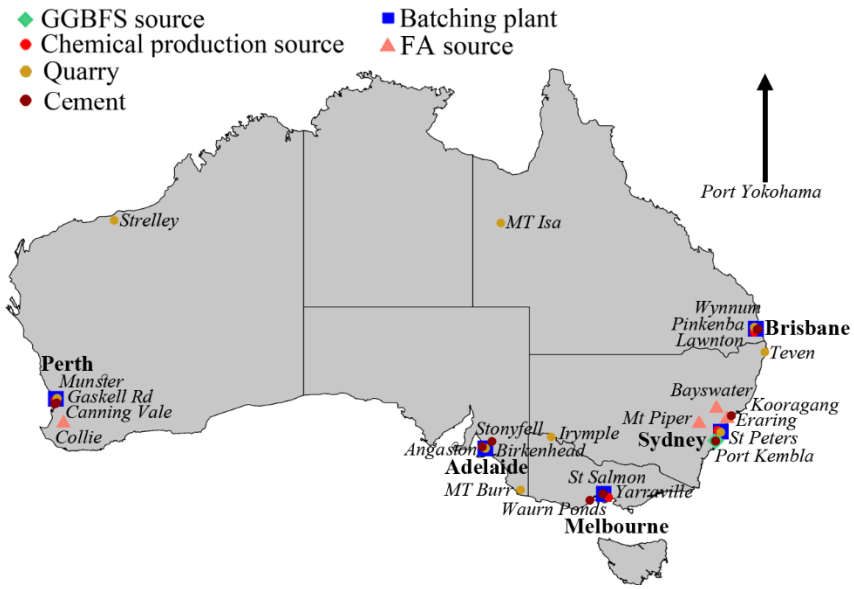

Fig. 8 Location of batching plants and material sources in Australia.

Table 3 Inputs for sensitivity analysis of transportation.

Batching Plant	Case	GGBFS		FA		Quarry (Intrastate)	Chemical Products	Cement
Sydney		Port Kembla		Eraring Power Station		St Peters	Sydney-based provider	Port Kembla
		Road (km)	Rail + road (km)	Road (km)	Rail + road (km)	Road (km)	Road (km)	Road (km)
	Min	95	89 + 3	124	127 + 12	7	28	95
		Port Yokohama		Collie Power Station		Teven	Perth-based provider	Kooragang
		Water (km)		Road (km)	Rail + road (km)	Road (km)	Road (km)	Road (km)
	Max	8021		3819	4540 + 74	731	3936	163
Melbourne		Port Kembla		Mt Piper Power Station		St Salmon	Melbourne-based provider	Yarraville
		Road (km)	Rail (km)	Road (km)	Rail + road (km)	Road (km)	Road (km)	Road (km)
	Min	845	973	835	1130 + 27	2	41	1.2

		Port Yokohama		Collie Power Station		Irymple	Perth-based provider	Waurn Ponds
		Water (km)		Road (km)	Rail + road (km)	Road (km)	Road (km)	Road (km)
	Max	9088		3302	4131 + 71	543	3420	90
Adelaide		Port Kembla		Mt Piper Power Station		Stonyfell	Adelaide-based provider	Angaston
		Road (km)	Rail + road (km)	Road (km)	Rail + road (km)	Road (km)	Road (km)	Road (km)
	Min	1370	1440 + 17	1280	1692 + 41	0.55	25	34
		Port Yokohama		Collie Power Station		Mt Burr	Perth-based provider	Birkenhead
		Water (km)		Road (km)	Rail + road (km)	Road (km)	Road (km)	Road (km)
	Max	9792		2590	3303 + 85	419	2708	98
Perth		Port Kembla		Collie Power Station		Strelley	Perth-based provider	Canning Vale
		Road (km)	Rail + road (km)	Road (km)	Rail + road (km)	Road (km)	Road (km)	Road (km)
	Min	3903	4441 + 21	219	188 + 92	13	10	42
		Port Yokohama		Eraring Power Station		Gaskell Rd	Brisbane-based provider	Munster
		Water (km)		Road (km)	Rail + road (km)	Road (km)	Road (km)	Road (km)
	Max	8317		3950	4479 + 30	1647	4302	53
Brisbane		Port Kembla		Bayswater Power Station		Lawnton	Brisbane - based provider	Pinkenba
		Road (km)	Rail	Road (km)	Rail + road (km)	Road (km)	Road (km)	Road (km)
	Min	1035	1135	756	900 + 35	16	34	15
		Port Yokohama		Collie Power Station		Mt Isa	Perth-based provider	Wynnum
		Water (km)		Road (km)	Rail + road (km)	Road (km)	Road (km)	Road (km)
	Max	7278		4211	5588 + 71	1853	4329	24

Table 4 Different scenarios for sensitivity analysis of transportation.

GP concrete					**OPC concrete**			
Case	**GGBFS (distance)**	**FA (distance)**	**Quarry (distance)**	**Chemical products (distance)**	**Case**	**Cement (distance)**	**Quarry (distance)**	**Chemical products (distance)**
1	Min	Min	Min	Min	1	Min	Min	Min
2	Max	Min	Min	Min				
3	Min	Max	Min	Min	2	Max	Min	Min
4	Max	Max	Min	Min				
5	Min	Min	Max	Min	3	Min	Max	Min
6	Max	Min	Max	Min				
7	Min	Max	Max	Min	4	Max	Max	Min
8	Max	Max	Max	Min				
9	Min	Min	Min	Max	5	Min	Min	Max
10	Max	Min	Min	Max				
11	Min	Max	Min	Max	6	Max	Min	Max
12	Max	Max	Min	Max				

13	Min	Min	Max	Max	7	Min	Max	Max
14	Max	Min	Max	Max				
15	Min	Max	Max	Max	8	Max	Max	Max
16	Max	Max	Max	Max				

Figs. 9 shows the $CO_{2\text{-eq}}$ emissions arising from different types of GP concretes for various sensitivity analysis scenarios with batching plants in five different cities when road and sea transportation are considered. It should be noted that since there is no GGBFS in FA GP concrete, the sensitivity analysis scenarios shown in Table 4 are limited to eight different cases for this type of GP concrete (cases 1 & 2, 3 & 4, …, 15 &16 are equivalent). A similar implication can also be drawn for GGBFS GP concrete since there is no FA in the mix design of this type of GP concrete (cases 1 & 3, 2 & 4, …, 14 & 16 are equivalent). For each scenario identified in Table 4, that the actual distances related to Max and Min are shown in Table 3 for each city and transportation mode. Examining these figures shows that $CO_{2\text{-eq}}$ emissions arising from the production of all types of GP concretes in different cities are minimum when the transport distances of all materials are minimum and vice versa. It is also clear that Perth and Brisbane have a higher range of $CO_{2\text{-eq}}$ emissions compared to other cities because they consider a wider range of transport distances for the supply of raw materials.

The results of the analysis in Fig. 9 show that while for batching plants in Sydney, Perth and Brisbane, FA GP concretes have lower $CO_{2\text{-eq}}$ emissions than OPC concrete for all cases of transportation except the cases in which transportation distances of FA and chemical products are both at their maximum (cases 11 &12 and 15 & 16), Fly Ash GP concrete has lower $CO_{2\text{-eq}}$ emissions than OPC concrete for batching plants in Adelaide and Melbourne for all the cases of transportation. However, OPC and GP concretes have similar $CO_{2\text{-eq}}$ emissions for batching plants in Melbourne when the transport distances of FA and chemical products are maximum. This indicates the importance of the transport distances of FA and chemical products in the sustainability of this type of GP concrete. Fig. 9 also indicates that for all cities except Perth, GGBFS GP concrete has lower $CO_{2\text{-eq}}$ emissions than OPC concrete for all the cases of transportation examined. However, for Perth, OPC concrete is more sustainable than GGBFS GP concrete when the transport distances of GGBFS and chemical products are maximum. The reason for this is that unlike OPC which can be produced locally, GGBFS is only produced at a single location nationally or imported internationally and therefore significantly more emissions arise from the transportation of GGBFS than the manufacture of OPC. It can also be seen from Fig. 9 that when batching concrete in Sydney, Melbourne, Adelaide and Brisbane, the manufacture of FA-GGBFS GP concrete has lower $CO_{2\text{-eq}}$ emissions than OPC concrete for all the cases of transportation, while when considering batching in Perth, OPC concrete and GP concrete have similar $CO_{2\text{-eq}}$ emissions because of the large transport distances. This case study therefore highlights the need to consider regional scale transport options when considering the manufacture of GP concrete because the source materials are often less widely available than those required to manufacture OPC.

The results in Fig. 9, are further broken down by contribution in Figure S1 in Supplementary Material C. In this breakdown it is shown that FA contributes the most to transportation related emissions when batching FA GP in Sydney, Melbourne and Adelaide, but in Perth and Brisbane quarry materials contribute more transportation related emissions because of the larger transport distances. When considering the manufacture of GGBFS and FA-GGBFS GP, similar trends are seen in all five cities that were modelled.

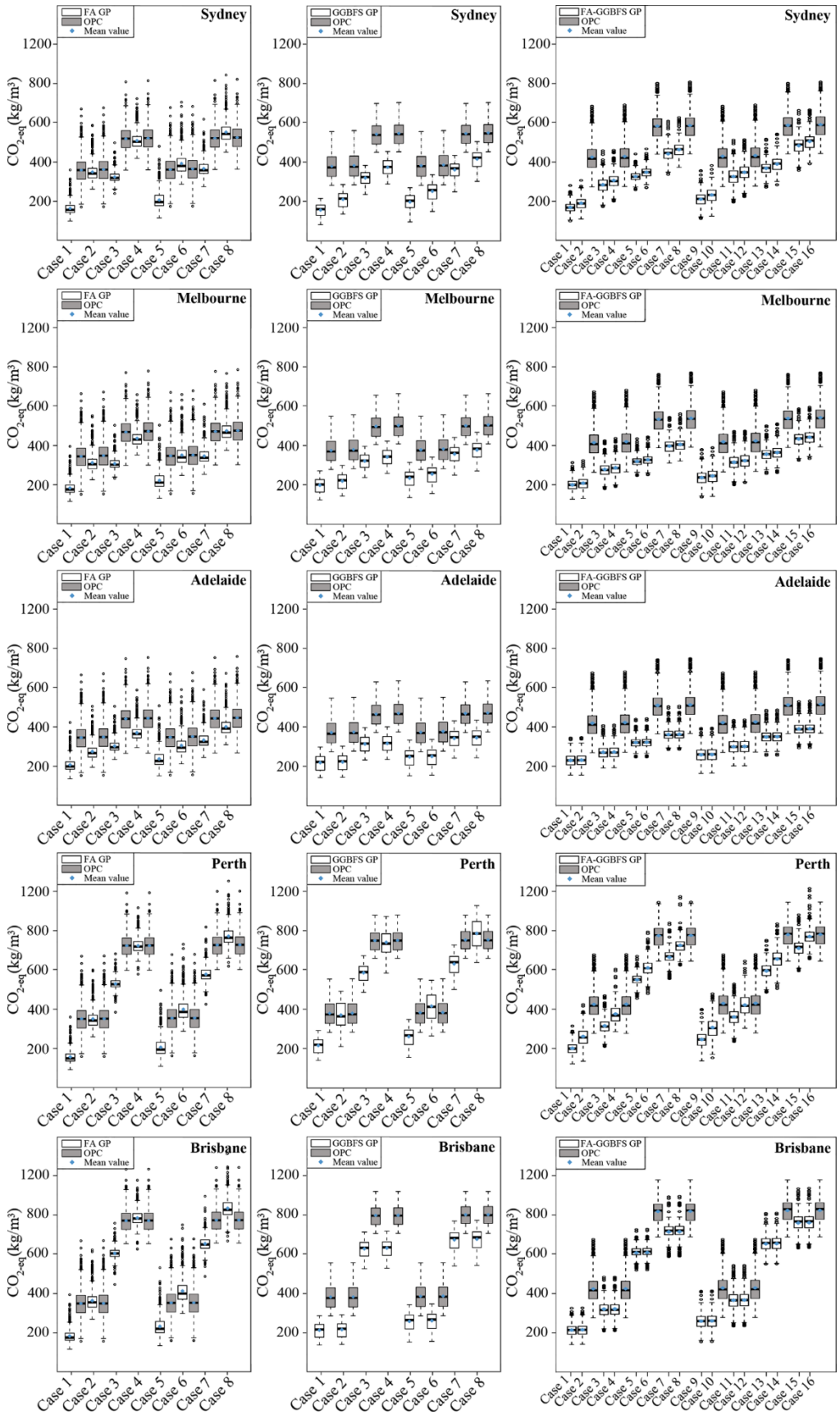

Fig.9 Distribution of $CO_{2\text{-eq}}$ emissions from GP and OPC concretes considering sensitivity analysis of road and sea transportation for batching plants in five different cities.

To better understand the importance of transportation mode, the transportation sensitivity analysis is now repeated considering the potential to use rail to transport FA and GGBFS. The results of the analysis (shown in Fig. 10) indicate that the use of rail decreases transport related emissions at all batching locations for all the three types of GP concrete. This finding highlights the importance of rail transportation where bulk transportation is required. Breaking down the sources of transportation emissions in Figure S2 (see Supplementary Material C) it is shown that a change in transportation mode from road to rail yields reductions in $CO_{2\text{-eq}}$ emissions of up to 25% from GGBFS and FA for all types of GP concrete in all cities. Figure S2 also shows that if using rail to transport FA and GGBFS then the largest contributor to transport emissions comes from quarry materials that are transported by road. This indicates the use of rail is preferred when transporting high bulk materials. Given that 80% of GGBFS in Australia is imported from Japan (Pink 2013; Grant 2015) and the remaining 20% is locally produced at Port Kembla, let us now examine the environmental impacts of providing GGBFS from domestic and international sources. Table 5 shows the CO_2 emissions of sourcing GGBFS from Port Kembla or importing it from Japan considering each of the five batching locations. Emissions factors for road, rail and sea transportation can be seen in Supplementary Material C and transportation distances from Port Yokohama to five cities in Australia are seen in Table 3.

The results show that while $CO_{2\text{-eq}}$ emissions would reduce for Sydney and Melbourne if GGBFS was provided from Port Kembla by road transportation, for Perth, GGBFS should be imported from Port Yokohama by sea freight because of lower sea transportation emissions. Sourcing GGBFS from Port Kembla or Japan has negligible impact on $CO_{2\text{-eq}}$ emissions when batching in Adelaide and Brisbane because of the relative weighting of the emissions factors and transport distances. If the mode of internal transport were changed from road to rail, emissions for all cities except Perth would be reduced if sourcing GGBFS at Port Kembla. It is interesting to note that small reductions in $CO_{2\text{-eq}}$ emissions are observed when batching in Perth and sourcing GGBFS from Port Kembla by rail transportation instead of importing it from Japan by sea transportation. This is because although the sea transportation distances from Perth to Port Yokohama are 90% greater than the rail transportation distance from Perth to Port Kembla, the emissions factor of rail transportation is 60% more than that of sea transportation.

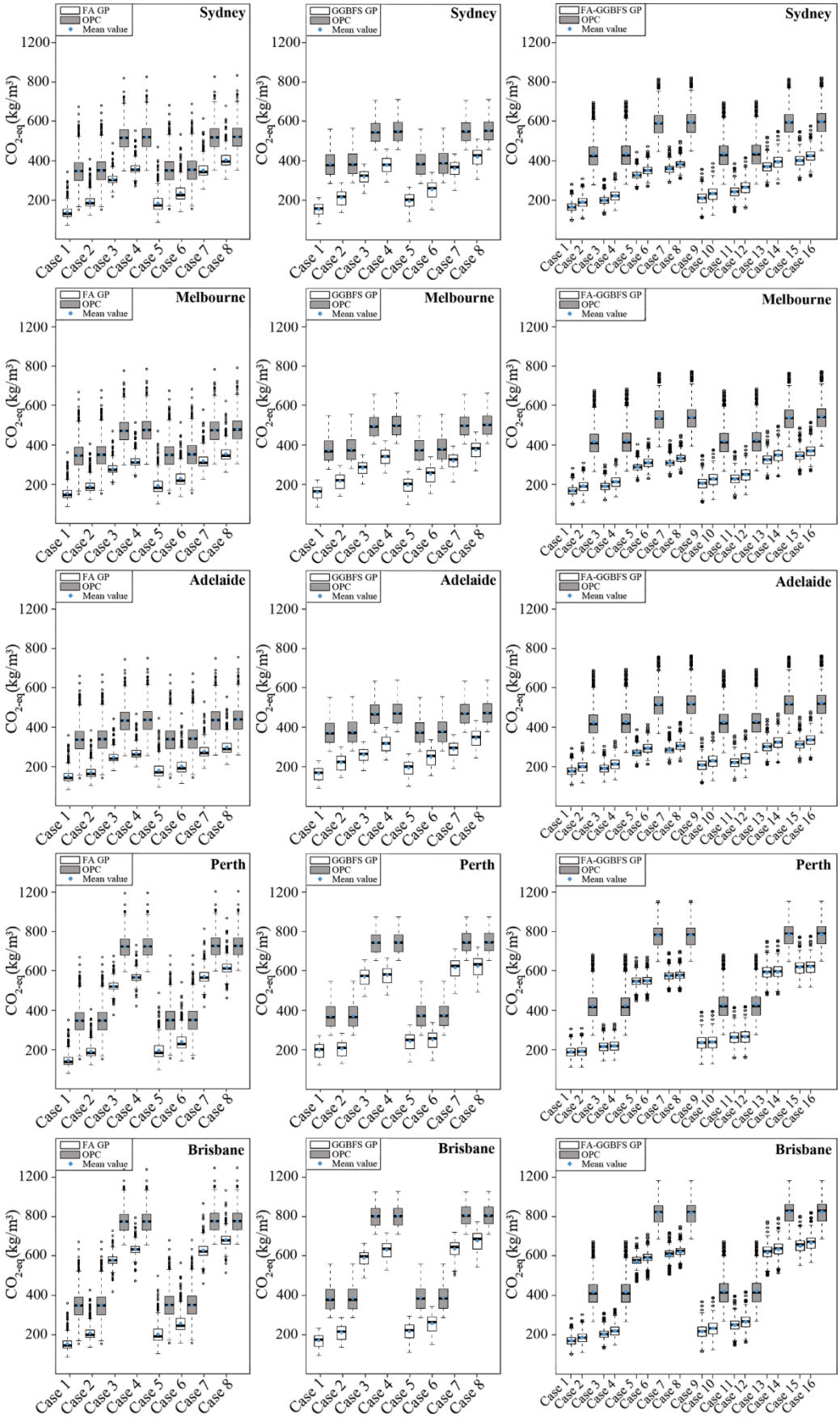

Fig.10 Distribution of $CO_{2\text{-eq}}$ emissions from GP and OPC concretes considering road, sea and rail transportation for batching plants in five different cities

Table 5 Transportation emissions for providing GGBFS from different sources

Batching Plant	Transportation emissions (kg/m^3)		
	Port Kembla		Port Yokohama
	Road	Rail	Water
Sydney	0.012	0.003	0.138
Melbourne	0.108	0.027	0.156
Adelaide	0.175	0.042	0.168
Perth	0.500	0.124	0.143
Brisbane	0.132	0.031	0.125

Having looked at a specific case study above, let us now consider a generalization, in which the maximum (or limiting) distance over which the materials required form manufacturing GP concretes can be sourced to ensure that the emissions associated with GP concrete are less than the equivalent strength OPC concrete. This limiting distance can be defined as

$$Limiting\ Distance = \frac{CO_{2-eq_{OPC}} - CO_{2-eq_{GP}}}{EF_{GP}} \quad (6)$$

where EF_{GP} is the total transportation emissions factor (kg CO_2/km) for GP concrete materials, $CO_{2-eq_{OPC}}$ is the $CO_{2\text{-eq}}$ emissions from OPC concrete considering emissions from transportation and $CO_{2-eq_{GP}}$ is $CO_{2\text{-eq}}$ emissions from GP concrete without emissions from transportation.

Detailed results obtained by solving Eq. (6) for each mix design considering all five different cities and either road, or road and rail transportation are shown in Figures S3 and S4 in Supplementary Material C and a summary of all of the results is presented here in Fig. 11. In both the detailed and summary plots, for clarity, only case 1 and case 8 (the minimum and maximum transportation distances for OPC concrete materials) in Table 4 are considered because these represent the absolute minimum and maximum limiting distances.

It is shown in Figures S3 and S4 that the limiting distance always increases as the compressive strength of the concrete increases regardless of the type of GP binder, transportation mode or the city in which the analysis is undertaken. This finding arises because the $CO_{2\text{-eq}}$ emissions of OPC concretes increase at a faster rate than for GP concretes at all compressive strengths (as shown in Fig. 3). Summarising the results independently of compressive strength in Fig. 11 shows by shifting from case 1 to case 8, the limiting distances can increase up to 340%. The reason for this is that $CO_{2\text{-eq}}$ emissions from OPC concrete in case 8 are much higher than that in case 1 resulting in more limiting distances for GP concretes to have the same $CO_{2\text{-eq}}$ emissions from OPC concrete. In case 8, Adelaide and Brisbane have respectively the least and most limiting distances for all types of GP concretes as they have the least and most $CO_{2\text{-eq}}$ emissions from OPC concrete. It is worth noting that by a change in transportation mode from road to rail for FA and GGBFS, the limiting distances can increase up to 20% indicating the importance of rail transportation for such materials.

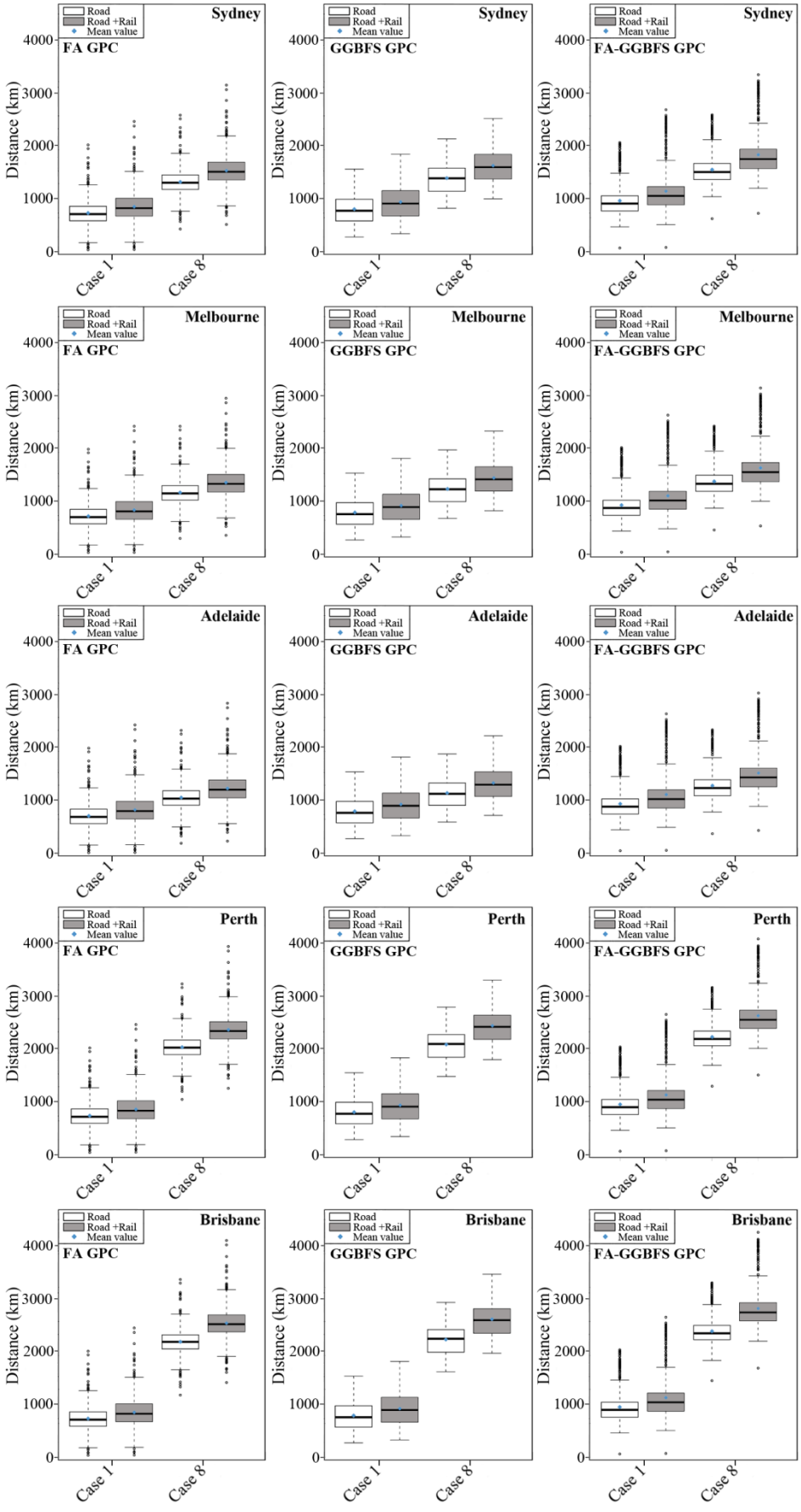

Fig. 11 Distribution of limiting distances for GP concretes considering different types of

transportation modes and cases for batching plants in five different cities

4.3. Allocation scenarios

A review of the literature on the LCA of concrete containing GGBFS and FA indicates that there is no general consensus on the inclusion of allocation procedures for FA and GGBFS production emissions (Habert et al. 2011; Van den Heede and De Belie 2012; Seto et al. 2017). There are several reasons for this, such as a lack of data on GGBFS and FA production quantities and the widely held assumption that GGBFS and FA are waste products having negligible environmental impacts as compared to overall environmental impacts of GP concretes (Athena 2005; Huntzinger and Eatmon 2009). To address these challenges, Chen et al. (2010) carefully examined the LCA of steel and coal power plants and suggested that GGBFS and FA should not be considered as waste products because they meet all the conditions set by the European Union directive on waste to be considered as by-products (EU 2008). Hence, in this section, the allocation principles proposed by Chen et al. (2010) are used to examine the variability in the $CO_{2\text{-eq}}$ emissions of GP concretes as a function with common emissions allocation scenarios.

Two forms of allocation scenarios are typically applied to industrial by-products: mass allocation and economic allocation (Chen et al. 2010); with each approach having its own benefits and limitations (Van den Heede and De Belie 2012; Seto et al. 2017).

In the case of mass allocation, the environmental impacts are split between the main product and by-product based on the mass ratio produced. That is:

$$C_m = \frac{m_{\text{by-product}}}{m_{\text{by-product}} + m_{\text{main product}}} \tag{7}$$

where C_m, $m_{\text{main product}}$ and $m_{\text{by-product}}$ are the mass allocation coefficients, the mass of main product (electricity and steel) and the mass of by-product (FA and GGBFS). For this analysis, mass quantities are taken from the LCI values of Chen et al. (2010) who states that 0.36 kg of hard coal is burnt to produce 0.052 kg of FA and 1.0 kWh of electricity and 0.24 kg of GGBFS is generated per kg of steel. Based on these values, C_m is calculated as 0.124 and 0.194 respectively for FA and GGBFS which means that 12.4% and 19.4 % of the environmental impact of a generation of 1 kWh of electricity and 1 kg of steel should be respectively allocated to the production of 0.052 kg of FA and 0.24 kg of GGBFS.

For economic allocation scenario, environmental impacts of main product and by-product can be calculated as (Chen et al. 2010):

$$C_e = \frac{(u_p \cdot m)_{\text{by-product}}}{(u_p \cdot m)_{\text{by-product}} + (u_p \cdot m)_{\text{main product}}} \tag{8}$$

where u_p is the unit price of the product. In this study, the value of FA between the years 2018 and 2027 was predicted assuming that the fly ash market grows globally from \$3.4 billion in 2018 to \$5.7 billion by 2027, at a compound annual growth rate (CAGR) of 6.0% (Fly Ash Market 2018). Electricity costs between these years were taken from the Australian electricity market analysis report, covering the years from 2020 and 2030 (Brinsmead et al. 2014) and steel price growth was predicted based on a CAGR of 2.6%, increasing from \$807 billion in 2016 to \$1.01 trillion in 2025 (Grand View Research 2017). Having the market value for

GGBFS between 2016 and 2025 (LP Information (LPI) 2020) and price range for GGBFS and FA respectively in 2016 and 2018 (Teh et al. 2017; Boral North America Investor Site Tour 2017), the economic allocation coefficients (C_e) based on the average price for FA and GGBFS can be obtained in various years as shown in Table 6.

Table 6 Economic allocation coefficients and emissions for FA and GGBFS based on average price in different consecutive years

Year	C_e (%)		F_i (kg/m^3)	
	FA	GGBFS	FA	GGBFS
2016	-	4.50	-	0.16
2017	-	5.31	-	0.19
2018	6.56	5.73	1.20	0.20
2019	6.68	6.10	1.22	0.22
2020	6.93	4.64	1.27	0.16
2021	6.95	6.04	1.27	0.21
2022	7.10	6.63	1.30	0.23
2023	7.15	7.09	1.31	0.25
2024	7.12	7.54	1.30	0.27
2025	7.11	7.84	1.30	0.28
2026	7.21	-	1.32	
2027	7.24	-	1.32	

It can be seen from Table 6 that C_e for GGBFS has increased faster than for FA; ranging from 4.50 in 2016 to 7.84 in 2025 (75% increase) compared to the 10% increase for FA between 2018 and 2027. This difference is because the price of GGBFS relative to steel has increased at a much faster rate than the price of FA relative to electricity.

Having quantified the allocation coefficients (C), the environmental impacts associated with by-product i (F_i) can be calculated as follows (Chen et al. 2010):

$$F_i = C \times F_{main\ product} + F_{by-product} \quad (9)$$

where $F_{main\ product}$ and $F_{by-product}$ are respectively allocation emissions from the main product (electricity and steel) and by-product (FA and GGBFS) which are taken from Chen et al. (2010). The results for the economic allocation emissions (F_i) of FA and GGBFS are shown in Table 6, from which it can be seen that the economic allocation of emissions associated with FA are higher than that for GGBFS.

To investigate the impacts of the change in the allocation scenario on the $CO_{2\text{-eq}}$ emissions of GP concretes, all mixes within the database were reanalyzed considering: no allocation, mass allocation and economic allocation scenarios and considering the base-case scenario outlined in Table 2 for all other inputs. The results of this analysis are shown in Fig. 12, from which it can be seen that while in the case of the no allocation scenario GP concrete has significantly lower $CO_{2\text{-eq}}$ emissions than OPC concrete; OPC concrete has significantly lower $CO_{2\text{-eq}}$ emissions than GP concrete when the mass allocation scenario is considered (i.e. the $CO_{2\text{-eq}}$ emissions from GPC when mass allocation is considered is around 260% of OPC concrete). It can also be observed that, in the case of the economic allocation scenario, OPC and GP concretes have similar $CO_{2\text{-eq}}$ emissions (ranging from 325 to 370 kg/m^3). These results suggest

that the change in $CO_{2\text{-eq}}$ emissions reported as arising from replacing OPC with FA and GGBFS GP depends greatly on the allocation procedure that is utilized and that the no allocation case represents a lower bound. Hence, this suggests that failing to consider allocation within LCA is not conservative.

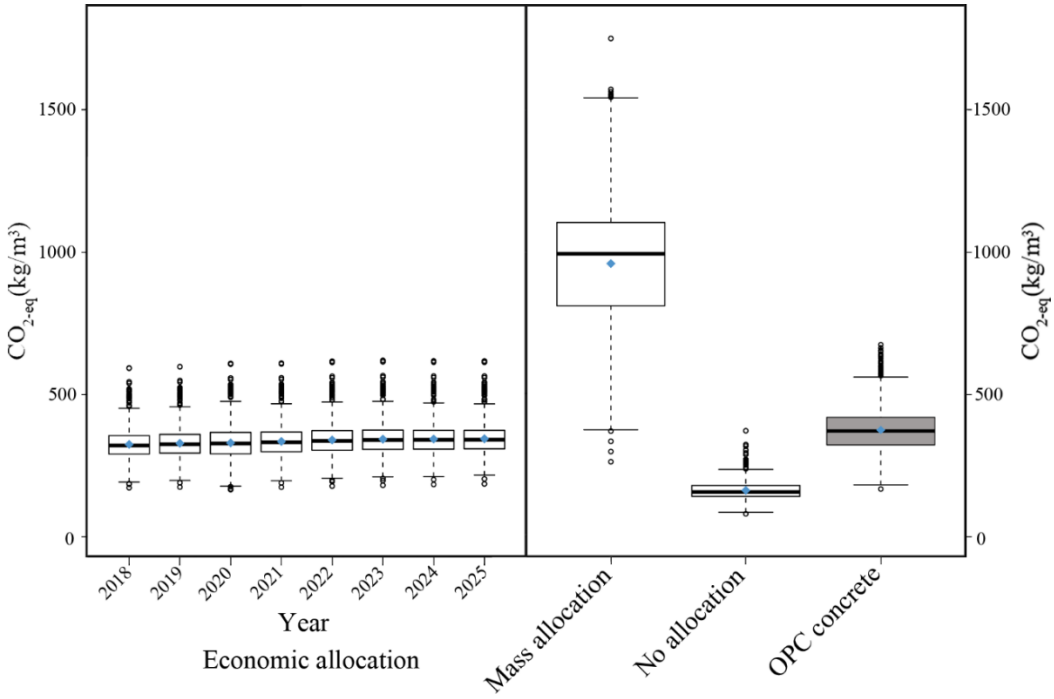

Fig.12 Distribution of $CO_{2\text{-eq}}$ emissions from GP concrete and equivalent OPC concrete considering different allocation scenarios

Further considering the results in Fig. 12, it appears that despite the variation in the price of FA, GGBFS, electricity and steel over time, in Fig. 12, economic allocation is relatively stable over time. This finding is contrary to the common assumption that economic allocation is affected by price variations (Van den Heede and De Belie 2012; Vendries Algarin et al. 2016; Teh et al. 2017) and arises because the price of FA and GGBFS generally varies with their utilization.

Now consider the impact of allocation scenario on the $CO_{2\text{-eq}}$ emissions from each process of the production of different types of GP concretes in Fig. 13 in which the year 2020 is considered for economic allocation. Although only the emissions from FA and GGBFS change due to allocation, breaking down all the emissions in this way is considered important to consider the relative weighting of emissions from each process.

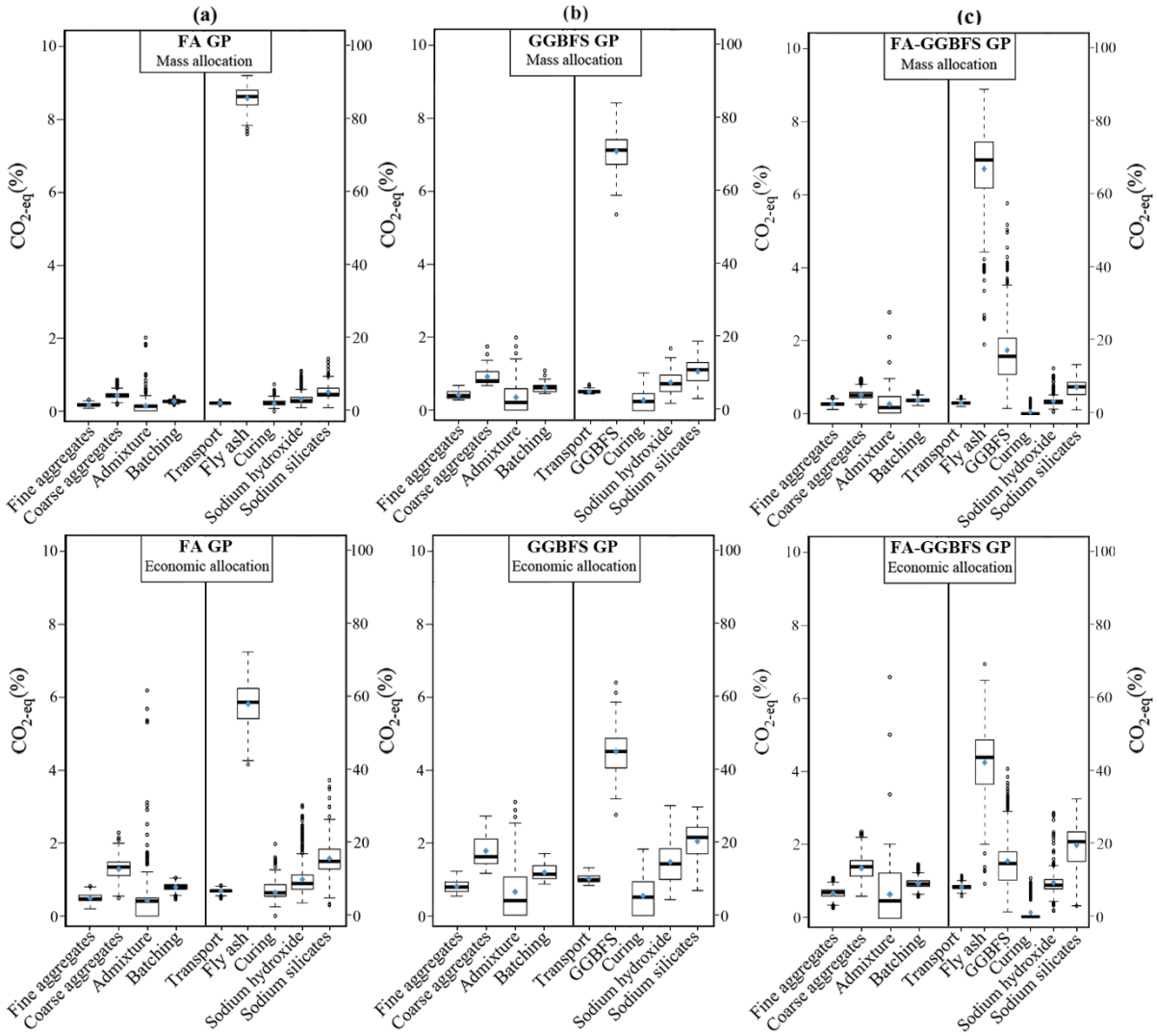

Fig.13 Contribution of GP concrete ingredients to $CO_{2\text{-eq}}$ emissions considering economic and mass allocation scenarios: (a) FA GP concrete; (b) GGBFS GP concrete; (c) FA-GGBFS GP concrete

The comparisons of results between those shown in Figs. 4(a-c) and Fig. 13 for all three types of GP concretes reveals that while $CO_{2\text{-eq}}$ emissions from GGBFS is higher than that from FA in the case of no allocation scenario, the $CO_{2\text{-eq}}$ emissions associated with FA is higher than that from GGBFS for economic and mass allocation scenarios. The reason for this can be attributed to the fact that in the case of economic and mass allocation scenarios, very little FA (0.052 kg) is generated per kWh of electricity compared to the mass of GGBFS (0.24 kg) generated per kg of steel. Therefore, the mass allocated impact of FA (19.2 kg) is much higher than that of GGBFS (4.2 kg) and hence leads to greater emissions. This is why, among all types of GP concretes with various allocation scenarios shown in Fig. 13, the $CO_{2\text{-eq}}$ emissions from FA GP concrete are affected the most when mass allocation scenario was applied. It also appears from Fig. 13 that for almost all types of GP concretes with different allocation scenarios, sodium silicates have the greatest contribution to $CO_{2\text{-eq}}$ emissions after FA and GGBFS. However, when the economic allocation scenario is considered for FA-GGBFS based GP concrete, $CO_{2\text{-eq}}$ emissions from sodium silicates are higher than that from GGBFS. The reason for this is the lower economic allocation of emissions from GGBFS compared to FA, and the energy-intensive production process of sodium silicates.

The allocation coefficients in Table 6 have been based on the average price of FA and GGBFS. There is however considerable uncertainty in the future price predictions and therefore in Fig. 14, change in allocation coefficient and $CO_{2\text{-eq}}$ emissions are shown based on the upper and lower bound predictions of the price of FA and GGBFS suggested by (Fly Ash Market 2018; LP Information (LPI) 2020).

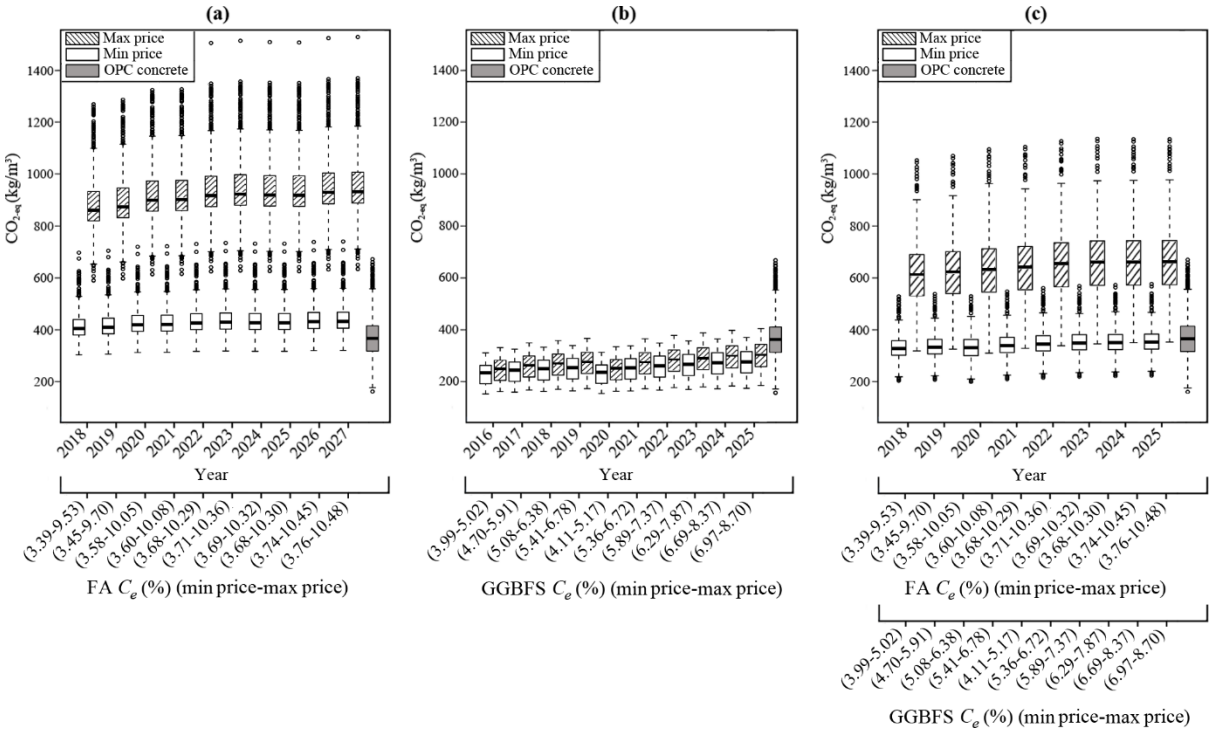

Fig.14 Distribution of $CO_{2\text{-eq}}$ emissions associated with different types of GP concretes with economic allocation scenario and maximum and minimum prices in various consecutive years: (a) FA GP; (b) GGBFS GP; (c) FA-GGBFS GP

The analysis in Fig. 14 shows that $CO_{2\text{-eq}}$ emissions associated with FA GP concrete, GGBFS GP concrete and FA-GGBFS GP concrete increase by approximately 100% for FA GP, 10% for GGBFS GP and 80% for FA-GGBFS GP when varying the price of FA and GGBFS from the expected minimum to the expected maximum. This shows that $CO_{2\text{-eq}}$ emissions from FA GP concrete and GGBFS GP concrete have respectively the highest and lowest sensitivity to the price change. The reason for this can be attributed to lower mass allocated impact as well as lower economic allocation emissions of GGBFS compared with FA (less than 20% as shown in Table 6). The results also show that if considering the best possible scenario for economic allocation (minimum price for FA and GGBFS), the mean $CO_{2\text{-eq}}$ emissions from GGBFS GP concrete and FA-GGBFS GP concrete are respectively 67% and 87% of that of those for OPC concretes. However, for the worst possible scenario (maximum price for fly ash and GGBFS), only GGBFS GP concretes have reduced mean $CO_{2\text{-eq}}$ emissions compared to OPC (72% of that of OPC concrete).

4.4. Combined transport and allocation scenarios

Given that regional scale transport and allocation of emissions from FA and GGBFS production have both been shown to significantly influence $CO_{2\text{-eq}}$ emissions, let us finally consider a scenario in which both factors are combined. Because of the large number of

combinations of transport and allocation scenarios let us consider the boundary cases outlined in Table 7 that yield the absolute minimum and absolute maximum $CO_{2\text{-eq}}$ emissions. For transportation, this corresponds to cases 1 and 16 shown in Table 4. It is interesting to note here that the results of this analysis reveal that the absolute maximum $CO_{2\text{-eq}}$ emissions for all cases correspond to mass allocation scenario with maximum transportation case and this combination may be suitable for use in future studies as a worst-case scenario.

Table 7 Different scenarios for allocation and transportation

Case	Allocation	Price of by-products	Transport distance*
1	No allocation	-	Min
2	No allocation	-	Max
3	Economic allocation	Min	Min
4	Economic allocation	Min	Max
5	Economic allocation	Max	Min
6	Economic allocation	Max	Max
7	Mass allocation	-	Min
8	Mass allocation	-	Max

*Min: minimum transport distance for all materials (case 1 in Table 4)
Max: maximum transport distance for all materials (case 16 in Table 4)

Fig.15 shows the distribution of $CO_{2\text{-eq}}$ emissions for the three different types of GP concretes arising from the absolute minimum and absolute maximum cases out of the cases set out in Table 7 compared against equivalent the minimum and maximum cases for OPC concretes. For each type of GP concrete the absolute minimum and maximum cases were case 1 and 8 respectively. FA the minimum occurs in Sydney and the maximum in Brisbane; for GGBFS GP the minimum occurs in Sydney and the maximum in Perth and for FA-GGBFS GP the minimum occurs in Sydney and the maximum in Perth. It can be seen that all three types of GP concrete have less $CO_{2\text{-eq}}$ emissions than OPC concrete when the absolute minimum case is considered. However, $CO_{2\text{-eq}}$ emissions from OPC concrete are much lower than those from all three types of GP concretes when the absolute maximum case is considered. The mean emissions from FA GP concrete, GGBFS GP concrete and FA-GGBFS GP concrete are respectively 80%, 80% and 65% of OPC concretes for the minimum case, while the mean emissions from those three types of GP concretes are respectively 245%, 153% and 194% of OPC concretes for the maximum case. This indicates the need for the targeted use of GP concretes as a replacement for OPC concretes, and that there is a need for modelling of emissions rather than the uniform application of the assumption that GP concretes will have lower emissions than OPC concretes due to their lack of cement.

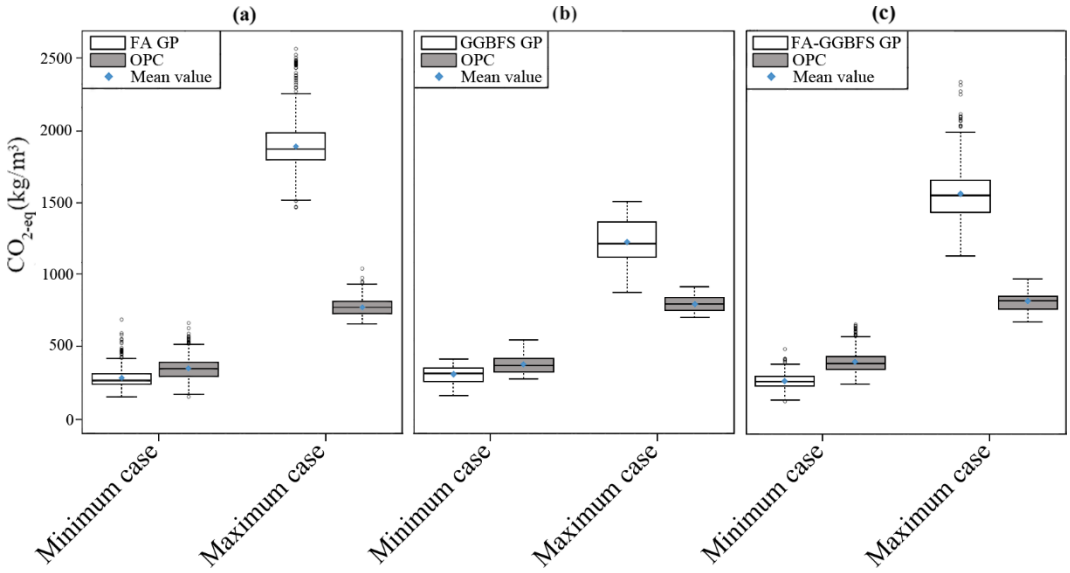

Fig.15 Distribution of $CO_{2\text{-eq}}$ emissions from different types of GP concretes considering the minimum and maximum cases: (a) FA GP; (b) GGBFS GP; (c) FA-GGBFS GP.

5. Conclusions

A detailed life-cycle assessment of 1404 geopolymer concrete mix designs collected from 110 studies has been conducted by taking into account the influence of curing, allocation and transportation on global warming potential of GP concretes. Considering batching plants in five major capital cities of Australia, a sensitivity analysis of material transportation with different transportation modes (road, rail and sea) was conducted to quantify the transport emissions from the GP and OPC concretes. Based on this analysis, the limiting distances for transportation of GP concrete materials were found so that their emissions benefits outweigh the emissions from OPC concretes. Different allocation scenarios combined with different transportation cases were studied to compare $CO_{2\text{-eq}}$ emissions from GP and OPC concretes. A sensitivity analysis was also conducted to study the effects of renewable energy sources, curing energy and alkali activator type on global warming potential of geopolymer concretes. Examination of the results of this analysis has indicated the following major findings:

1. $CO_{2\text{-eq}}$ emissions from GP concrete are less dependent to the compressive strength than those of OPC concrete.
2. A sensitivity analysis of the effects of curing energy, alkali activator type and electricity grid mix on overall emissions showed that the $CO_{2\text{-eq}}$ emissions from GP concretes can decrease more than 30% by changing the curing energy and sodium silicate type. This finding indicates the importance of considering these factors in the development of new mix designs.
3. It is possible to achieve up to a 30% reduction in the overall $CO_{2\text{-eq}}$ emissions by converting the energy grid from the Australian national average grid mix to 100% renewables. This emissions reduction can be the result of 90%, 90%, 15%, 55% and 65% reduction in the $CO_{2\text{-eq}}$ emissions from curing, batching and the production of FA, aggregates and GGBFS respectively.
4. The results of transport sensitivity analysis showed that the $CO_{2\text{-eq}}$ emissions of GP concrete can vary widely depending on the locations of batching plants, type of GP concrete and transport distances and mode. It is also shown that a change in the transportation mode from road to rail can yield up to 25% reduction in emissions. The

environmental assessment of importing slags from abroad or providing it from local sources also reveals that, depending on the location of batching plants and transportation mode, slags should either be provided from local sources or imported from abroad. The limiting distance at which emissions arising from the transportation of raw materials required for GP production negates the benefit of their use has been quantified. Analysis shows that the limiting distance increases with compressive strength, and therefore the materials required to manufacture high strength concrete can be sourced from further away while still maintaining an overall improvement in GWP.

5. An assessment of the impacts of different allocation scenarios indicate that while no allocation and mass allocation scenarios have respectively the smallest and largest emissions (as high as 42% and 260% of those of OPC concrete), GP concrete and OPC concrete can have similar $CO_{2\text{-eq}}$ emissions when economic allocation scenario is considered. The results of analysis for combination of different types of allocation scenarios with different transportation cases also reveal that the production of GP concretes generally (but not always) leads to lower $CO_{2\text{-eq}}$ emissions than OPC concretes when no allocation and minimum transportation distances are considered, while when considering mass allocation with maximum transportation distances GP concretes emit higher $CO_{2\text{-eq}}$ emissions than OPC concretes. This indicates that depending on the type of allocation scenario and transportation case, GP concretes can have either lower or higher $CO_{2\text{-eq}}$ emissions than OPC of the same compressive strength. This is contrary to the underlying assumption that GP concretes are always more sustainable than OPC concretes.

Appendix

Table A1 UNESCO conversion factors (UNESCO 1971)

Specimen Shape	Specimen Size	Conversion Factor
Cylinder	150 × 300 mm	1.00
	100 × 200 mm	0.97
	250 × 500 mm	1.05

Table A2 Relationship between 150 × 300 mm cylinders, 150 mm cubes and 100 mm cubes strength (BS EN 206-1; Wong 2013)

Compressive strength class	Cylinder/150 mm cube strength ratio	Cylinder/100 mm cube strength ratio
C8/10	0.80	0.73
C12/15	0.80	0.75
C16/20	0.80	0.76
C20/25	0.80	0.74
C25/30	0.83	0.78
C30/37	0.81	0.77
C35/45	0.78	0.73
C40/50	0.80	0.75
C45/55	0.82	0.78
C50/60	0.83	0.79

C55/67	0.82	0.77
C60/75	0.80	0.76
C70/85	0.82	0.78
C80/95	0.84	0.80
C90/105	0.86	0.81
C100/115	0.87	0.83

Acknowledgments

Vahid Shobeiri was supported by an Australian Government Research Training Program Scholarship.

References

Abbas, R., Khereby, M. A., Ghorab, H. Y., & Elkhoshkhany, N. (2020). Preparation of geopolymer concrete using Egyptian kaolin clay and the study of its environmental effects and economic cost. Clean Technologies and Environmental Policy, 1-19.

ACI 2011. American Concrete Institute. Building Code Requirements for Structural Concrete (ACI 318-11) and Commentary.

Albitar, M., Ali, M. M., Visintin, P., & Drechsler, M. (2015). Effect of granulated lead smelter slag on strength of fly ash-based geopolymer concrete. Construction and Building Materials, 83, 128-135.

Albitar, M., Ali, M. M., Visintin, P., & Drechsler, M. (2017). Durability evaluation of geopolymer and conventional concretes. Construction and Building Materials, 136, 374-385.

Alyousef, R. A. M., Alabduljabbar, H. A. M., & El-Zeadani, M. (2020). Clean production and properties of geopolymer concrete; A review.

Asadollahfardi, G., Katebi, A., Taherian, P., & Panahandeh, A. (2019). Environmental life cycle assessment of concrete with different mixed designs. International Journal of Construction Management, 1-12.

Assi, L. N., Deaver, E. E., ElBatanouny, M. K., & Ziehl, P. (2016). Investigation of early compressive strength of fly ash-based geopolymer concrete. Construction and Building Materials, 112, 807-815.

Athena, (2005). Cement and Structural Concrete Products: Life Cycle Inventory Update #2. Athena Sustainable Materials Institute, Ottawa.

Bajpai, R., Choudhary, K., Srivastava, A., Sangwan, K. S., & Singh, M. (2020). Environmental impact assessment of fly ash and silica fume based geopolymer concrete. Journal of Cleaner Production, 254, 120147.

Bakharev, T. (2005). Durability of geopolymer materials in sodium and magnesium sulfate solutions. Cement and Concrete Research, 35(6), 1233-1246.

Bare, J.C., 2002. TRACI: The tool for the reduction and assessment of chemical and other environmental impacts. *Journal of industrial ecology*, *6*(3-4), pp.49-78.

Bellum, R. R., Muniraj, K., & Madduru, S. R. C. (2020). Exploration of mechanical and durability characteristics of fly ash-GGBFS based green geopolymer concrete. SN Applied Sciences, 2, 1-10.

Bergman, T. L., Lavine, A., Incropera, F. P., & Dewitt, D. P. (2017). Fundamentals of heat and mass transfer (pp. 533-534). New York: John Wiley & Sons.

Bernal, S. A., Provis, J. L., De Gutiérrez, R. M., & van Deventer, J. S. (2015). Accelerated carbonation testing of alkali-activated slag/metakaolin blended concretes: effect of exposure conditions. Materials and Structures, 48(3), 653-669.

Bernal, S. A., Provis, J. L., Walkley, B., San Nicolas, R., Gehman, J. D., Brice, D. G., ... & van Deventer, J. S. (2013). Gel nanostructure in alkali-activated binders based on slag and fly ash, and effects of accelerated carbonation. Cement and Concrete Research, 53, 127-144.

Boral North America Investor Site Tour presentation, 12 September 2017. https://www.boral.com/news-announcements/management-presentations

Brinsmead T.S., J. Hayward and P. Graham (2014) Australian Electricity Market Analysis report to 2020 and 2030, CSIRO Report No. EP141067.

BS, EN 206-1 (2000). Concrete–part 1: specification, performance, production and conformity. British Standard.

Butler, D. B. (1906). THE SPECIFIC GRAVITY OF PORTLAND CEMENT. In Minutes of the Proceedings of the Institution of Civil Engineers (Vol. 166, No. 1906, pp. 342-345). Thomas Telford-ICE Virtual Library.

Chen, C., Habert, G., Bouzidi, Y., Jullien, A., & Ventura, A. (2010). LCA allocation procedure used as an incitative method for waste recycling: An application to mineral additions in concrete. Resources, Conservation and Recycling, 54(12), 1231-1240.

Chindaprasirt, P., & Chalee, W. (2014). Effect of sodium hydroxide concentration on chloride penetration and steel corrosion of fly ash-based geopolymer concrete under marine site. Construction and Building Materials, 63, 303-310.

Chithambaram, S. J., Kumar, S., Prasad, M. M., & Adak, D. (2018). Effect of parameters on the compressive strength of fly ash based geopolymer concrete. Structural Concrete, 19(4), 1202-1209.

Dal Pozzo, A., Carabba, L., Bignozzi, M. C., & Tugnoli, A. (2019). Life cycle assessment of a geopolymer mixture for fireproofing applications. The International Journal of Life Cycle Assessment, 24(10), 1743-1757.

Damineli, B. L., Kemeid, F. M., Aguiar, P. S., & John, V. M. (2010). Measuring the eco-efficiency of cement use. Cement and Concrete Composites, 32(8), 555-562.

De Larrard, F. (1999). Concrete mixture proportioning: a scientific approach. CRC Press.

Di Maria, A., & Van Acker, K. (2018). Turning industrial residues into resources: an environmental impact assessment of goethite valorization. Engineering, 4(3), 421-429.

Dontriros, S., Nooaek, P., & Supakata, N. (2020). Geopolymer Bricks from Concrete Residue and Palm Oil Fuel Ash: Evaluating Physical-mechanical Properties, Life Cycle Assessment and Economic Feasibility. EnvironmentAsia, 13(1).

Duxson, P., Provis, J. L., Lukey, G. C., & Van Deventer, J. S. (2007). The role of inorganic polymer technology in the development of 'green concrete'. Cement and Concrete Research, 37(12), 1590-1597.

Elwell, D. J., & Fu, G. (1995). Compression testing of concrete: cylinders vs. cubes (No. FHWA/NY/SR-95/119).

Fawer, M., Concannon, M., & Rieber, W. (1999). Life cycle inventories for the production of sodium silicates. The International Journal of Life Cycle Assessment, 4(4), 207.

Fly Ash Market (2018). https://www.marketsandmarkets.com/Market-Reports/fly-ash-market-76345803.html

Freight rates in Australia (2017). Bureau of Infrastructure, Transport and Regional Economics. https://www.bitre.gov.au/publications/2017/is_090

Gautam, N., Krishna, V., & Srivastava, A. (2014). Sustainability in the concrete construction. International Journal of Environmental Research and Development, 4(1), 81-90.

Grand View Research (2017). https://www.grandviewresearch.com/press-release/global-steel-market

Grant TF (2015) Life Cycle Inventory of Cement & Concrete produced in Australia. Life Cycle Strategies Pty Ltd, Melbourne, Australia.

Gursel, A.P. (2014). Life-cycle Assessment of Concrete: Decision-Support Tool and Case Study Application (UC Berkeley).

Habert, G., & Roussel, N. (2009). Study of two concrete mix-design strategies to reach carbon mitigation objectives. Cement and Concrete Composites, 31(6), 397-402.

Habert, G., D'Espinose de Lacaillerie, J. B., Lanta, E., & Roussel, N. (2010, June). Environmental evaluation for cement substitution with geopolymers. In Proceedings of the 2nd international conference on sustainable construction materials and technologies (pp. 1607-1615).

Habert, G., De Lacaillerie, J. D. E., & Roussel, N. (2011). An environmental evaluation of geopolymer based concrete production: reviewing current research trends. Journal of cleaner production, 19(11), 1229-1238.

Hardjito, D., Wallah, S. E., Sumajouw, D. M., & Rangan, B. V. (2004). On the development of fly ash-based geopolymer concrete. Materials Journal, 101(6), 467-472.

Hassan, A., Arif, M., & Shariq, M. (2019a). Use of geopolymer concrete for a cleaner and sustainable environment–A review of mechanical properties and microstructure. Journal of cleaner production, 223, 704-728.

Hassan, A., Arif, M., & Shariq, M. (2019b). Mechanical behaviour and microstructural investigation of geopolymer concrete after exposure to elevated temperatures. Arabian Journal for Science and Engineering, 1-19.

Hassan, A., Arif, M., & Shariq, M. (2019c). Effect of curing condition on the mechanical properties of fly ash-based geopolymer concrete. SN Applied Sciences, 1(12), 1694.

Hassan, A., Arif, M., & Shariq, M. (2020a). A review of properties and behaviour of reinforced geopolymer concrete structural elements-A clean technology option for sustainable development. Journal of Cleaner Production, 245, 118762.

Hassan, A., Arif, M., & Shariq, M. (2020b). Structural performance of ambient-cured reinforced geopolymer concrete beams with steel fibres. Structural Concrete.

Heath, A., Paine, K., & McManus, M. (2014). Minimising the global warming potential of clay based geopolymers. Journal of cleaner production, 78, 75-83.

Helsel, M. A., Ferraris, C. F., & Bentz, D. (2016). Comparative study of methods to measure the density of Cementitious powders. Journal of testing and evaluation, 44(6), 2147-2154.

Huntzinger, D., Eatmon, T., 2009. A life-cycle assessment of Portland cement manufacturing: comparing the traditional process with alternative technologies. J. Clean. Prod. 17, 668e675

Khan, M. S. H., Castel, A., & Noushini, A. (2017). Carbonation of a low-calcium fly ash geopolymer concrete. Magazine of Concrete Research, 69(1), 24-34.

Law, D. W., Adam, A. A., Molyneaux, T. K., Patnaikuni, I., & Wardhono, A. (2015). Long term durability properties of class F fly ash geopolymer concrete. Materials and Structures, 48(3), 721-731.

LP Information (LPI) 2020. Global Ground Granulated Blast-Furnace Slag (GGBFS) Market Growth 2020-2025

McLellan, B. C., Williams, R. P., Lay, J., Van Riessen, A., & Corder, G. D. (2011). Costs and carbon emissions for geopolymer pastes in comparison to ordinary portland cement. Journal of cleaner production, 19(9-10), 1080-1090.

Mohamed, S., Nuruddin, F., Halim, N. S. A., & Kamal, S. A. (2011). Compressive Strength and Workability of Blended and Unblended Self Compacting Geopolymer Concrete.

Naik, T. R. (2008). Sustainability of concrete construction. Practice Periodical on Structural Design and Construction, 13(2), 98-103.

Nath, P., & Sarker, P. K. (2014). Effect of GGBFS on setting, workability and early strength properties of fly ash geopolymer concrete cured in ambient condition. Construction and Building Materials, 66, 163-171.

Neville, A.M. (1981 3rd edition). Properties of Concrete, Pitman Pub. Ltd. London, 529-604.

Nuruddin, M. F., Demie, S., & Shafiq, N. (2011). Effect of mix composition on workability and compressive strength of self-compacting geopolymer concrete. Canadian Journal of Civil Engineering, 38(11), 1196-1203.

O'Brien, K. R., Ménaché, J., & O'Moore, L. M. (2009). Impact of fly ash content and fly ash transportation distance on embodied greenhouse gas emissions and water consumption in concrete. The International Journal of Life Cycle Assessment, 14(7), 621-629.

Pan, Z., Sanjayan, J. G., & Rangan, B. V. (2011). Fracture properties of geopolymer paste and concrete. Magazine of concrete research, 63(10), 763-771.

Passuello, A., Rodríguez, E. D., Hirt, E., Longhi, M., Bernal, S. A., Provis, J. L., & Kirchheim, A. P. (2017). Evaluation of the potential improvement in the environmental footprint of geopolymers using waste-derived activators. Journal of Cleaner Production, 166, 680-689.

Pasupathy, K., Berndt, M., Castel, A., Sanjayan, J., & Pathmanathan, R. (2016). Carbonation of a blended slag-fly ash geopolymer concrete in field conditions after 8 years. Construction and Building Materials, 125, 661-669.

Pasupathy, K., Berndt, M., Sanjayan, J., Rajeev, P., & Cheema, D. S. (2017). Durability of low-calcium fly ash based geopolymer concrete culvert in a saline environment. Cement and Concrete Research, 100, 297-310.

Petrillo, A., Cioffi, R., De Felice, F., Colangelo, F., & Borrelli, C. (2016). An environmental evaluation: A comparison between geopolymer and OPC concrete paving blocks manufacturing process in italy. Environmental Progress & Sustainable Energy, 35(6), 1699-1708.

Pink, B. (2013). "Waste Account, Australia, Experimental Estimates."

Prakasan, S., Palaniappan, S., & Gettu, R. (2020). Study of Energy Use and CO 2 Emissions in the Manufacturing of Clinker and Cement. Journal of The Institution of Engineers (India): Series A, 101(1), 221-232.

Puertas, F., Martínez-Ramírez, S., Alonso, S., & Vazquez, T. (2000). Alkali-activated fly ash/slag cements: strength behaviour and hydration products. Cement and concrete research, 30(10), 1625-1632.

Ramujee, K., & PothaRaju, M. (2017). Mechanical properties of geopolymer concrete composites. Materials Today: Proceedings, 4(2), 2937-2945.

Ryu, G. S., Ahn, G. H., Koh, K. T., & Lee, J. H. (2013). Compressive Strength Properties of Fly Ash-based Geopolymer Concrete. In Advanced Materials Research (Vol. 741, pp. 49-54). Trans Tech Publications Ltd.

Salas, D. A., Ramirez, A. D., Ulloa, N., Baykara, H., & Boero, A. J. (2018). Life cycle assessment of geopolymer concrete. Construction and Building Materials, 190, 170-177.

Seto, K. E., Churchill, C. J., & Panesar, D. K. (2017). Influence of fly ash allocation approaches on the life cycle assessment of cement-based materials. Journal of Cleaner Production, 157, 65-75.

Shahmansouri, A. A., Bengar, H. A., & Ghanbari, S. (2020). Compressive strength prediction of eco-efficient GGBS-based geopolymer concrete using GEP method. Journal of Building Engineering, 101326.

Shi, C., & Day, R. L. (1999). Early strength development and hydration of alkali-activated blast furnace slag/fly ash blends. Advances in Cement Research, 11(4), 189-196.

Smith, M. A., & Osborne, G. J. (1977). Slag/fly ash cements. World Cement Technology, 8(6).

Snell, C., Tempest, B., & Gentry, T. (2017). Comparison of the thermal characteristics of portland cement and geopolymer cement concrete mixes. Journal of Architectural Engineering, 23(2), 04017002.

Song, K. I., Song, J. K., Lee, B. Y., & Yang, K. H. (2014). Carbonation characteristics of alkali-activated blast-furnace slag mortar. Advances in Materials Science and Engineering, 2014.

Struble, L. (2006). Hydraulic Cements—Physical Properties. In Significance of Tests and Properties of Concrete and Concrete-Making Materials. ASTM International.

Stuart, M., 2017. The Future of Australian Energy Generation. Institution of Engineers Australia, Australian Capital Territory, Australia, 2017. Institution of Engineers Australia.

Teh, S. H., Wiedmann, T., Castel, A., & de Burgh, J. (2017). Hybrid life cycle assessment of greenhouse gas emissions from cement, concrete and geopolymer concrete in Australia. Journal of Cleaner Production, 152, 312-320.

Turner, L. K., & Collins, F. G. (2013). Carbon dioxide equivalent (CO2-e) emissions: A comparison between geopolymer and OPC cement concrete. Construction and Building Materials, 43, 125-130.

UNESCO. Reinforced Concrete: An International Manual. London: Butterworths, 1971, p. 20.

Van den Heede, P., & De Belie, N. (2012). Environmental impact and life cycle assessment (LCA) of traditional and ‘green’concretes: literature review and theoretical calculations. Cement and Concrete Composites, 34(4), 431-442.

van Deventer, J. S., Provis, J. L., Duxson, P., & Brice, D. G. (2010). Chemical research and climate change as drivers in the commercial adoption of alkali activated materials. Waste and Biomass Valorization, 1(1), 145-155.

Vendries Algarin, J., Hawkins, T. R., Marriott, J., & Khanna, V. (2017). Effects of Using Heterogeneous Prices on the Allocation of Impacts from Electricity Use: A Mixed-Unit Input-Output Approach. Journal of Industrial Ecology, 21(5), 1333-1343.

Vinothkumar, A., Kalaivani, M., & Easwaran, P. (2019). Development of Fly ash-GGBS based Self Compacting Geopolymer Concrete: a Review. International Research Journal of Multidisciplinary Technovation, 1(6), 373-377.

Vora, P. R., & Dave, U. V. (2013). Parametric studies on compressive strength of geopolymer concrete. Procedia Engineering, 51, 210-219.

Weil, M., Dombrowski, K., & Buchwald, A. (2009). Life-cycle analysis of geopolymers. In Geopolymers (pp. 194-210). Woodhead Publishing.

Wernet, G., Bauer, C., Steubing, B., Reinhard, J., Moreno-Ruiz, E., & Weidema, B. (2016). The Ecoinvent database version 3 (part I): overview and methodology. The International Journal of Life Cycle Assessment, 21(9), 1218-1230.

Wong, H. D. (2013). Cylinder Strength versus Cube Strength. In Standing Committee on Concrete Technology Annual Concrete Seminar, CEDD, Hong Kong.

Xie, T., Visintin, P., Zhao, X., & Gravina, R. (2020). Mix design and mechanical properties of geopolymer and alkali activated concrete: Review of the state-of-the-art and the development of a new unified approach. Construction and Building Materials, 256, 119380.

Yang, K. H., Song, J. K., & Song, K. I. (2013). Assessment of CO2 reduction of alkali-activated concrete. Journal of Cleaner Production, 39, 265-272.

Zain, H., Abdullah, M. M. A. B., Hussin, K., Ariffin, N., & Bayuaji, R. (2017). Review on various types of geopolymer materials with the environmental impact assessment. In MATEC Web of Conferences (Vol. 97, p. 01021). EDP Sciences.

Zhuguo, L. I., & Sha, L. I. (2018). Carbonation resistance of fly ash and blast furnace slag based geopolymer concrete. Construction and Building Materials, 163, 668-680.

Supplementary Material A

Supplementary Material A provides a detailed description of the model and inventory used to derive the specific solutions for OPC based concretes described in the main paper. The reader is referred to the work of Gursel (2016) for a more detailed description of the modelling of OPC based concretes and a detailed discussion of potential inventories.

In the remainder of Supplementary Material A, the approach taken to modelling each component of concrete manufacture is provided based on the Green Concrete Tool (Gursel 2016), which was originally developed for OPC concretes and adapted in this work for geopolymers), the inventories for implementing a specific solution are then provided.

Cement quarrying:

$$Mass_{Meal} = Mass_{PortlandCement} \times TotalRawMaterial \quad (1)$$

$$Electrcity_{Quarrying} = Electricty_{Factor\_Quarrying} \times Mass_{Meal} \quad (2)$$

$$Fuel_{Quarrying_i} = Fuel_{Factor\_Quarrying_i} \times Mass_{Meal} \quad (3)$$

$$Quarrying_{CO_{2-eq}{}_{electricty}} = Electrcity_{Quarrying} \times ElectricityGidMix_{Factor} \quad (4)$$

$$Quarrying_{CO_{2-eq}{}_{Precombustion}} = \sum_{i=1}^{n} [Fuel_{Quarrying_i} \times Precombust_i] \quad (5)$$

$$Quarrying_{CO_{2-eq}{}_{Combustion}} = \sum_{i=1}^{n} [Fuel_{Quarrying_i} \times Combust_i] \quad (6)$$

where, $TotalRawMaterial$ can be determined from Table S1 according to the kiln type and $Mass_{PortlandCement}$ is the total mass of Portland cement. $Electricty_{Factor\_Quarrying}$ and $Fuel_{Factor\_Quarrying_i}$ can be obtained from Table S2. $Precombust_i$ and $Combust_i$ are obtained from Tables S3 and S4. $ElectricityGidMix_{Factor}$ can be taken as 0.683 kg $CO_{2\text{-}eq}$/kWh (the Australian average).

Table S1. Cement raw material quantities by cement kiln type (Marceau et al. 2006)

		Kiln type				
	Unit	**Wet kiln**	**Long dry kiln**	**Preheater kiln**	**Preheater/Precalciner kiln**	**US Average kiln**
Total raw meal	kg/tonne of cement	1752	1612	1492	1606	1612

Table S2. Input data for CO_2 emissions factors from cement quarrying (NREL 2012)

Input	Unit	Per tonne of raw material
Bituminous (hard) coal	kg	0.036
Natural gas	m^3	0.140
Distillate (diesel or light) fuel oil	l	0.584
Gasoline	l	0.051
Electricity	kWh	4.230

Table S3. Precombustion CO_2 emissions factors (Bhatty and Bohan 2004; Deru and Torcellini 2007; EIA 2010; EIA 2011; NREL 2012)

	Unit	Bituminous coal	Lignite coal	Distillate (diesel) fuel oil	Gasoline	Kerosene	LPG	Residual (heavy) fuel oil	Natural gas	Nuclear
$CO_{2\text{-eq}}$	kg	1.85E-01	1.37E-01	4.92E-01	4.19E-01	4.59E-01	3.07E-01	5.35E-01	4.46E-01	3.86E+03

Table S4. Combustion CO_2 emissions factors (Bhatty and Bohan 2004; Deru and Torcellini 2007; EIA 2010; EIA 2011; NREL 2012)

	Unit	Bituminous coal	Lignite coal	Petroleum coke	Natural gas	Residual (heavy) fuel oil	Distillate (diesel) fuel oil	Gasoline
$CO_{2\text{-eq}}$	kg/kg	2.66E+00	2.47E+00	3.68E+00	1.94E+00	3.00E+00	2.66E+00	2.42E+00

Cement raw material preparation:

$$Electrcity_{CementRawPrep} = Electricty_{Factor\_CementRawPrep} \times Mass_{Clinker} \quad (7)$$

$$CementRawPrep_{CO_{2-eq}{}_{electricty}} = Electrcity_{CementRawPrep} \times ElectricityGidMix_{Factor} \quad (8)$$

where, $Mass_{Clinker}$ is the total mass of clinker and $Electricty_{Factor\_CementRawPrep}$ is obtained from Table S5 according to the technology utilised.

Table S5. Input data for CO_2 emissions factors for cement raw material preparation (Cembureau 1997; Bhatty and Bohan 2004; APP 2008; EPA 2012)

Technology Options	Electricity (kWh/tonne clinker)
Raw Materials Prehomogenization Technology	
Dry process raw storing, nonpreblending	0.250
Dry process raw storing, preblending	0.500
Wet process raw storing	0.375
Raw Materials Grinding Technology	
Dry raw grinding, ball mill	23.000
Dry raw grinding, tube mill	18.500
Dry raw grinding, vertical roller mill	15.500
Wet raw grinding, tube mill	13.000
Wet raw grinding, wash mill	6.5000
Raw Meal Blending/Homogenization Technology	
Raw meal homogenization, blending, and storage	1.080
Slurry blending homogenization and storage	0.400

Cement pyroprocessing:

$$Electrcity_{KilnFuelPreparation} = \sum_{i=1}^{n} [Fuel_{Percent_i} \times Electricity_{Factor_{KilnFuelPreparation}}] \times Mass_{PortlandCement} \quad (9)$$

$$Electrcity_{KilnPoweringEquipment} = Electricty_{Factor\_KilnPoweringEquipment} \times Mass_{Clinker} \quad (10)$$

$$Electrcity_{Pyroprocessing} = Electrcity_{KilnFuelPreparation} + Electrcity_{KilnPoweringEquipment} \quad (11)$$

$$Energy_{KilnThermal} = Eenergy_{Factor\_KilnThermal} \times Mass_{Clinker} \quad (12)$$

$$Fuel_{Pyroprocessing_i} = \frac{Fuel_{Percent_i} \times Energy_{KilnThermal}}{Fuel_{HHV_i}} \quad (13)$$

$$PyroprocessingCalcination_{CO_{2-eq}} = EF_{Calcination} \times Mass_{Clinker} \quad (14)$$

$$Pyroprocessing_{CO_{2-eq}{}_{electricty}} = Electrcity_{Pyroprocessing} \times ElectricityGidMix_{Factor} \quad (15)$$

$$Pyroprocessing_{CO_{2-eq}{}_{Precombustion}} = \sum_{i=1}^{n} [Fuel_{Pyroprocessing_i} \times Precombust_i] \quad (16)$$

$$Pyroprocessing_{CO_{2-eq}{}_{Combustion}} = \sum_{i=1}^{n} [Fuel_{Pyroprocessing_i} \times Combust_i] \quad (17)$$

In which $Electricity_{Factor_{KilnFuelPreparation}}$, $Fuel_{Percent_i}$, $Electricty_{Factor\_KilnPoweringEquipment}$, $Eenergy_{Factor\_KilnThermal}$ and $Fuel_{HHV_i}$ are respectively taken from Tables S6-S10 according the kiln technology, and $EF_{Calcination}$ is taken to be 522 kg/tonne of clinker according to Gursel (2016).

Table S6. Electricity use factors for kiln fuel preparation (cement pyroprocessing) (Gursel 2016)

Kiln Fuels	**kWh/tonne Cement**
Bituminous coal	40
Lignite coal	35
Distillate (diesel or light) fuel oil	0
Petroleum coke (petcoke)	45
Residual (heavy) fuel oil	3
Natural gas	0
Waste oil	3
Waste solvent	3
Waste tire (whole)	3
Waste tire (shredded)	45
Waste (other) (non-hazardous)	25
Waste paper, cardboard, wood	25
Waste plastics	43
Waste sewage sludge (dry)	8
Waste (other) (hazardous)	45

Table S7**.** Cement pyroprocessing fuel use options (PCA 2008)

Fuel Options	**US Average Fuel**	**AUS Average Fuel**
Bituminous coal	64.1%	57%
Lignite coal	0.0%	0.0%
Distillate (diesel or light) fuel oil	0.8%	1.00%
Petroleum coke (pet coke)	21.2%	1.33%
Residual (heavy) fuel oil	0.2%	0.0%
Natural gas	3.7%	34%
Waste oil	0.3%	2.67%
Waste solvent	4.0%	0.0%
Waste tire (whole)	1.8%	1.33%
Waste tire (shredded)	1.8%	0.0%
Waste (other) (non-hazardous)	2.3%	2.67%
Waste paper, cardboard	0.0%	0.0%
Waste plastics	0.0%	0.0%
Waste sewage sludge (dry)	0.0%	0.0%
Waste (other) (hazardous)	0.0%	0.0%

Table S8. Electricity use factors for powering kiln drive, kiln fan, etc. (pyroprocessing) (Marceau et al. 2006; Bhatty and Bohan 2004; Bureau 2009; CEMBUREAU 1999).

Cement Pyroprocessing	**Electricity Use (kWh/tonne Clinker)**		
Technology Options	**Avg**	**Max**	**Min**
Wet kiln	21	25	17
Long dry kiln	25	30	20
Preheater kiln	25	25	25
Preheater/precalciner kiln	25	25	25
Average kiln, United States	25	25	25

Table S9. Thermal energy consumption for pyroprocessing (Marceau et al. 2006; Bhatty and Bohan 2004; Bureau 2009; CEMBUREAU 1999)

Cement Pyroprocessing	**Thermal Energy Consumption Use (MJ/kg Clinker)**		
Technology Options	**Avg**	**Max**	**Min**
Wet kiln	6.2	6.9	5.4
Long dry kiln	5.0	5.4	4.6
Preheater kiln	3.5	3.8	3.1
Preheater/precalciner kiln	3.3	3.6	3.0
Average kiln, United States	3.5	3.8	3.1

Table S10. Average higher heating value (HHV) (heat content) of fuel (Bhatty and Bohan 2004; Deru and Torcellini 2007; EIA 2010; EIA 2011; NREL 2012; Boesch and Hellweg 2010; Bureau 2009; Boesch et al. 2009; Alsop 2007; CARB 2008)

Fuel Options	**HHV (MJ/Fuel unit)**
Bituminous coal	27.9
Lignite coal	15.1
Distillate (diesel or light) fuel oil	38.3
Petroleum coke (pet coke)	35.7
Residual (heavy) fuel oil	41.72
Natural gas	38.23
Waste oil	32.03
Waste solvent	29.4
Waste tire (whole)	31.4
Waste tire (shredded)	37.26
Waste (other) (non-hazardous)	18.76
Waste paper, cardboard	9.98

Waste plastics	29.93
Waste sewage sludge (dry)	11.03
Waste (other) (hazardous)	31.31

Clinker cooling:

$$Electricity_{Cooling} = (Electricity_{Factor_{Cooler}} + Electricity_{Factor_{PM\ Control}}) \times Mass_{PortlandCement} \quad (18)$$

$$Cooling_{CO_{2-eq_{electricty}}} = Electricity_{Cooling} \times ElectricityGidMix_{Factor} \quad (19)$$

where, $Electricity_{Factor_{PM\ Control}}$ and $Electricity_{Factor_{Cooler}}$ are obtained from Tables S11 and S12 according to the technology utilised.

Table S11. Electricity use for PM control technology options (clinker cooling) (EPA 1994; CEMBUREAU 1999; Marceau et al. 2006)

Cement Clinker Cooling	**Electricity use (kWh/tonne Cement)**		
Technology Options	**Avg**	**Max**	**Min**
Fabric Filter (FF)	1.902	2.092	1.712
Electrostatic Precipitators (ESP)	1.664	1.902	1.427

Table S12. Electricity use for common kiln cooling technology options (EPA 1994; CEMBUREAU 1999; Marceau et al. 2006)

Clinker Coolers	**Electricity use (kWh/tonne Cement)**		
Technology Options	**Avg**	**Max**	**Min**
Rotary (Tube) Cooler	3.563 + (FF or ESP)	3.800 + (FF or ESP)	3.325 + (FF or ESP)
Planetary (Satellite) Cooler	0.950 + (FF or ESP)	1.425 + (FF or ESP)	0.475 + (FF or ESP)
Reciprocating Grate Cooler (Conventional)	4.750 + (FF or ESP)	4.750 + (FF or ESP)	4.750 + (FF or ESP)
Reciprocating Grate Cooler (Modern)	5.700 + (FF or ESP)	7.600 + (FF or ESP)	3.800 + (FF or ESP)
Vertical Gravity Cooler with Grate Cooler (G-Cooler)	8.075 + (FF or ESP)	8.075 + (FF or ESP)	8.075 + (FF or ESP)
Grate Cooler (Recirculating Excess Air)	9.025 + (FF or ESP)	9.025 + (FF or ESP)	9.025 + (FF or ESP)

Cement Finish Milling, Grinding, and Blending:

$$Electricity_{FinishGrid} = Electricity_{Factor_{FinishGrid}} \times Grinding_{Factor} \quad (20)$$

$$FinishGrid_{CO_{2-eq}{}_{electricty}} = Electricity_{FinishGrid} \times ElectricityGidMix_{Factor} \quad (21)$$

where $Grinding_{Factor}$ and $Electricity_{Factor_{FinishGrid}}$ are obtained from Tables S13 and S14.

Table S13. Blaine fineness and grindability factors for cement finish milling and grinding (Gursel 2016)

	Grindability factor with respect to Blaine fineness		
Cement Types	**Ave**	**Max**	**Min**
Portland cement Normal Type I	1.09	1.42	0.89

Table S14. Electricity factors for milling and grinding technology options (CEMBUREAU 1999; Worrell et al. 2000; Alsop 2007; Worrell et al. 2008; LBNL/ERI 2008)

Cement Finish Milling and Grinding	**Electricity use (kWh/tonne Cement)**		
Technology Options	Ave	Max	Min
Tube Mill	34.675	34.675	34.675
Vertical Roller Mill	27.100	29.200	25.000
Ball Mill	36.000	42.000	30.000
Roller Press	27.500	33.000	22.000
Horizontal Roller Mill (Horomill)	25.500	28.000	23.000

Cement plant conveying:

$$Electricity_{Conveying} = \sum_i^n Electricity_{Factor_{Conveying\_type}}[Distance_{CementMaterial_i} \times Mass_{CementMaterial_i}] \quad (22)$$

$$Conveying_{CO_{2-eq}{}_{electricty}} = Electricity_{Conveying} \times ElectricityGidMix_{Factor} \quad (23)$$

where $Distance_{CementMaterial_i}$ and $Mass_{CementMaterial_i}$ are respectively the distance and mass for conveying cement material *i* and $Electricity_{Factor_{conveying\_type}}$ is obtained from Table S15.

Table S15**.** Electricity factors for cement conveyer technology (Gursel 2016)

Conveyor technology	**Screw pump**	**Airlift**	**Dense phase pump**	**Bucket elevator**

Conveying electricity use factor (kWh/kg.m)	1.20E-06	1.10E-05	5.90E-06	4.10E-06

Non-process related electricity and fuel use for cement plants:

$$Electricity_{CementFacility} = Electricity_{Factor_{CementFacility}} \times Mass_{Cement} \quad (24)$$

$$CementFacility_{CO_{2-eq}{}_{electricty}} = Electricity_{CementFacility} \times ElectricityGidMix_{Factor} \quad (25)$$

in which $Electricity_{Factor_{CementFacility}}$ is obtained from Table S16 row 7.

Table S16. Non-process electricity factors for cement plant (EIA 2010)

NAICS Code: 327310 Cements	Electricity use (kWh per kg of cement)
Facility HVAC	0.007793
Facility Lighting	0.006336
Other Facility Support	0.003698
Onsite Transportation	0.000815
Other Non-process Use	0.000733
Total	**0.019375**

Gypsum production:

$$Electricity_{Gypsum} = Electricity_{Factor_{Gypsum}} \times Mass_{Gypsum} \quad (26)$$

$$Fuel_{Gypsum} = Fuel_{Factor_{Gypsum}} \times Mass_{Gypsum} \quad (27)$$

$$Gypsum_{CO_{2-eq}{}_{electricty}} = Electricity_{Gypsum} \times ElectricityGidMix_{Factor} \quad (28)$$

$$Gypsum_{CO_{2-eq}{}_{Precombustion}} = Fuel_{Gypsum} \times Precombust \quad (29)$$

$$Gypsum_{CO_{2-eq}{}_{Combustion}} = Fuel_{Gypsum} \times Combust \quad (30)$$

where $Electricity_{Factor_{Gypsum}}$ and $Fuel_{Factor_{Gypsum}}$ are obtained from Table S17.

Table S17. Input data for CO_2 emissions from gypsum production (Kellenberger et al. 2007; NREL 2012)

Input	Unit	per kg of gypsum
Diesel (distillate) fuel oil	l	4.67E-04
Electricity	kWh	9.16E-04

Aggregates products:

$$Electrcity_{Aggregates} = Electricty_{Factor\_aggregates} \times Mass_{Aggregates} \quad (31)$$

$$Fuel_{Aggregates_i} = Fuel_{Factor\_aggregates_i} \times Mass_{Aggregates} \quad (32)$$

$$Aggregates_{CO_{2-eq}{}_{electricty}} = Electrcity_{Aggregates} \times ElectricityGidMix_{Factor} \quad (33)$$

$$Aggregates_{CO_{2-eq}{}_{Precumbustion}} = \sum_{i=1}^{n} [Fuel_{Aggregates_i} \times Precombust_i] \quad (34)$$

$$Aggregates_{CO_{2-eq}{}_{Cumbustion}} = \sum_{i=1}^{n} [Fuel_{Aggregates_i} \times Combust_i] \quad (35)$$

where, $Mass_{Aggregates}$ is mas either the mass of coarse or fine aggregates and $Electricty_{Factor\_aggregates}$ and $Fuel_{Factor\_aggregates_i}$ are obtained from Table S18.

Table S18. Input data for CO_2 emissions from aggregates (Marceau et al. 2007; Choate 2003)

Input	Unit	Fine aggregates	Coarse aggregates
Electricity	kWh/kg	2.65E-03	3.42E-03
Natural gas	m^3/kg	4.15E-11	4.53E-10
Residual (Heavy) fuel oil	l/kg	5.26E-05	6.05E-05
Distillate (Diesel or Light) fuel oil	l/kg	2.35E-04	3.89E-04
Gasoline	l/kg	2.27E-05	3.92E-05

Admixture production:

$$Admixture_{CO_{2-eq}} = Admixture_{Factor_{CO_{2-eq}}} \times Mass_{Admixture} \quad (36)$$

where, $Mass_{Admixture}$ is the mass of admixture and $Admixture_{Factor_{CO_{2-eq}}}$ is obtained from Table S19.

Table S19. Admixture production CO_2 emissions factors (EFCA Eco-Profiles 2006)

	Water-reducing (Plasticizer)	Superplasticiser	Set-retarding (Retarder)	Accelerating	Air entraining	Waterproofing

				(Accelerator)		(Water resisting)
$CO_{2\text{-}eq}$ (kg/kg)	2.29E-01	7.67E-01	1.42E+00	1.26E+00	1.03E-01	3.74E-01

Alkali activators : CO_2 emissions from alkali activators are taken from Ecoinvent 3.2 and Fawer et al. (1999) and are detailed according to production method in the main body of the paper.

Supplementary materials production:

$$Electrcity_{Supplementary} = Electricty_{Factor\_Supplementary} \times Mass_{Supplementary} \quad (37)$$

$$Fuel_{Supplementary_i} = Fuel_{Factor\_Supplementary_i} \times Mass_{Supplementary} \quad (38)$$

$$Supplementary_{CO_{2-eq}{}_{electricty}} = Electrcity_{Supplementary} \times ElectricityGidMix_{Factor} \quad (39)$$

$$Supplementary_{CO_{2-eq}{}_{Precumbustion}} = \sum_{i=1}^{n} [Fuel_{Supplementary_i} \times Precombust_i] \quad (40)$$

$$Supplementary_{CO_{2-eq}{}_{Cumbustion}} = \sum_{i=1}^{n} [Fuel_{Supplementary_i} \times Combust_i] \quad (41)$$

Where, fuel and energy usage for supplementary materials can be obtained from Table S20.

Table S20**.** Input data for CO_2 emissions from supplementary materials productions (Dunlap 2003, Chen et al. 2010)

Supplementary material		**Fly ash**	**Slag**
Input	**Unit**	**Per tonne of fly ash**	**per tonne of slag**
Natural gas	m^3	7.59E+00	8.96E+00
Distillate (Diesel or Light) fuel oil	l	1.03E+00	1.26E+00
Electricity	kWh	6.82E+00	9.47E+01

Concrete Mixing and Batching Processes:

$$Electrcity_{MixingBatching} = Electricty_{Factor\_MixingBatching} \times V_{concrete} \quad (42)$$

$$Fuel_{MixingBatching_i} = Fuel_{Factor\_MixingBatching_i} \times V_{concrete} \quad (43)$$

$$MixingBatching_{CO_{2-eq}{}_{electricty}} = Electrcity_{MixingBatching} \times ElectricityGidMix_{Factor} \quad (44)$$

$$MixingBatching_{CO_{2-eq}{}_{Precumbustion}} = \sum_{i=1}^{n} [Fuel_{MixingBatching_i} \times Precombust_i] \quad (45)$$

$$MixingBatching_{CO_{2-eq}{}_{Cumbustion}} = \sum_{i=1}^{n} [Fuel_{MixingBatching_i} \times Combust_i] \quad (46)$$

where, $V_{concrete}$ is the volume of concrete produced, and $Electrcity_{MixingBatching}$ and $Fuel_{MixingBatching_i}$ are obtained from Table S21.

Table S21. Input data for CO_2 emissions from concrete mixing and batching (Marceau et al. 2007)

Input	Unit	per m^3 of concrete
Natural gas	m^3	3.28E-09
Distillate (Diesel or Light) fuel oil	l	4.38E-07
Electricity	kWh	4.11E+00

Fright Transportation:

$$Transportation_{CO_{2-eq_i}} = Transportation_{Factor_{CO_{2-eq_i}}} \times Distance_i \times Mass_i \quad (47)$$

where $Transportation_{CO_{2-eq_i}}$ is obtained from Table S22; and $Distance_i$ and $Mass_i$ are respectively the transportation distance and mass of material *i*.

Table S22. Input data for CO_2 emissions factors from transportation (Facanha and Horvath 2007; Weber and Matthews 2008; Nealer et al. 2012)

Mode	Unit	Road Class 8b (Model 2005)	Road Class 5 (Model 2005)	Road Class 2b (Model 2005)	Rail Diesel Electric Locomotive	Water Generic
$CO_{2\text{-}eq}$	kg/tonne-km	1.28E-04	1.58E-04	1.98E-04	2.74E-05	1.72E-05

References

Alsop, P. A. (2007). Cement plant operations handbook: for dry process plants. Tradeship Publications Ltd.

APP (2008). Energy Efficiency and Resource Saving Technologies in Cement Industry, in, Asia Pacific Partnership on Clean Development and Climate.

Bhatty, J. I., & Bohan, R. (2004). Innovations in Portland cement manufacturing (Vol. 2004). F. M.

Boesch, M. E., & Hellweg, S. (2010). Identifying improvement potentials in cement production with life cycle assessment. Environmental science & technology, 44(23), 9143-9149.

Boesch, M. E., Koehler, A., & Hellweg, S. (2009). Model for cradle-to-gate life cycle assessment of clinker production. Environmental science & technology, 43(19), 7578-7583.

Bureau, I. P. P. C. (2009). Draft reference document on best available techniques in the cement, lime and magnesium oxide manufacturing industries. European IPPC Bureau.

CARB (2008), Instructional Guidance for Mandatory GHG Emissions Reporting - Chapter 13 Common Calculation Methods (Guidence for Regulation Section 95125), in, California Air Resources Board Sacramento, California.

Cembureau-The European Cement Association. (1997). Best Available Techniques for the Cement Industry. A Contribution from the European Cement Industry to the Exchange of Information and Preparation of the IPPC BAT Reference Document for the Cement Industry on BAT. Brussels.

Cembureau (1999). Best Available Techniques for the Cement Industry, in, The European Cement Association [CEMBUREAU], Brussels.

Choate, W. T. (2003). Energy and emission reduction opportunities for the cement industry. BCS Inc., Laurel, MD (United States).

Deru, M., Torcellini, P. (2007). Source Energy and Emission Factors for Energy Use in Buildings, in,National Renewable Energy Laboratory, Golden, Colorado.

Dunlap, R. (2003). Life cycle inventory of slag cement manufacturing process: project CTL. No. 312012. Construction Technology Laboratories, Illinois.

EFCA, EFCA Environmental Product Declarations, (EPD), in, European Federation of Concrete Admixtures Associations, 2006.

EIA (2010), 2006 Energy Consumption by Manufacturers-Data Tables.

EIA, Annual Coal Report (2010), in, U.S. Energy Information Administration - Office of Oil, Gas, and Coal Supply Statistics. U.S. Department of Energy, Washington, DC.

EIA, Annual Energy Outlook (2011) with Projections to 2035, in, U.S. Energy Information Administration, Washington, DC.

EPA, WebFIRE (2012). Technology Transfer Network Clearinghouse for Inventories & Emissions Factors, in, U.S. Environmental Protection Agency.

EPA (1994). Compilation of Air Pollution Emission Factors, Emission Factor Documentation for AP-42. Section 11.6. Portland Cement Manufacturing_Final Report, in, U. S. Environmental Protection Agency - Office of Air Quality Planning and Standards. Emission Inventory Branch, Research Triangle Park, NC.

Facanha, C., & Horvath, A. (2007). Evaluation of life-cycle air emission factors of freight transportation. Environmental Science & Technology, 41(20), 7138-7144.

Gursel, A.P. (2014). Life-cycle Assessment of Concrete: Decision-Support Tool and Case Study Application (UC Berkeley).

Kellenberger, D., Althaus, H. J., Jungbluth, N., Künniger, T., Lehmann, M., & Thalmann, P. (2007). Life cycle inventories of building products. Final report ecoinvent data v2.0 No, 7.

LBNL/ERI (2008), Guidebook for Using the Tool BEST Cement: Benchmarking and Energy Savings Tool for the Cement Industry, in, Lawrence Berkeley National Laboratory (LBNL) - Environmental and Energy Technologies Division and China Energy Research Institute (ERI), Berkeley, CA and Beijing, China.

Marceau, M., Nisbet, M. A., & Van Geem, M. G. (2007). Life cycle inventory of portland cement concrete. Portland Cement Association.

Marceau, M., Nisbet, M. A., & Van Geem, M. G. (2006). Life cycle inventory of portland cement manufacture (No. PCA R&D Serial No. 2095b). Skokie, IL: Portland Cement Association.

Miller, & S. H. Kosmatka (Eds.). Washington^ eDC DC: Portland Cement Association.

Nealer, R., Matthews, H. S., & Hendrickson, C. (2012). Assessing the energy and greenhouse gas emissions mitigation effectiveness of potential US modal freight policies. Transportation Research Part A: Policy and Practice, 46(3), 588-601.

NREL (2012). U.S. Life-Cycle Inventory Database: Electricity, bituminous coal, at power plant, in, National Renewable Energy Laboratory.

NREL (2012), U.S. Life-Cycle Inventory Database: Mining (except Oil and Gas) - Uranium-Radium-Vanadium Ore Mining, in, National Renewable Energy Laboratory.

NREL (2012), U.S. Life-Cycle Inventory Database: Gasoline, combusted in equipment, in, National Renewable Energy Laboratory.

Portland Cement Association (2008). US and Canadian Portland Cement Industry: Plant Information Summary, in. Portland Cement Association [PCA]-Economic Research Department, Skokie, IL.

Weber, C. L., & Matthews, H. S. (2008). Food-miles and the relative climate impacts of food choices in the United States.

Worrell, E., Galitsky, C., & Price, L. (2008). Energy efficiency improvement and cost saving opportunities for cement making. LBNL-54036-Revision. Ernest Orlando Lawrence Berkeley National Laboratory, University of California, March.

Worrell, E., Martin, N., & Price, L. (2000). Potentials for energy efficiency improvement in the US cement industry. Energy, 25(12), 1189-1214.

Supplementary Material C

Figures S1 and S2 provide a breakdown of the sources of emissions for each GP mix design considered in the transportation sensitivity analysis and Figures S3 and S4 provide limiting distances for each GP mix design with different transportation modes and cases.

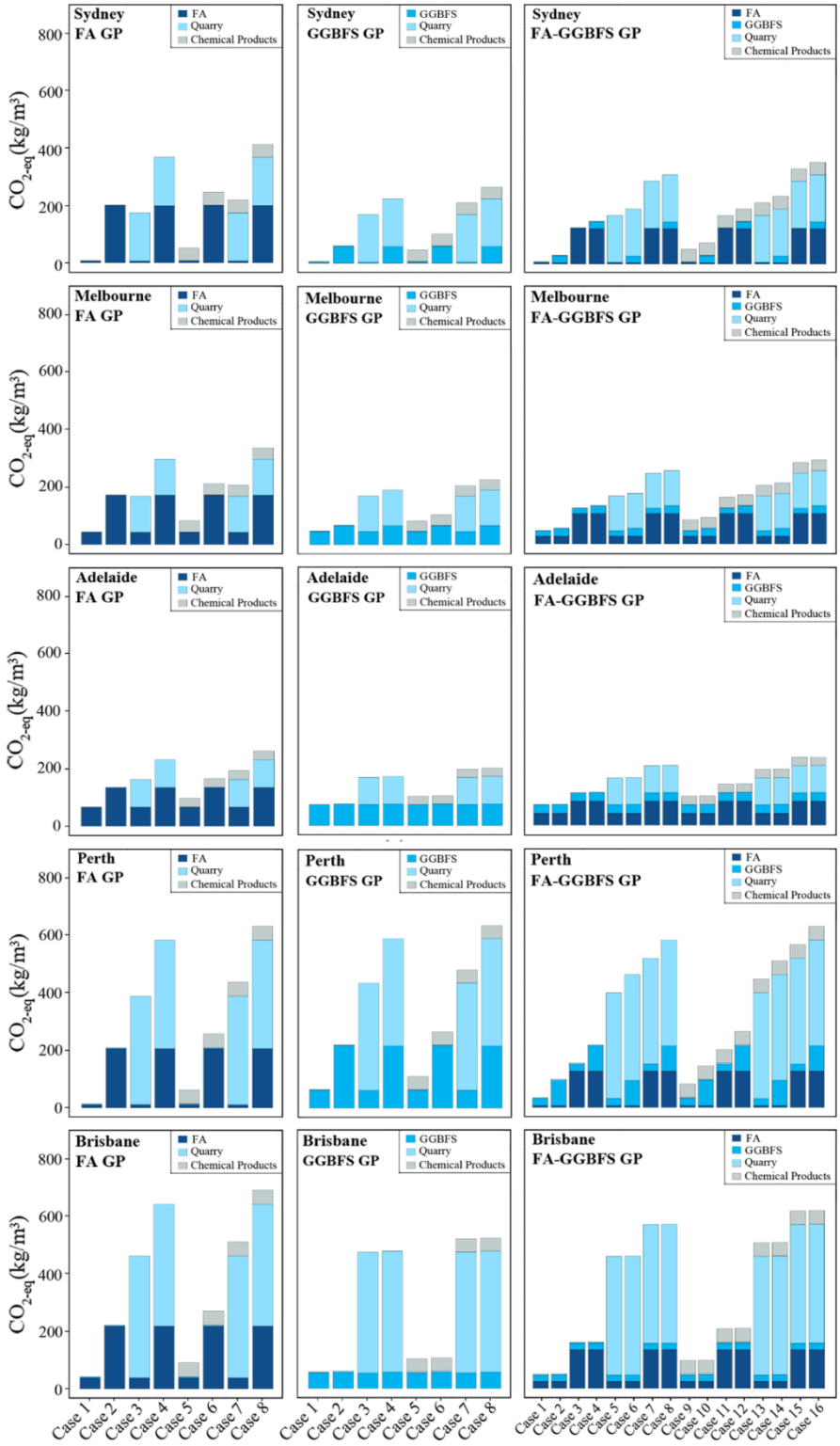

Fig. S1 Contribution of road transportation of each GP concrete material to $CO_{2\text{-eq}}$ emissions in five different cities

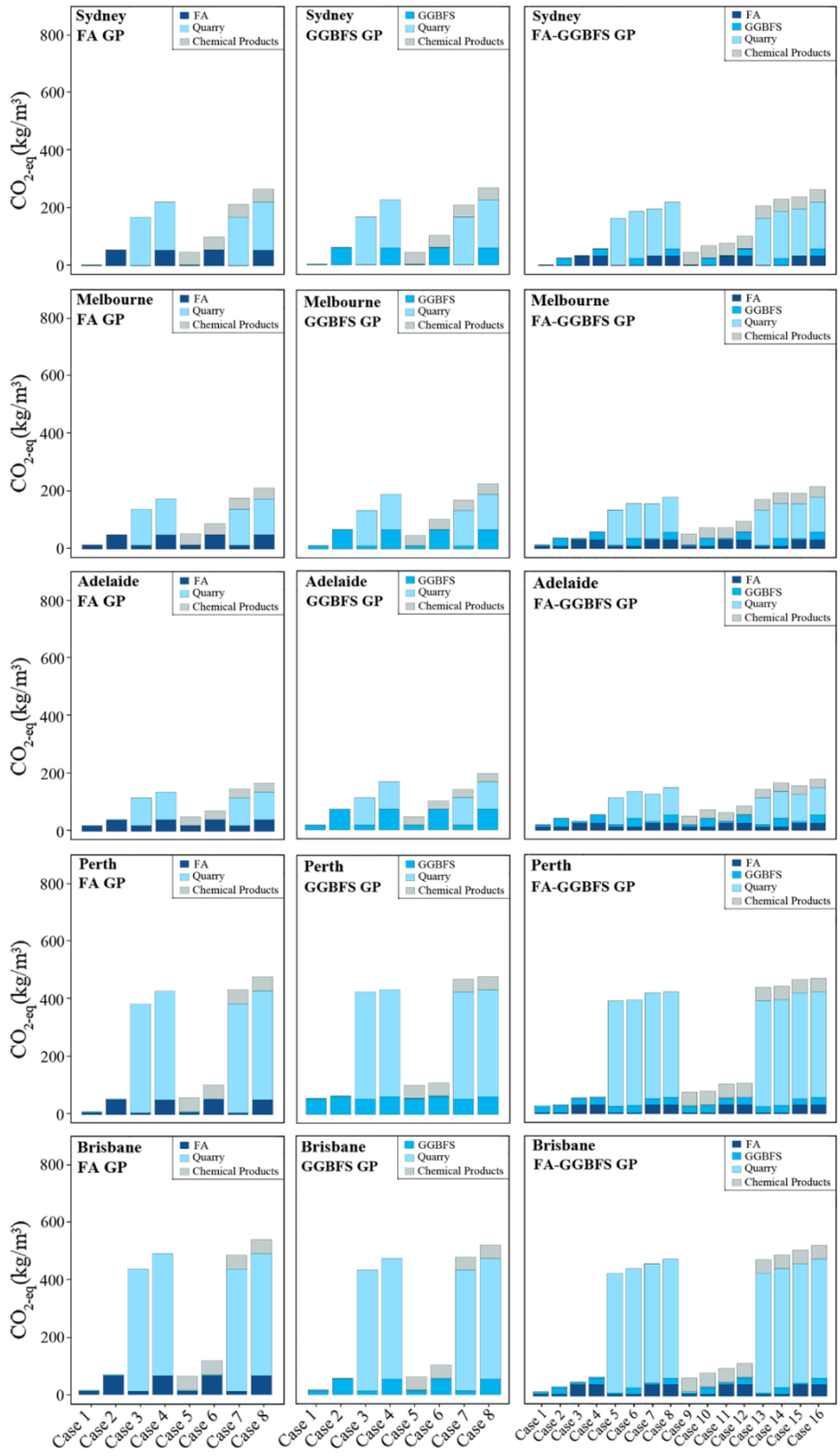

Fig.S2 Contribution of rail and road transportation of each GP concrete material to $CO_{2\text{-eq}}$ emissions in five different cities

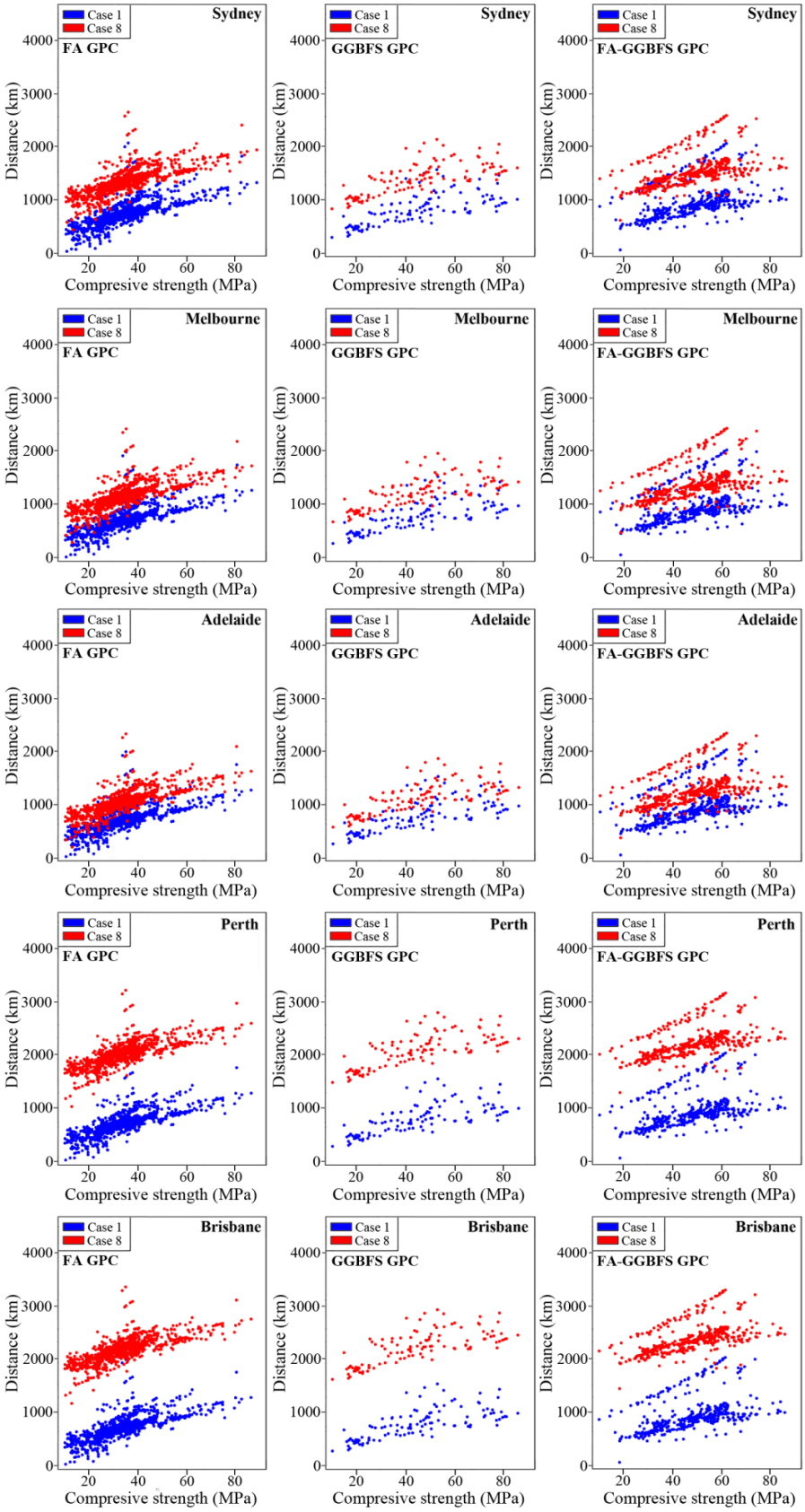

Fig.S3 Distribution of limiting distances for GP concretes considering only road transportation for batching plants in five different cities

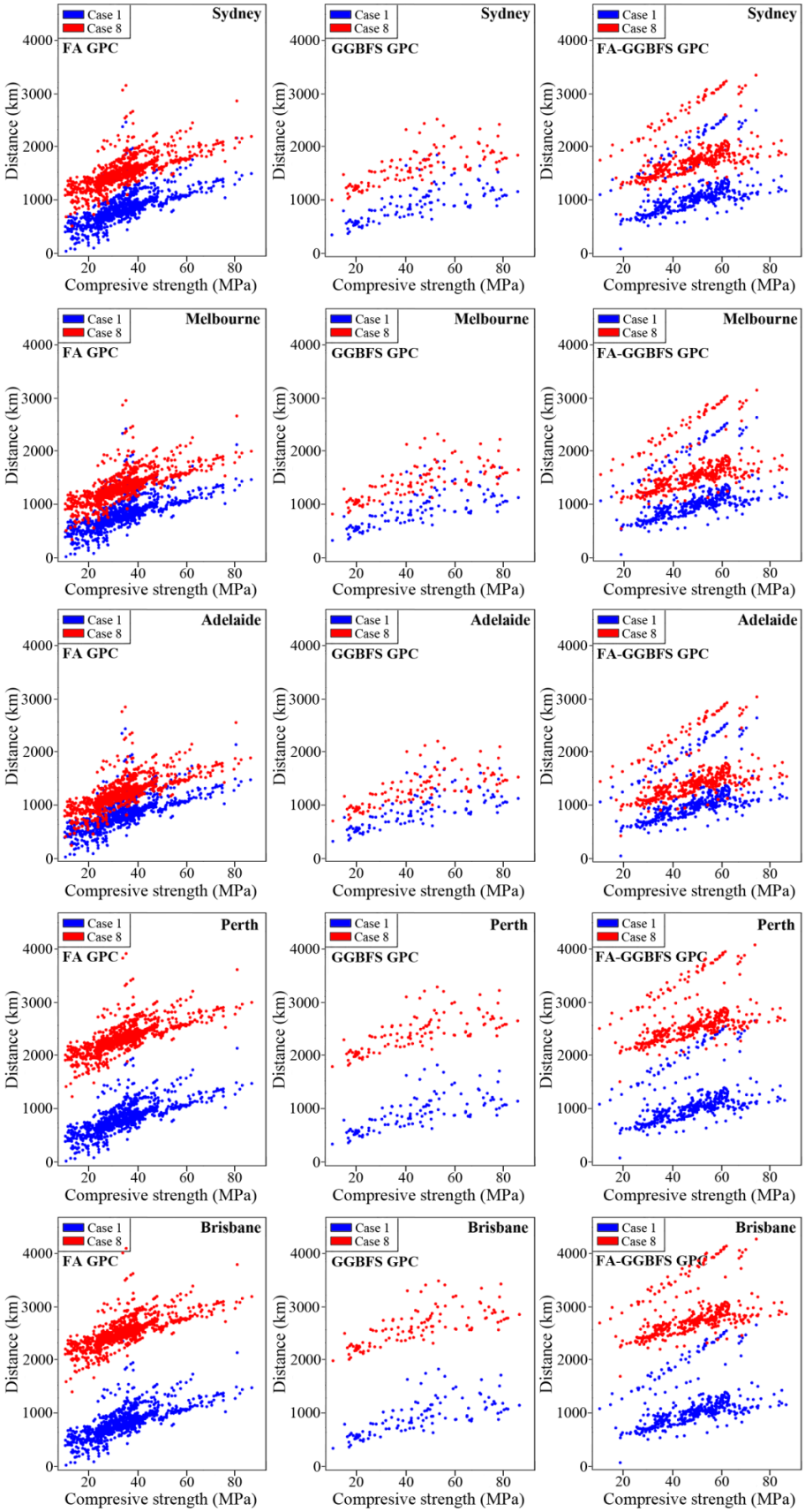

Fig.S4 Distribution of limiting distances for GP concretes considering road and rail transportation for batching plants in five different cities

CHAPTER 2

Background

In this chapter, a generic concrete mix design optimization framework is developed to find optimal mixes for concrete with alternative binders. The developed framework is implemented by integrating an ANN model based on the chemical makeup of binders, a multi-objective genetic algorithm (GA) optimization, a detailed life-cycle assessment developed in the previous chapter and financial models to find optimum mix designs with desired properties (e.g., compressive strength and slump) in terms of carbon dioxide emissions and mix cost based on several case studies.

The first publication *"A generic framework for augmented concrete mix design: Optimisation of geopolymer concrete considering environmental, financial and mechanical properties"* investigates the mix design optimization of geopolymer concrete using single and multi-objective optimization techniques for the purpose of minimizing carbon dioxide emissions and mix cost by examining the impact of regional scale transportation scenarios and the chemical composition of binders and alkali activators on the optimum mix designs.

The second publication *"Mix Design Optimization of Concrete Containing Fly Ash and Slag for Global Warming Potential and Cost Reduction"* explores optimum mixes of concrete with supplementary cementitious materials (SCMs) in terms of carbon dioxide equivalent emissions ($CO_{2\text{-}eq}$) and mix cost through investigating the impact of chemical composition of cement and SCMs, minimum cement content, regional transportation, emissions allocation, and binder type.

List of manuscripts

Shobeiri, V., Bennett, B., Xie, T., & Visintin, P. (2022). "A generic framework for augmented concrete mix design: Optimisation of geopolymer concrete considering environmental, financial and mechanical properties". *Journal of Cleaner Production*, 369, 133382.

Shobeiri, V., Bennett, B., Xie, T., & Visintin, P. (2023). "Mix Design Optimization of Concrete Containing Fly Ash and Slag for Global Warming Potential and Cost Reduction". *Case Studies in Construction Materials*, e01832.

STATEMENT OF AUTHORSHIP

"A generic framework for augmented concrete mix design: Optimisation of geopolymer concrete considering environmental, financial and mechanical properties"
Journal of Cleaner Production, 369, 133382.

Shobeiri, V. (Candidate)

Prepared manuscript, performed all analyses, and developed model and theory (70%)

This paper reports on original research I conducted during the period of my Higher Degree by Research candidature and is not subject to any obligations or contractual agreements with a third party that would constrain its inclusion in this thesis. I am the primary author of this paper.

Signed… Date16/03/2023

Bennett, B.

Supervised and contributed to research, and acted as corresponding author (10%)

I certify that the candidate's stated contribution to the publication is accurate (as detailed above); permission is granted for the candidate in include the publication in the thesis; and the sum of all co-author contributions is equal to 100% less the candidate's stated contribution.

Signed… Date 17/04/2023

Xie, T.

Supervised and contributed to research (10%)

I certify that the candidate's stated contribution to the publication is accurate (as detailed above); permission is granted for the candidate in include the publication in the thesis; and the sum of all co-author contributions is equal to 100% less the candidate's stated contribution.

Signed… Date 17/04/2023

Visintin, P.

Supervised and contributed to research (10%)

I certify that the candidate's stated contribution to the publication is accurate (as detailed above); permission is granted for the candidate in include the publication in the thesis; and the sum of all co-author contributions is equal to 100% less the candidate's stated contribution.

Signed… Date 04/04/2023

A generic framework for augmented concrete mix design: optimisation of geopolymer concrete considering environmental, financial and mechanical properties

Vahid Shobeiri, Bree Bennett, Tianyu Xie and Phillip Visintin
Word count (main body): 9625

Abstract
While concrete mix design has typically focused on the development of low-cost concretes that achieve a particular set of material characteristics, it is now becoming increasingly important to consider environmental impact. This is a challenging problem because concrete mix design, particularly when involving waste materials, is impacted not only by the concrete mix performance but also on material availability and local variation in chemical composition. This variation impacts material performance, financial cost and environmental sustainability. This paper presents a generic framework for mix design optimisation based on a material design and profiling tool coupled with an optimisation algorithm. The framework is then demonstrated for geopolymer concrete (GPC) using a new data-driven mix design tool based on an artificial neutral network to predict mechanical properties (compressive strength and slump) coupled with life-cycle assessment and financial models to quantify mix performance. Together these inputs are used as the basis for single and multi-objective optimisation using a genetic algorithm as part of set of scenarios examining the impact of regional scale transportation scenarios and the chemical composition of binders on the resultant mix properties. The framework's implementation for GPC enabled up to a 50% reduction in $CO_{2\text{-eq}}$ emissions compared to equivalent strength experimental mixes, and demonstrated that for a given strength, slump and transportation case the overall $CO_{2\text{-eq}}$ emissions can increase by up to 30% where multi-objective optimisation is used (financial and $CO_{2\text{-eq}}$ emissions minimization) when compared to minimisation of $CO_{2\text{-eq}}$ emissions alone.

Keywords: *Geopolymer concrete; optimal mixtures; machine learning; global warming; carbon dioxide emissions; industrial wastes*

1 Introduction

The building and construction sector accounts for approximately 20% of all greenhouse gas emissions and 24% of total energy consumption in Australia (Yu et al. 2017). More generally, the Paris Agreement Commitment and the United Nations (UN) Sustainable Development Goals both identify the building and construction sector as having a significant impact on the environment in terms of carbon dioxide equivalent ($CO_{2\text{-eq}}$) emissions. Therefore, decarbonisation of the building and construction sector is vital to meeting the reductions in emissions necessary to limit climate change.

Approaches to reduce reliance on cement are of great interest as cement-based concrete is the most commonly used material, and the production of cement is responsible for a significant portion of the sector's $CO_{2\text{-eq}}$ emissions. A widely proposed alternative to Ordinary Portland Cement (OPC) binders are geopolymers, which are produced by the reaction of aluminosilicate precursors sourced from industrial wastes with alkali activators. Initially, the term 'geopolymer' was strictly applied to the alkali-activation of aluminosilicate precursors, later the term alkali-activated materials (AAMs) was introduced to describe materials in which aluminosilicate sources with calcium are chemically activated. It should be noted that more

recently both terms are commonly used interchangeably in the concrete technology community (Xiao et al. 2020a) and therefore both geopolymer and AAMs are considered in this study using the single term geopolymer. This proposal is based on the proposition that the use of geopolymers enables the reduction of OPC consumption and therefore leads to lower CO_2 emissions (McLellan et al. 2011; Turner and Collins 2013; Heath et al. 2014; Salas et al. 2018; Sangwan 2020; Zhang et al. 2021). In addition to reducing $CO_{2\text{-eq}}$ emissions, the use of commonly available aluminosilicate wastes such as fly ash and slags, other potentially new waste materials such as waste glass powder, sewage sludge or palm oil fuel ash have been investigated for use as precursor materials (Xiao et al. 2021a; Xiao et al. 2022; Khankhaje et al. 2016; Zhang et al. 2017; Azad and Samarakoon 2021). The use of these alternative precursors has the benefit of reducing the environmental burden associated with their safe handling and disposal and is important because materials such as fly ash are becoming increasingly difficult to source as coal burning power generation is reduced and the price of slags increases due to demand (Xiao et al. 2020b; Amer et al. 2022). However, the diversity of raw materials that can be used as precursors for geopolymer binders makes geopolymer concrete highly versatile (Provis 2018). This variability in chemical composition and reactivity due to the variations in the integrated technology and local resources, and also in the regional availability of raw materials can be a barrier to the wide acceptance of geopolymer concrete (Xiao et al. 2020b). To address the challenges of material variability thermodynamic modelling has been applied to design precursors for geopolymer concrete in which reaction products can be directly predicted (Xiao et al. 2020a; Xiao et al. 2021b; Xie and Zhao 2022). A similar approach is taken in this study by considering the chemical composition of geopolymer ingredients in addition to their regional transportation requirements. With these proposed environmental benefits as a motivating driver, numerous studies have been conducted citing GPC as an alternative for OPC concrete and investigating its improved strength and durability properties (Hardjito et al. 2004; Bakharev 2005; Chindaprasirt & Chalee 2014; Law et al. 2015; Albitar et al. 2017; Jiang et al. 2020; Jiang et al. 2022).

Although a significant number of geopolymer concrete mix designs have been reported, mix design approaches which allow for the optimum selection of raw materials to achieve a concrete with the required fresh and hardened properties are not well developed (Shi et al. 2015; DeRousseau et al. 2018; Boindala and Arunachalam 2020). This is likely due to the complexity of factors affecting concrete properties. In general, there are two approaches for concrete mix design optimization: traditional and non-traditional. Traditional approaches are generally based on statistical methods such as response surface methodology (RSM) and the Taguchi method, in which experimental tests are done and best fit plots are drawn for similar mixture materials (Khan et al. 2016; Abellán et al. 2020; Sharif et al 2020; Li et al. 2021, Karthik and Mohan 2021). These approaches need a large number of trial mixes to identify satisfactory combinations of materials, and hence can be inefficient (Lim et al. 2004). In an attempt to minimize the number of trial mixes, non-traditional approaches based on soft computing techniques such as fuzzy logic, metaheuristic algorithms, genetic algorithms and artificial neural networks have been developed because they can generally provide good results once appropriately calibrated (Dan and Barai 2014).

The use of soft computing approaches to identify economical mix designs for OPC concretes with a set of minimum fresh and hardened properties (e.g. compressive strength and workability) has been the focus of several previous studies (Habibi and Ghomashi 2018; Naseri 2019; Golafshania and Behnood 2019; Zhang et al. 2020; Sadrossadat et al. 2021). However, with the increase in the global awareness regarding the environmental impact of the concrete industry, there has recently been a growing interest in developing ‘eco-friendly’ concrete

mixtures (Wang 2019; Lee et al. 2019; Wang 2020; Zhang et al. 2021). A summary of the existing studies on concrete mixture optimization using soft-computing methods is presented in Table 1, where it can be seen that although many studies have considered cost and mechanical considerations, only a few studies have considered environmental impact (i.e. CO_2 emissions). Importantly for soft-computing approaches, these previous studies also only consider relatively limited concrete databases (e.g. between 77 and 232 mix designs).

While there is limited research on mix design optimization of geopolymer concrete using statistical methods (Dao and Trinh 2020; Karthik and Mohan 2021), at present no study has considered mix design optimization of geopolymer concrete using data-driven soft-computing methods (see Table 1). This is important because unlike traditional cement-based concrete, geopolymer concretes consist of materials including slag, fly ash and alkaline solutions and hence mixture optimization of geopolymer concrete is more complex. Given that the chemical composition of the binders has been shown to significantly influence material properties (Hardjito and Rangan 2005; Diaz-Loya et al. 2011; Nagalia et al 2016; Arimanwa et al. 2016) it is expected that there is a need to consider the chemical composition of the binders rather than the material name or class (Cho et al. 2019). Despite the importance of binder chemical composition, to date no study has attempted to include the impact of this variable when predicting concrete mechanical properties. Additionally, although cement is generally locally produced, the precursors to geopolymer are only available at a limited number of geographic locations (coal power stations and smelters), the impacts of transportation emissions and cost on the optimal mix designs have generally been ignored (see Table 1). The need to consider geographical location is also highly linked to the need to consider chemical composition of the binders because materials such as fly ash and slag have highly variable chemical compositions depending on the source material and therefore geographical location can influence the mechanical properties of the resulting concrete (Shi et al. 1995; Kumar et al. 2007; Zhang et al. 2012; Glosser 2019; Xie et al. 2020).

Table 1 A summary of previous studies in the literature on concrete mixture optimization using soft-computing methods

Source	Database feature		Mechanical properties		Objective		Factors considered	
	Binder	Size	Compressive strength	Slump	Cost	CO_2	Regional scale transportation	Binder chemical composition
Noguchi et al. (2003)	OPC SCMs*		✓	✓	✓			
Lim et al. (2004)	OPC SCMs	189	✓	✓				
Yeh (2007)	OPC SCMs	103	✓	✓	✓			
Jayaram et al. (2009)	OPC SCMs	350	✓					
Lee et al. (2009)	OPC SCMs		✓		✓			
Lee et al. (2012)	OPC SCMs	189	✓	✓				
Cheng et al. (2014)	OPC SCMs	1030	✓		✓			
Dan and Barai (2014)	OPC SCMs		✓		✓			
Habibi and Ghomashi (2018)	OPC SCC+	42	✓	✓	✓			
Golafshania and Behnood (2019)	OPC SCMs	1030	✓		✓			
Kwon and Wang (2019)	OPC SCMs	77	✓	✓		✓		
Naseri (2019)	OPC SCMs	96	✓		✓			
Lee et al. (2019)	OPC SCMs	103	✓	✓		✓		
Wang (2020)	OPC SCMs		✓	✓		✓		
Zhang et al. (2020)	OPC SCMs	1030	✓	✓	✓			

Naseri et al. (2020)	OPC SCMs	232	✓		✓	✓		
Sadrossadat et al. (2021)	OPC SCMs	41	✓	✓	✓			
Zhang et al. (2021a)	OPC SCMs	1030	✓		✓	✓		
This study	GPC	1178	✓	✓	✓	✓	✓	✓

[*] ***Supplementary Cementitious Materials*** [+]***Self-compacting concrete***

This paper fills a significant research gap by introducing a generic conceptual framework that can be applied to find optimum mix designs considering a range of adaptable factors (e.g. mechanical, financial and environmental) for a range of concrete types. Similarly, application of the generic framework to investigate optimum geopolymer concrete mix designs using soft-computing methods is also novel (see Table 1) because to date these techniques have only been applied to OPC based concretes. Demonstration scenarios are presented and used to investigate the impact of considering binder chemical composition on optimal geopolymer mix designs in the context of single-objective optimisation (i.e. CO_2-eq minimisation) as well as the impact of transportation emissions and cost while meeting a minimum set of mechanical properties (strength and workability) from a single- and multi-objective perspective. This is significant as it acknowledges that the precursor materials applied in geopolymer concrete production have varying chemical compositions and are not necessarily locally available.

The paper first presents a generic conceptual framework for concrete mixture optimization incorporating environmental, financial and mechanical properties in Section 2 which can be adapted to concrete types and applications of interest. The specific implementation of the framework used in this paper, including a description of the database used to develop the geopolymer mix design tool, are detailed separately in Section 3. Scenarios used to illustrate the approach and evaluate influences on optimal geopolymer mixes, including a sensitivity analysis of binder chemical compositions and transport emissions, are detailed in Sections 4 and 5. Although presented via different Australian demonstration scenarios the framework is applicable anywhere in the world provided a local inventory for life-cycle assessment and binder chemical composition is available.

2 Conceptual framework for augmented mix design

This paper presents a generic conceptual framework for concrete mix design incorporating environmental, financial and mechanical properties so that it can be tailored to a range of concrete applications and types.

The conceptual framework is formalized as an approach with three main components: (i) the mix design tool, (ii) the material attribute calculator that augments standard mix design information with complementary information (e.g. financial and environmental information), and (iii) an optimisation algorithm that updates the mix design components and evaluates with respect to the defined objective function(s). The first two components essentially form a material design and profiling tool for concrete and the third leverages the information to optimize the mix design. The framework is also sufficiently generic such that it can be extended to look at additional material properties beyond mechanical, environmental and financial considerations, with adaption of the material attribute calculator.

The three framework components above are represented schematically in Fig 1 where the solid boxes represent the underlying tools employed and the dashed boxes represent key components and attributes of the optimisation algorithm.

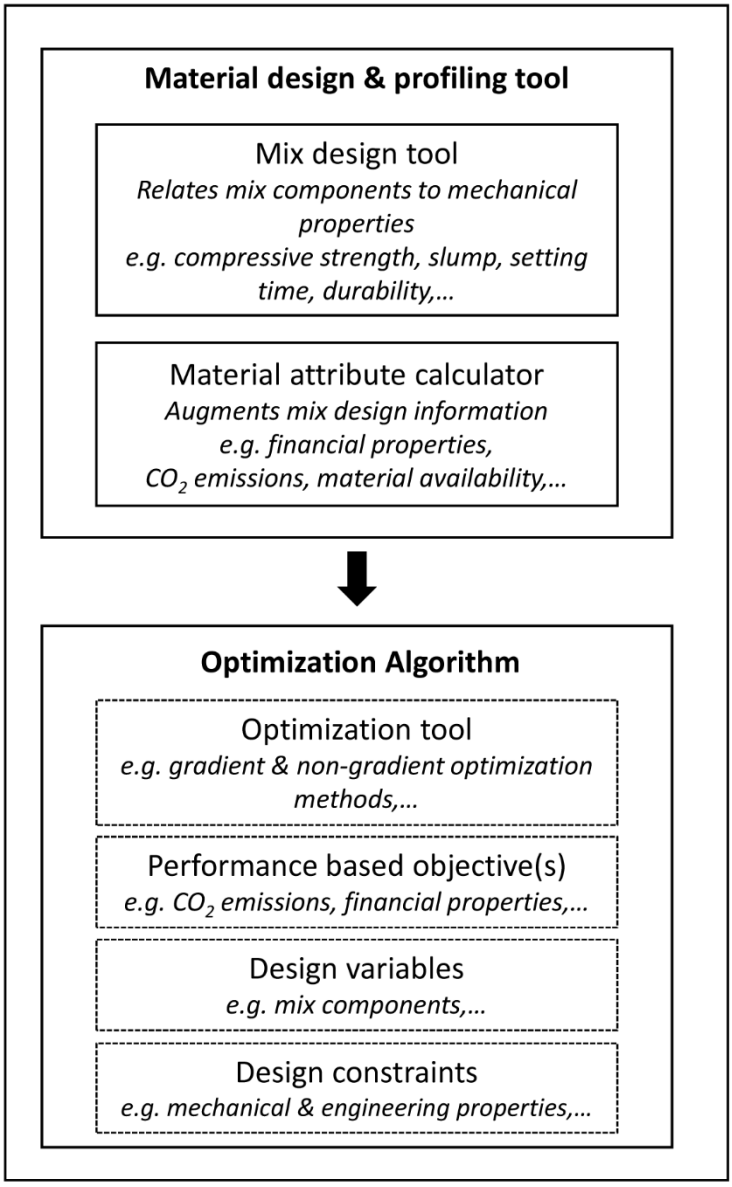

Fig.1 Schematic of the generic framework

The three framework components are outlined here including a discussion of the necessary considerations for choosing data and tools to implement the framework.

1. *Material design and profiling tool: mix design tool*
   The mix design tool relates defined mix components (i.e. the quantities and properties of the concrete mixture) to the mechanical properties of the resultant mix that are of interest (e.g. compressive strength and slump). The mix design tool must provide satisfactory predictions of mechanical properties for the type of concrete (or concretes) of interest such that changes to the mix components result in reasonable mechanical property predictions.

2. *Material design and profiling tool: material attribute calculator*
   The material attribute calculator augments the traditional outputs of a concrete mix design tool (i.e. the mechanical properties) by further describing the resultant mix in terms of other attributes of interest (i.e. CO_2 emissions, financial implications). This material attribute calculator uses the mix components in conjunction with contextual information related to the mix components and the end use of the concrete. For example, the source of the raw

materials for a given type of concrete, the transport mode and location of utilisation of concrete may be input to the life-cycle assessment to determine CO_2 emissions associated with the considered concrete mixture.

3. *Optimisation algorithm*
   The mix design properties and attributes generated by the mix design and profiling tool are used as inputs to the optimisation algorithm. That is, the mix design components are used as the design variable (i.e. decision variables) which are updated based on the objective function(s) which incorporates desired performance measures derived from the material attribute calculator (e.g. CO_2 emissions) within a set of prescribed design constraints (e.g. mechanical properties including target compressive strength and slump which is an important mix design outcome in terms of workability as well as limits in terms of feasible mix design). The chosen optimization scheme must have the capacity to deal with high dimensionality problems with highly nonlinear constraints and many decision variables due to the complexity of factors affecting the concrete mix design properties (Wang 2019; Kwon and Wang 2019; Nunez et al. 2020)

3 Framework implementation

This paper implements the conceptual framework for augmented mix design (see Section 2) on geopolymer concrete considering environmental, financial and mechanical properties. The specific implementation employs a new data-driven mix design tool to predict geopolymer mechanical properties, a material attribute calculator comprising a detailed life-cycle assessment (LCA) of concrete developed by Shobeiri et al. (2020) and a simple summative financial model to predict the cost of the concrete coupled using a GA to optimise the concrete mixture with respect to desired performance measures. The overall framework implementation is shown in Fig. 2.

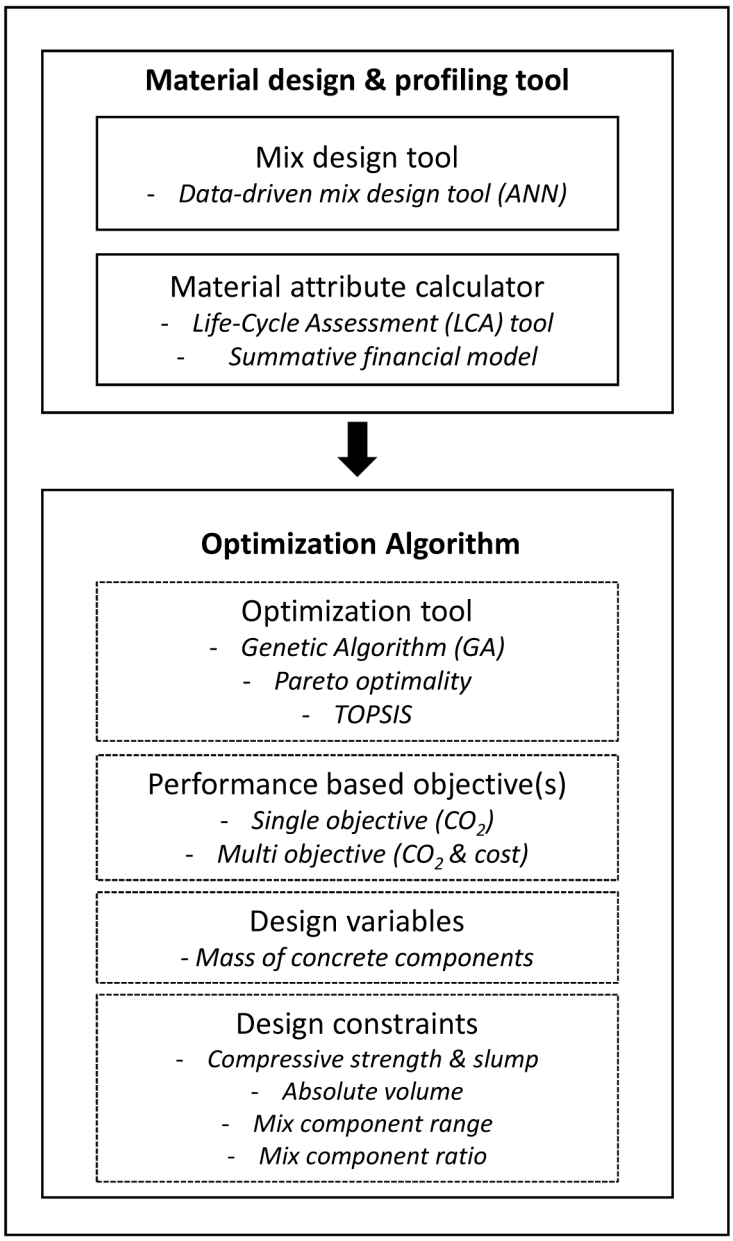

Fig. 2 Framework implementation for geopolymer

3.1 Material design and profiling tool: mix design tool

This study develops and employs a data-driven mix design tool to relate mix design components to mechanical properties. The mix design tool uses an ANN which is trained using a large database of 1178 mix designs and associated mechanical properties. The mix design tool and the database are now described in turn.

3.1.1 Mix design tool: Artificial Neural Networks

Artificial neural networks, due to their ability to map complex and nonlinear problems (Akpinar and Uwanuakwa 2016), are used herein to relate mix components and desired mechanical properties. ANNs as a non-parametric model have been widely used for the prediction of various concrete properties (Yaman et al. 2017; Naderpour et al. 2018; García et al. 2020; Liu et al. 2021) and for a detailed review of ANN mathematical models, the reader is

referred to Dreiseitl and Ohno-Machado (2002) and Demuth et al. (2009).

The ANN model used in this study (The MathWorks Inc. 2020a) contains a single hidden layer and uses the following as input variables: total mass of SiO_2, total mass of Al_2O_3, total mass of Fe_2O_3, total mass of CaO, total mass of Na_2O, mass of fine aggregates, mass of coarse aggregates, total mass of water, mass of superplasticizer, age of concrete at the time of compression testing, temperature of accelerated curing, time of accelerated curing and relative humidity of accelerated curing. Where ambient curing is used the accelerated curing time, temperature and relative humidity are specified as zero, 25°C and 50%. For oven curing, relative humidity is specified as 10% (Wedatalla et al. 2019). For the prediction of slump, curing variables are not used as inputs because curing does not play role in the fresh properties of concrete.

In the developed ANN model, training (70%), testing (15%) and validation (15%) sets are randomly selected from the database. To obtain an unbiased estimation of the model performance the accuracy of the model is measured through several statistical indicators including root mean square error (*RSME*), mean absolute error (*MAE*), coefficients of multiple determination (R^2) and correlation coefficient (R) as described follows:

$$RMSE = \sqrt{\frac{\sum_{i=1}^{n}(x_i - y_i)^2}{n}} \quad (1)$$

$$MAE = \frac{\sum|x-y|}{n} \quad (2)$$

$$R^2 = 1 - \frac{\sum(x_i - y_i)^2}{\sum(x_i - \bar{x})^2} \quad (3)$$

$$R = \frac{\sum(x-\bar{x})(y-\bar{y})}{\sqrt{\sum(x-\bar{x})^2 \sum(x-\bar{y})^2}} \quad (4)$$

where x is the observed value, $\bar{x}$ is the mean of observed value, y is the predicted value, $\bar{y}$ is the mean of predicted value, and n is the total number of observations in the database.
An existing experimental database for GPC, containing 1756 geopolymer concrete mix designs with alkaline activators containing sodium silicates and sodium hydroxide from 110 previously published studies, originally collated by Xie et al. (2020), was used. For use in the ANN, the database was further refined as follows:

(g) Due to the difficulty in quantifying emissions associated with the processing of other aluminosilicate materials only mixes having fly ash and GGBFS are considered. This approach ensures a large quantity of experimental data is available and allow the development of chemically-informed models for predicting the strength of geopolymer concrete.
(h) Only ambient and oven cured geopolymer concrete are considered, steam cured GPC is not considered in this work owing to the small number of data points.
(i) Only mixes with a compressive strength of greater than 10 MPa are considered due to their broader applications in civil engineering.

Using the above criteria, 1178 mix designs remained for calibrating the ANN. Prior to calibration, all compressive strength results obtained from cube testing were converted to an equivalent cylindrical strength using the procedure described in UNESCO (1971), British Standards Institution (2013) and Wong (2013). Reporting of workability via slump testing is far less common than reporting of compressive strength and as a result only 292 mix designs could be collated to train the ANN for prediction of slump.

Figure 3 shows the distribution of geopolymer concrete ingredients by weight (Fig. 3 (a)) and chemical compositions of binders as percentages (Fig. 3 (b)) in the database. Figure 3(a) illustrates that the concrete mixtures within the database cover a wide range of variability and include concretes with either fly ash or GGBFS as binders or blended fly ash/GGBFC binders. For clarity, the distributions of chemical compositions of binders in the database including SiO_2, Al_2O_3, Fe_2O_3, CaO which generally constitute more than 90% of the mass of binders are shown in Fig. 3(b). It can be seen that the database covers different classes of fly ash and GGBFS with the chemical compositions ranging widely for each chemical component.

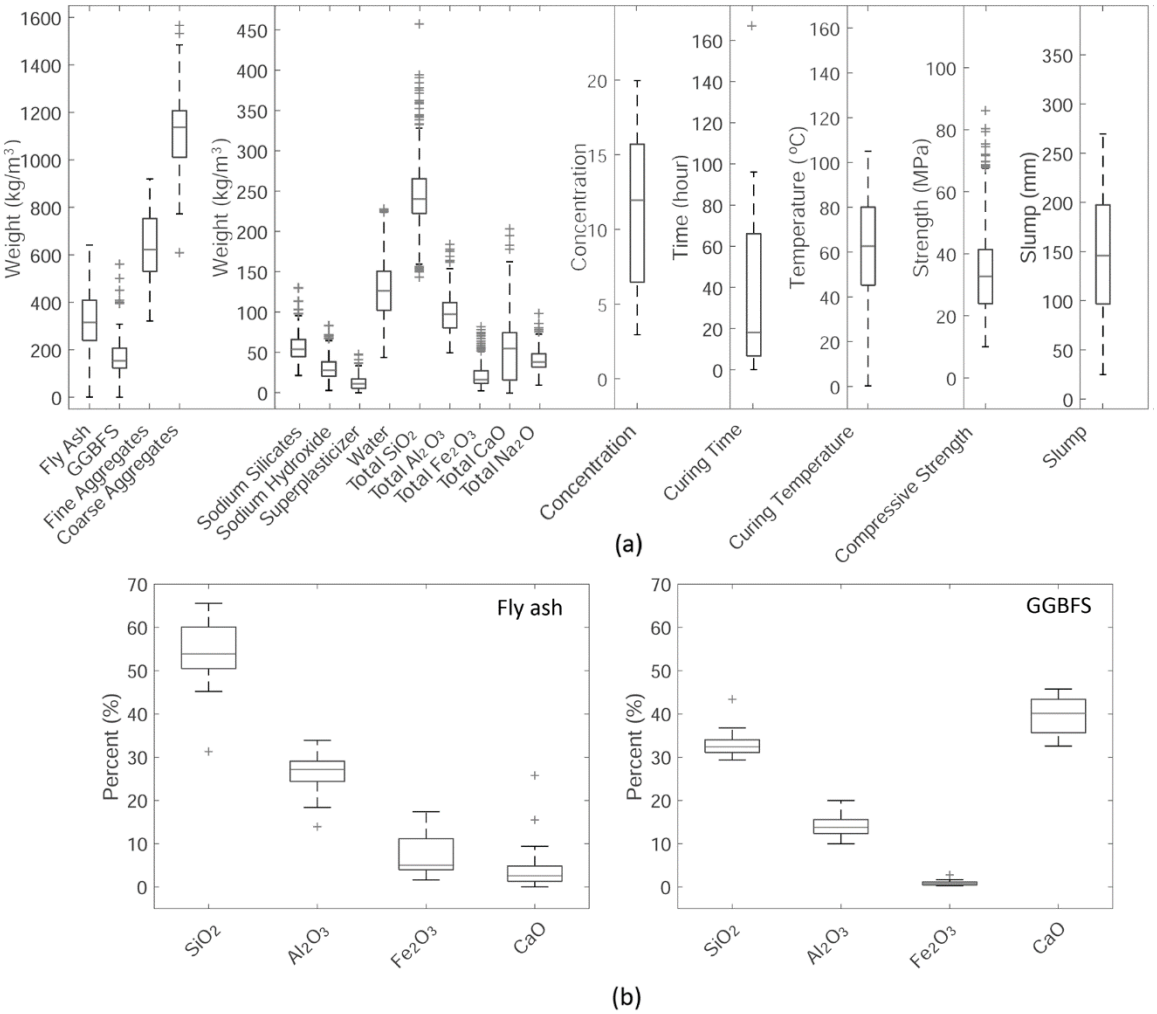

Fig. 3 Distribution of (a) geopolymer concrete ingredients in database (b) chemical compositions of binders in the database.

The total masses of SiO_2, Al_2O_3, Fe_2O_3, CaO and Na_2O in the mixture are the sum of the mass of the related chemicals in binders (fly ash and GGBFS), dried sodium silicates (Na_2SiO_3 comprising Na_2O and SiO_2) and dried sodium hydroxide (NaOH comprising Na_2O and a small component of H_2O). The calculation of total masses of chemical components is given by:

$$m_{SiO_2} = P_{SiO_2}^{FA} \cdot m_{FA} + P_{SiO_2}^{GGBFS} \cdot m_{GGBFS} + P_{SiO_2}^{Na_2SiO_3(dry)} \cdot m_{Na_2SiO_3(dry)} \quad (5)$$

$$m_{Al_2O_3} = P_{Al_2O_3}^{FA} \times m_{FA} + P_{Al_2O_3}^{GGBFS} \times m_{GGBFS} \quad (6)$$

$$m_{Fe_2O_3} = P_{Fe_2O_3}^{FA} \times m_{FA} + P_{Fe_2O_3}^{GGBFS} \times m_{GGBFS} \quad (7)$$

$$m_{CaO} = P_{CaO}^{FA} \times m_{FA} + P_{CaO}^{GGBFS} \times m_{GGBFS} \quad (8)$$

$$m_{Na_2O} = P_{Na_2O}^{Na_2SiO_3(dry)} \times m_{Na_2SiO_3(dry)} + P_{Na_2O}^{NaOH(dry)} \times m_{NaOH(dry)} \quad (9)$$

where m_z indicates the mass in kg of chemical component z and P_z^A is the percentage of chemical component z in mix ingredient A and the chemical components are indicated in terms of their chemical symbols (e.g. NaOH) with the form (i.e. dry or solution) indicated in brackets where relevant. The total water is calculated based on the amount of additional water, water in alkali solutions (Na_2SiO_3 and NaOH) and water in dried sodium hydroxide as follows:

$$m_{H_2O} = m_{H_2O\_additional} + P_{H_2O}^{Na_2SiO_3(solution)} \times m_{Na_2SiO_3(solution)} + P_{H_2O}^{NaOH(solution)} \times m_{NaOH(solution)} + P_{H_2O}^{NaOH(dry)} \times m_{NaOH(dry)} \quad (10)$$

3.2 Material design and profiling tool: material attribute calculator

In this study, the results of a cradle to gate life-cycle assessment (LCA) model are used to quantify the environmental impacts in terms of global warming potential measured in terms of carbon dioxide equivalent ($CO_{2\text{-eq}}$) emissions to produce 1 m^3 of concrete (Shobeiri et al. 2021). The LCA includes emissions associated with raw material extraction through to production and manufacture. Throughout the analysis, the emissions released from three major processes including fuel pre-combustion, fuel combustion and electricity generation for the production of fine and coarse aggregates, superplasticizer, fly ash, GGBFS, alkali activators and concrete batching are calculated for the assessment of global warming potential (see Shobeiri et al. 2021 for the detailed information concerning LCA calculations of geopolymer concrete).

For each constituent material, the $CO_{2\text{-eq}}$ emissions per kg taken from Shobeiri et al (2021) are presented in Table 2 along with the production cost of geopolymer concrete ingredients identified by Teh et al. (2017). Comparing the variations in $CO_{2\text{-eq}}$ emissions and cost per kg it can be seen that there is typically a strong correlation between these variables. Table 2 also summarises $CO_{2\text{-eq}}$ emissions and costs per kg-km for road, rail and sea where road transport is the greatest emitter and most expensive per kg-km.

Table 2 Unit $CO_{2\text{-eq}}$ emissions, unit cost and specific gravity of geopolymer concrete components and unit $CO_{2\text{-eq}}$ emissions and cost of transportation modes (Gursel 2014; Teh et al. 2017; Freight rates in Australia 2017; Shobeiri et al. 2021).

Component	Unit $CO_{2\text{-eq}}$ (kg/kg)	Unit Cost (AUD/kg)	Specific gravity
Fly ash	0.0260	0.045	2.20
GGBFS	0.0901	0.140	2.80
Fine aggregates	0.0028	0.012	2.61
Coarse aggregates	0.0039	0.019	2.70
Water	0.0002	0.002	1.00
Superplasticizer (liquid)	0.2290	0.424	1.22
Sodium silicates (dried)	1.0670	0.400	1.40
Sodium hydroxide (dried)	1.2700	0.200	1.04-1.26*
Transportation mode		**Unit $CO_{2\text{-eq}}$ (kg/kg-km)**	**Unit Cost (AUD/kg-km)**
Road		12.80×10^{-5}	9.08×10^{-5}
Rail		2.74×10^{-5}	4.32×10^{-5}
Sea		1.72×10^{-5}	3.14×10^{-5}

* ***Depending on concentration***

3.3 Optimisation algorithm

This study employs a genetic algorithm (GA) to optimise mix design components to achieve performance-based criteria (The MathWorks Inc. 2020b). GAs use objective functions based on the fitness criteria to find the optimal solutions using reproduction, crossover and mutation operators imitating biological evolution (Rani et al. 2013; Filipovic 2019; Yang 2020) and have been successfully used for the mix design optimization of different types of concrete (Dan and Barai 2014; Lee et al. 2019; Wang 2020; Naseri et al. 2020).

Single- and multi-objective optimization is used depending on the investigated scenario where the multi-objective optimization for a GA problem minimizes k single-objective functions (where $k = 1$ for the single-objective case) in the vector $F(x)$ where x is a d-dimensional design variable vector $x = x_1, \dots, x_d$ in the decision space as follows (Gen & Cheng 1999):

$$\text{Minimize: } F(x) = \big(f_1(x), \dots f_k(x)\big) \tag{11}$$

In the case of multi-objective optimization where the objectives conflict with one another, a single solution cannot optimize all the objective functions in $F(x)$ simultaneously. Where this occurs the notion of Pareto optimality and Technique for Order Preference by Similarity to an Ideal Solution (TOPSIS), which is a multi-criteria decision-maker (Méndez et al. 2020), are used to make a trade-off between conflicting objectives. For a detailed review on the mathematical models of Pareto optimality and TOPSIS, the reader is referred to Chinchuluun and Pardalos (2007) and Méndez et al. (2020).

3.3.1 Design variables

To limit the search space, the fundamental mixing factors that govern the performance of the geopolymer concrete were designated as the design variables. The eight design variables specified for the GA were: the mass of fly ash, GGBFS, fine aggregates, coarse aggregates, superplasticizer, total water (additional water plus water in alkali solutions) and dried mass of sodium silicates and sodium hydroxide.

It should be noted that as the chemical compositions and mass of materials are respectively used as ANN and GA inputs, the GA-design variables are converted to ANN-input variables using Equations 5 - 10 for prediction purposes.

3.3.2 Objective function(s)

The total $CO_{2\text{-eq}}$ emissions and cost arising from the production of a cubic meter of geopolymer concrete with a given set of mechanical properties are designated as objectives for minimization. The total $CO_{2\text{-eq}}$ emissions and cost are calculated as the sum of the emissions or cost of the production and transportation of each component material i as follows:

$$C_t = \sum_i m_i(C_{prod_i} + C_{trans_i} \times d_i) \tag{12}$$
$$F_t = \sum_i m_i(F_{prod_i} + F_{trans_i} \times d_i) \tag{13}$$

where C_t and F_t are the total $CO_{2\text{-eq}}$ emissions and cost of concrete, m_i is the mass of each mix component, d_i is the distance in km the component is transported, C_{prod_i} and F_{prod_i} are the unit $CO_{2\text{-eq}}$ emissions and unit cost of the production of individual components of concrete,

and C_{trans_i} and F_{trans_i} are the unit emissions and cost associated with transportation per km (see Table 2).

3.3.3 Design constraints

Due to the importance of compressive strength and slump for specifying 'fit for purpose' concrete, these mechanical properties are designated as the main constraints. To achieve a target predicted compressive strength ($f_{c_{target}}$) and slump (S_{target}), the ANN predicted compressive strength, f_{c_p}, and slump, S_p, are constrained within a tolerance (tol_{f_c} and tol_S respectively) Eqs. (14-15). Tolerances applied for investigated scenarios are given in Section

$$f_{c_{target}} - tol_c \leq f_{c_p} \leq f_{c_{target}} + tol_c \quad (14)$$

$$S_{target} - tol_S \leq S_p \leq S_{target} + tol_S \quad (15)$$

Further constraints are employed to ensure physical feasibility of the optimized mix including, design variable constraints (i.e. mix component masses), the absolute volume constraint and component ratio constraint. The lower and upper bounds for the design variables are constrained within the lower and upper limits observed in the database as given by Eq. (16) where m_i is the mass of each mix component, i. The absolute volume constraint ensures the sum of the volume of concrete ingredients minus the volume of the entrapped air (V_{air}) is 1 m^3 is considered as another main constraint given by Eq. (17) where m_i and ρ_i are respectively the mass and specific gravity of concrete components listed in Table 2. The component ratio constraint (r_j) specifies that the ratios of concrete components in the optimal mixes (including water-to-binder ratio, binder-to-total aggregates ratio, fine aggregates-to-coarse aggregates ratio, superplasticizer-to-binder ratio and binder-to-paste ratio) should fall within their lower and upper limits in the database (Eq. 18). Accordingly, the design constraints employed to ensure physical feasibility can be defined as follows:

$$m_i^{min} \leq m_i \leq m_i^{max} \quad i = 1,2,\dots,8 \quad (16)$$

$$\sum_{i=1}^{8} \frac{m_i}{\rho_i} = 1 - V_{air} \quad (17)$$

$$r_j^{min} \leq r_j \leq r_j^{max} \quad j = 1,2,\dots,5 \quad (18)$$

It should be noted that in Eq. (14), the concrete compressive strength is bracketed by an acceptable range as a constraint. This is approach has been commonly applied in the optimisation of other concrete types (e.g. see Naseri 2019; Golafshania and Behnood 2019; Zhang et al. 2021a) as a designer typically specifies the compressive strength based on concrete's intended application (Lee et al. 2009). However, to check whether by relaxing the upper strength limit it is possible to find optimum mixes with higher strengths, a sensitivity analysis is performed in which the upper strength limit is removed (i.e. the constraint becomes $f_{c_{target}} \leq f_{c_p}$) and the optimum mixes derived from this approach are compared to those found when both lower and upper strength limits are considered. This comparison is shown in Supplementary Material A. The results of this analysis show that even with different transportation cases there is a negligible difference between the compressive strengths and $CO_{2\text{-eq}}$ emissions of optimum mixes obtained from these two strength constraint approaches (see Fig A-1 (bottom row)). This can be attributed to the fact that the mix emissions generally increase with an increase in the concrete's compressive strength and that the optimisation algorithm tries to find mixes that minimize emissions (as required by the objective function) while satisfying design constraints (e.g., compressive strength and slump). Hence, in this study

Eq. (14) is applied to minimise the difference between the predicted and target strength considering the intended application of concrete as part of problem formulation.

4 Scenario demonstration

Two different scenarios are evaluated. The first investigates the effects of the chemical compositions of binders on the optimal mixtures of geopolymer concrete in the context of single-objective optimization ($CO_{2\text{-eq}}$ minimization). The second deals with the additional effects of transport emissions and cost in quantifying optimal mixtures of geopolymer concrete. In both scenarios, target compressive strengths, $f_{c_{target}}$, of between 25 and 50 MPa in 5 MPa increments are considered with an allowable deviation from target (tol_c) of 1 MPa. The target slump, S_{target}, of each mix is considered to be 150 mm with a tolerance (tol_S) of 5 mm as these designated properties meet the common requirements of concrete for municipal applications. For each target compressive strength, oven and ambient curing of the geopolymer concrete are evaluated separately.

In both scenarios the following parameters are held constant at the following values as these reflect the properties of the most frequently used practices in the database:

- chemical compositions of sodium silicates (SiO_2: 30.7%, Na_2O: 11.40%; H_2O:57.9%)
- concentration of the sodium hydroxide is 12 molar
- strength test age is 28 days
- oven curing time 24 hours
- oven curing temperature is 60°C

4.1 Scenario 1: sensitivity analysis of chemical compositions of binders

Scenario one investigates the effects of binder chemical compositions on optimal geopolymer concrete mixes ($CO_{2\text{-eq}}$ minimization) by evaluating the impact of procuring binders (fly ash and GGBFS) from different sources in Australia. The sources and chemical compositions of the binders evaluated are shown in Table 3. While Port Kembla is the only source of GGBFS in Australia various types of fly ash are sourced from different power stations in Australia.

Table 3 Chemical compositions of fly ash sourced from different Australian power stations (Yu et al. 2012; Ngu et al. 2007; Williams and Van Riessen 2010) and GGBFS sourced from Port Kembla (Heaton et al. 1981) in Australia.

Power Station	**Chemical Composition of fly ash (%)**			
	SiO_2	**Al_2O_3**	**Fe_2O_3**	**CaO**
Eraring Power Station	61.60	24.50	5.40	3.50
Collie Power Station	54.00	28.30	10.50	1.70
Mt Piper Power Station	68.60	25.50	1.30	0.22
Bayswater Power Station	64.79	23.50	4.98	2.26
Location	**Chemical Composition of GGBFS (%)**			
	SiO_2	**Al_2O_3**	**Fe_2O_3**	**CaO**
Port Kembla	38.80	16.80	0.70	38.40

For each combination of binder source and compressive strength investigated, the optimal mixtures are reported in terms of the mass of constituent components (i.e. fly ash, GGBFS, fine aggregate, coarse aggregate, sodium silicates, sodium hydroxide, superplasticizer and extra water) with oven and ambient cured mixes reported separately. The environmental performance of optimal mixtures developed using the framework and experimental mixes of the same strength in the database are compared using the $CO_{2\text{-eq}}$ intensity indicator (C_i) which

is defined as the $CO_{2\text{-eq}}$ emissions of delivering one unit of compressive strength (Yang et al. 2013).

4.2 Scenario 2: sensitivity analysis of transportation

The second scenario study investigates the impact of transport emissions and cost on the optimal geopolymer mixes in two parts considering: single- and multi-objective optimisation. Considering the $CO_{2\text{-eq}}$ emissions minimization as the single objective, a sensitivity analysis is first done to analyze the cases for the five major capital cities in Australia (Sydney, Melbourne, Adelaide, Perth and Brisbane). Within the context of this scenario it is assumed that:

(i) sodium silicates, sodium hydroxide and superplasticizer as chemical products are sourced from the same suppliers;
(ii) the same type of GGBFS can be provided locally from the steel factories in Port Kembla or imported from Port Yokohama (Japan); fly ash can be sourced from the same four Australian coal power stations (Table 3);
(iii) quarry materials can only be transported within the state, while fly ash and GGBFS can be transported by rail from interstate if they are not available locally; and
(iv) batching plants are assumed to be within each state, where the minimum and maximum distances between the batching plants and material sources are both considered in the scenarios.

The locations of batching plants and material sources; the transportation distances and modes of raw materials for each city; and different transportation scenarios for raw materials for each city are presented in Fig. 4, Table 4 and Table 5. For each transportation scenario (location and transportation mode/distance combination) the optimal mixtures are reported in terms of the mass of constituent materials (i.e. fly ash, GGBFS, fine aggregate, coarse aggregate, sodium silicates, sodium hydroxide, superplasticizer and extra water) for each compressive strength investigated. Again, mixes considering oven and ambient curing are reported separately.

In practice, the assessment of multiple concrete performance indicators may be required or desired (De Munck et al. 2015, Afshari et al. 2019; Kayabekir et al. 2020; Dave et al. 2021; Chen et al. 2022; Boindala et al. 2022). Therefore, having investigated the impact of regional scale transport, optimal mixes of geopolymer concrete in Sydney are then found in the context of multi-objective optimization ($CO_{2\text{-eq}}$ and cost minimization) using the notion of Pareto optimality. The same assumptions and scenarios for the transportation of raw materials are used for the multi-objective analysis. In this analysis, while the TOPSIS technique is used to find the final optimal mixtures from the Pareto optimal solutions, the trade-off between the objectives ($CO_{2\text{-eq}}$ emissions and cost) is discussed for different transportation scenarios.

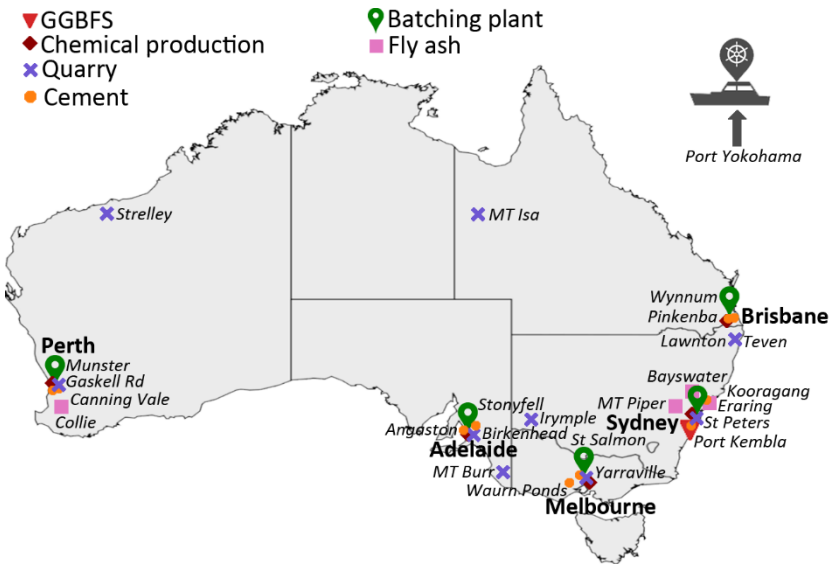

Fig. 4 Location of batching plants and material sources for geopolymer concrete in Australia

Table 4 Transportation distance and mode of source materials for the transport scenarios (adapted from Shobeiri et al. 2021).

Batching Plant	Case	GGBFS		FA		Quarry (Intrastate)	Chemical Products
Sydney		Port Kembla		Eraring Power Station		St Peters	Sydney-based provider
		Road (km)	Rail + road (km)	Road (km)	Rail + road (km)	Road (km)	Road (km)
	Min	95	89 + 3	124	127 + 12	7	28
		Port Yokohama		Collie Power Station		Teven	Perth-based provider
		Water (km)		Road (km)	Rail + road (km)	Road (km)	Road (km)
	Max	8021		3819	4540 + 74	731	3936
Melbourne		Port Kembla		Mt Piper Power Station		St Salmon	Melbourne-based provider
		Road (km)	Rail (km)	Road (km)	Rail + road (km)	Road (km)	Road (km)
	Min	845	973	835	1130 + 27	2	41
		Port Yokohama		Collie Power Station		Irymple	Perth-based provider
		Water (km)		Road (km)	Rail + road (km)	Road (km)	Road (km)
	Max	9088		3302	4131 + 71	543	3420
Adelaide		Port Kembla		Mt Piper Power Station		Stonyfell	Adelaide-based provider
		Road (km)	Rail + road (km)	Road (km)	Rail + road (km)	Road (km)	Road (km)
	Min	1370	1440 + 17	1280	1692 + 41	0.55	25
		Port Yokohama		Collie Power Station		Mt Burr	Perth-based provider

		Water (km)		Road (km)	Rail + road (km)	Road (km)	Road (km)
	Max	9792		2590	3303 + 85	419	2708
Perth		Port Kembla		Collie Power Station		Strelley	Perth-based provider
		Road (km)	Rail + road (km)	Road (km)	Rail + road (km)	Road (km)	Road (km)
	Min	3903	4441 + 21	219	188 + 92	13	10
		Port Yokohama		Eraring Power Station		Gaskell Rd	Brisbane-based provider
		Water (km)		Road (km)	Rail + road (km)	Road (km)	Road (km)
	Max	8317		3950	4479 + 30	1647	4302
Brisbane		Port Kembla		Bayswater Power Station		Lawnton	Brisbane - based provider
		Road (km)	Rail	Road (km)	Rail + road (km)	Road (km)	Road (km)
	Min	1035	1135	756	900 + 35	16	34
		Port Yokohama		Collie Power Station		Mt Isa	Perth-based provider
		Water (km)		Road (km)	Rail + road (km)	Road (km)	Road (km)
	Max	7278		4211	5588 + 71	1853	4329

Table 5 Different transport scenarios (adapted from Shobeiri et al. 2021).

Scenario	GGBFS (distance)	FA (distance)	Quarry (distance)	Chemical products (distance)
1	Min	Min	Min	Min
2	Max	Min	Min	Min
3	Min	Max	Min	Min
4	Max	Max	Min	Min
5	Min	Min	Max	Min
6	Max	Min	Max	Min
7	Min	Max	Max	Min
8	Max	Max	Max	Min
9	Min	Min	Min	Max
10	Max	Min	Min	Max
11	Min	Max	Min	Max
12	Max	Max	Min	Max
13	Min	Min	Max	Max
14	Max	Min	Max	Max
15	Min	Max	Max	Max
16	Max	Max	Max	Max

5 Results and discussion

In this section, the performance of the mix design tool in predicting mechanical properties including strength and slump is first discussed. The effects of binder and activator chemical composition and transport emissions on the optimal mix designs are then investigated in the context of single and multi-objective optimization.

5.1 Mix design tool performance: ANN

The mix design tool was evaluated considering two structural specifications: the base case where chemical compositions of binders and alkali activators are ignored, and a second case where chemical composition is considered to examine the effect on performance. The input mixture variables for the two cases are given in Table 6.

Table 6 Input mix variables with and without chemical compositions of binders and activators for ANN

Item No.	Without chemical compositions	With chemical compositions
1	Fine Aggregate (kg)	
2	Coarse Aggregate (kg)	
3	Total water (kg)	
4	Superplasticizer (kg)	
5	Age (day)	
6	Curing Temp (°C)	
7	Curing Time (day)	
8	Curing RH (%)	
9*	FA (kg)	
10*	GGBFS (kg)	
11*	Dried Na_2SiO_3 (kg)	
12*	Dried NaOH (kg)	
9#		Total SiO_2 (kg)
10#		Total Al_2O_3 (kg)
11#		Total Fe_2O_3 (kg)
12#		Total CaO (kg)
13#		Total Na_2O (kg)

indicates input only used for ANN base case (without chemical compositions)

 # indicates input only used for ANN second case (with chemical compositions)

Table 7 reports the performance of the ANN mix design tool in terms of the statistical indicators for the predictive performance on training, validation and test sets both with (left side) and without (right side) consideration of the chemical composition as inputs. To further show the goodness-of-fit, Fig. 5 shows the variation between the measured and predicted strength and slump for each mix in the database, broken down in terms of the training, validation and test sets. For completeness, Supplementary Material B reports the predictions errors for both cases. Considering the general performance summarized in Table 7 it can be seen that the *RMSE* improved up to 33% on the validation set and 35% on the test set for the compressive strength model and up to 53% on the validation set and 20% on the test set for the slump model when the chemical compositions are defined as inputs. This result shows that changing the input structure to reflect the breakdown of binders and alkali activators in terms of the chemical composition can significantly improve the performance of the mix design tool.

Table 7 Statistical results for ANN model with and without the chemical compositions of binders and alkali activators as inputs.

		With chemical compositions				**Without chemical compositions**			
Output	**Data set**	***RMSE***	***MAE***	R^2	***R***	***RMSE***	***MAE***	R^2	***R***
	Training	3.56	2.75	0.916	0.957	4.49	3.42	0.862	0.929

Compressive strength	**Validation**	3.93	3.12	0.888	0.942	5.84	4.33	0.736	0.858
	Test	4.15	3.42	0.868	0.931	6.41	5.00	0.692	0.832
Slump	**Training**	5.52	3.84	0.990	0.995	16.00	12.88	0.904	0.950
	Validation	9.99	7.58	0.961	0.980	21.60	16.26	0.893	0.944
	Test	14.50	11.67	0.893	0.944	18.20	14.62	0.856	0.925

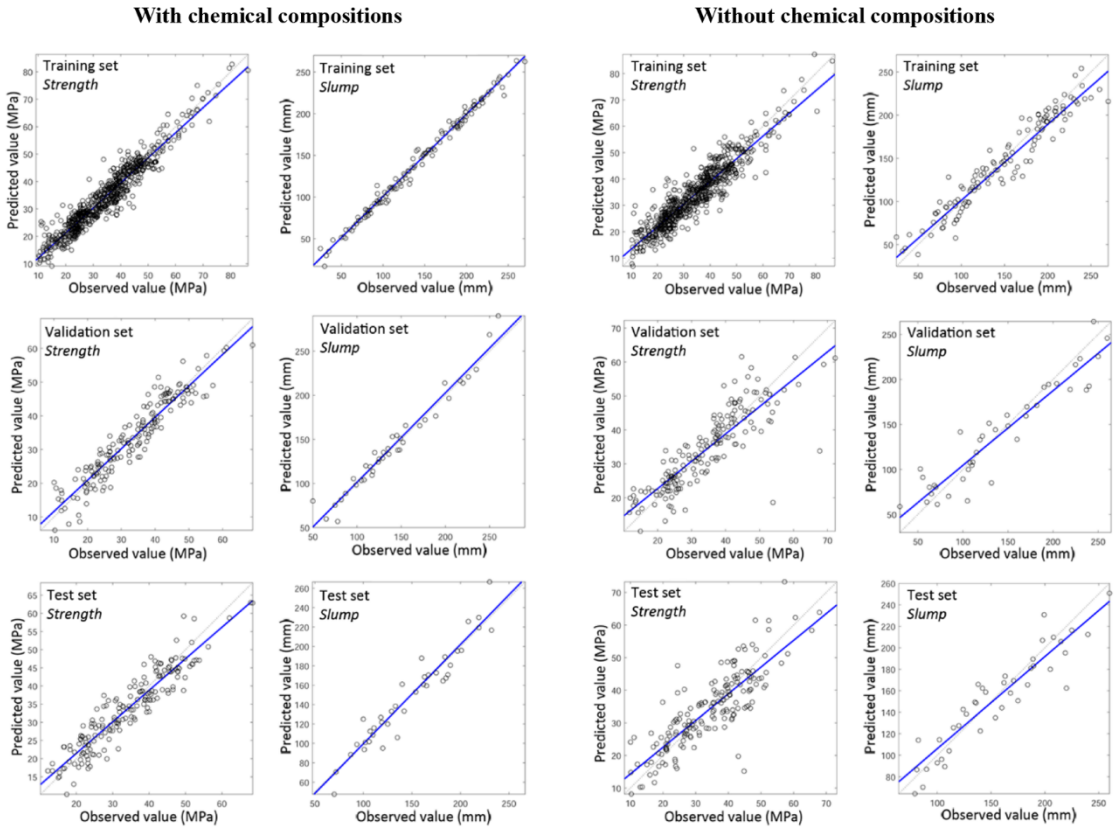

Fig. 5 Actual versus predicted compressive strength and slump for training set, test set and validation set with (left) and without (right) considering chemical compositions as inputs.

5.2 Scenario analysis

5.2.1 Scenario 1: sensitivity analysis of chemical compositions of binders

The optimal mix for oven and ambient cured GPC containing fly ash sourced from different power stations in Australia are shown in Fig. 6. It can be seen for both oven and ambient cured GPC that as compressive strength increases the fly ash quantities either remain constant or decrease while the quantity of GGBFS increases. This variation is because GGBFS is the primary source of calcium and a higher calcium content will generally increase both hydration and geopolymerization (Smith and Osborne 1977; Shi and Day 1999; Puertas et al., 2000; Nath and Sarker 2014).

As compressive strength increases no significant change in the coarse aggregate content is observed for either oven or ambient curing. The fine aggregate content can however be seen to decrease by up to 10% when the compressive strength increases from 25 MPa to 50 MPa under ambient curing conditions. This observation is likely because coarse-fine aggregate interactions (e.g. interlock effects) support higher strength in ambient cured GPC as a lower matrix strength is obtained in comparison to that when oven curing.
The extra water (which is the lowest contributor to $CO_{2\text{-eq}}$ emissions per unit per Table 2)

remains relatively constant for all compressive strengths for both oven and ambient curing and this is because it is being predominately used to maintain concrete slump which remains unchanged throughout the analysis. For ambient curing the mass of superplasticizer generally increases with increasing GGBFS content and strength. The bias towards superplasticizer addition is likely to correct the dilution of the activator caused by water addition would require an increase in activator content and the emissions associated with activator are significantly higher than those associated with superplasticizer.

For both oven and ambient cured concretes, the amount of sodium silicates and sodium hydroxide (the largest unit producers of $CO_{2\text{-eq}}$) are constant for most compressive strengths. However, for ambient cured GPC with compressive strengths above 45 MPa the mass of sodium hydroxide increases when there is a higher quantity of GGBFS and this is required to maintain workability (Xie et al. 2020).

When considering oven cured GPC, for almost all compressive strengths the quantity of fly ash increases as the proportion of SiO_2 (%) in the fly ash decreases. This observation can be explained by the need to increase the SiO_2 content in the overall mix design in order to make (semi-) crystalline polymer products which form the Si-O-Al and Si-O-Si bonds (Reddy et al. 2016; Xie et al. 2020). The inclusion of additional fly ash over additional sodium silicate can be explained by the significant difference in their emissions (sodium silicate is approximately 41 times more carbon-intensive than fly ash). The impact of this can be seen by comparing the mass of fly ash in the optimal mixtures sourced from Collie Power Station (i.e. the lowest SiO_2 content fly ash source, see barchart in Fig. 6) which has up to 30% more fly ash than the optimal mix if fly ash is sourced from Mt Piper Power Station (i.e. the highest SiO_2 content fly ash source, see barchart in Fig. 6).

Sodium silicates are another source of soluble silica in the mixture, although, the amount is typically minimized due to the more carbon-intensive nature of its production process (i.e. 41 times more carbon-intensive than fly ash). This above outcome is different to that observed for ambient cured GPC in which GGBFS is a more efficient silica and calcium source than fly ash. For instance, the optimal mixtures with fly ash sourced from Collie Power Station can have up to 70% more GGBFS than those sourced from Mt Piper Power Station for the compressive strength of 50 MPa. The reason for this is that an ambient cured GPC tends to use more GGBFS than fly ash as GGBFS spontaneously supports both hydration and geopolymerization.

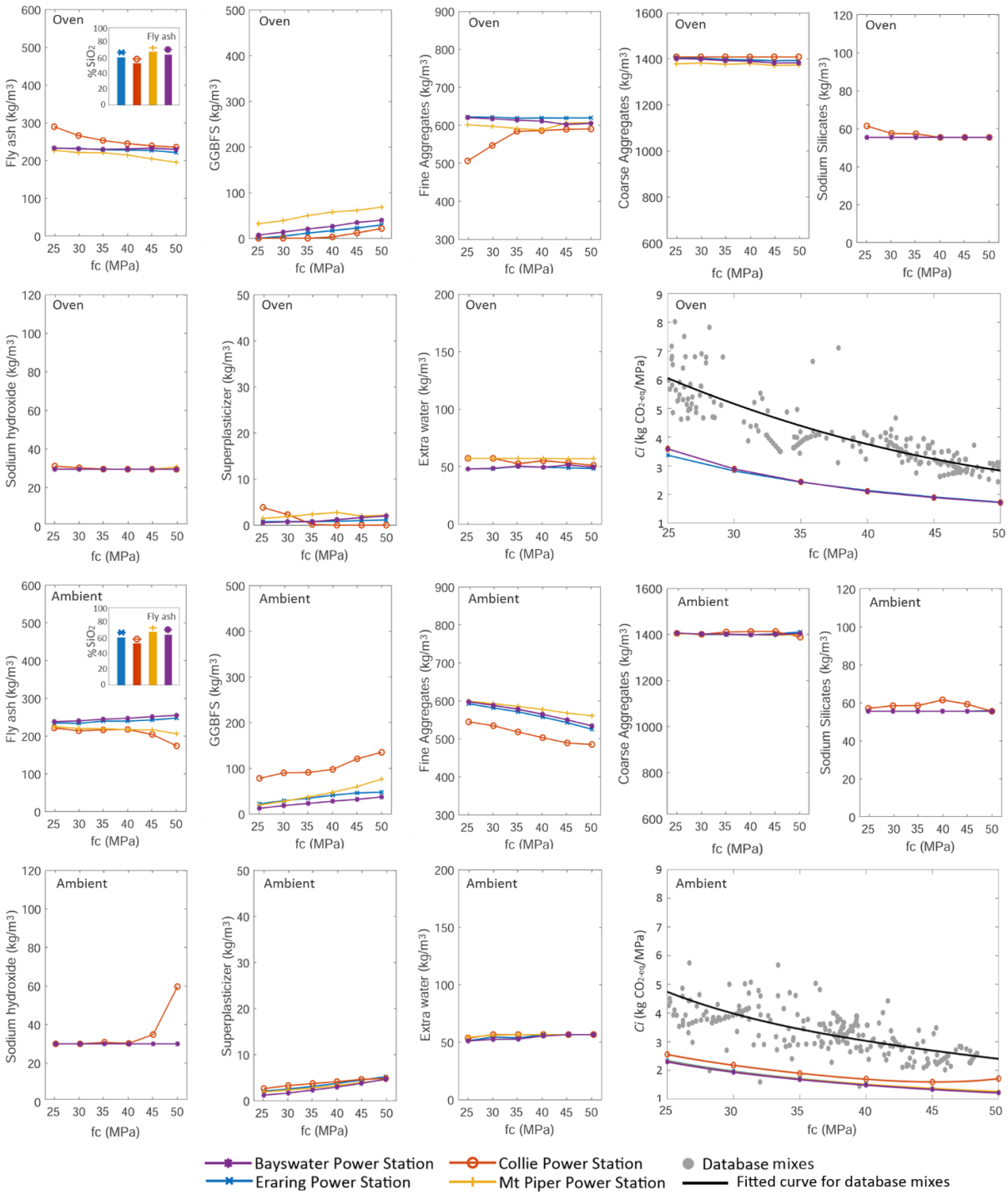

Fig. 6 Optimal mixtures of oven and ambient cured GPC considering fly ash sourced from different power stations and corresponding $CO_{2\text{-eq}}$ intensity indicator (C_i).

Fig. 6 compares the environmental performance of the experimental mix in the database and the simulated optimal mix using the $CO_{2\text{-eq}}$ intensity indicator (C_i), which is defined as the $CO_{2\text{-eq}}$ emissions of delivering one unit of compressive strength (Yang et al. 2013). For ambient curing, simulated optimal mixes have 47% less $CO_{2\text{-eq}}$ intensity than database mixes and for oven curing the optimal mixes have 33-44% less (depending on fly ash source) $CO_{2\text{-eq}}$ intensity than database mixes. The optimization framework generally produces mix designs with lower $CO_{2\text{-eq}}$ emissions. Although a few mix designs with lower $CO_{2\text{-eq}}$ emissions were identified by traditional methods in the database for ambient curing (see grey dots below colored regression

lines).

5.2.2 Scenario 2: sensitivity analysis of transportation

Figure 7 shows the optimal mixes for oven- and ambient- cured GPC with the road and rail transportation for batching plants in Sydney when the minimum and maximum transportation scenarios (transport scenarios 1 & 16 shown in Table 5) are considered (see Supplementary Material C for all transportation scenarios in all cities). Examining these figures shows that the emissions generated during the transport of a GPC binder significantly affect its use (i.e. mass) in the concrete mixture. That is, where a binder (either fly ash or GGBFS) emits more $CO_{2\text{-eq}}$ during its transportation the amount used is decreased to reduce overall $CO_{2\text{-eq}}$ emissions. For instance, for road transportation, the total emissions (sum of the transport and production emissions per kg) of fly ash to GGBFS can increase up to 6 times when the transport distance of all ingredients changes from minimum to maximum, which results in a greater amount of GGBFS than fly ash in the mixture (Fig. 7).

For oven cured GPC, as compressive strength increases, the mass of fly ash in mix designs that are based predominately on GGBFS increases considerably to increase the overall silica content. In contrast, the mass of GGBFS in mix designs which are predominately FA-based only increases slightly. For ambient cured concretes that are predominately GGBFS-based, as the target compressive strength increases, the fly ash content is further replaced with GGBFS to increase the calcium content.

It also appears from Fig. 7 for both ambient and oven cured GPC of all strengths and in all transportation cases that the optimal mix design is achieved by keeping the dry sodium silicate weight constant (as the minimum value in the database). The sodium silicates-to-sodium hydroxide ratio can then be seen to gradually decrease with an increase in compressive strength in predominately FA-based ambient cured concretes. This can be attributed to the fact that a reduction in sodium silicate to sodium hydroxide ratio can result in improved workability of the mix due to a decrease in the viscosity of alkali activators and a higher compressive strength arising from sodium oxide content (Xie et al. 2020; Shukla et al. 2020). Likewise, enhanced workability can also be seen in mixes that are predominately GGBFS based but have some fly ash, this is because the spherical shape of fly ash particles provides additional lubricant to enhance the rheological properties (Bondar et al. 2019, Rossow 2003). Similar trends in optimal mix design can also be seen in the other cities considered (see Supplementary Material C) and the differences in magnitude arise from the differences in transportation distances of source materials to the batching plants as shown in Table 4, and the varied chemical compositions of binders as shown in Table 3. For instance, the optimal oven cured mixtures in Melbourne contain more GGBFS than those in Perth when transportation distance of fly ash is minimum because the emissions per kg of GGBFS compared to fly ash is more for Perth than Melbourne.

In Fig. 7, it can also be seen that the transportation distances of fly ash and GGBFS are a significant influence on optimal mix design because they are the largest component of concrete by mass after aggregates, and they have the most impact on mechanical properties of concrete (Pasupath et al. 2021).

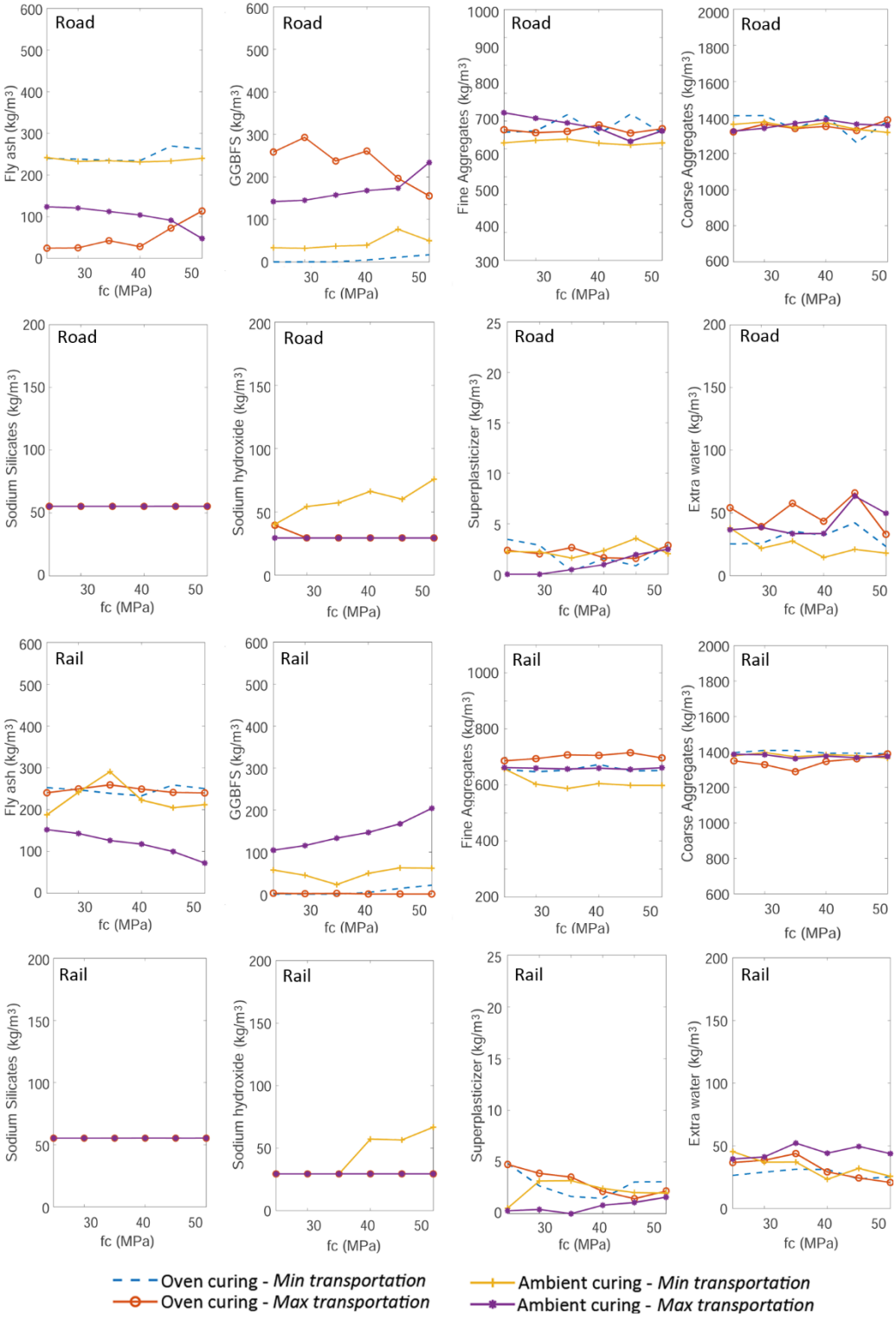

(1)

Fig. 7 Optimal mixes considering minimum and maximum transportation distance scenarios for oven and ambient cured GPC.

It can also be seen that when the transport distances of all ingredients are at their minimum, the difference between road and rail transport distances are small (see Table 4) and hence little variation in optimal mix design is observed (see Fig. 7). A more significant change is observed for oven cured concrete when considering the maximum transportation scenario for all ingredients. In this case the change from road to rail transportation causes GGBFS to become more highly emitting than fly ash, and as a result fly ash is preferred over GGBFS to minimise

emissions due to transport. Although the same trends can be observed in both ambient and oven cured GPC, this behaviour is less pronounced in ambient cured GPC because GGBFS is generally required to support both the hydration and geopolymerisation reactions required to meet the target strength (Xie et al. 2020).

Similar trends can also be seen in Supplementary Material D where the results for the remaining full set of transportation cases are presented. For example, optimal mixes in Melbourne and Brisbane are seen to have either more fly ash or GGBFS depending on the specific transportation distances, but in all transportation cases for Adelaide and Perth fly ash is preferred over GGBFS because of the emissions associated with long transport distances. This finding highlights the importance of transportation mode and distance when optimising mix design.

The $CO_{2\text{-eq}}$ intensities of optimal mix designs with road and rail transportation for all cities are shown in Fig. 8 when transport distance of all ingredients is either minimum or maximum (see Supplementary Material E for other transportation scenarios in all cities). It can be seen that, as expected, the optimal mixes for batching plants in Adelaide and Brisbane have respectively the lowest and highest $CO_{2\text{-eq}}$ intensity when the transport distances of all materials are maximum as they generally have the shortest and longest transport distances for maximum transportation distances of aggregates, fly ash and chemical components. Significantly, the total emissions per kg of GGBFS, fly ash and chemical products, for Sydney can be seen to increase by up to 2.5, 12, and 3 times, respectively, by a change from the minimum to maximum distances and up to 20 times for aggregates, given they are the primary component by mass of concrete. It is also evident that the optimal mixtures for batching plants in Adelaide and Perth have respectively the lowest and highest $CO_{2\text{-eq}}$ intensity as they generally have the shortest and longest transportation distances for maximum transportation distances of aggregates, fly ash and chemical components.

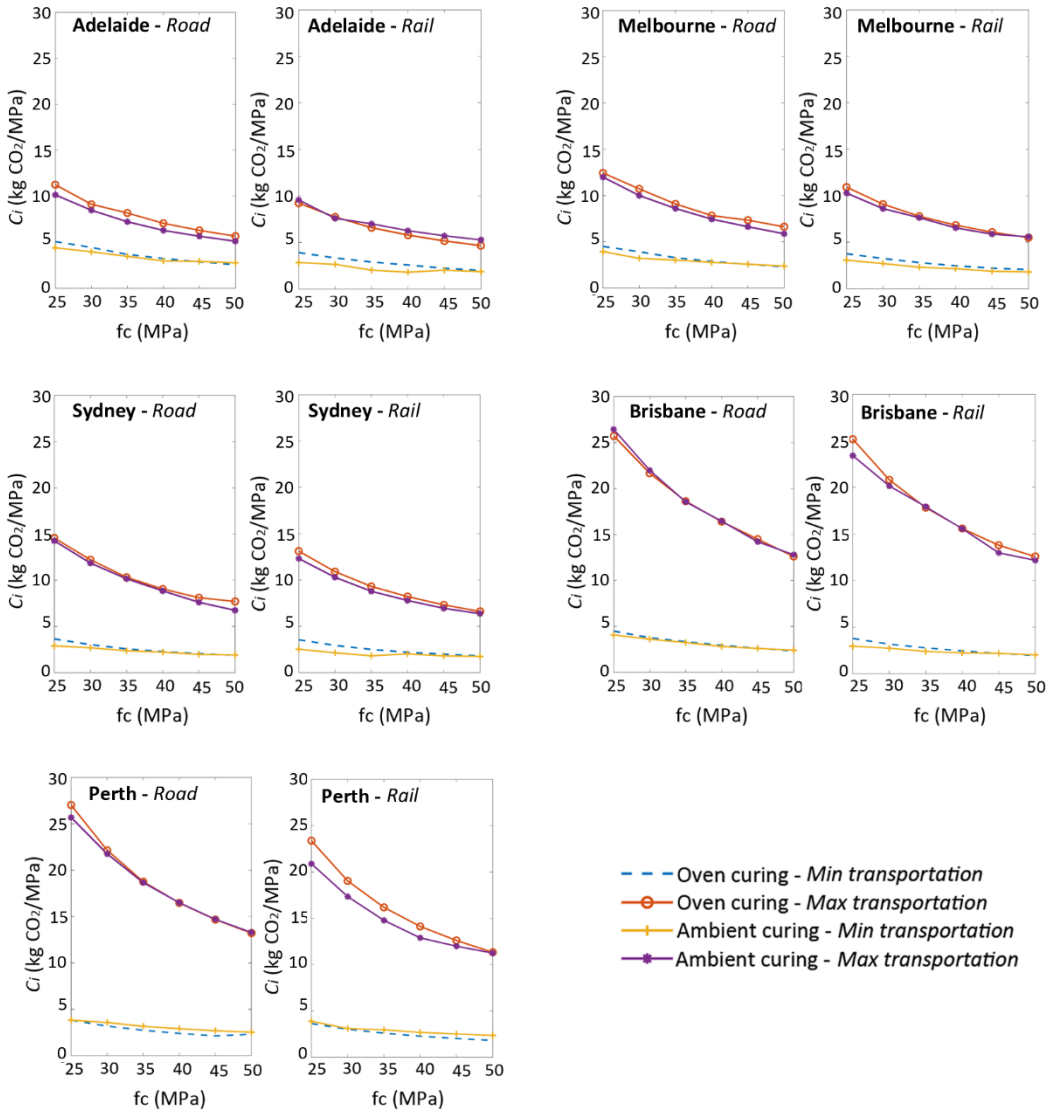

Fig. 8 $CO_{2\text{-eq}}$ intensity of optimal mixes for Adelaide, Melbourne, Sydney, Brisbane and Perth considering the minimum and maximum transportation distance scenarios for oven and ambient cured GPC for different transportation modes.

For the transportation sensitivity analysis, the only objective was to minimize $CO_{2\text{-eq}}$ emissions subject to the compressive strength and slump constraints. However, another key driver for the optimal mixtures of GPC is to minimize the cost since financial considerations can be a significant driver in construction projects. To address this, let us now consider minimizing both the $CO_{2\text{-eq}}$ emissions and cost as the objective functions while using the same compressive strength and slump as the constraints in the context of multi-objective optimisation.

Considering the sensitivity analysis for Sydney using road transportation, the TOPSIS technique is used to find the final optimal mixtures of oven curing from the Pareto optimal sets for each transportation distance case in Table 5 when the target compressive strength is 30 MPa and the target slump is 150 mm. The Pareto front sets for the optimal mixtures with different transportation cases are shown in Supplementary Material F, from which it can be seen that there is a strong relationship between the cost of production and $CO_{2\text{-eq}}$ emissions for all mixes, which indicates that for a given strength and slump, the $CO_{2\text{-eq}}$ emissions increase with an increase in the material cost. This link is likely a result of a more energy-intensive production

process or longer transportation distances.

The distribution of the final optimal mixes chosen by the TOPSIS for all transportation cases is illustrated in Fig. 9, from which it can be seen that while the contents of fine and coarse aggregates change slightly for all transportation cases, the contents of fly ash and GGBFS can change considerably depending on their local availability. Similarly, the contents of sodium silicates and sodium hydroxide can increase up to 25% by weight while extra water content can be tripled depending on the transportation distances of the source materials and required mechanical properties.

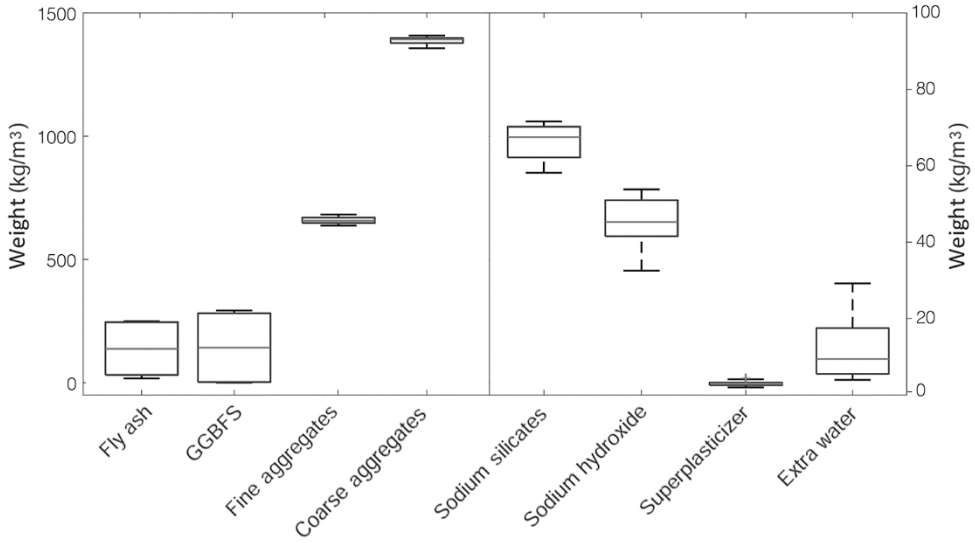

Fig. 9 Distribution of final optimal mixes within all transportation cases for Sydney.

The objective values for the final optimal mixtures with different transportation scenarios are shown in Fig. 10 where, as expected, a linear relationship with R^2 value of 0.93 can be seen between the mixture cost and $CO_{2\text{-eq}}$ emissions for all transportation cases. It can also be seen that those cases having the maximum transport distances for aggregates generate more $CO_{2\text{-eq}}$ and cost due to the higher volume of aggregates compared to other materials in the mixture. For instance, $CO_{2\text{-eq}}$ emissions and cost for cases 1, 2, 3, 4, 9, 10, 11, and 12 where the transport distance of aggregates is maximum is higher than those for other cases with minimum transport distance for aggregates. It is also clear that $CO_{2\text{-eq}}$ emissions and cost can increase up to 5 times when the transportation distances for all materials change from minimum (case 1) to maximum (case 16), showing the significance of transportation of source materials to the environmental and economic sustainability of optimal mixtures.

Importantly, when compared to the cases in which the only objective is the emissions minimization, the $CO_{2\text{-eq}}$ emissions from the optimal mixtures of the same strength, slump and transportation cases in Sydney can increase up to 30% when the emissions and cost are considered together as the objectives. The reason for this can be attributed to the Pareto optimality principle in which one objective cannot be improved without deteriorating the other objective (Ngatchou et al. 2005). For instance, the amount of sodium hydroxide can increase up to 80% when the objectives are the production cost and $CO_{2\text{-eq}}$ emissions together compared to when the single objective is the emissions minimization. The reason for this is that while sodium hydroxide is the largest contributor to the overall concrete $CO_{2\text{-eq}}$ emissions, it is not the most expensive GPC component (Table 2).

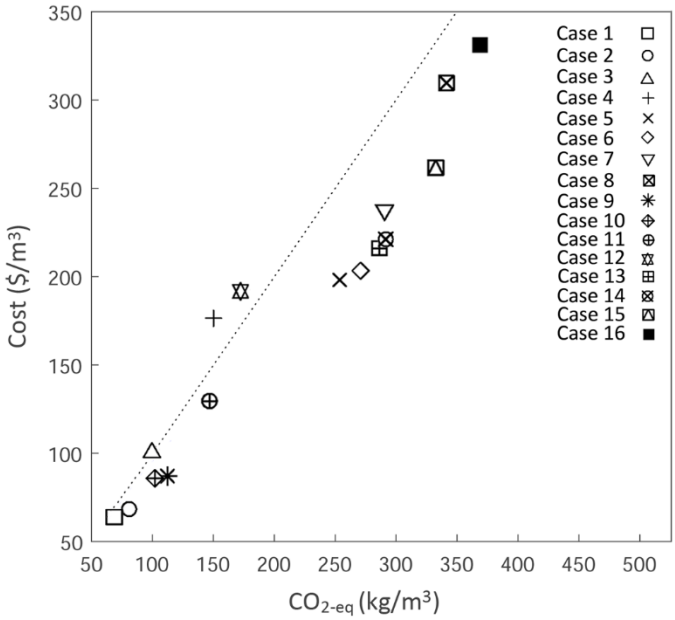

Fig. 10 Objective values for optimal mixtures with different transportation cases for Sydney

6 Conclusions

The optimisation of concrete mix design is becoming increasingly important. The task now extends beyond achieving low-cost concretes that meet the required material characteristics to now needing to also consider environmental impact. The proportioning of concretes, in particular those that rely on waste materials, is made challenging because not only is the ratio of mix components important, but so too is the underlying chemical composition of the materials. To improve concrete mix design, this paper has developed a generic framework for mix design optimisation based on a material design and profiling tool (incorporating financial and environmental models to predict cost and global warming potential) coupled with an optimisation algorithm.

The framework is implemented in this paper in the context of optimising geopolymer mix design using either a single or multi-objective GA that profiles materials with properties generated using an ANN trained, validated and tested using 1178 existing mix designs covering a broad range of binder and activator ingredients and chemical compositions. The mechanical properties of the concrete generated by the ANN are augmented with cost and global warming potential data generated by a simply sum product financial model and an existing life-cycle assessment tool developed specifically for geopolymer concrete.

Examination of the results has indicated the following major findings:

1. The use of an ANN to predict the compressive strength and slump of geopolymer concrete mix designs can be improved by between 33% and 53% if the chemical composition of the materials is used in place of material types (i.e. mass of critical oxides in fly ash in place of mass of fly ash).
2. Varying the source of binder material can significantly influence the mass of binder in the optimal mix design. For example, considering the optimal mix design when using fly ash with the lowest SiO_2 content compared to the highest SiO_2 content was shown to change the total mass of fly ash by up to 70%. This finding further shows the importance of considering the chemical composition of constituent materials rather than simply material type.

3. The results of transportation analysis for five major capital cities in Australia showed that the transportation distance and mode of GPC ingredients play a significant role in the optimal mixtures of oven and ambient cured GPC. It was shown that depending on the transport distance and mode of fly ash and GGBFS, optimal mixtures can either be FA-based GPC or GGBFS-based GPC and that the amount of fly ash and GGBFS with the same type of GPC (FA or GGBFS-based GPC) can change depending on their transportation distance and mode.
4. When minimising both the $CO_{2\text{-}eq}$ emissions and cost, a strong relationship between the mixture cost and $CO_{2\text{-}eq}$ emissions is observed for all the considered transportation cases. This finding indicates that $CO_{2\text{-}eq}$ emissions increase with an increase in the mixture cost because higher cost materials generally have either more energy-intensive manufacturing process or longer transportation distances.
5. It was also shown that for a given strength, slump and transportation case, the overall $CO_{2\text{-}eq}$ emissions can increase up to 30% when the $CO_{2\text{-}eq}$ emissions and production cost are considered together in the context of multi-objective optimization compared to when the single objective is the $CO_{2\text{-}eq}$ emissions minimization. This can be attributed to the Pareto Optimality principle in which an objective cannot be improved without deteriorating the other objective.

The above outcomes suggest that generic concrete mix design frameworks that can be locally calibrated to the chemical composition and transport distances of local materials should be developed rather than traditional mix design proportioning techniques that focus only on the broad definitions of material type.

Acknowledgments

Vahid Shobeiri was supported by an Australian Government Research Training Program Scholarship.

References

Abellán García, J., Fernández Gómez, J., & Torres Castellanos, N. (2020). Properties prediction of environmentally friendly ultra-high-performance concrete using artificial neural networks. European Journal of Environmental and Civil Engineering, 1-25.

Abellán, J., Fernández, J., Torres, N., & Núñez, A. (2020). Statistical optimization of ultra-high-performance glass concrete. ACI Materials Journal, 117(1), 243-254.

Afshari, H., Hare, W., & Tesfamariam, S. (2019). Constrained multi-objective optimization algorithms: Review and comparison with application in reinforced concrete structures. Applied Soft Computing, 83, 105631.

Albitar, M., Ali, M. M., Visintin, P., & Drechsler, M. (2017). Durability evaluation of geopolymer and conventional concretes. Construction and Building Materials, 136, 374-385.

Althnian, A., AlSaeed, D., Al-Baity, H., Samha, A., Dris, A. B., Alzakari, N., ... & Kurdi, H. (2021). Impact of dataset size on classification performance: an empirical evaluation in the medical domain. Applied Sciences, 11(2), 796.

Alyousef, R. A. M., Alabduljabbar, H. A. M., & El-Zeadani, M. (2020). Clean production and properties of geopolymer concrete; A review.

Amer, O. A., Rangaraju, P., & Rashidian-Dezfouli, H. (2022). Effectiveness of binary and ternary blended cements of class C fly ash and ground glass fibers in improving the durability of concrete. Journal of Sustainable Cement-Based Materials, 11(2), 181-195.

Arimanwa, M. C., Onwuka, D. O., & Arimanwa, J. I. (2016). Effect of Chemical Composition of Ordinary Portland cement on the Compressive Strength of Concrete. International refereed journal of Engineering and Science, 5(3), 20-31.

Asadollahfardi, G., Katebi, A., Taherian, P., & Panahandeh, A. (2019). Environmental life cycle assessment of concrete with different mixed designs. International Journal of Construction Management, 1-12.

Assi, L. N., Deaver, E. E., ElBatanouny, M. K., & Ziehl, P. (2016). Investigation of early compressive strength of fly ash-based geopolymer concrete. Construction and Building Materials, 112, 807-815.

Azad, N. M., & Samarakoon, S. M. (2021). Utilization of Industrial By-Products/Waste to Manufacture Geopolymer Cement/Concrete. Sustainability, 13(2), 873.

Bakharev, T. (2005). Durability of geopolymer materials in sodium and magnesium sulfate solutions. Cement and Concrete Research, 35(6), 1233-1246.

Bellum, R. R., Muniraj, K., & Madduru, S. R. C. (2020). Exploration of mechanical and durability characteristics of fly ash-GGBFS based green geopolymer concrete. SN Applied Sciences, 2, 1-10.

Bernal, S. A., Provis, J. L., De Gutiérrez, R. M., & van Deventer, J. S. (2015). Accelerated carbonation testing of alkali-activated slag/metakaolin blended concretes: effect of exposure conditions. Materials and Structures, 48(3), 653-669.

Bernal, S. A., Provis, J. L., Walkley, B., San Nicolas, R., Gehman, J. D., Brice, D. G., ... & van Deventer, J. S. (2013). Gel nanostructure in alkali-activated binders based on slag and fly ash, and effects of accelerated carbonation. Cement and Concrete Research, 53, 127-144.

Boindala, S. P., & Arunachalam, V. (2020). Concrete mix design optimization using a multi-objective cuckoo search algorithm. In Soft Computing: Theories and Applications (pp. 119-126). Springer, Singapore.

Bondar, D., Basheer, M., & Nanukuttan, S. (2019). Suitability of alkali activated slag/fly ash (AA-GGBS/FA) concretes for chloride environments: Characterisation based on mix design and compliance testing. Construction and Building Materials, 216, 612-621.

Bondar, D., Nanukuttan, S. V., Soutsos, M. N., Basheer, P. M., & Provis, J. L. (2017, January). Suitability of alkali activated GGBS/Fly ash concrete for chloride environments. In ACI Special Publications (Vol. 320, No. SP 320, pp. 35-1). American Concrete Institute.

British Standards Institution (2013). BS EN 206: Concrete – Specification, performance, production and conformity, London, 2013.

Chen, Hongyu, Tingting Deng, Ting Du, Bin Chen, Miroslaw J. Skibniewski, and Limao Zhang. "An RF and LSSVM–NSGA-II method for the multi-objective optimization of high-performance concrete durability." Cement and Concrete Composites (2022): 104446.

Cheng, M. Y., Prayogo, D., & Wu, Y. W. (2014). Novel genetic algorithm-based evolutionary support vector machine for optimizing high-performance concrete mixture. Journal of Computing in Civil Engineering, 28(4), 06014003.

Chinchuluun, A., & Pardalos, P. M. (2007). A survey of recent developments in multiobjective optimization. Annals of Operations Research, 154(1), 29-50.

Chindaprasirt, P., & Chalee, W. (2014). Effect of sodium hydroxide concentration on chloride penetration and steel corrosion of fly ash-based geopolymer concrete under marine site. Construction and Building Materials, 63, 303-310.

Chithambaram, S. J., Kumar, S., Prasad, M. M., & Adak, D. (2018). Effect of parameters on the compressive strength of fly ash based geopolymer concrete. Structural Concrete, 19(4), 1202-1209.

Cho, Y. K., Jung, S. H., & Choi, Y. C. (2019). Effects of chemical composition of fly ash on compressive strength of fly ash cement mortar. Construction and Building Materials, 204, 255-264.

Coolidge, F. (2012). An introduction to correlation and regression. Statistics: A Gentle Introduction, 211-267.

Dan, S., & Barai, S. V. (2014, August). Sustainable concrete mix—Design: Evolutionary algorithm approach. In 2014 International Conference on Data Science & Engineering (ICDSE) (pp. 94-99). IEEE.

Dao, D. V., & Trinh, S. H. (2020). Design method for optimizing geopolymer concrete proportions utilising entirely steel slag aggregates. In CIGOS 2019, Innovation for Sustainable Infrastructure (pp. 459-464). Springer, Singapore.

Demuth, H., Beale, M., Hagan, M. 2009. Neural Network Toolbox™ 6 User's Guide. The MathWorks Inc., New York

De Munck, M., De Sutter, S., Verbruggen, S., Tysmans, T., & Coelho, R. F. (2015). Multi-objective weight and cost optimization of hybrid composite-concrete beams. Composite Structures, 134, 369-377.

DeRousseau, M. A., Kasprzyk, J. R., & Srubar III, W. V. (2018). Computational design optimization of concrete mixtures: A review. Cement and Concrete Research, 109, 42-53.

Diaz-Loya, E. I., Allouche, E. N., & Vaidya, S. (2011). Mechanical properties of fly-ash-based geopolymer concrete. ACI materials journal, 108(3), 300.

Dreiseitl, S., & Ohno-Machado, L. (2002). Logistic regression and artificial neural network classification models: a methodology review. Journal of biomedical informatics, 35(5-6), 352-359.

Filipovic, N. (2019). Computational Modeling in Bioengineering and Bioinformatics. Academic Press.

Freight rates in Australia (2017). Bureau of Infrastructure, Transport and Regional Economics. https://www.bitre.gov.au/publications/2017/is_090

Gen, M., & Cheng, R. (1999). Genetic algorithms and engineering optimization (Vol. 7). John Wiley & Sons.

Glosser, D., Choudhary, A., Isgor, O. B., & Weiss, W. J. (2019). Investigation of reactivity of fly ash and its effect on mixture properties. ACI Materials Journal, 116(4), 193-200.

Golafshani, E. M., & Behnood, A. (2019). Estimating the optimal mix design of silica fume concrete using biogeography-based programming. Cement and Concrete Composites, 96, 95-105.

Gursel, A.P. (2014). Life-cycle Assessment of Concrete: Decision-Support Tool and Case Study Application (UC Berkeley).

Habibi, A., & Ghomashi, J. (2018). Development of an optimum mix design method for self-compacting concrete based on experimental results. Construction and Building Materials, 168, 113-123.

Hardjito, D., & Rangan, B. V. (2005). Development and properties of low-calcium fly ash-based geopolymer concrete.

Hardjito, D., Wallah, S. E., Sumajouw, D. M., & Rangan, B. V. (2004). On the development of fly ash-based geopolymer concrete. Materials Journal, 101(6), 467-472.

Hashemi, M., Shafigh, P., Karim, M. R. B., & Atis, C. D. (2018). The effect of coarse to fine aggregate ratio on the fresh and hardened properties of roller-compacted concrete pavement. Construction and Building Materials, 169, 553-566.

Hassan, A., Arif, M., & Shariq, M. (2019). Use of geopolymer concrete for a cleaner and sustainable environment–A review of mechanical properties and microstructure. Journal of cleaner production, 223, 704-728.

Heath, A., Paine, K., & McManus, M. (2014). Minimising the global warming potential of clay based geopolymers. Journal of cleaner production, 78, 75-83.

Heaton, B. S., Down, F. W., & Emery, J. J. (1981). Properties of Ground Granulated Slags in Cement Blends. In The Second Australian Conference on Engineering Materials, held at Sydney, July 6-8, 1981.

Jayaram, M. A., Nataraja, M. C., & Ravikumar, C. N. (2009). Elitist genetic algorithm models: optimization of high performance concrete mixes. Materials and Manufacturing Processes, 24(2), 225-229.

Jiang, X., Xiao, R., Bai, Y., Huang, B., & Ma, Y. (2022). Influence of waste glass powder as a supplementary cementitious material (SCM) on physical and mechanical properties of cement paste under high temperatures. Journal of Cleaner Production, 130778.

Jiang, X., Xiao, R., Zhang, M., Hu, W., Bai, Y., & Huang, B. (2020). A laboratory investigation of steel to fly ash-based geopolymer paste bonding behavior after exposure to elevated temperatures. Construction and Building Materials, 254, 119267.

Karen, P. (2016). Assessing the Fit of Regression Models. Manitab.com. Retrieved 28th Aug.

Khan, A., Do, J., & Kim, D. (2016). Cost effective optimal mix proportioning of high strength self-compacting concrete using response surface methodology. Computers and Concrete, 17(5), 629-638.

Karthik, S., & Mohan, K. S. R. (2021). A taguchi approach for optimizing design mixture of geopolymer concrete incorporating fly ash, ground granulated blast furnace slag and silica fume. Crystals, 11(11), 1279.

Kayabekir, A. E., Arama, Z. A., Bekdaş, G., Nigdeli, S. M., & Geem, Z. W. (2020). Eco-friendly design of reinforced concrete retaining walls: multi-objective optimization with harmony search applications. Sustainability, 12(15), 6087.

Khan, M. S. H., Castel, A., & Noushini, A. (2017). Carbonation of a low-calcium fly ash geopolymer concrete. Magazine of Concrete Research, 69(1), 24-34.

Khankhaje, E., Hussin, M. W., Mirza, J., Rafieizonooz, M., Salim, M. R., Siong, H. C., & Warid, M. N. M. (2016). On blended cement and geopolymer concretes containing palm oil fuel ash. Materials & Design, 89, 385-398.

Kumar, S., Kumar, R., Alex, T. C., Bandopadhyay, A., & Mehrotra, S. P. (2007). Influence of reactivity of fly ash on geopolymerisation. Advances in Applied Ceramics, 106(3), 120-127.

Kwon, S. J., & Wang, X. Y. (2019). Optimization of the mixture design of low-CO2 high-strength concrete containing silica fume. Advances in Civil Engineering, 2019.

Kwon, S. J., & Wang, X. Y. (2019). Optimization of the mixture design of low-CO2 high-strength concrete containing silica fume. Advances in Civil Engineering, 2019.

Law, D. W., Adam, A. A., Molyneaux, T. K., Patnaikuni, I., & Wardhono, A. (2015). Long term durability properties of class F fly ash geopolymer concrete. Materials and Structures, 48(3), 721-731.

Lee, B. Y., Kim, J. H., & Kim, J. K. (2009). Optimum concrete mixture proportion based on a database considering regional characteristics. Journal of Computing in Civil Engineering, 23(5), 258-265.

Lee, H. S., Lim, S. M., & Wang, X. Y. (2019). Optimal Mixture Design of Low-CO 2 High-Volume Slag Concrete Considering Climate Change and CO 2 Uptake. International Journal of Concrete Structures and Materials, 13(1), 1-13.

Lee, J. H., Yoon, Y. S., & Kim, J. H. (2012). A new heuristic algorithm for mix design of high-performance concrete. KSCE Journal of Civil Engineering, 16(6), 974-979.

Lee, S. C. (2003). Prediction of concrete strength using artificial neural networks. Engineering structures, 25(7), 849-857.

Li, Z., Lu, D., & Gao, X. (2020). Optimization of mixture proportions by statistical experimental design using response surface method-A review. Journal of Building Engineering, 102101.

Lim, C. H., Yoon, Y. S., & Kim, J. H. (2004). Genetic algorithm in mix proportioning of high-performance concrete. Cement and Concrete Research, 34(3), 409-420.

Liu, Q. F., Iqbal, M. F., Yang, J., Lu, X. Y., Zhang, P., & Rauf, M. (2021). Prediction of chloride diffusivity in concrete using artificial neural network: Modelling and performance evaluation. Construction and Building Materials, 268, 121082.

M. S.H.K. (2011) Standard Deviation. In: Lovric M. (Eds) International Encyclopedia of Statistical Science. Springer, Berlin, Heidelberg. https://doi.org/10.1007/978-3-642-04898-2_535

McLellan, B. C., Williams, R. P., Lay, J., Van Riessen, A., & Corder, G. D. (2011). Costs and carbon emissions for geopolymer pastes in comparison to ordinary Portland cement. Journal of cleaner production, 19(9-10), 1080-1090.

Méndez, M., Frutos, M., Miguel, F., & Aguasca-Colomo, R. (2020). Topsis decision on approximate Pareto fronts by using evolutionary algorithms: Application to an engineering design problem. Mathematics, 8(11), 2072.

Mohamed, S., & Tayeb, B. (2019). Effect of coarse aggregates and sand contents on workability and static stability of self-compacting concrete. Advances in concrete construction, 7(2), 97.

Mohamed, S., Nuruddin, F., Halim, N. S. A., & Kamal, S. A. (2011). Compressive Strength and Workability of Blended and Unblended Self Compacting Geopolymer Concrete.

Naderpour, H., Rafiean, A. H., & Fakharian, P. (2018). Compressive strength prediction of environmentally friendly concrete using artificial neural networks. Journal of Building Engineering, 16, 213-219.

Nagalia, G., Park, Y., Abolmaali, A., & Aswath, P. (2016). Compressive strength and microstructural properties of fly ash–based geopolymer concrete. Journal of Materials in Civil Engineering, 28(12), 04016144.

Naseri, H. (2019). Cost optimization of no-slump concrete using genetic algorithm and particle swarm optimization. International Journal of Innovation, Management and Technology, 10(1), 33-37.

Naseri, H., Jahanbakhsh, H., Hosseini, P., & Nejad, F. M. (2020). Designing sustainable concrete mixture by developing a new machine learning technique. Journal of Cleaner Production, 258, 120578.

Nath, P., & Sarker, P. K. (2014). Effect of GGBFS on setting, workability and early strength properties of fly ash geopolymer concrete cured in ambient condition. Construction and Building materials, 66, 163-171.

Nath, P., Sarker, P.K., 2014. Effect of GGBFS on setting, workability and early strength properties of fly ash geopolymer concrete cured in ambient condition. Construct. Build. Mater. 66, 163-171

Neupane, K., Chalmers, D., & Kidd, P. (2018). High-strength geopolymer concrete-properties, advantages and challenges. Advances in Materials, 7(2), 15-25.

Ngatchou, P., Zarei, A., & El-Sharkawi, A. (2005, November). Pareto multi objective optimization. In Proceedings of the 13th International Conference on, Intelligent Systems

Application to Power Systems (pp. 84-91). IEEE.

Ngu, L. N., Wu, H., & Zhang, D. K. (2007). Characterization of ash cenospheres in fly ash from Australian power stations. Energy & Fuels, 21(6), 3437-3445.

Noguchi, T., Maruyama, I., & Kanematsu, M. (2003, May). Performance based design system for concrete mixture with multi-optimizing genetic algorithm. In Proceedings of the 11th international congress on the chemistry of cement "Cements Contribution to the Development in the 21st Century", Durban.

Nunez, I., Marani, A., & Nehdi, M. L. (2020). Mixture Optimization of Recycled Aggregate Concrete Using Hybrid Machine Learning Model. Materials, 13(19), 4331.

Nuruddin, M. F., Demie, S., & Shafiq, N. (2011). Effect of mix composition on workability and compressive strength of self-compacting geopolymer concrete. Canadian Journal of Civil Engineering, 38(11), 1196-1203.

Öztaş, A., Pala, M., Özbay, E., Kanca, E., Caglar, N., & Bhatti, M. A. (2006). Predicting the compressive strength and slump of high strength concrete using neural network. Construction and building materials, 20(9), 769-775.

Pan, Z., Sanjayan, J. G., & Rangan, B. V. (2011). Fracture properties of geopolymer paste and concrete. Magazine of concrete research, 63(10), 763-771.

Park, W. (2013). Genetic-algorithm-based mix proportion design method for recycled aggregate concrete. Transactions of the Canadian Society for Mechanical Engineering, 37(3), 345-354.

Passuello, A., Rodríguez, E. D., Hirt, E., Longhi, M., Bernal, S. A., Provis, J. L., & Kirchheim, A. P. (2017). Evaluation of the potential improvement in the environmental footprint of geopolymers using waste-derived activators. Journal of Cleaner Production, 166, 680-689.

Pasupathy, K., Berndt, M., Castel, A., Sanjayan, J., & Pathmanathan, R. (2016). Carbonation of a blended slag-fly ash geopolymer concrete in field conditions after 8 years. Construction and Building Materials, 125, 661-669.

Pasupathy, K., Berndt, M., Sanjayan, J., Rajeev, P., & Cheema, D. S. (2017). Durability of low-calcium fly ash based geopolymer concrete culvert in a saline environment. Cement and Concrete Research, 100, 297-310.

Pasupathy, K., Sanjayan, J., & Rajeev, P. (2021). Evaluation of alkalinity changes and carbonation of geopolymer concrete exposed to wetting and drying. Journal of Building Engineering, 35, 102029.

Provis, J. L. (2018). Alkali-activated materials. Cement and Concrete Research, 114, 40-48.

Prusa, J., Khoshgoftaar, T. M., & Seliya, N. (2015, December). The effect of dataset size on training tweet sentiment classifiers. In 2015 IEEE 14th International Conference on Machine Learning and Applications (ICMLA) (pp. 96-102). IEEE.

Puertas, F., Martínez-Ramírez, S., Alonso, S., & Vázquez, T. (2000). Alkali-activated fly ash/slag cements: strength behaviour and hydration products. Cement and concrete research,

30(10), 1625-1632.

Ramujee, K., & PothaRaju, M. (2017). Mechanical properties of geopolymer concrete composites. Materials Today: Proceedings, 4(2), 2937-2945.

Rani, D., Jain, S. K., Srivastava, D. K., & Perumal, M. (2013). Genetic algorithms and their applications to water resources systems. Metaheuristics in Water, Geotechnical and Transport Engineering, 43.

Reddy, M. S., Dinakar, P., & Rao, B. H. (2016). A review of the influence of source material's oxide composition on the compressive strength of geopolymer concrete. Microporous and Mesoporous Materials, 234, 12-23.

Rodríguez, F., Florez-Tapia, A. M., Fontán, L., & Galarza, A. (2020). Very short-term wind power density forecasting through artificial neural networks for microgrid control. Renewable energy, 145, 1517-1527.

Rossow, M. (2003). Fly Ash Facts for Highway Engineers. New York NY Continuing Education and Development.

Ryu, G. S., Ahn, G. H., Koh, K. T., & Lee, J. H. (2013). Compressive Strength Properties of Fly Ash-based Geopolymer Concrete. In Advanced Materials Research (Vol. 741, pp. 49-54). Trans Tech Publications Ltd.

Sadrossadat, E., Basarir, H., Karrech, A., & Elchalakani, M. (2021). Multi-objective mixture design and optimisation of steel fiber reinforced UHPC using machine learning algorithms and metaheuristics. Engineering with Computers, 1-14.

Sarkar, A., Rano, R., Udaybhanu, G., & Basu, A. K. (2006). A comprehensive characterisation of fly ash from a thermal power plant in Eastern India. Fuel Processing Technology, 87(3), 259-277.

Salas, D. A., Ramirez, A. D., Ulloa, N., Baykara, H., & Boero, A. J. (2018). Life cycle assessment of geopolymer concrete. Construction and Building Materials, 190, 170-177.

Sangwan, K. S. (2020). Environmental impact assessment of fly ash and silica fume based geopolymer concrete. Journal of Cleaner Production.

Shahmansouri, A. A., Bengar, H. A., & Ghanbari, S. (2020). Compressive strength prediction of eco-efficient GGBS-based geopolymer concrete using GEP method. Journal of Building Engineering, 101326.

Sharifi, E., Sadjadi, S. J., Aliha, M. R. M., & Moniri, A. (2020). Optimization of high-strength self-consolidating concrete mix design using an improved Taguchi optimization method. Construction and Building Materials, 236, 117547.

Shi, C., & Day, R. L. (1995). Acceleration of the reactivity of fly ash by chemical activation. Cement and Concrete Research, 25(1), 15-21.

Shi, C., & Day, R. L. (1999). Early strength development and hydration of alkali-activated blast furnace slag/fly ash blends. Advances in Cement Research, 11(4), 189-196.

Shi, C., Wu, Z., Lv, K., & Wu, L. (2015). A review on mixture design methods for self-compacting concrete. Construction and Building Materials, 84, 387-398.

Shobeiri, V., Bennett, B., Xie, T., & Visintin, P. (2021). A comprehensive assessment of the global warming potential of geopolymer concrete. Journal of Cleaner Production, 297, 126669.

Smith, M. A., & Osborne, G. J. (1977). Slag/fly ash cements. World Cement Technology, 8(6).

Song, K. I., Song, J. K., Lee, B. Y., & Yang, K. H. (2014). Carbonation characteristics of alkali-activated blast-furnace slag mortar. Advances in Materials Science and Engineering, 2014.

Teh, S. H., Wiedmann, T., Castel, A., & de Burgh, J. (2017). Hybrid life cycle assessment of greenhouse gas emissions from cement, concrete and geopolymer concrete in Australia. Journal of Cleaner Production, 152, 312-320.

The MathWorks, Inc. (2020a) Neural Network Toolbox, Natick, Massachusetts, United State. Available at: https://au.mathworks.com/help/deeplearning/ref/nftool.html

The MathWorks, Inc. (2020b) Optimisation Toolbox, Natick, Massachusetts, United State. Available at: https://au.mathworks.com/help/optim.

Turner, L. K., & Collins, F. G. (2013). Carbon dioxide equivalent (CO2-e) emissions: A comparison between geopolymer and OPC cement concrete. Construction and Building Materials, 43, 125-130.

UNESCO. Reinforced Concrete: An International Manual. London: Butterworths, 1971, p. 20.

Vinothkumar, A., Kalaivani, M., & Easwaran, P. (2019). Development of Fly ash-GGBS based Self Compacting Geopolymer Concrete: a Review. International Research Journal of Multidisciplinary Technovation, 1(6), 373-377.

Vora, P. R., & Dave, U. V. (2013). Parametric studies on compressive strength of geopolymer concrete. Procedia Engineering, 51, 210-219.

Wang, X. Y. (2019). Impact of Climate Change on the Optimization of Mixture Design of Low-CO2 Concrete Containing Fly Ash and Slag. Sustainability, 11(12), 3394.

Wang, X. Y. (2019). Simulation for optimal mixture design of low-CO2 high-volume fly ash concrete considering climate change and CO2 uptake. Cement and Concrete Composites, 104, 103408.

Wang, X. Y. (2020). Optimal mix design of low-CO2 blended concrete with limestone powder. Construction and Building Materials, 263, 121006.

Wedatalla, A. M., Jia, Y., & Ahmed, A. A. (2019). Curing effects on high-strength concrete properties. Advances in Civil Engineering, 2019.

Williams, R. P., & Van Riessen, A. (2010). Determination of the reactive component of fly ashes for geopolymer production using XRF and XRD. Fuel, 89(12), 3683-3692.

Wong, H. D. (2013). Cylinder Strength versus Cube Strength. In Standing Committee on Concrete Technology Annual Concrete Seminar, CEDD, Hong Kong.

Xiao, R., Jiang, X., Zhang, M., Polaczyk, P., & Huang, B. (2020a). Analytical investigation of phase assemblages of alkali-activated materials in CaO-SiO2-Al2O3 systems: The management of reaction products and designing of precursors. Materials & Design, 194, 108975.

Xiao, R., Ma, Y., Jiang, X., Zhang, M., Zhang, Y., Wang, Y., ... & He, Q. (2020b). Strength, microstructure, efflorescence behavior and environmental impacts of waste glass geopolymers cured at ambient temperature. Journal of Cleaner Production, 252, 119610.

Xiao, R., Jiang, X., Wang, Y., He, Q., & Huang, B. (2021a). Experimental and thermodynamic study of alkali-activated waste glass and calcium sulfoaluminate cement blends: shrinkage, efflorescence potential, and phase assemblages. Journal of Materials in Civil Engineering, 33(11), 04021312.

Xiao, R., Zhang, Y., Jiang, X., Polaczyk, P., Ma, Y., & Huang, B. (2021b). Alkali-activated slag supplemented with waste glass powder: Laboratory characterization, thermodynamic modelling and sustainability analysis. Journal of Cleaner Production, 286, 125554.

Xiao, R., Huang, B., Zhou, H., Ma, Y., & Jiang, X. (2022). A state-of-the-art review of crushed urban waste glass used in OPC and AAMs (geopolymer): Progress and challenges. Cleaner Materials, 100083.

Xie, T., Visintin, P., Zhao, X., & Gravina, R. (2020). Mix design and mechanical properties of geopolymer and alkali activated concrete: Review of the state-of-the-art and the development of a new unified approach. Construction and Building Materials, 256, 119380.

Xie, T., & Zhao, X. (2022). A mix-design procedure for alkali-activated concrete based on the concept of reactive modulus. In *Handbook of Advances in Alkali-Activated Concrete* (pp. 15-40). Woodhead Publishing.

Yaman, M. A., Abd Elaty, M., & Taman, M. (2017). Predicting the ingredients of self-compacting concrete using artificial neural network. Alexandria Engineering Journal, 56(4), 523-532.

Yang, K. H., Song, J. K., & Song, K. I. (2013). Assessment of CO2 reduction of alkali-activated concrete. Journal of Cleaner Production, 39, 265-272.

Yang, X. S. (2020). Nature-inspired optimization algorithms. Academic Press.

Yeh, I. C. (2007). Computer-aided design for optimum concrete mixtures. Cement and Concrete Composites, 29(3), 193-202.

Yu, J., Li, X., Fleming, D., Meng, Z., Wang, D., & Tahmasebi, A. (2012). Analysis on characteristics of fly ash from coal fired power stations. Energy Procedia, 17, 3-9.

Yu, M., Wiedmann, T., Crawford, R., & Tait, C. (2017). The carbon footprint of Australia's construction sector. Procedia engineering, 180, 211-220.

Zhang, Y., Gong, H., Jiang, X., Lv, X., Xiao, R., & Huang, B. (2021). Environmental impact assessment of pavement road bases with reuse and recycling strategies: A comparative study on geopolymer stabilized macadam and conventional alternatives. Transportation Research Part D: Transport and Environment, 93, 102749.

Zhang, J., Huang, Y., Ma, G., & Nener, B. (2021a). Mixture optimization for environmental, economical and mechanical objectives in silica fume concrete: A novel frame-work based on machine learning and a new meta-heuristic algorithm. Resources, Conservation and Recycling, 167, 105395.

Zhang, J., Huang, Y., Wang, Y., & Ma, G. (2020). Multi-objective optimization of concrete mixture proportions using machine learning and metaheuristic algorithms. Construction and Building Materials, 253, 119208.

Zhang, Z., Wang, H., & Provis, J. L. (2012). Quantitative study of the reactivity of fly ash in geopolymerization by FTIR. Journal of Sustainable Cement-Based Materials, 1(4), 154-166.

Zhang, Z., Zhu, Y., Yang, T., Li, L., Zhu, H., & Wang, H. (2017). Conversion of local industrial wastes into greener cement through geopolymer technology: A case study of high-magnesium nickel slag. Journal of Cleaner Production, 141, 463-471.

Zhao, J., Tong, L., Li, B., Chen, T., Wang, C., Yang, G., & Zheng, Y. (2021). Eco-friendly geopolymer materials: A review of performance improvement, potential application and sustainability assessment. Journal of Cleaner Production, 307, 127085.

Zhuguo, L. I., & Sha, L. I. (2018). Carbonation resistance of fly ash and blast furnace slag based geopolymer concrete. Construction and Building Materials, 163, 668-680.

Supplementary Material A: Sensitivity on the compressive strength constraint

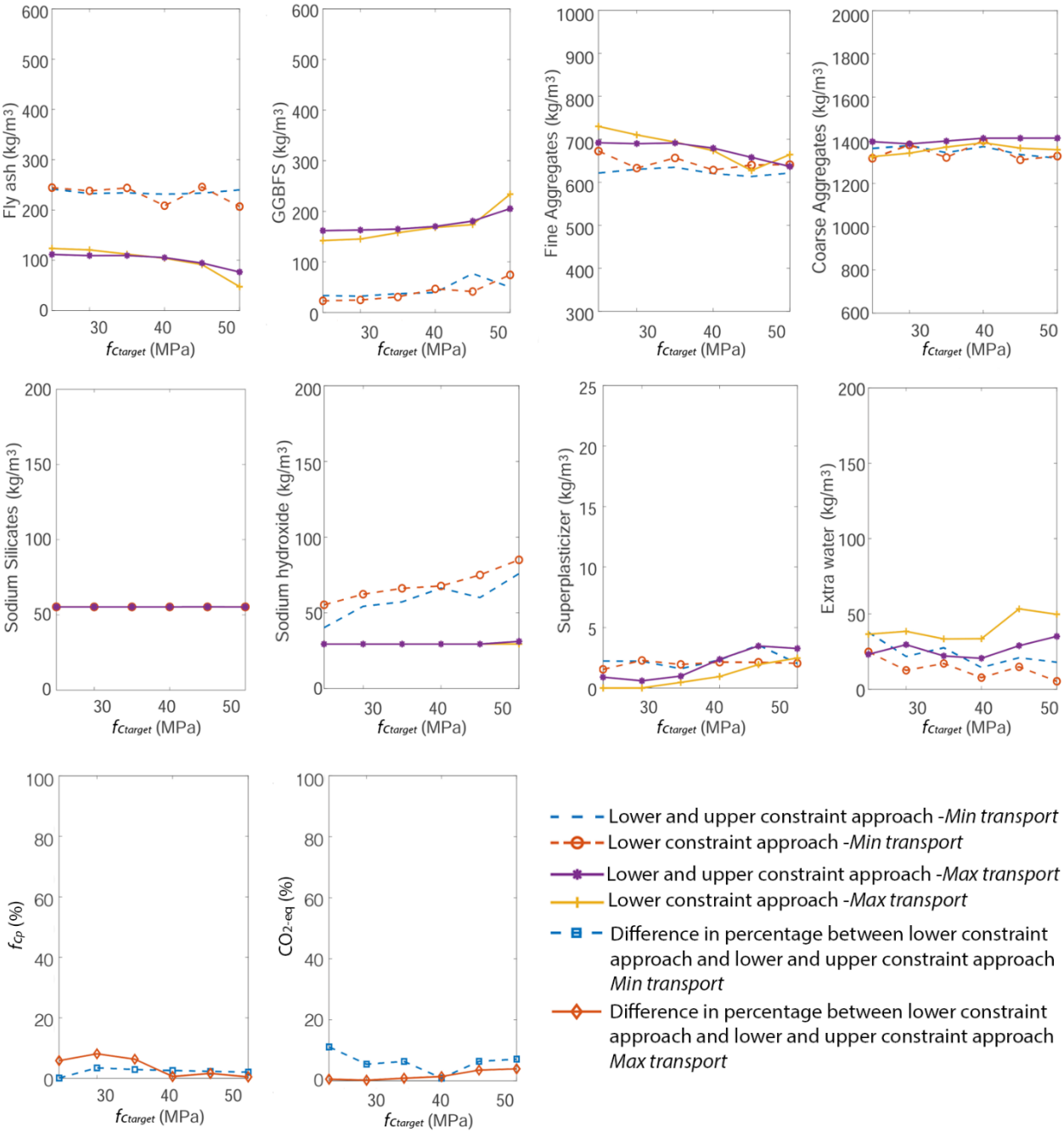

Fig. A-1 The effects of considering or relaxing the upper strength constraint on the optimum mix designs, and their strength and $CO_{2\text{-eq}}$ emissions considering minimum and maximum transportation distances in Sydney

Supplementary Material B: Mix design tool performance

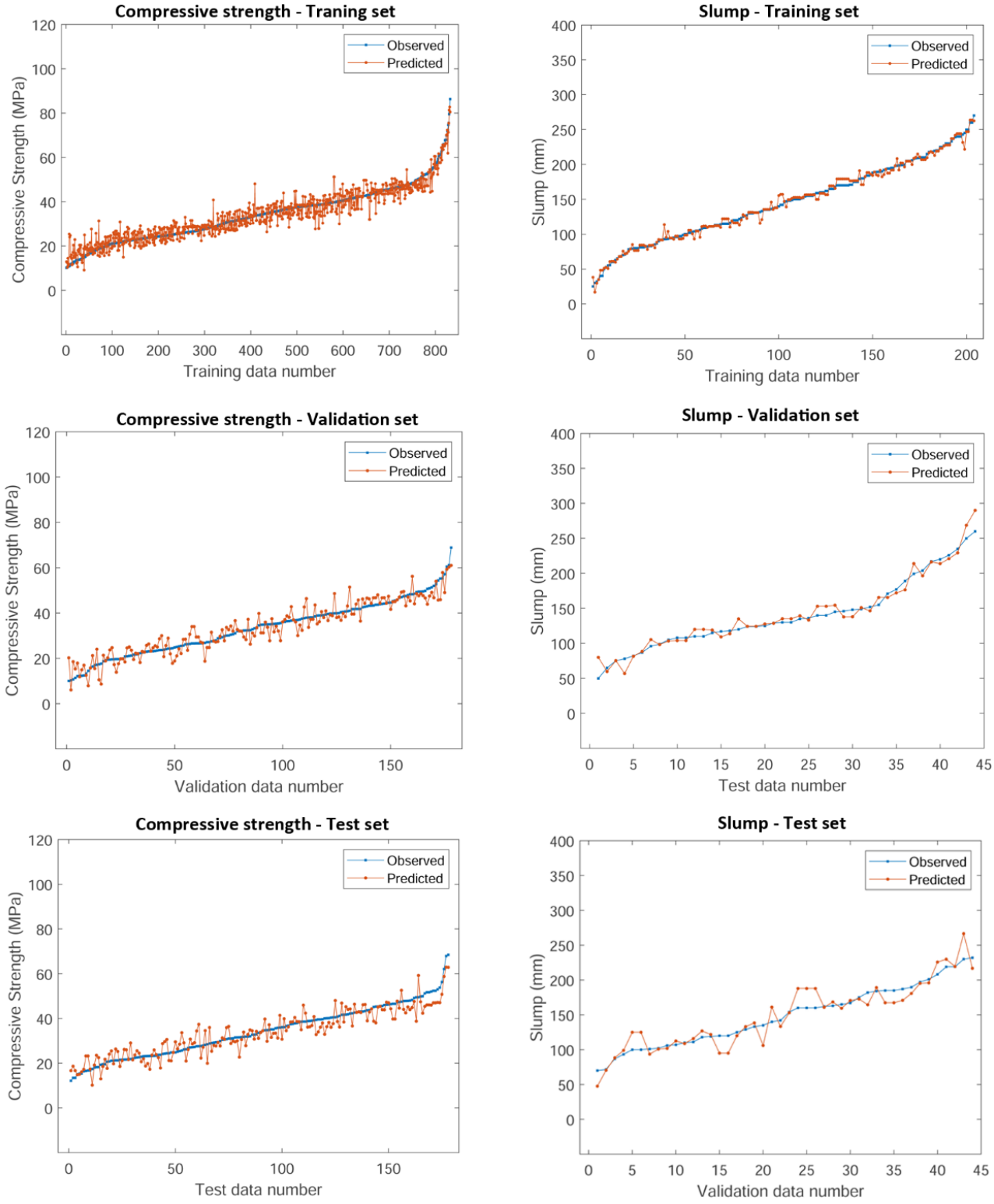

Fig. B-1 Prediction errors of compressive strength and slump for training set, test set and validation set considering chemical compositions as inputs

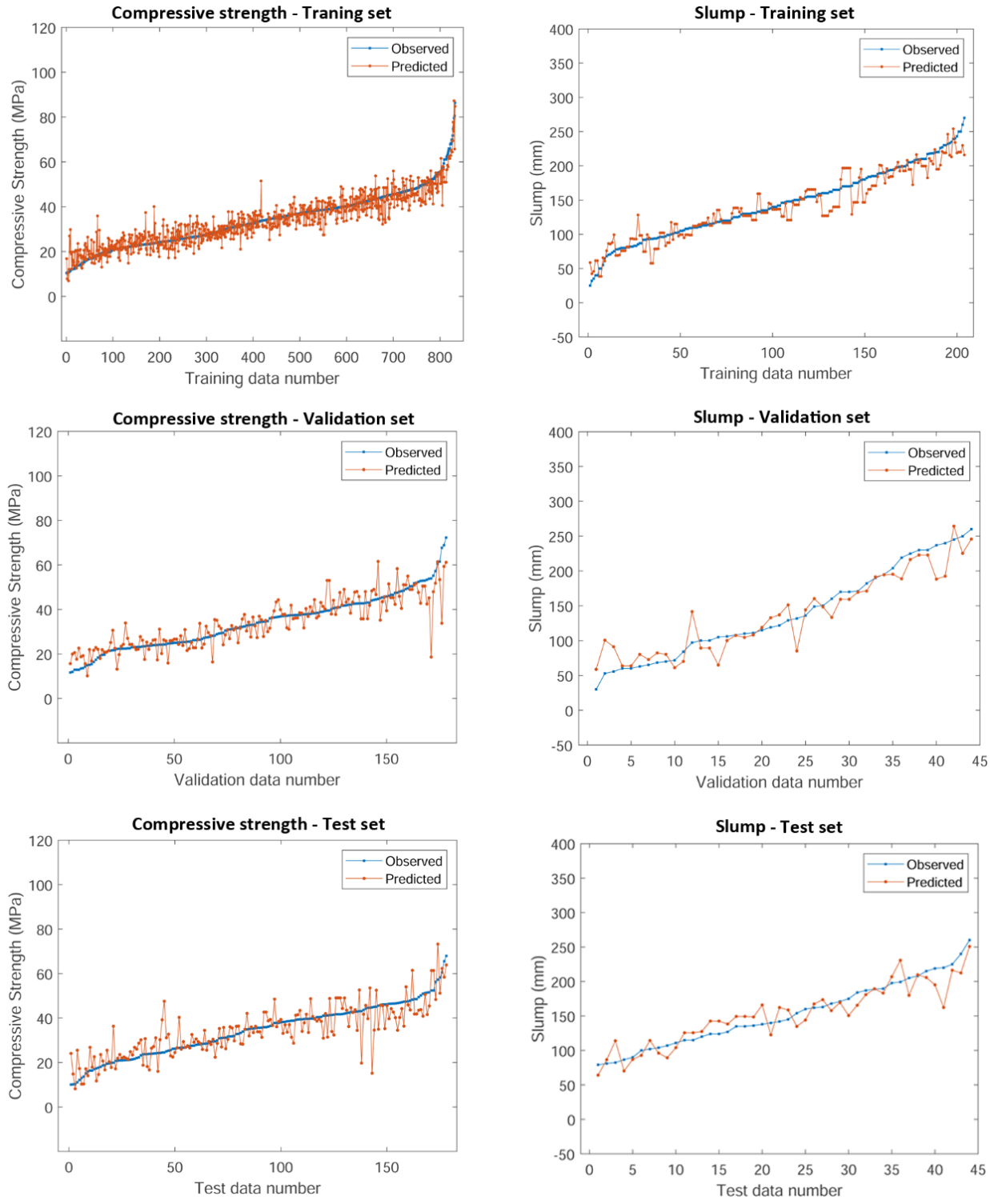

Fig. B-2 Prediction errors of compressive strength and slump for training set, test set and validation set ignoring chemical compositions as inputs.

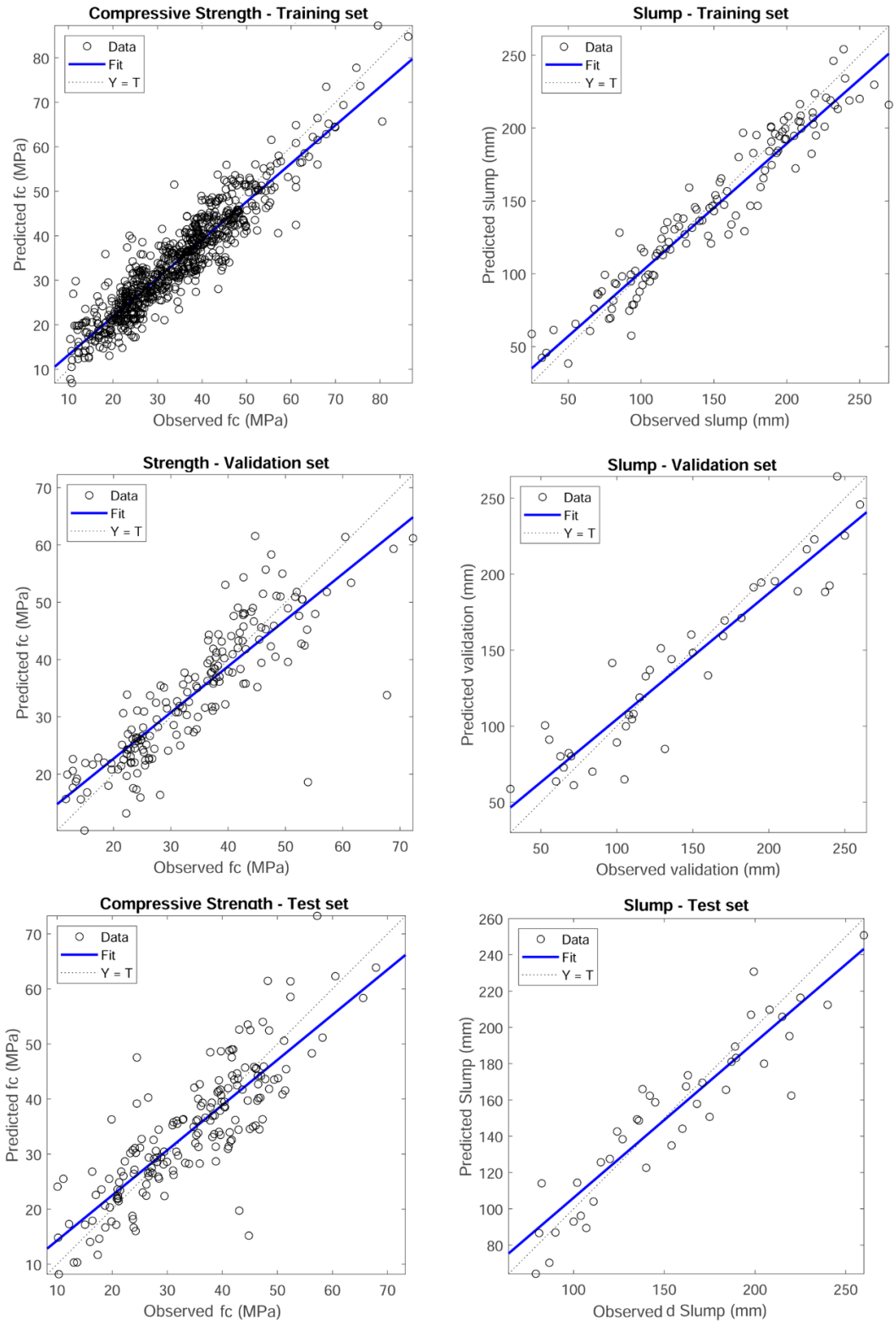

Fig. B-3 Actual versus predicted compressive strength and slump for training set, test set and validation set ignoring chemical compositions as inputs.

Supplementary Material C: Scenario 2: sensitivity analysis of transportation (sea & road)

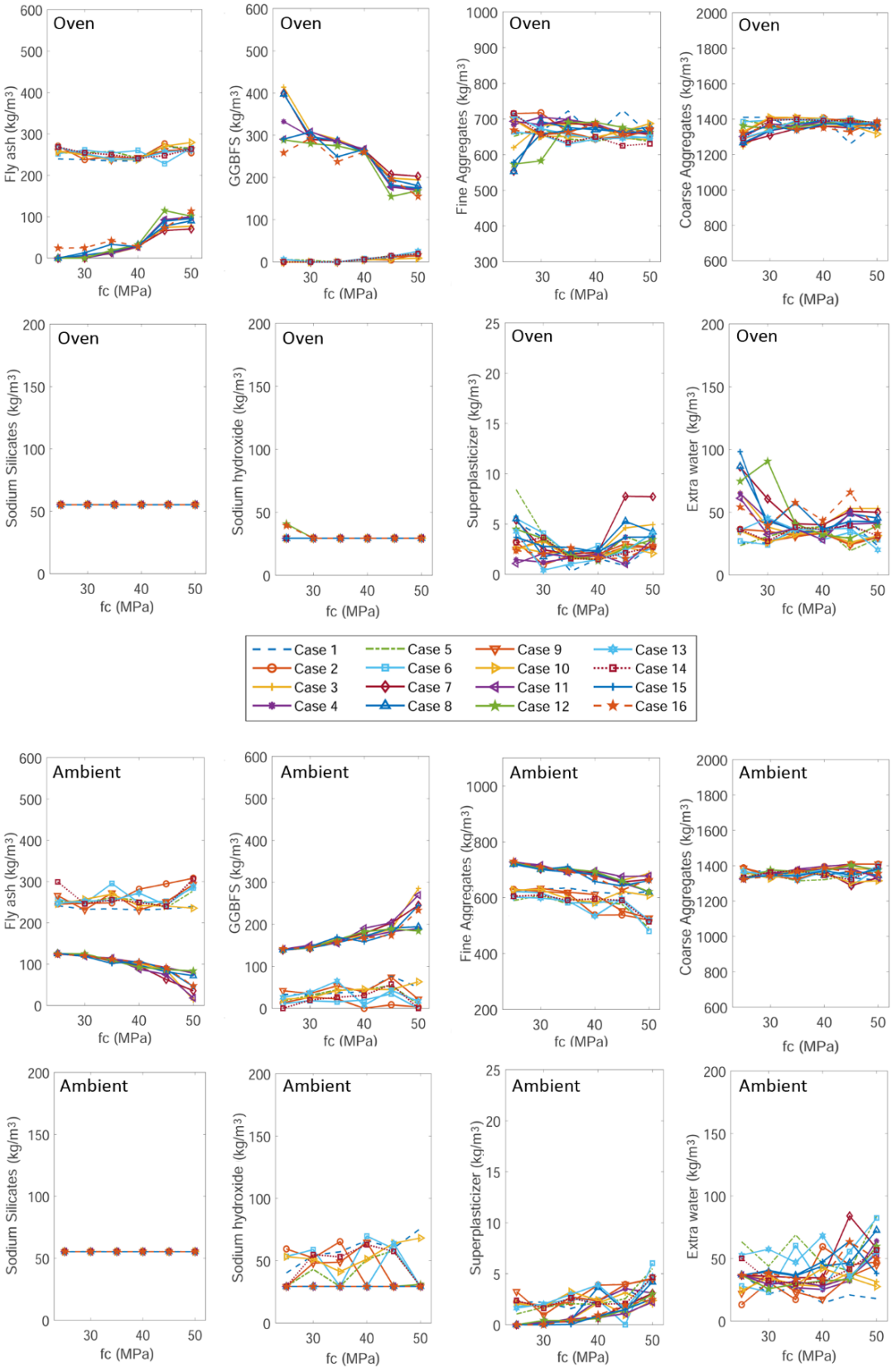

Fig. C-1 Optimal mixtures considering sensitivity analysis of sea and road transportation for batching plants in Sydney

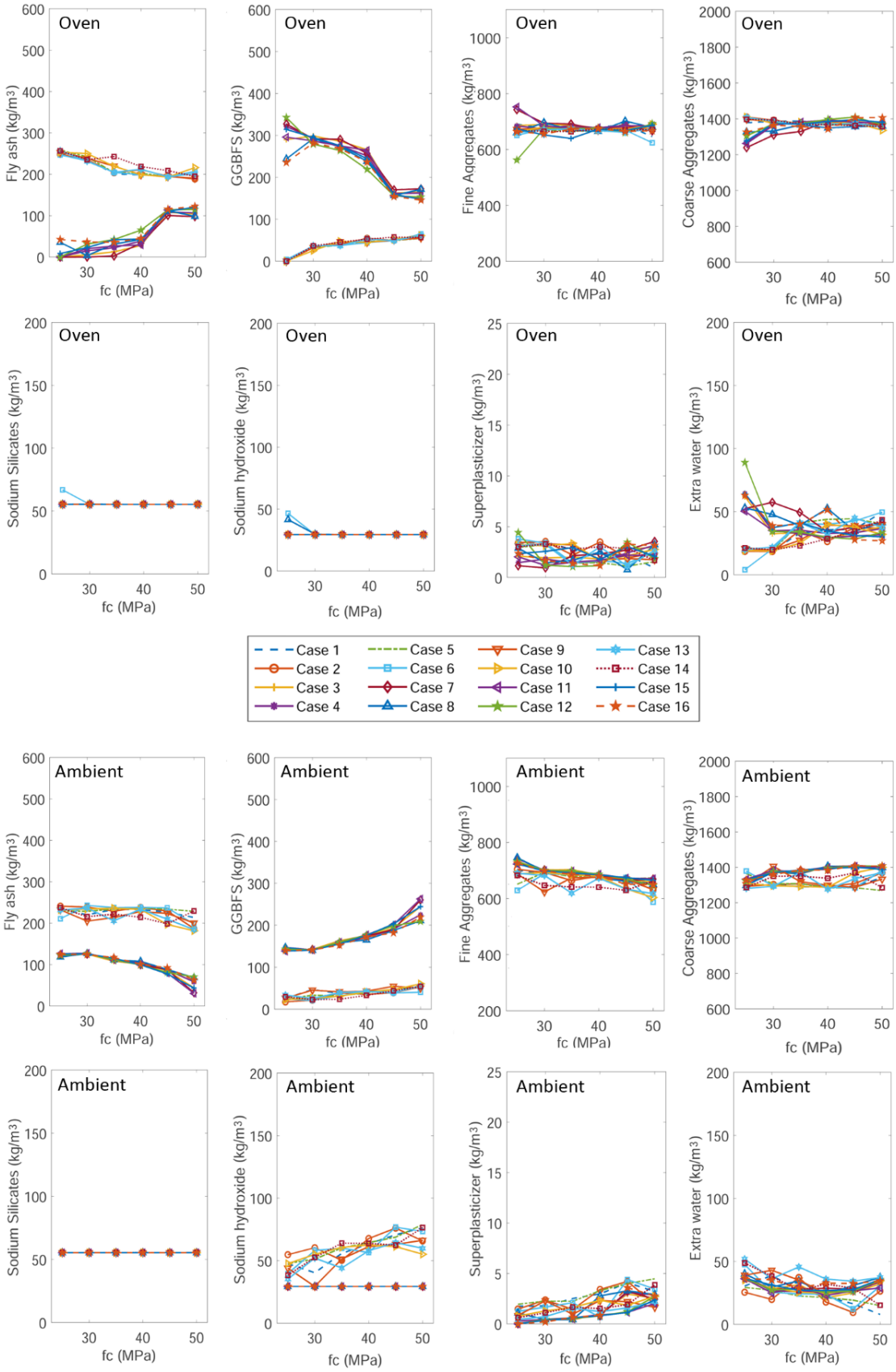

Fig. C-2 Optimal mixes considering sensitivity analysis of sea and road transportation for batching plants in Melbourne

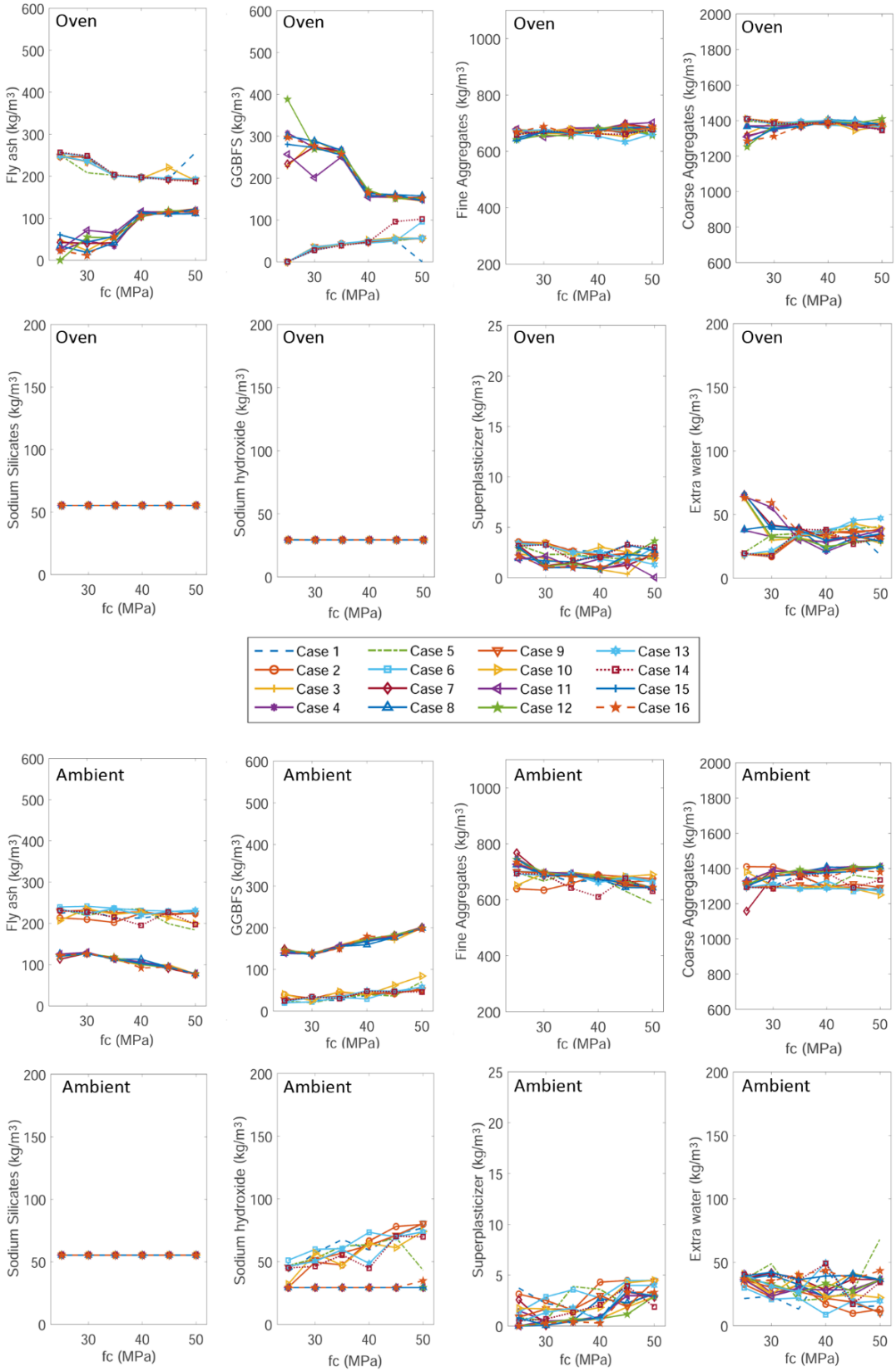

Fig. C-3 Optimal mixes considering sensitivity analysis of sea and road transportation for batching plants in Adelaide

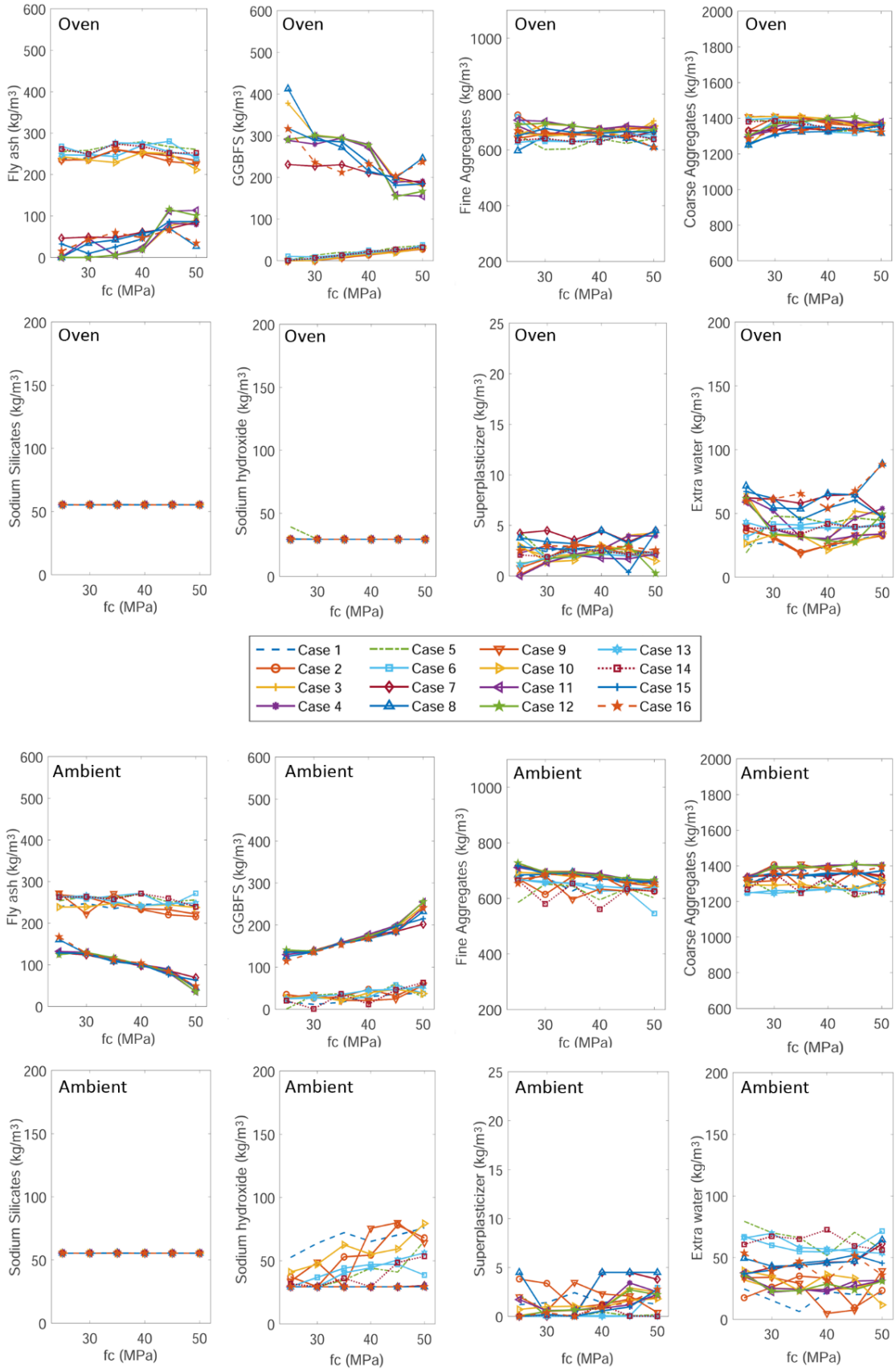

Fig. C-4 Optimal mixes considering sensitivity analysis of sea and road transportation for batching plants in Brisbane

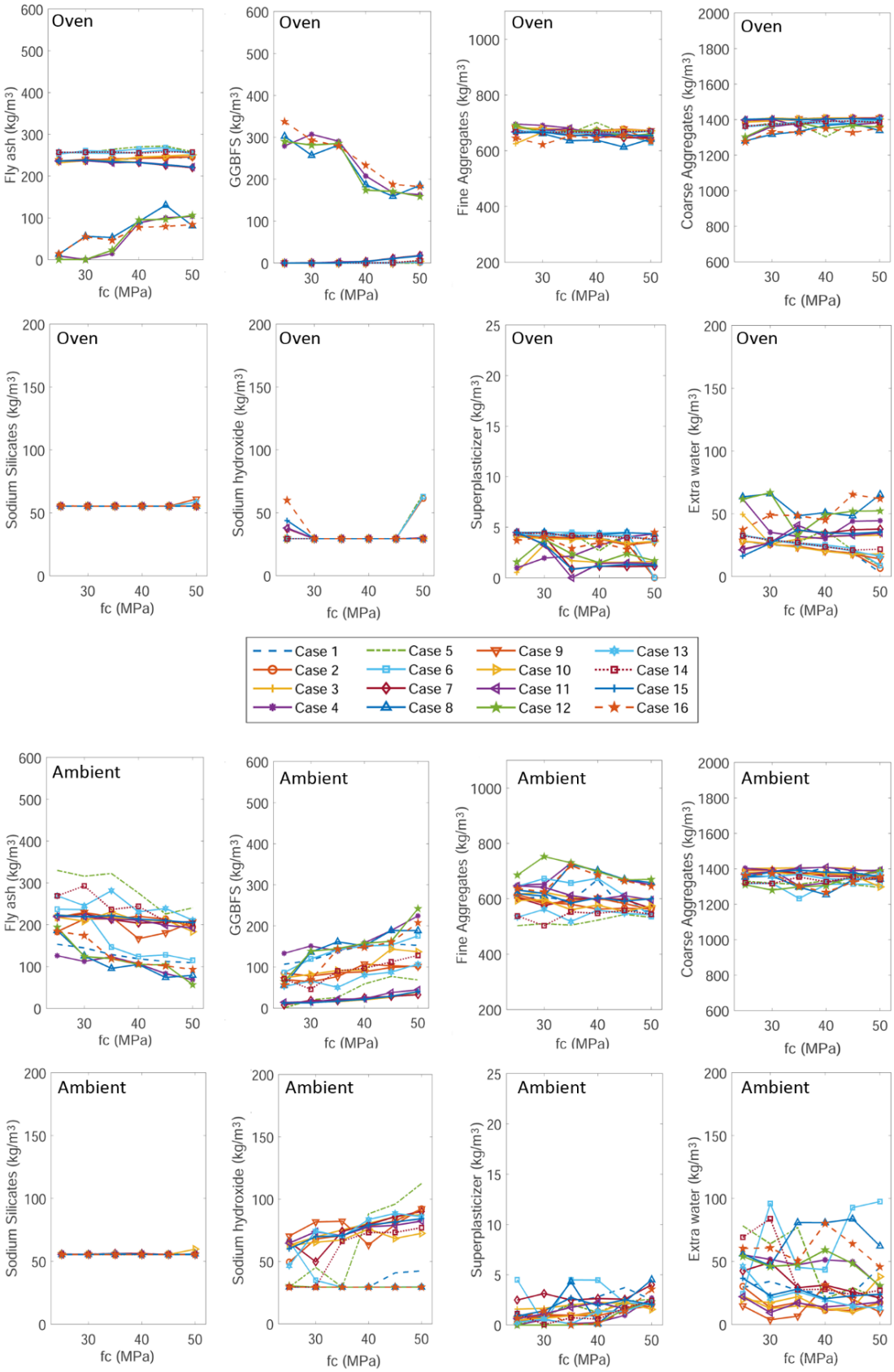

Fig. C-5 Optimal mixes considering sensitivity analysis of sea and road transportation for batching plants in Perth

Supplementary Material D: Scenario 2: sensitivity analysis of transportation (sea, road & rail)

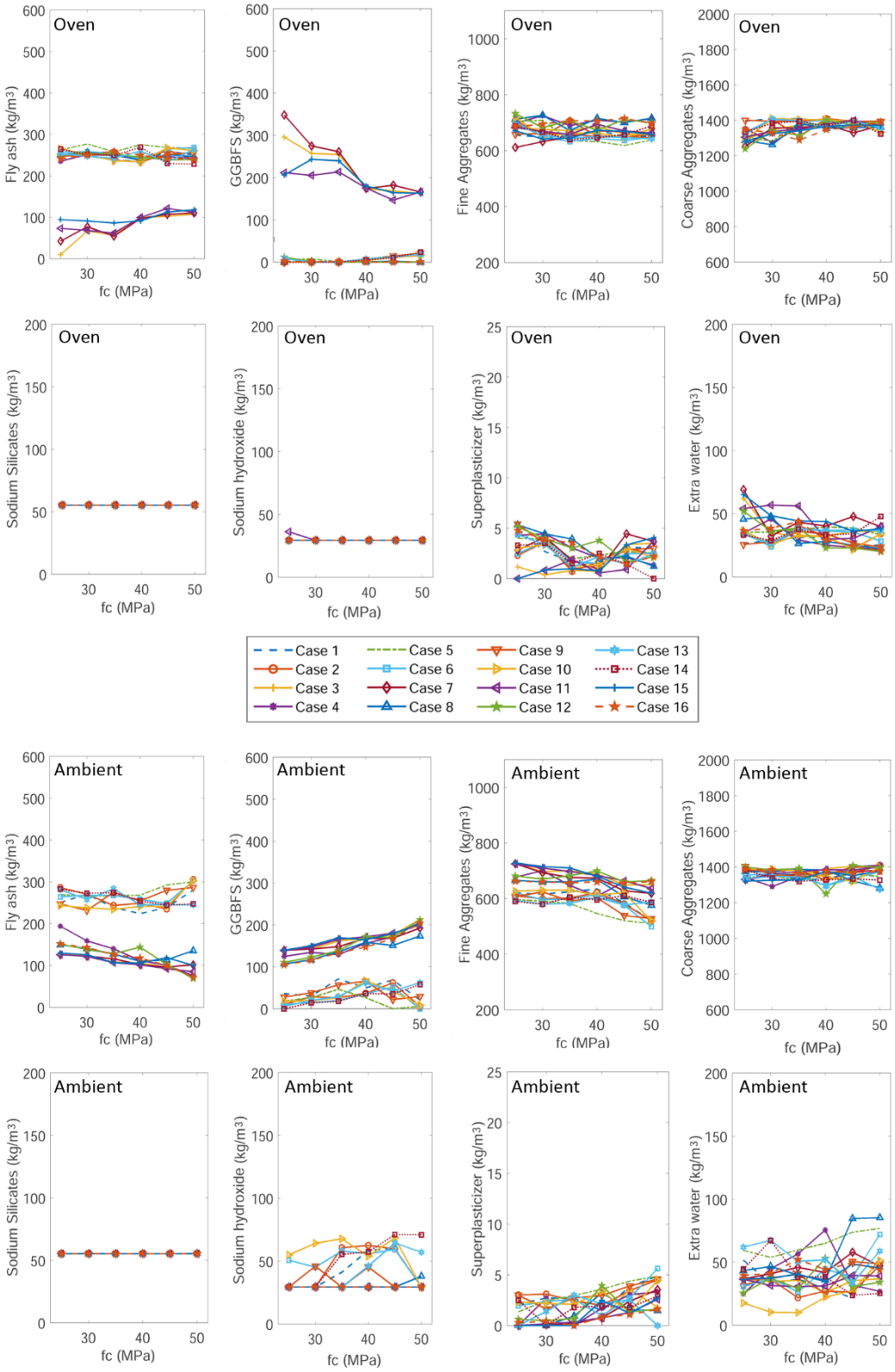

Fig. D-1 Optimal mixtures considering sensitivity analysis of sea, rail and road transportation for batching plants in Sydney

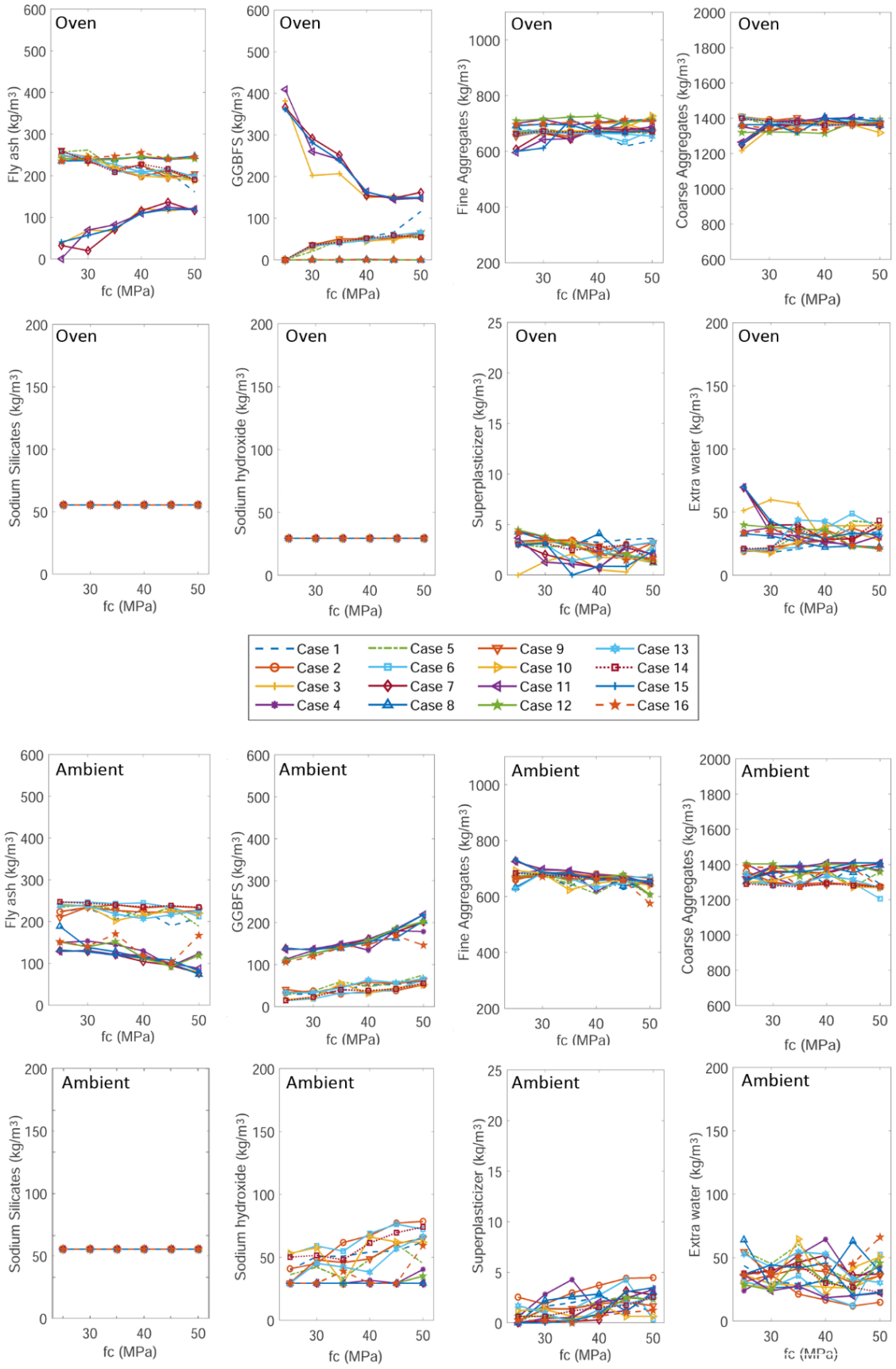

Fig. D-2 Optimal mixes considering sensitivity analysis of sea, rail and road transportation for batching plants in Melbourne

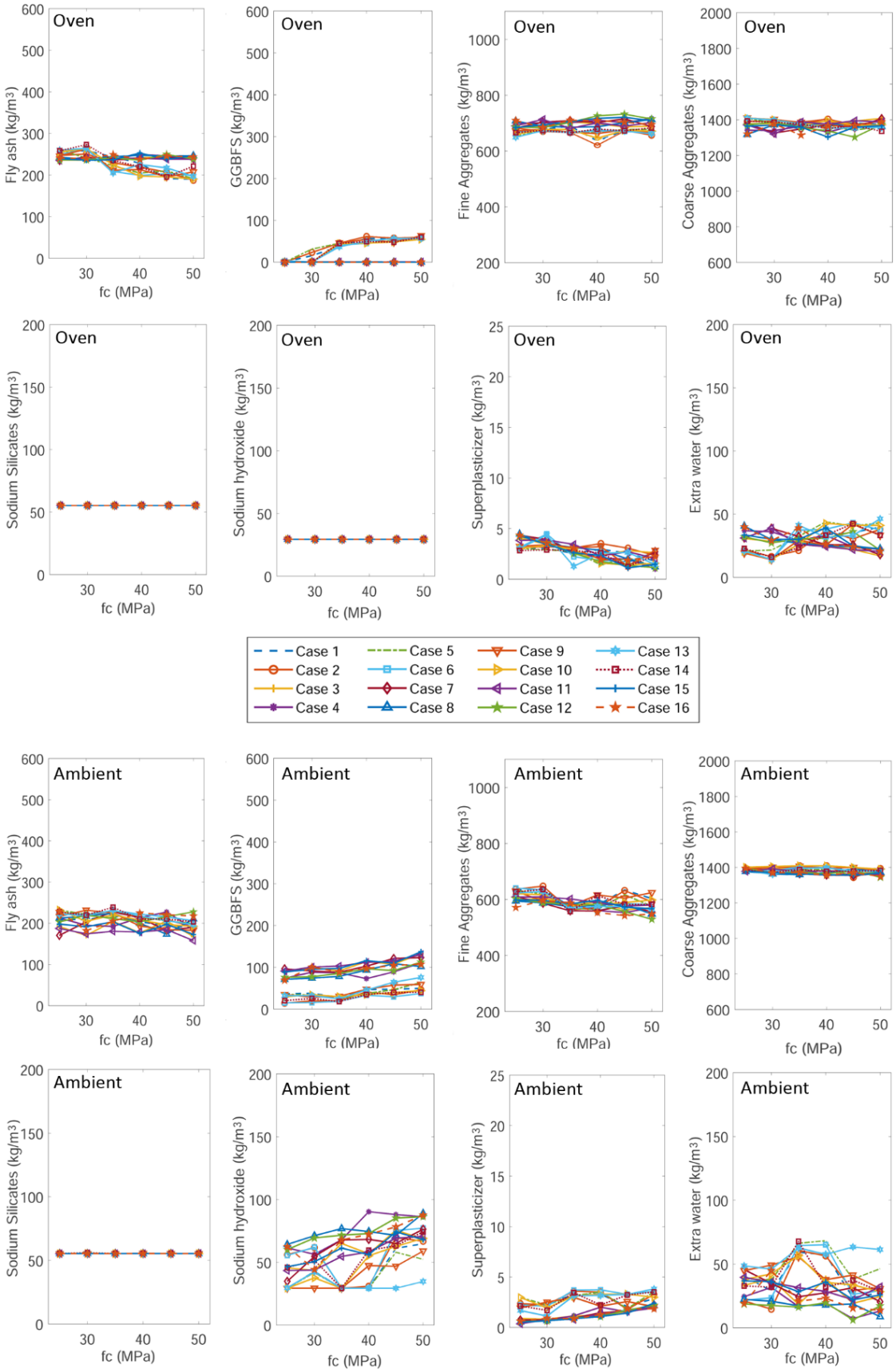

Fig. D-3 Optimal mixes considering sensitivity analysis of sea, rail and road transportation for batching plants in Adelaide

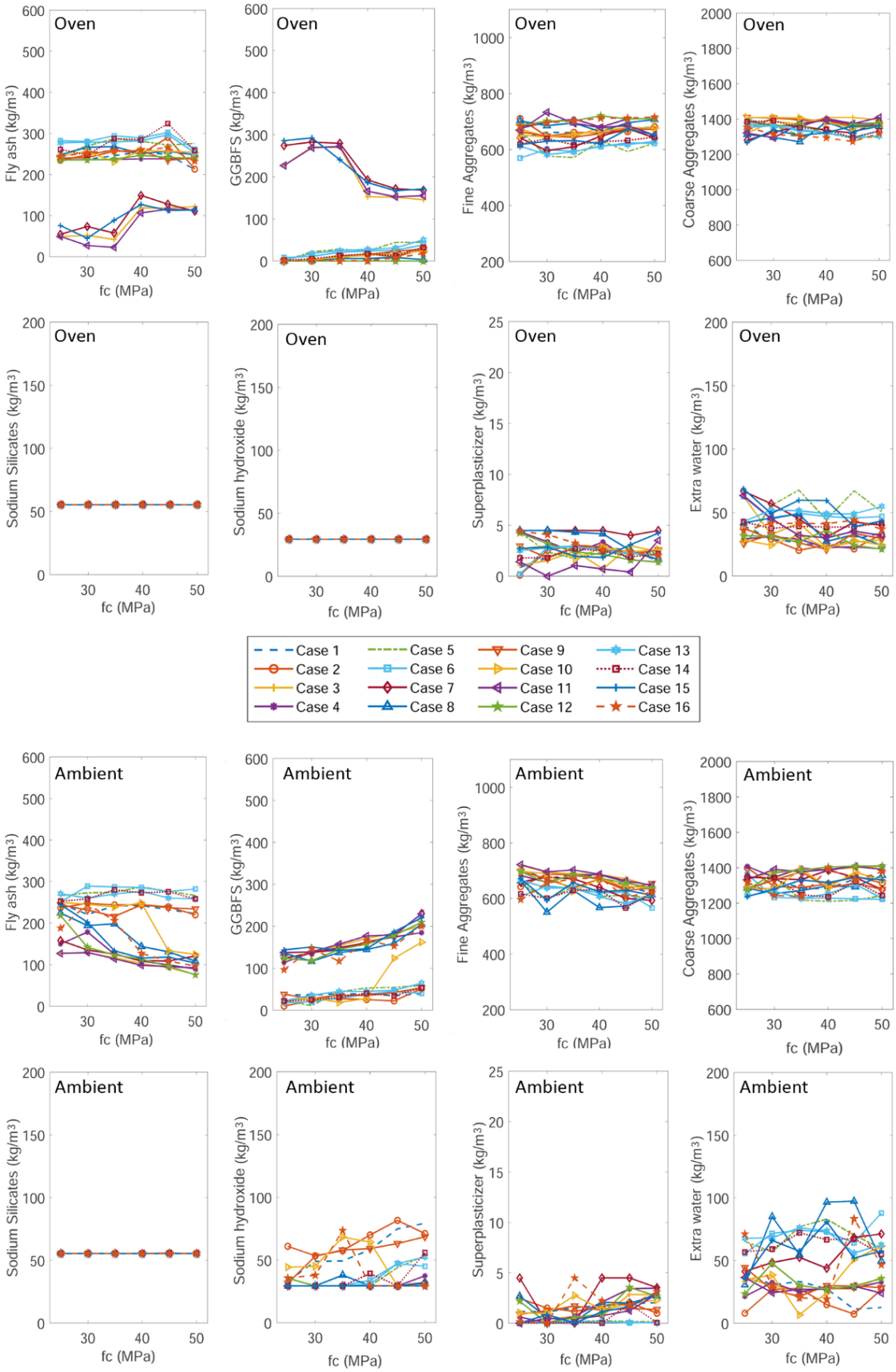

Fig. D-4 Optimal mixes considering sensitivity analysis of sea, rail and road transportation for batching plants in Brisbane

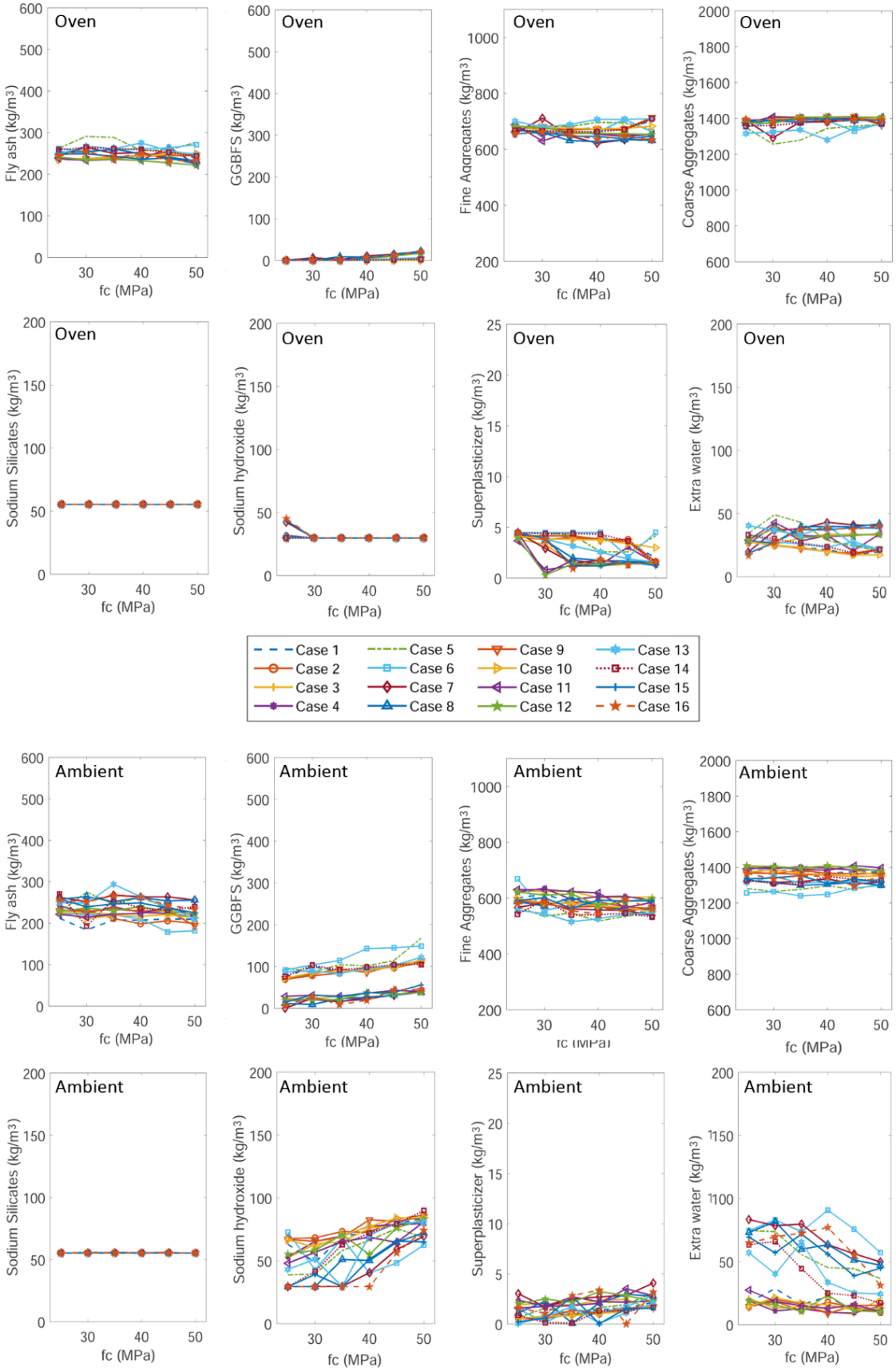

Fig. D-5 Optimal mixes considering sensitivity analysis of sea, rail and road transportation for batching plants in Perth

Supplementary Material E: $CO_{2\text{-eq}}$ intensity of optimal mixes

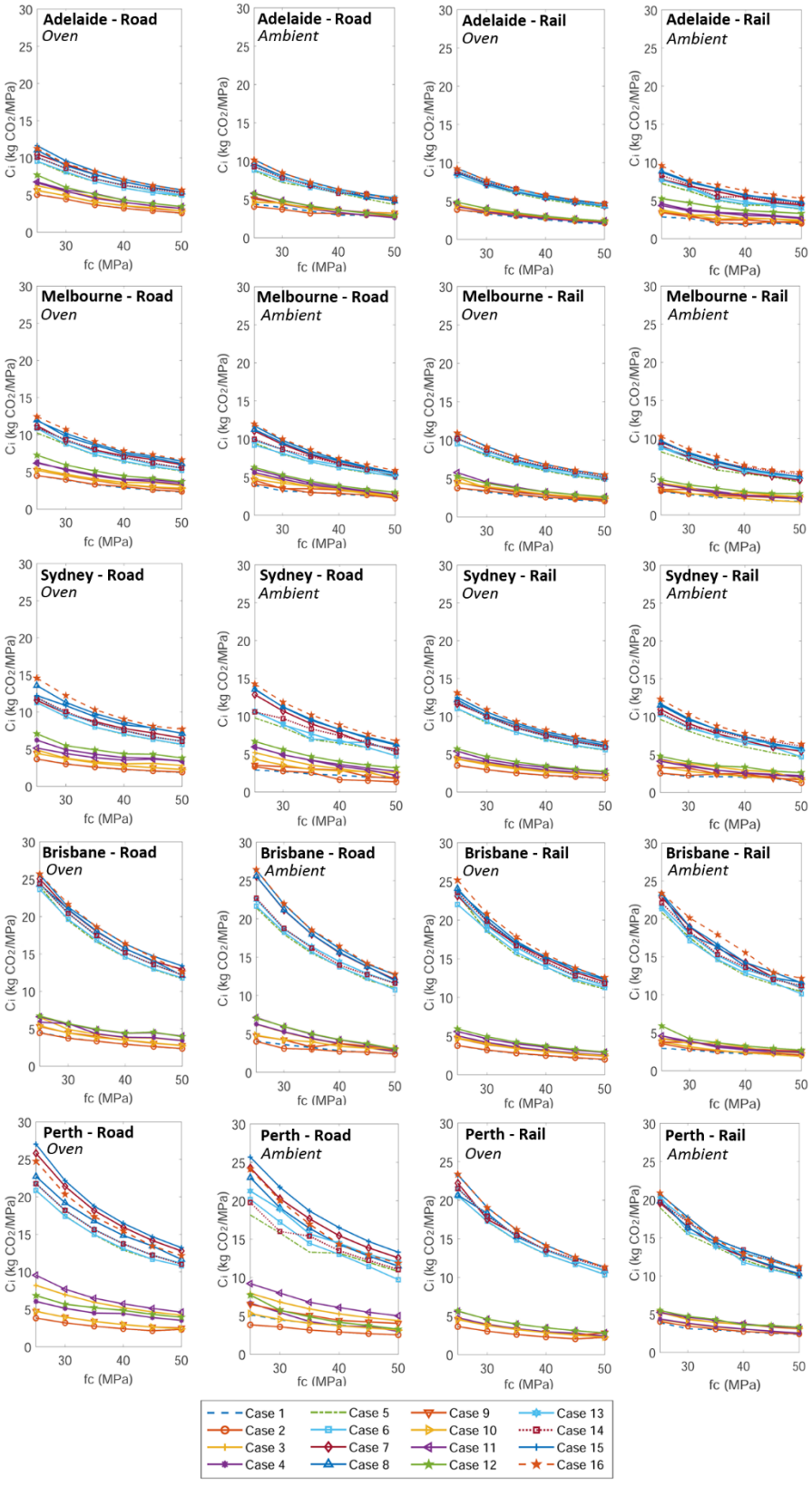

Fig. E-1 $CO_{2\text{-eq}}$ intensity of optimal mixes for Adelaide, Melbourne, Sydney, Brisbane and Perth considering all the possible transportation scenarios for oven and ambient cured GPC for different transportation modes.

Supplementary Material F: Scenario 2 – multi-objective optimisation

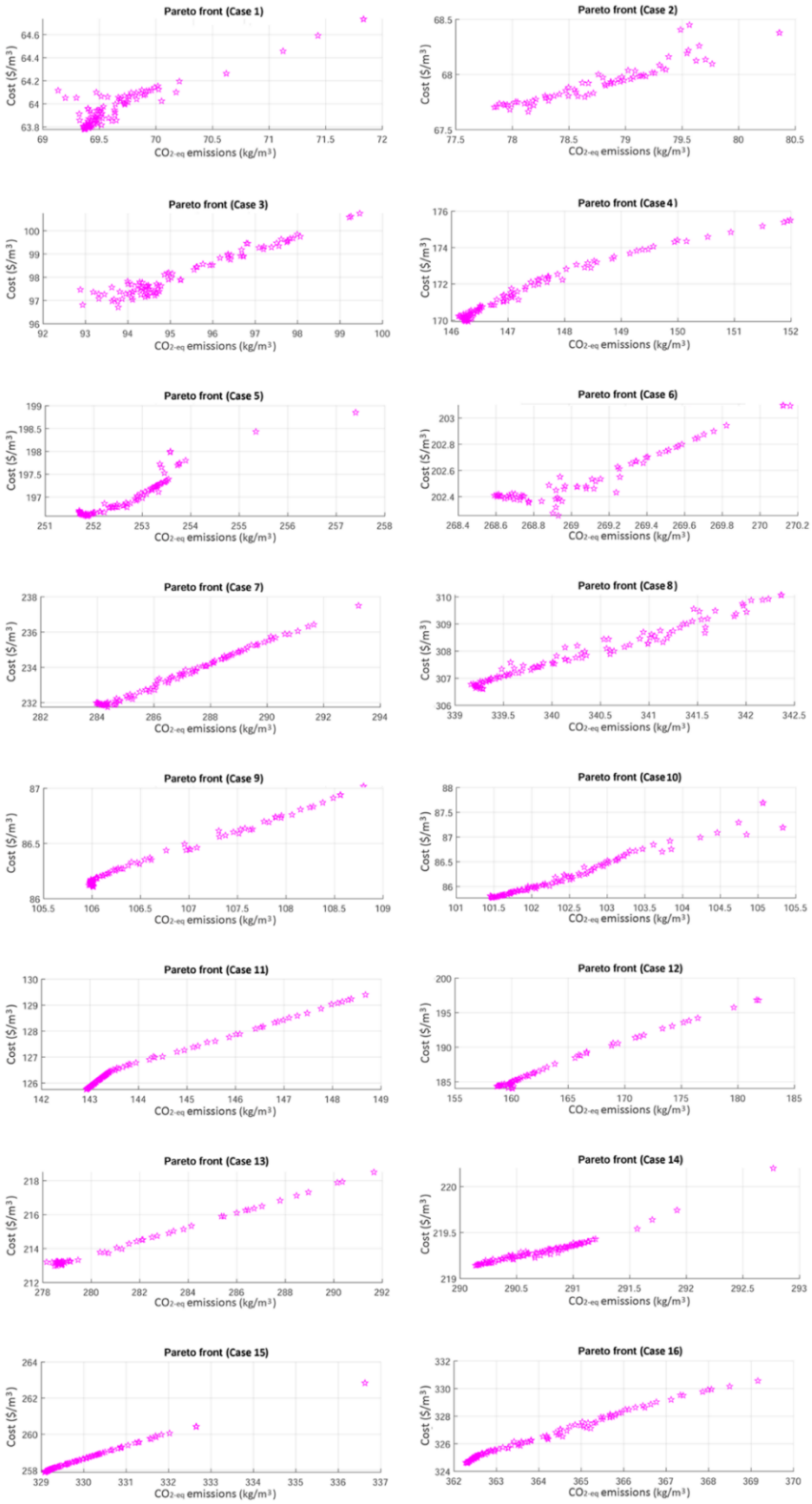

Fig. F-1 Pareto front showing a trade-off between $CO_{2\text{-eq}}$ emissions and cost for optimal mixes with different transportation cases for Sydney

STATEMENT OF AUTHORSHIP

"Mix Design Optimization of Concrete Containing Fly Ash and Slag for Global Warming Potential and Cost Reduction"
Case Studies in Construction Materials, e01832.

Shobeiri, V. (Candidate)

Prepared manuscript, performed all analyses, and developed model and theory (70%)

This paper reports on original research I conducted during the period of my Higher Degree by Research candidature and is not subject to any obligations or contractual agreements with a third party that would constrain its inclusion in this thesis. I am the primary author of this paper.

Signed… Date16/03/2023

Bennett, B.

Supervised and contributed to research (10%)

I certify that the candidate's stated contribution to the publication is accurate (as detailed above); permission is granted for the candidate in include the publication in the thesis; and the sum of all co-author contributions is equal to 100% less the candidate's stated contribution.

Signed… Date 17/04/2023

Xie, T.

Supervised and contributed to research, and acted as corresponding author (10%)

I certify that the candidate's stated contribution to the publication is accurate (as detailed above); permission is granted for the candidate in include the publication in the thesis; and the sum of all co-author contributions is equal to 100% less the candidate's stated contribution.

Signed… Date 17/04/2023

Visintin, P.

Supervised and contributed to research (10%)

I certify that the candidate's stated contribution to the publication is accurate (as detailed above); permission is granted for the candidate in include the publication in the thesis; and the sum of all co-author contributions is equal to 100% less the candidate's stated contribution.

Signed… Date 04/04/2023

Mix Design Optimization of Concrete Containing Fly Ash and Slag for Global Warming Potential and Cost Reduction

Vahid Shobeiri, Bree Bennett, Tianyu Xie and Phillip Visintin

Abstract

Mix design optimization is challenging because the properties of concrete depend on both the chemical and physical properties of the components and their relative proportions. In this paper a mix design optimization approach based on the application of artificial intelligence, genetic algorithm optimisation, life-cycle assessment to quantify global warming potential (GWP) and simple economic modelling is developed and applied to identify the optimal use of fly ash and granulated blast furnace slag (GGBFS) in concretes with blended binders. A database including 892 mixes with supplementary cementitious materials (SCMs) is used to predict the concrete compressive strength and slump. Five case studies are presented investigating the influence of: chemical makeup of cement and SCMs, minimum cement content, regional transportation, emissions allocation, and binder type on the GWP and cost of optimal mix designs. The results show that the tool developed can reduce GWP by up to 60% and cost by up to 40% when compared to experimental results with equivalent strength.

Keywords: *supplementary cementitious materials; mix optimization; carbon dioxide emissions; mix cost; industrial waste*

6. Introduction

As the primary binder in concrete, the global production of Ordinary Portland Cement (OPC) is responsible for approximately 4-8% of carbon dioxide equivalent $CO_{2\text{-eq}}$ emissions [1-3]. The high global warming potential (GWP) for OPC and concrete coupled with the expected rapid growth in concrete demand [4] make it essential that effective low carbon approaches to mix design are developed to enable the targets set in the Paris Agreement to be met [5].

One of the most well-developed technologies for minimising the GWP of concrete is to partially replace OPC with supplementary cementitious materials (SCMs) [6-8] such as fly ash, ground granulated blast furnace slag (GGBFS), waste glass powder, palm oil fuel ash [9] and limestone powder and calcinated clay [10-11]. In this study fly ash and GGBFS are used as SCMs in the analysis as they are commonly reported in literature and easy to get data. These SCMs not only minimise reliance on OPC (being industrial wastes from the coal and iron industries), their use in concrete also provides a pathway for their safe disposal and minimises reliance on natural resource utilisation [12-13].

Although many studies have been conducted to quantify the impact of SCMs on the engineering properties of concrete [14-16], limited research has considered the development of concrete mix design approaches, particularly those which aim to measure and minimise environmental impact and cost while meeting the performance criteria required for practical application [17].

Concrete mix design approaches can be broadly divided into three categories: (i) experimental approaches, (ii) robust design methods, and (iii) intelligent techniques. Experimental methods require extensive experimentation, often on a trial-and-error basis, and therefore are best suited to the optimisation of a narrow range of materials [18-19]. To reduce the quantity of expensive and time-consuming experimentation, some problem-solving techniques have been developed

based on the robust design of experiments. In these approaches experimental tests are designed to cover a selected range of proportions for each ingredient and the results are used to construct best-fit plots for similar ingredients [20-22]. To further minimise the need for trial mixing while also maximising the number of design parameters that can be considered, novel intelligent techniques based on artificial intelligence (AI) have recently been applied to concrete mix design. These approaches have been shown to be able to provide reliable predictions when provided with an appropriate range of existing experimental data [23-24].

To date, studies utilising intelligent techniques for concrete mix optimization have primarily sought to reduce the total cost of ingredients while satisfying a set of performance criteria. Table 1 summarizes the scope of each study in terms of the input parameters, the objective that is being minimised (e.g. cost or GWP) and the constraints of the analysis (e.g. target strength or slump). From this summary it is clear that many studies have been conducted with the aim of minimising cost, few have aimed to minimise GWP and only two previous studies have considered the minimisation of both cost and GWP.

Table 1 also highlights significant gaps in the inputs used as the basis for optimisation. For example, despite these approaches being data-driven, most studies have considered a very small number of mix designs as inputs (between 41 and 189 mix designs) and only a few studies have considered relatively large-scale databases for prediction purposes (between 350 and 1030 mix designs). Further, although it is widely accepted that the chemical makeup of SCMs strongly impacts the physical properties of concrete mixture [25-27], this parameter has not previously been considered in concrete with SCMs. The consideration of binder chemical makeup is also strongly related to the need to consider emissions arising from material transportation, that is, although transportation distances are generally small for cement, fewer sources of SCMs generally exist and therefore significant emissions from long transportation distances may occur [28-30]. These transportation distances can be further increased if an SCM with a specific chemical composition is required.

While traditionally considered waste materials, GGBFS and fly ash are no longer classified as waste since they meet all the conditions necessary for by-products [31]. This shift in classification requires that a proportion of the emissions associated with the production of fly ash and GGBFS be allocated to the concrete that they are used to produce [32-33]. Although this allocation process can significantly impact the GWP of concrete containing SCMs it has not previously been considered in mix design optimisation tools.

Finally, despite the development of alternative binder chemistries (e.g. alkali activated or geopolymer concretes), to date there is also no approach that is able determine which concrete technology should be applied in a given location when targeting a given set of performance criteria. That is, it is now important that we be able to identify not only the optimal mix design, but also more broadly the type of material that should be produced. For example, when provided with fly ash and GGBFS of a given chemical makeup, is it better to use the material as an SCM in an OPC based concrete or as the binders in a geopolymer concrete.

To bridge the above gaps, the aim of this paper is to find the optimal mix design of concretes that minimise both cost and GWP of concretes that utilise a combination of OPC, fly ash and GGBFS. To do so, a design optimisation approach which is an extension of that developed by Shobeiri et al. 2022 [27] for geopolymer concrete mix design to allow it to consider OPC based concrete and the inclusion of emissions allocation. The modified framework is then demonstrated using five case studies investigating the impact of: (i) the chemical makeup of binders, (ii) minimum cement content (iii) transportation distances of raw materials to the factory gate (iv) emissions allocation and (v) binder type.

Table 1: Published papers related to intelligent techniques in concrete optimization with SCMs

Reference	Binder type (SCMs type)	No of mixes	Compressive strength	Slump	Cost	Emissions	Transport	chemical makeup	Allocation
[34]	OPC-SCMs (GGBFS)		✓	✓	✓				
[35]	OPC-SCMs (FA*, SF**)	189	✓	✓					
[36]	OPC-SCMs (FA, GGBFS)	103	✓	✓	✓				
[37]	OPC-SCMs (FA)	350	✓						
[38]	OPC-SCMs (FA,SF)	189	✓	✓					
[39]	OPC		✓	✓	✓	✓			
[40]	OPC-SCMs (FA, GGBFS)	1030	✓		✓				
[41]	OPC-SCMs (FA, SF)		✓		✓				
[42]	OPC-SCMs (SF)	1030	✓		✓				
[43]	OPC-SCMs (SF)	77	✓	✓		✓			
[44]	OPC-SCMs (SF)	96	✓		✓				
[45]	OPC-SCMs (GGBFS)	103	✓	✓		✓			
[46]	OPC-SCMs (FA, GGBFS)	1030	✓	✓	✓				
[47]	OPC-SCMs (SF)	41	✓	✓	✓				
[48]	OPC-SCMs (SF)	1030	✓		✓	✓			
[27]	GPC	1178	✓	✓	✓	✓	✓	✓	
This study	OPC-SCMs (FA, GGBFS) GPC***	892	✓	✓	✓	✓	✓	✓	✓

****Fly ash*** ****Silica fume*** *****Geopolymer***

7. Review of framework

This paper extends and implements a mix design optimization approach proposed by Shobeiri et al. (2022) [27] including three major components as shown in Fig. 1. As can be seen, the concrete performance in terms of strength, slump, cost and GWP is related to the mix components using a set of mix design outcomes and the components are optimized using the optimization algorithm according to the desired objectives, variables and constraints. The framework components are outlined in the following sections.

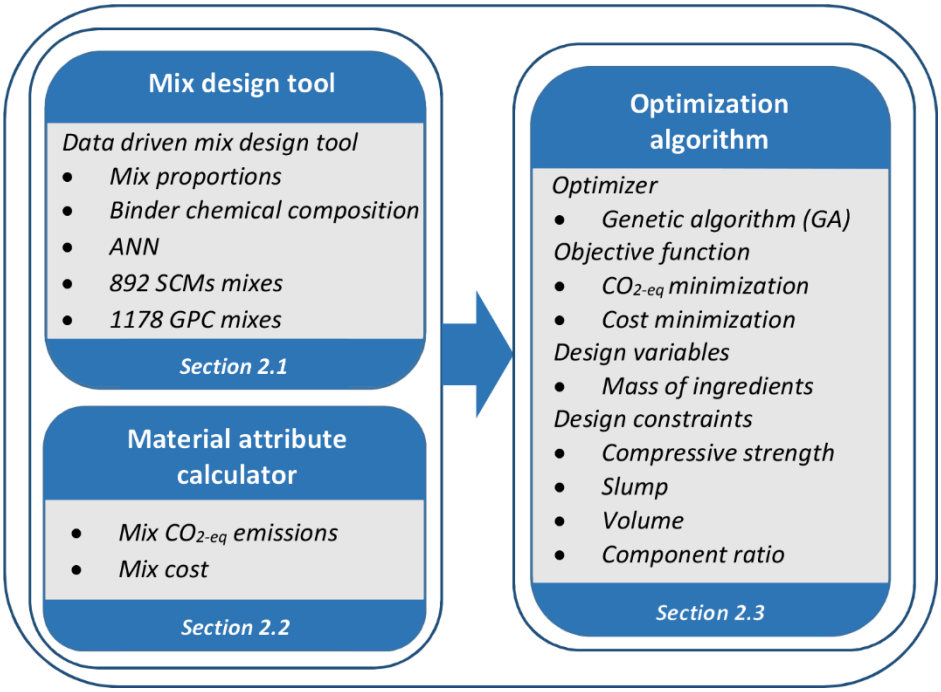

Fig. 1 Mix design framework implementation (extended from Shobeiri et al. (2022) [27])

2.1 Mix design tool

The artificial neural network (ANN) available in Matlab [50] is used for OPC based concretes with SCMs. An ANN has been chosen as the basis for the mix design tool because of its proven ability to predict the performance of concrete mix designs [20, 51-53].

In this study the ANN input variables are taken to be the mass of mix design components, where importantly, to allow for the influence of chemical makeup of cement and SCMs, instead of considering their masses, the total mass of reactive oxides (SiO_2, Al_2O_3, Fe_2O_3 and CaO) within each of these materials is used. Further, when considering geopolymer mixes, according to Shobeiri et al. (2022) [27] the composition of the activator solution is disaggregated into the dried mass of SiO_2 and Na_2O contained in Na_2SiO_3 and NaOH and the water required to turn these solids into a solution.

The ANN input variables for the production of 1 m^3 concrete are therefore the total mass of: (1) SiO_2, (2) Al_2O_3, (3) Fe_2O_3, (4) CaO, (5) Na_2O (6) fine aggregates, (7) coarse aggregates (8) total water (mixing water and any water contained in activators), (9) superplasticizer (10) the age of the concrete at the time of measuring the compressive strength, and the (11) time and (12) temperature of accelerated curing of a geopolymer concrete (e.g. where oven curing is used). From these input variables the ANN predicts the compressive strength at the time of testing and the slump at the time of mixing. It should be noted that in this study SiO_2, Al_2O_3, Fe_2O_3 and CaO are used as the reactive oxides within binding materials because these oxides are the most commonly available chemical makeup which generally occupy the majority (>90%) of binder chemical composition [87-89]. The mix design tool is based on the application of an ANN containing a single hidden layer which has been trained using a database of mix designs containing blended OPC, fly ash and GGBFS binders collected by Xie and Visintin (2018) [54]. Within this database 892 mix designs with strengths ranging from 10 MPa to 109 MPa were identified. The source papers were then reassessed to identify if workability

data was available and a separate database was established for the 185 mix designs in which slump was also reported. The compressive strengths reported in the database are measured on both cubic and cylindrical specimens and so all results were converted to those of an equivalent a 100 diameter × 200 mm height cylinder using the approaches suggested in [55-56].

The distribution of SCMs mix ingredients and binder chemical makeup in the database can be found in Supplementary Material A. It is observed that the database covers a broad range of ingredients and chemical makeup of SCMs which can affect the concrete mechanical properties.

2.2 Material attribute calculator

GWP on the basis of a unit volume (cubic meter) of concrete are calculated based on a life-cycle assessment tool limited to GWP developed in Shobeiri et al. (2021) [49] for geopolymer concretes and OPC concretes containing SCMs. This cradle-to-gate analysis includes emissions associated with all cycles of production of concrete materials as shown Table 2 (see Shobeiri et al. (2021) [49] for complete details on the sources of the values shown in Table 2).

The material attribute calculator also contains a simple economic model that calculates the total cost of a unit volume of the concrete based on a simple sum-product of the unit price and mass of the component material. A summary of the unit prices of each component material is provided in Table 2. It should be noted that however the values shown in Table 2 can change based on the local sources and technologies, the proposed framework is generic enough to incorporate any emissions factor and unit cost from raw materials.

Table 2 Emissions factors and unit cost for concrete mix components [49, 57-59]

Ingredient	**Emissions factor ($\mathbf{kg\ CO_{2-eq}/kg}$)**			**$\mathbf{AUD^*/kg}$**
	Manufacture	Economic	Mass al**location**	
Fly ash	26.0×10^{-3}	1300.0×10^{-3}	2267.0×10^{-3}	45.0×10^{-3}
GGBFS	90.1×10^{-3}	230.0×10^{-3}	685×10^{-3}	140.0×10^{-3}
Cement	896.6×10^{-3}			293.0×10^{-3}
Fine aggregates	2.8×10^{-3}			12.0×10^{-3}
Coarse aggregates	3.9×10^{-3}			19.0×10^{-3}
Water	0.2×10^{-3}			2.0×10^{-3}
Superplasticizer	229.0×10^{-3}			424×10^{-3}
Sodium silicates	1067.0×10^{-3}			400.0×10^{-3}
Sodium hydroxide	1270.0×10^{-3}			200.0×10^{-3}
Transport type mode	**$\mathbf{kg\ CO_{2-eq}/kg-km}$**			**$\mathbf{AUD/kg-km}$**
Road	0.128×10^{-3}			0.091×10^{-3}
Sea	0.017×10^{-3}			0.031×10^{-3}

* *Australian dollar*

2.3 Optimization algorithm

Within the mix design framework, the optimisation algorithm generates trial mix designs, these mix designs are then parsed to the mix design tool which calculates and returns the material compressive strength and slump, and also to the material attribute calculator that returns the GWP and cost of a unit volume of the concrete. In this study a genetic algorithm (GA) is implemented as the optimiser. A GA is implemented because it is able to optimise highly nonlinear constraints and models and it has been shown to yield good results when applied in previous studies on concrete mix design [41, 45, 60-61]. This approach follows objectives and constraints of a similar nature that have been broadly utilized in the literature [42, 44, 48] but

also considers transport emissions and cost as in Shobeiri et al. (2022) [27] .

2.3.1 Objective function

The objective function is to minimize the GWP and cost of producing a unit volume of concrete considering desired mechanical properties, importantly, in this minimisation the resulting concrete can be either an OPC concrete (containing SCMs) or a geopolymer concrete. For analysis the total GWP and cost are quantified by:

$$C_t = \sum_i m_i (C_{prod_i} + C_{trans_i} \times d_i) \quad (1)$$

$$F_t = \sum_i m_i (F_{prod_i} + F_{trans_i} \times d_i) \quad (2)$$

In which C_t and F_t are the total GWP and cost of the concrete resulting from the i mix components, where m_i is the mass of ingredient i, d_i is the transport distance of ingredient i (km), C_{prod_i} and F_{prod_i} are the emissions and cost of a unit mass of each component material which is defined in Table 2, and C_{trans_i} and F_{trans_i} are emissions and cost for transportation of a unit volume of material (kg) per kilometre as shown in Table 2.

2.3.2 Design variables

The design variables are taken as the mass of concrete materials. These masses are parsed to the mix design tool which predicts the corresponding compressive strength and slump. It should be noted that in addition to the mass of other concrete ingredients such as water, aggregates and admixture, the reactivity of cementitious materials calculated from major oxides is considered in this study as inputs to help distinguish the difference in the reactivity of fly ash or GGBFS from different sources [87-89].

2.3.3 Design constraints

Constraints are applied to the optimisation process to ensure the optimiser returns concrete mix designs that are feasible and suitable for real-world application. To do this, constraints are applied as follows and mixes are only considered to be valid if all constraints are met.

1. The compressive strength and slump are constrained to be within a tolerance of the target value. That is:

$$f_{c_t} - tol_{f_c} \leq f_{c_p} \leq f_{c_t} + tol_{f_c} \quad (3)$$

$$S_t - tol_S \leq S_p \leq S_t + tol_S \quad (4)$$

   where, f_c refers to the compressive strength, S refers to the slump and *tol* refers to tolerance and the subscripts p refer to predicted values and t to target values.
2. The total volume of the concrete mix components (with densities provided in Table 2) minus the entrapped air should be 1 m^3. Note that in this study, in the absence of an air entraining agent (AEA), the volume of entrapped air is assumed to be 2% [86].
3. Each component of the mix design has an upper and lower bound based on the limits in the database. This is especially important for minimum cement content as it is a necessary restriction on the mix design of OPC SCM blends [62-63].
4. The ratios of mix components must be between their allowable ranges in the existing database.

8. Scenario analysis

To demonstrate the potential of the framework described above and to highlight the importance of the input parameters five scenarios are presented as follows:

1. *Scenario one* – this first scenario examines the influence of chemical makeup of cement and SCMs on the resulting mix designs. This effect in investigated because it has previously been shown that variation in the chemical makeup of SCMs of the same class (e.g. Class-F fly ash) can strongly affect the resulting concrete mechanical properties [25-26]. This scenario focuses on the blended OPC SCM binders only (the reader is referred to Shobeiri et al. (2022) [27] for geopolymer binders). For this analysis we consider fly ash provided from two coal-fired power plants in Australia with varying chemical makeup: Mt Piper Coal-fired Power Station (chemical makeup : SiO_2: 68.6%, Al_2O_3:25.5%, Fe_2O_3:1.3%, CaO:0.22%) and Collie Coal-fired Power Station (chemical makeup: SiO_2:54.0%, Al_2O_3:28.3%, Fe_2O_3: 10.5%, CaO:1.7%) ([64-66]). These fly ash sources were chosen because although they have the same country of origin and are designated as Class-F fly ash (ASTM C618) they have significantly different reactivity as SCMs due to the variation in the locally available coal's chemical makeup. For simplicity, throughout this analysis the chemical makeup of both cement and GGBFS are constant, but they can easily be varied in the same way.
2. *Scenario two* – The second scenario examines the effects of imposing a minimum cement content while trying to minimize GWP and cost. The definition of a minimum cement content is an important boundary condition in the optimisation process because national standards often impose a minimum content in their definition of concrete, and cement content in OPC based concretes strongly influences total GWP. In this analysis, the lower bound for cement content in the mixes is considered to be between 100 kg/m^3 and 200 kg/m^3.
3. *Scenario three* – Scenario three investigates the influence of materials transport adding additional complexity to the analysis. Previous LCA has shown transportation of materials to be a significant contributor to a concrete's GWP [49-28-30]. Note that scenarios one and two ignore the role of materials transport. Here two capital cities in Australia: Melbourne and Perth (Fig. 2) corresponding to the locations of the Mt Piper and Coolie Power stations respectively have been chosen for analysis. The point of generation of concrete, and the assumed maximum and minimum transportation distances for each material are summarized in Supplementary Material B.
   Two different transportation cases are considered as part of scenario three. They are: (1) transportation distances of all concrete materials are set to the minimum, and (2) transportation distances of all concrete materials are set to the maximum but do not cross state boundaries. Given that the difference between the minimum and maximum transport distances of cement for each city is negligible compared to that of other ingredients, only the maximum assumed transportation distance of cement for each city is considered for this analysis. It should be noted that this study only considers the impact of emissions arising from material transportation to the factory gate before it is transported to the consumer.
4. *Scenario four* – The fourth scenario investigates the effects of emissions allocation on the optimal mixes and their carbon and cost intensities. This is of great importance as considering fly ash and GGBFS as a by-product rather than a waste product can significantly influence their production emissions (see Table 2 and [32, 67]) When examining emissions allocation, the impacts of allocation type including: no allocation, economic allocation and mass allocation are considered. When applying economic and mass allocation, the approach defined in [57] based on product mass as by-products is applied, for economic allocation the price and the cost of iron and electricity in Australia in 2022 has been taken from [68-71]. The purpose of this investigation is to demonstrate the impact of assumptions surrounding allocation, in particular the sensitivity of outcomes to inputs rather than absolute values and does not seek to

provide guidance on what assumptions should be applied in practice.

5. *Scenario five* – The final scenario investigates mix design optimization that crosses material types, that is, for a given target strength and slump, and using identical transportation cases, the final scenario identifies if the optimal use of the available source materials arises from the batching of an OPC concrete containing SCMs or a geopolymer concrete.

In all scenarios, it is assumed that at all locations the chemical makeup of OPC is the mean of the chemical makeup ranges defined in Guirguis (1998) [72] and for scenarios 3, 4 and 5 the chemical makeup of fly ash varies depending on the local source and is defined in [64-66, 73]. In all scenarios the emissions factors, unit costs and densities of the materials is as defined in Table 2. Where applicable, the minimum cement content is considered to be 150 kg as it is the most common mass of cement in the database.

The 28-day compressive strength of less than 25 MPa and larger than 50 MPa is not considered and the target slump is fixed at 150 mm for all compressive strengths as this range is widely used in practical applications. The tolerance on compressive strength and slump in Eqns. 3 and 4 are taken to be 1 MPa and 5 mm respectively.

When presenting results, the mix GWP and cost is presented in terms of a carbon intensity (C_i) and cost intensity (F_i) which simplify comparison by normalizing against the material compressive strength. That is, C_i and F_i refer respectively to the GWP and cost to deliver 1 MPa of compressive strength.

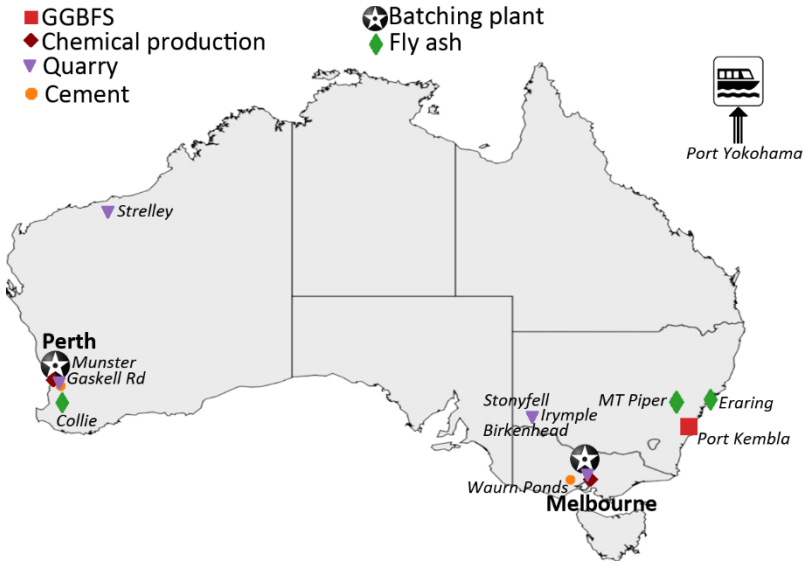

Fig. 2 Points of generation of source materials for SCMs concrete

9. Results and Discussion

The reliability of the integrated ANN for f_c and slump of OPC concretes with SCMs is first presented and the reader is referred to Shobeiri et al. (2022) [27] for validation when considering geopolymer concretes. For geopolymer concrete, two different scenarios including chemical compositions of binders (fly ash and GGBFS) and alkaline solutions (sodium silicates and sodium hydroxide) as well as transport emissions were considered in the context of single- and multi-objective optimisation (emissions and cost) in five major capital cities Australia [27]. The optimal oven and ambient curing geopolymer mixes were found using a genetic algorithm and ANN based on a large database of 1178 geopolymer mixes in terms of the mass of fly ash,

GGBFS, fine aggregate, coarse aggregate, sodium silicates, sodium hydroxide, superplasticizer and extra water [27]. The results of each of the five scenarios considered in this study are then presented and discussed.

9.1. Mix design tool performance: ANN

The error and correlation between the observed and predicted values for compressive strength and slump on training, validation, test, and all-data sets are shown in Supplementary Material C in Supplementary Material. In these plots it is shown a good correlation exists between the observed and ANN-predicted values for both compressive strength and slump in each different data set. The statistical indicators in Table 3 show that the ANN model is a reliable tool to accurately predict the f_c and slump with R^2 larger than 94%. It can be seen that the compressive strength model has better *RMSE* and *MAE* values on all different data sets than slump model. The reason for this can be attributed to the difference between the absolute and relative measure of different model fits, smaller database size for slump and the fact that slump data has a wider range than the compressive strength data leading to more errors for absolute model fits.

Table 3 Error metrics of ANN model for compressive strength and slump on different data sets

Output	Data set	*RMSE*	*MAE*	R^2	*R*
Compressive strength	Training	3.12	2.35	0.977	0.988
	Validation	4.96	3.46	0.944	0.972
	Test	4.40	3.47	0.945	0.972
	All data	3.81	2.78	0.965	0.982
Slump	Training	7.39	5.17	0.985	0.992
	Validation	14.41	13.00	0.942	0.970
	Test	14.40	12.65	0.948	0.974
	All data	15.0	13.12	0.939	0.969

$RMSE = \sqrt{\frac{\sum_{i=1}^{n}(x_i - y_i)^2}{n}}$, $MAE = \frac{\sum|x-y|}{n}$, $R^2 = 1 - \frac{\sum(x_i - y_i)^2}{\sum(x_i - \bar{x})^2}$, $R = \frac{\sum(x-\bar{x})(y-\bar{y})}{\sqrt{\sum(x-\bar{x})^2 \sum(x-\bar{y})^2}}$ in which x is the actual observation, $\bar{x}$ is the mean of actual observations, y is estimated value, $\bar{y}$ is the mean of estimated value and n is the sample size.

9.2. Scenarios to evaluate parametric sensitivity

The following scenarios are presented to evaluate the parametric sensitivity to binder chemical makeup , minimum cement content, transportation distance and binder chemistry (i.e. OPC and SCM based concretes versus geopolymer concretes).

4.2.1 Scenario one: sensitivity analysis of chemical makeup of fully blended binders

The resulting mixtures for OPC based concretes including fly ash produced in either the Mt Piper or Collie Coal-fired Power stations (see Fig. 3). The results show that as the target compressive strength increases the cement content tends towards the lower bound (150 kg/m^3) and an increasing proportion of the total binder is comprised of the SCMs. This outcome is expected because, 1) in general, the SCM content must increase to increase the compressive strength; 2) higher SCM content (especially FA due to its spherical shaped particles) reduces the water demand for a given slump (150 mm); and 3) SCMs have a lower carbon and cost intensity than cement [74-75].

For the mix with fly ash produced in Mt Piper Coal-fired Power Station, as f_c increases fly ash

content increases rapidly while the GGBFS content reduces and cement content remain relatively stable. This behaviour is in contrast to what is observed when sourcing fly ash from the Coolie power station in which the fly ash content reduces and the GGBFS content increases. This behaviour can be attributed to the difference in SiO_2 content between the power stations (68.6% *vs* 54%) which makes Mt Piper fly ash a less carbon and cost intensive source of SiO_2 than Collie fly ash, which subsequently reduces the demand for GGBFS that contains an even lower proportion of SiO_2 (38.8 %) when applying Mt Piper fly ash. For lower strength concrete, the amount of fly ash in the mixture increased up to 200% with a reduction in SiO_2 percentage in fly ash from 68.6% to 54%. This is likely related to the beneficial effects of silicon dioxide on the pozzolanic reactions in concrete. This increase in fly ash quantity was accompanied by a decrease in cement content resulting in an improvement of up to 20% and 12% in C_i and F_i respectively. For high-strength concrete, however, GGBFS can increase up to 100% when fly ash with a lower level of SiO_2 (54%) is used. This is likely because GGBFS being a valuable source of SiO_2 and CaO is preferable to fly ash with lower levels of SiO_2 for higher strength concretes [76].

Also observed in Fig. 3 is that as the compressive strength increases no significant changes in the quantity of fine aggregates occurs, but coarse aggregates slightly decrease and mixing water and superplasticizer increase to maintain the workability of the developed mixes [77-79]. It is also observed that the amount of mixing water and superplasticizer generally increase more for the mix with fly ash produced in Collie Coal-fired Power Station as it generally has more GGBFS leading to a higher demand for water and/or superplasticizer to maintain the workability [62, 80-81].

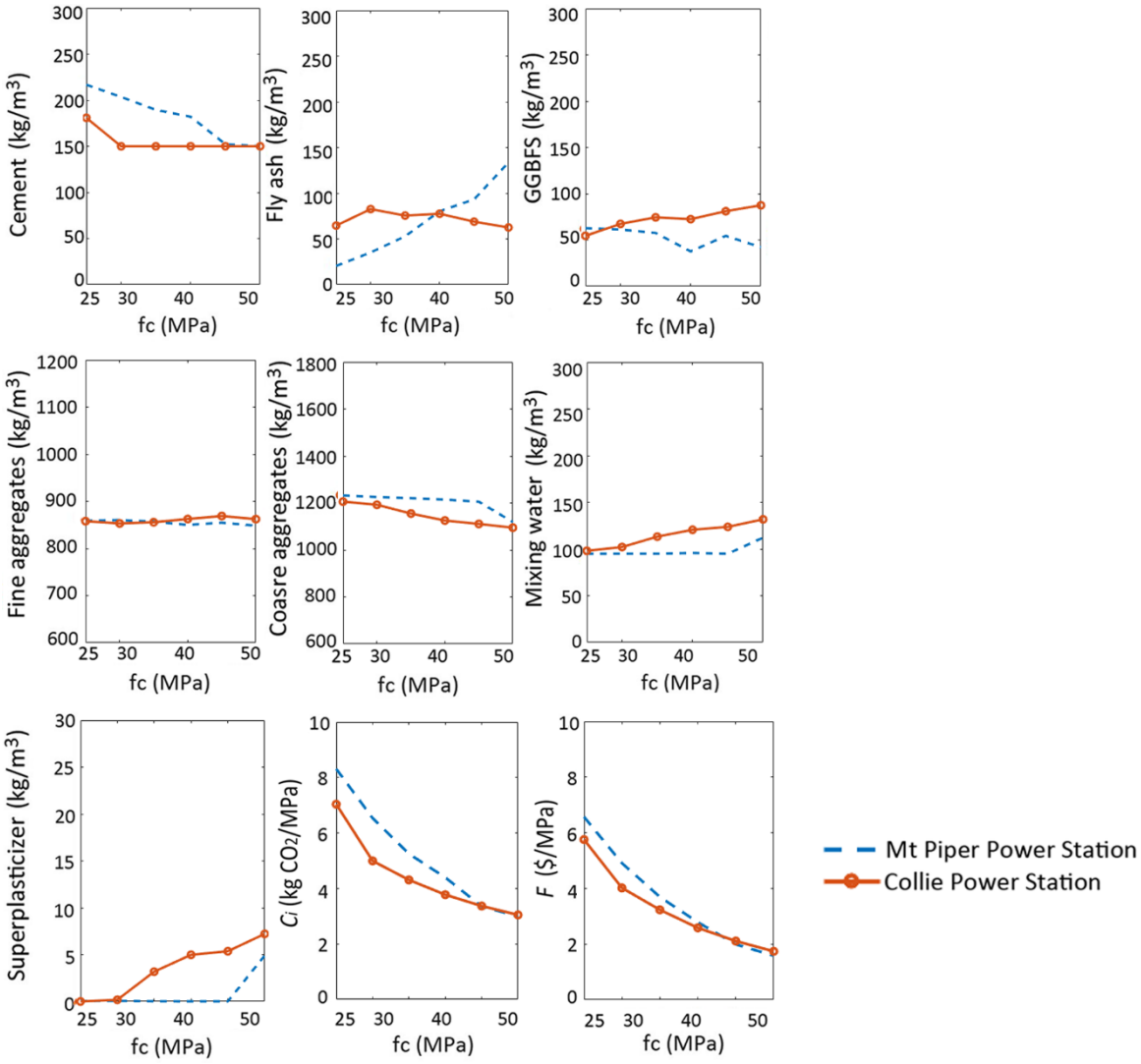

Fig. 3 Optimal SCMs mixes with fly ash generated in different coal-fired power stations

4.2.2 Scenario two: sensitivity analysis of cement content

As national codes of practice (e.g., Australian standard) generally define a minimum cement content in concrete, and because a minimum cement content needs to be defined in the optimizer because of a lack of data at very low cement contents, let us now examine the effects of the minimum cement content on the optimal OPC mixes containing SCMs. The optimal SCMs mixes with different limits on minimum cement content along with the corresponding carbon and cost intensities are shown in Fig. 4.

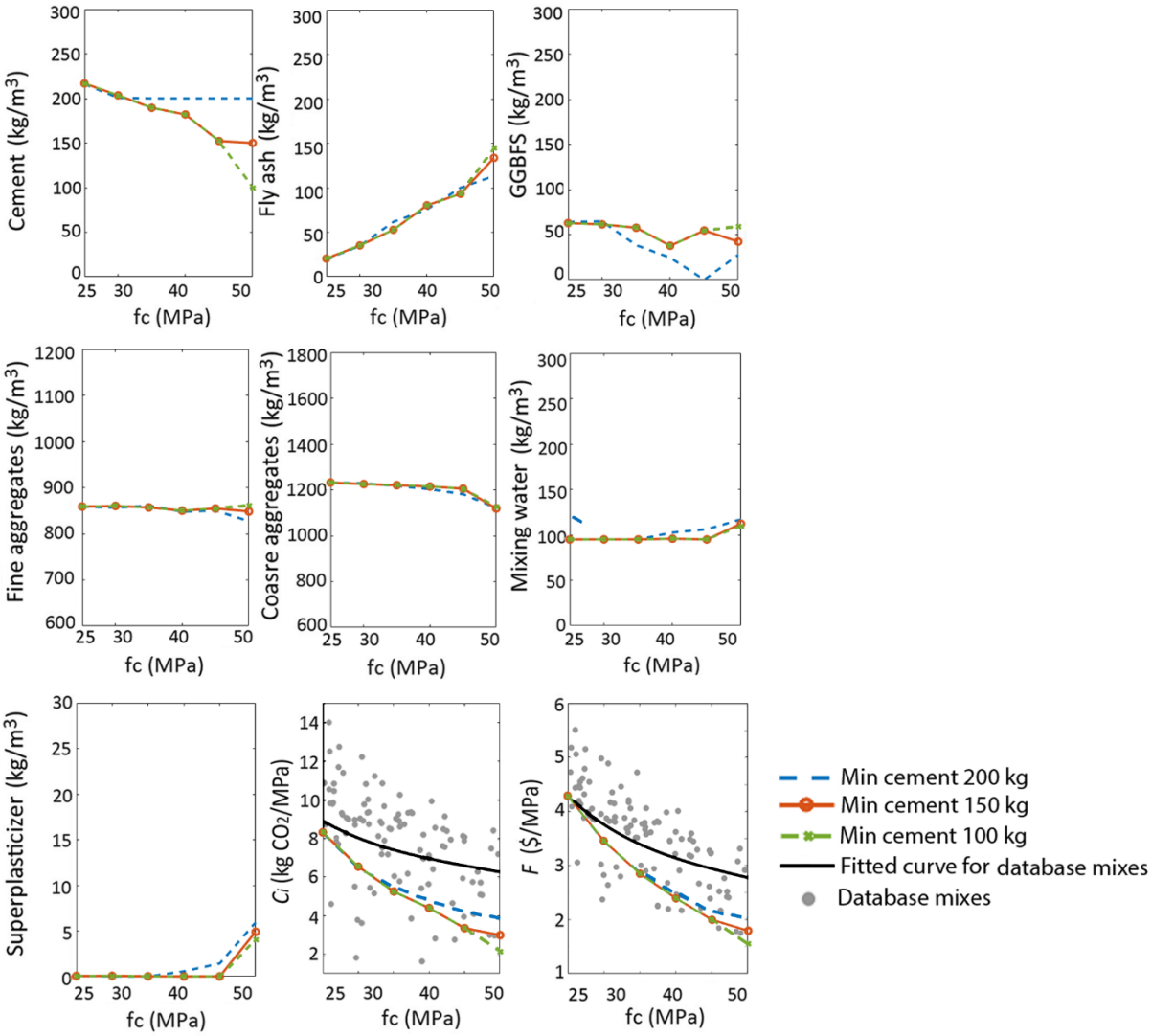

Fig. 4 Optimal SCMs mixes and their $CO_{2\text{-eq}}$ intensity (C_i) and the cost intensity (F_i) with different minimum cement contents

It can be seen that while for lower strength concrete (f_c < 40 MPa), the carbon intensity of the optimal mixes with different limits on cement content is very similar, for higher strength concrete (e.g. f_c > 45 MPa), the carbon intensity is correlated to the minimum cement content (i.e. with the lowest minimum cement content resulting in lower carbon intensity and vice versa for higher minimum cement contents). A similar trend is also observed for cost intensity (F_i). This outcome can be explained by the fact that while for lower strength concrete, more than 70% of the total binder content for optimal mixes is cement, but for 50 MPa concrete the proportion of cement in the binder reduces to between 58% and 33% as the minimum cement content is reduced from 200 to 100 kg/m^3. This result shows that to achieve a higher strength of concrete, it is feasible to increase the proportion of cement replaced by SCMs (usually by up to 50%). This is beneficial in that it not only improves in mechanical properties but also carbon and cost intensities [82-84].

Figure 4 also presents a comparison of the carbon and cost intensities of the optimized mixes to mixes in the experimental database with the same strength range and age (28-day). From this comparison, it can be seen that for lower strength concrete the carbon intensity of optimal mixes with different limits on minimum cement content can be between 20% and 30% lower

than that of experimental mixes, and the cost intensity can be up to 15% lower. For 50 MPa concretes, the optimal mixes with minimum cement content of 200 kg, 150 kg and 100 kg have between 35% and 60% lower carbon intensity and between 20% and 40% lower cost intensity than the experimentally derived mixes that produce the concrete with a similar strength in the database. The higher reductions in emissions compared to cost can be explained simply by the differences in emissions and cost relative to reactivity between cement and SCMs. The findings indicate that as the compressive strength increases the emissions and cost of the concrete can be avoided by replacing cement with SCMs.

4.2.3 Scenario three: sensitivity analysis of transport emissions

As the transportation emissions were not considered in the above analysis (i.e. scenarios one and two), let us now consider the effects of emissions arisen from the transportation on the resulting SCMs concrete mixes. Figure 5 shows the resulting mixes with minimum and maximum transportation distances when sourcing each material within the home state of Melbourne and Perth (see Fig. 2). For both the cities the total emissions associated with cement manufacture and transport are almost identical (~0.9 kg $CO_{2\text{-eq}}$/kg) and water is assumed to be free of transport emissions and so the following discussion focuses on the remaining mix components.

Similar to when transport associated emissions were ignored (Fig. 4), for both transportation cases and cities and with an increase in f_c, cement quantity reduces and binder is increasingly comprised of SCMs. This behavior observed because even though the emissions relating to transporting SCMs are higher than cement, the emissions associated with producing the SCMs is much less than cement when allocation emissions are ignored. For example, emissions from production and transportation of fly ash to cement is 50% and 60% respectively for Melbourne and Perth in the case that the fly ash is transported at the maximum distance. Similarly, the emissions from production and transportation of GGBFS to cement are 27% and 65% for the same cities and transportation case. It can be seen from Fig. 5 that the optimal mixes in Melbourne with minimum transport distances are similar to those ignoring transport emissions. The reason for this is that minimizing the effects of transport emissions, both mixes possess the largely same binder chemical makeup as shown in Fig. 3 by the overlaid blue dash and green dot-dash series and Table S1. However, when the transport distances in Melbourne for the maximum case, the emissions associated with using fly ash in place of GGBFS can be up to three times higher because of the increased transport distances, and therefore in this scenario the optimal mix designs in Melbourne tend to have significantly higher quantities of GGBFS than fly ash as shown in Fig. 5.

A similar outcome is also observed in Perth where the emissions associated with transporting fly ash can be five times higher than those associated with transporting GGBFS. Also of significance in Fig. 5 is that regardless of the transportation cases the quantities of aggregates do not change significantly. The small variation in the mass of aggregates can be explained by their relatively low environmental impact and cost in comparison to that which would be incurred by replacing them with additional binders.

Importantly, comparison of results including transport emissions and cost with those in Section 4.2.1 where binder chemical makeup but not transport was considered show that if transportation is ignored, optimal mix design will be strongly dependent on binder chemical makeup , however, when both chemical makeup of SCMs and cement and the emissions arisen from transportation are considered, the optimal mix designs are more strongly influenced by transportation distances.

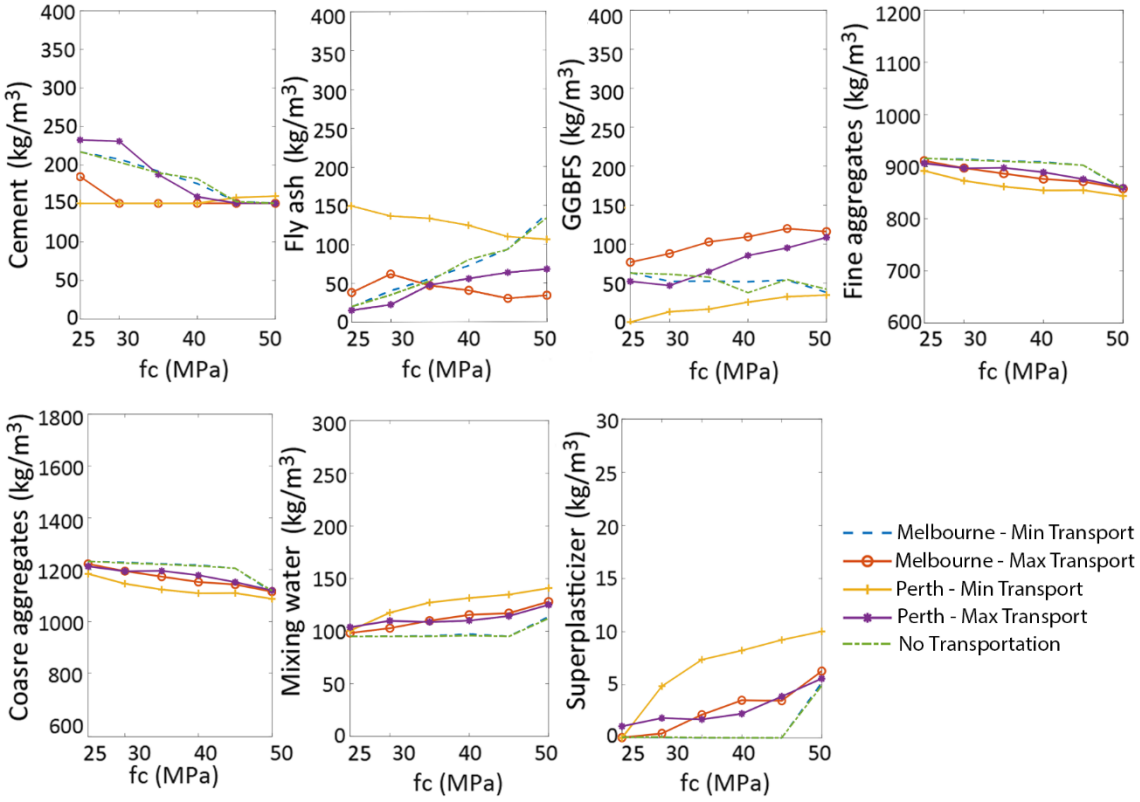

Fig. 5 Optimal SCMs mixes with different transportation cases

4.2.4 Scenario four: impact of allocation of emissions

The findings presented in the above case studies are expected to be highly sensitive to the role of emissions allocation when quantifying the environmental impact of fly ash and GGBFS. That is, if fly ash and GGBFS are considered to be a by-product rather than a waste product, a proportion of the emissions associated with burning the coal to generate electricity and smelting the steel to produce the slag must be allocated to the emissions factors of fly ash and GGBFS respectively. This allocation can be done on the basis of the mass of the by-products (fly ash or GGBFS) relative to the primary products (coal burned or steel produced) or on the basis of cost (cost of fly ash and GGBFS relative to the cost of electricity and steel), and can lead to an increase in fly ash and GGBFS emissions factors of up to 88 and 9 times respectively.

The allocation emissions factors for fly ash and GGBFS are shown in Table 2 [57] where it is seen that when an allocation by cost or mass is chosen, $CO_{2\text{-eq}}$ emissions per kg of fly ash (1.3 and 2.267 respectively for cost and mass allocation) are respectively 45% and 150% higher than $CO_{2\text{-eq}}$ emissions per kg of cement (0.896). However, the impact of allocation for GGBFS is less than that for fly ash making its emissions 74% and 24% lower than that of cement for economic and mass allocation respectively. Fig. 6 shows the binders of optimal concrete mix designs when no allocation is applied (top row) (taken from Fig. 5), economic allocation (middle row) and mass allocation are considered (bottom row) (see Supplementary Material D) for the remainder of optimal mix proportions).

From this analysis, it is clear that while in the case of no allocation cement content is pushed to the lower limit (150 kg) and mixes can either have more fly ash or GGBFS depending on

their transport emissions. For mix designs considering economic or mass allocation the optimal mixes have much more cement than SCMs regardless of their transport emissions and strongly preference the use of cement above fly ash and GGBFS in contrast to their no allocation counterparts. This is due to the lower emissions from cement than total emissions from SCMs when allocation emissions are applied. For example, for both allocation types and transportation cases the emissions per unit volume of fly ash are higher than those of cement (between 1.5 and 3 times) leading to optimum mix designs with negligible fly ash content (Fig. 6 middle and bottom rows). However, for economic allocation, GGBFS has lower emissions than cement for both transportation cases resulting in optimal mix designs having more GGBFS when considering economic allocation compared to those when considering mass allocation. It is clear that as expected from Fig. 6 that the mass of fly ash in the case of economic and mass allocation is close to zeros. This is because considering emissions minimization as the objective, while in case of no allocation, emissions from cement is 35 time more than emissions from fly ash, in economic and mass allocation, emissions from fly ash is respectively 1.5 and 2.5 times more than emissions from cement.

The results of this analysis show that ignoring allocation emissions, optimal mixes can be affected more either by binder chemical makeup when the transport emissions are ignored or by transport emissions when it is also considered as discussed in Section 4.2.1 and 4.2.3. However, when allocation procedures are also considered, optimal mixes are more strongly affected by allocation emissions of SCM. The purpose of this analysis has been to show the impact of allocation assumptions on optimal mixes–it does not suggest what should be applied in practice. As noted in Chen et al. (2010) [57] each allocation method possesses strengths and weaknesses but none are ‘incontestable’.

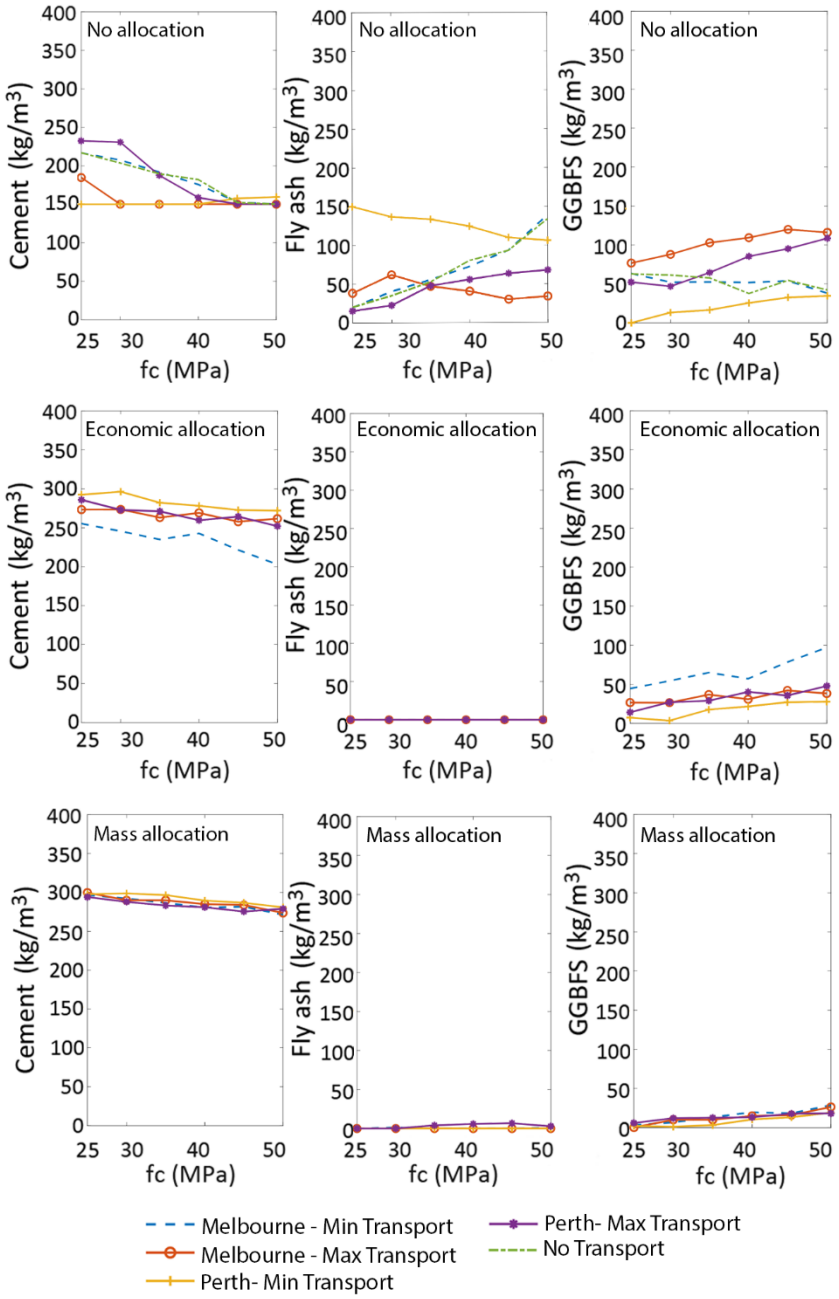

Fig. 6 Optimal SCMs binders with different allocation and transportation scenarios

4.2.5 Scenario five: sensitivity analysis of binder type

Given that the transport and allocation emissions have been shown to significantly influence the optimal mixes, let us finally examine their effects on the $CO_{2\text{-eq}}$ intensity and cost intensity of optimal SCMs mixes when compared to another type of concrete with alternative binders made from alkali activated aluminosilicate or geopolymer concrete (GPC). Supplementary Material E presents optimal GPC mixes adopted from Shobeiri et al. (2022) [27] with different allocation scenarios where it is seen that in the absence of allocation, optimal GPC mixes can either have more GGBFS or fly ash depending on their transport emissions. However, when allocation (either mass or economic) is adopted there is more GGBFS than fly ash regardless of transport emissions.

Fig. 7 shows the $CO_{2\text{-eq}}$ intensity (C_i) and the cost intensity (F_i) of optimal GPC and SCMs mixes with the same strength, slump and transportation cases. It is clear that when the allocation

of emissions is ignored (see the green series in Fig. 7), ambient cured GPC have a relative reduction in carbon intensity of between 10% and 40% (depending on the selected transportation case and compressive strength) when compared to SCMs mixes for both cities. However, oven cured GPC can have either lower or similar carbon intensity values compared to SCMs mixes depending on the transportation case. For instance, while for both cities, oven cured GPC can have a $CO_{2\text{-eq}}$ intensity of up to 30%, on average, lower than that for SCMs mixes with minimum transport distances, SCMs mixes in both cities possess similar carbon intensities to GPC when considering maximum transport distances. The reason for this can be attributed to the fact that while with minimum transport distances, emissions from cement are much higher than that from alkali activators, when considering maximum transport distances, emissions from cement can be partly compensated by the emissions from alkali activators, fly ash and GGBFS as GPC generally have much more fly ash and/or GGBFS than SCMs mixes.

When economic allocation is applied (see the blue series in Fig. 7), either GPC or SCMs mixes can have lower $CO_{2\text{-eq}}$ intensity depending on the transportation scenario. For instance, SCMs mixes with ambient or oven cured GPC in Melbourne can have a similar $CO_{2\text{-eq}}$ intensity in the case that all concrete ingredients are transported at the minimum distances. However, for the minimum transport distance case in Perth, SCMs mixes have $CO_{2\text{-eq}}$ intensity of between 10% and 25% lower (depending on the compressive strength) than GPC (ambient or oven cured). This is because the total emissions from GGBFS in Perth is 90% more than that in Melbourne as its minimum transportation distance is much longer (4.6 times).

When mass allocation is applied (see the red series in Fig. 7), the SCMs mixes possess lower carbon intensities than GPC mixes for both transportation cases and cities as emissions from GPC considering mass allocation is higher than that from economic allocation (due to having more fly ash and GGBFS in the GPC mixes than SCMs mixes). However, the $CO_{2\text{-eq}}$ intensity of SCMs mixes GPC in this scenario can vary by transport emissions. For instance, SCMs mixes can have a $CO_{2\text{-eq}}$ intensity of between 20% and 70% lower than that for GPC depending on the transportation distances and curing type.

The cost intensity (F_i) of optimal mixes is also impacted by transport emissions, curing type and allocation emissions (see bottom row of Fig. 7). Ignoring the allocation of emissions (see the green series in Fig. 7), while either SCMs or ambient cured GPC in Melbourne can be more cost-effective depending on the transportation case, they can have similar costs for both transportation cases in Perth. However, SCMs mixes can have a lower cost intensity by between 10% and 30% (depending on the compressive strength and city) than oven cured GPC with maximum transport distances. It is seen that both allocation scenarios slightly affect the mixes' cost intensity unless there is a considerable replacement of low-cost fly ash with high-cost GGBFS due to allocation emissions. For instance, the cost intensity of oven cured GPC in Perth increases by up to 125% when either economic (blue series) or mass (red series) allocation where minimum transportation distances are applied. The reason for this is that for the no allocation case, fly ash is chosen as the single binder, whereas when considering economic and mass allocation fly ash is completely replaced with GGBFS with a total cost (sum of the transportation and production cost) of 700% more than fly ash. This binder change due to allocation can lead to an increase of up to 60% in cost intensity compared to SCMs mixes with the same transportation case and city.

The above finding shows the importance of several factors including transport emissions and cost, curing type and allocation scenarios in the evaluating the sustainability of concrete with different binders. This adds additional insights to the current literature as some of these factors have previously been ignored which has formerly led to assumptions such as GPC always having lower $CO_{2\text{-eq}}$ emissions than SCMs concrete of same strength (e.g. [85]). Again, it is

not the purpose of this investigation to suggest a preferred approach for use in practice.

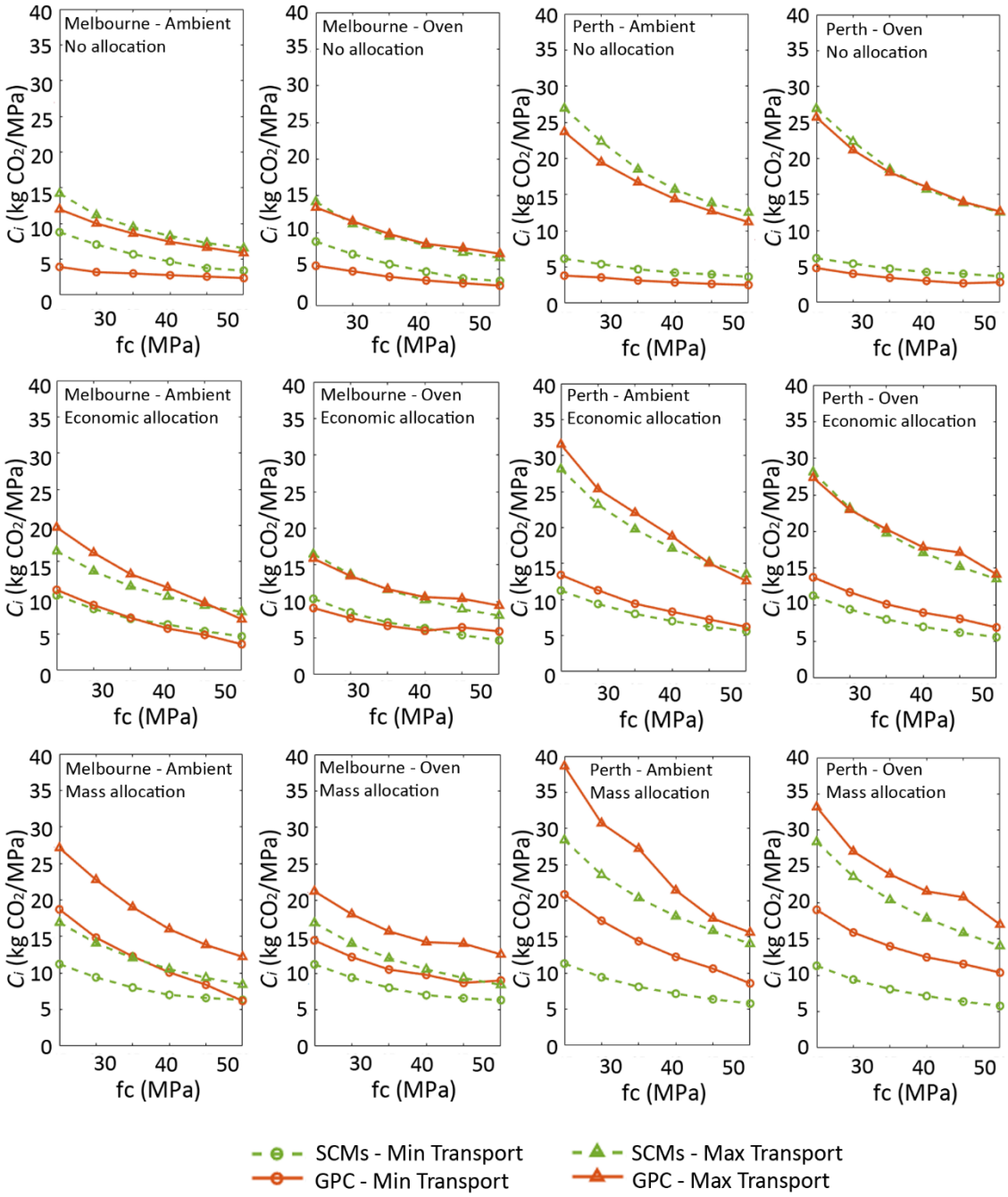

Fig. 7 $CO_{2\text{-eq}}$ intensity (C_i) of optimal GPC and SCMs mixes (ambient and oven cured) comparing different allocation approaches and transportation cases

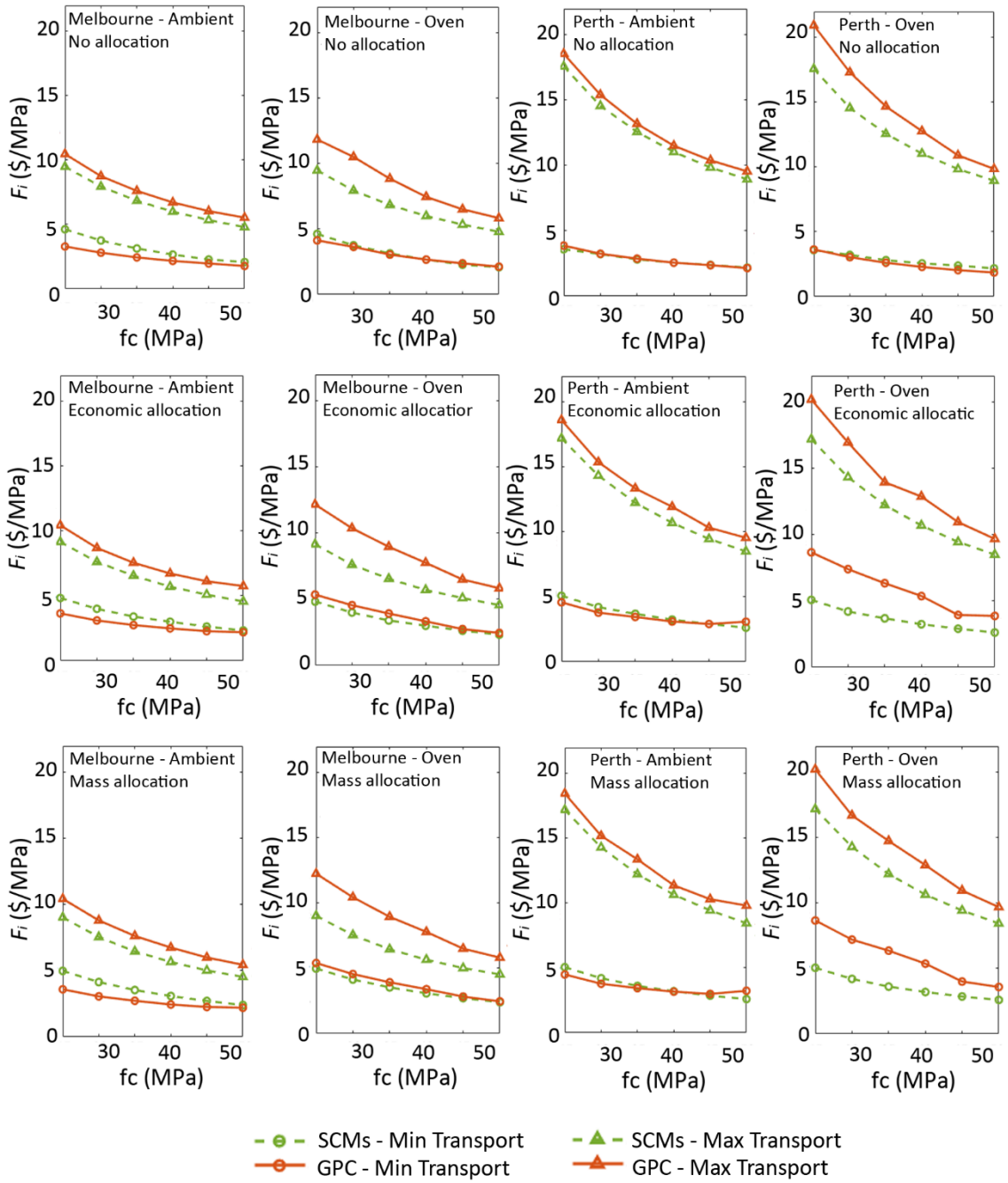

Fig. 8 Cost intensity (F_i) of optimal GPC and SCMs mixes (ambient and oven cured) comparing different allocation approaches and transportation cases

10. Conclusions

An augmented framework considering environmental and economic factors is implemented for the mix design optimization of SCMs concrete. In this study, artificial intelligence and genetic algorithm due to their capabilities in handling highly nonlinear models and as a substitution to traditional time and resource-consuming approaches, were utilized to reduce the emissions and cost of the SCMs concrete. Integrating a comprehensive database including 892 mixes with a wide range of chemical makeup for binders, the artificial neural network was able to fairly

predict the compressive strength and slump of optimal mixes which were considered as constraints for the optimization process. The analysis results on different scenarios have shown the following findings:

1- Scenario one: the results show that the mass of binder can be significantly affected by a variation in the binder's source. This indicates the important role that chemical makeup of SCMs and cement can play when it comes to the design of sustainable concretes.
2- Scenario two: the results show that for low-strength concrete (f_c < 40 MPa), the environmental and economic performance of optimal SCMs mixes with different limits on minimum cement contents is similar, for high-strength concrete, their environmental and economic performance can improve when the minimum limit on cement content decreases. The results also found that it is possible to achieve a significant reduction in emissions and cost depending on the target strength and minimum cement content compared to the experimental SCMs of the same strength in the database using the proposed approach.
3- Scenarios three and four: through a transportation sensitivity analysis combined with different allocation scenarios it was shown that with an increase in the compressive strength, mixes with no allocation scenario tend to have less cement and more SCMs based on their transport emissions. However, mixes with economic and mass allocation scenarios tend to have more cement than SCMs regardless of their transport emissions.
4- Scenario five: it was shown that the $CO_{2\text{-eq}}$ intensity and cost intensity of SCMs and GPC mixes are highly sensitive to the curing type, transport emissions and emissions allocation approach.

The framework presented is generic and can be tailored to any local application vie modification of the input parameters. In the implementation of the framework the user can make their own choice regarding what local values are suited for their application. In terms of the work presented in this study, the specific outcomes are unique, and the scenarios presented can be adapted to any local application for the purpose of reducing emissions and cost of SCMs concrete having the potential of providing additional insights.

Acknowledgments

Vahid Shobeiri was supported by an Australian Government Research Training Program Scholarship.

References

[1] Fattah, K. P., Al-Tamimi, A. K., Hamweyah, W., & Iqbal, F. (2017). Evaluation of sustainable concrete produced with desalinated reject brine. International Journal of Sustainable Built Environment, 6(1), 183-190.

[2] Tschakert, P., Waisman, H., Abdul Halim, S., Antwi-Agyei, P., Dasgupta, P., Hayward, B., & Suarez, A. Chapter 5: Sustainable Development, Poverty Eradication and Reducing Inequalities in: Global Warming of 1.5 C, An IPCC Special Report on the impacts of global warming of 1.5 C above pre-industrial levels and related global gre. IPCC SPECIAL REPORT Global Warming of 1.5 C, 445-538 (2018).

[3] Winnefeld, F., Leemann, A., German, A., & Lothenbach, B. (2022). CO2 storage in cement and concrete by mineral carbonation. Current Opinion in Green and Sustainable Chemistry, 100672.

[4] Andrew, R. M. (2018). Global CO 2 emissions from cement production. Earth System Science Data, 10(1), 195-217.

[5] Emissions, Beyond Zero. Zero carbon industry plan: rethinking cement. Beyond Zero Emissions, 2016.

[6] Hossain, M. U., Poon, C. S., Dong, Y. H., & Xuan, D. (2018). Evaluation of environmental impact distribution methods for supplementary cementitious materials. Renewable and Sustainable Energy Reviews, 82, 597-608.

[7] Xie, T., Yang, G., Zhao, X., Xu, J., & Fang, C. (2020). A unified model for predicting the compressive strength of recycled aggregate concrete containing supplementary cementitious materials. Journal of Cleaner Production, 251, 119752.

[8] Arrigoni, A., Panesar, D. K., Duhamel, M., Opher, T., Saxe, S., Posen, I. D., & MacLean, H. L. (2020). Life cycle greenhouse gas emissions of concrete containing supplementary cementitious materials: Cut-off vs. substitution. Journal of Cleaner Production, 263, 121465.

[9] Xiao, R., Jiang, X., Zhang, M., Polaczyk, P., & Huang, B. (2020). Analytical investigation of phase assemblages of alkali-activated materials in CaO-SiO2-Al2O3 systems: The management of reaction products and designing of precursors. Materials & Design, 194, 108975.

[10] Wang, D., Shi, C., Farzadnia, N., Shi, Z., & Jia, H. (2018). A review on effects of limestone powder on the properties of concrete. Construction and building materials, 192, 153-166.

[11] Jaskulski, R., Jóźwiak-Niedźwiedzka, D., & Yakymechko, Y. (2020). Calcined clay as supplementary cementitious material. Materials, 13(21), 4734.

[12] Gamage, N., Liyanage, K., Fragomeni, S., & Setunge, S. (2011). Overview of different types of fly ash and their use as a building and construction material.

[13] Panda, R., & Sahoo, T. K. (2021). Effect of Replacement of GGBS and Fly Ash with Cement in Concrete. In Recent Developments in Sustainable Infrastructure (pp. 811-818). Springer, Singapore.

[14] Skibsted, J., & Snellings, R. (2019). Reactivity of supplementary cementitious materials (SCMs) in cement blends. Cement and Concrete Research, 124, 105799.

[15] Burris, L. E., & Juenger, M. C. (2020). Effect of calcination on the reactivity of natural clinoptilolite zeolites used as supplementary cementitious materials. Construction and Building Materials, 258, 119988.

[16] Elahi, M. M. A., Shearer, C. R., Reza, A. N. R., Saha, A. K., Khan, M. N. N., Hossain, M. M., & Sarker, P. K. (2021). Improving the sulfate attack resistance of concrete by using supplementary cementitious materials (SCMs): A review. Construction and Building Materials, 281, 122628.

[17] DeRousseau, M. A., Kasprzyk, J. R., & Srubar III, W. V. (2018). Computational design optimization of concrete mixtures: A review. Cement and Concrete Research, 109, 42-53.

[18] Oner, A. D. N. A. N., Akyuz, S., & Yildiz, R. (2005). An experimental study on strength development of concrete containing fly ash and optimum usage of fly ash in concrete. Cement and Concrete Research, 35(6), 1165-1171.

[19] Lian, C., & Zhuge, Y. (2010). Optimum mix design of enhanced permeable concrete–an experimental investigation. Construction and Building Materials, 24(12), 2664-2671.

[20] Abellán García, J., Fernández Gómez, J., & Torres Castellanos, N. (2020). Properties prediction of environmentally friendly ultra-high-performance concrete using artificial neural networks. European Journal of Environmental and Civil Engineering, 1-25.

[21] Sharifi, E., Sadjadi, S. J., Aliha, M. R. M., & Moniri, A. (2020). Optimization of high-strength self-consolidating concrete mix design using an improved Taguchi optimization method. Construction and Building Materials, 236, 117547.

[22] Li, Z., Lu, D., & Gao, X. (2021). Optimization of mixture proportions by statistical experimental design using response surface method-A review. Journal of Building Engineering, 102101.

[23] Bhamare, D., & Suryawanshi, P. (2018). Review on reliable pattern recognition with machine learning techniques. Fuzzy Information and Engineering, 10(3), 362-377.

[24] Falcone, R., Lima, C., & Martinelli, E. (2020). Soft computing techniques in structural and earthquake engineering: a literature review. Engineering Structures, 207, 110269.

[25] Arimanwa, M. C., Onwuka, D. O., & Arimanwa, J. I. (2016). Effect of Chemical Composition of Ordinary Portland cement on the Compressive Strength of Concrete. International refereed journal of Engineering and Science, 5(3), 20-31.

[26] Cho, Y. K., Jung, S. H., & Choi, Y. C. (2019). Effects of chemical composition of fly ash on compressive strength of fly ash cement mortar. Construction and Building Materials, 204, 255-264.

[27] Shobeiri, V., Bennett, B., Xie, T., & Visintin, P. (2022). A generic framework for augmented concrete mix design: Optimisation of geopolymer concrete considering environmental, financial and mechanical properties. Journal of Cleaner Production, 133382. https://doi.org/10.1016/j.jclepro.2022.133382

[28] Miller, S. A., Horvath, A., Monteiro, P. J., & Ostertag, C. P. (2015). Greenhouse gas emissions from concrete can be reduced by using mix proportions, geometric aspects, and age as design factors. Environmental Research Letters, 10(11), 114017.

[29] Adesina, A. (2020). Recent advances in the concrete industry to reduce its carbon dioxide emissions. Environmental Challenges, 1, 100004.

[30] Caldas, L. R., & Sposto, R. M. (2017). CO 2 emissions related to building materials transportation in Brazil: comparative study on structural ceramic and concrete bricks. Ambiente Construído, 17, 91-108.

[31] Directive 2008/98/Ec on Waste (Waste Framework Directive) - Environment - European Commission

[32] Anastasiou, E. K., Liapis, A., & Papayianni, I. (2015). Comparative life cycle assessment of concrete road pavements using industrial by-products as alternative materials. Resources, Conservation and Recycling, 101, 1-8.

[33] Seto, K. E., Churchill, C. J., & Panesar, D. K. (2017). Influence of fly ash allocation approaches on the life cycle assessment of cement-based materials. Journal of Cleaner Production, 157, 65-75.

[34] Noguchi, T., Maruyama, I., & Kanematsu, M. (2003, May). Performance based design system for concrete mixture with multi-optimizing genetic algorithm. In Proceedings of the 11th international congress on the chemistry of cement "Cements Contribution to the Development in the 21st Century", Durban.

[35] Lim, C. H., Yoon, Y. S., & Kim, J. H. (2004). Genetic algorithm in mix proportioning of

high-performance concrete. Cement and Concrete Research, 34(3), 409-420.

[36] Yeh, I. C. (2007). Computer-aided design for optimum concrete mixtures. Cement and Concrete Composites, 29(3), 193-202.

[37] Jayaram, M. A., Nataraja, M. C., & Ravikumar, C. N. (2009). Elitist genetic algorithm models: optimization of high performance concrete mixes. Materials and Manufacturing Processes, 24(2), 225-229.

[38] Lee, J. H., Yoon, Y. S., & Kim, J. H. (2012). A new heuristic algorithm for mix design of high-performance concrete. KSCE Journal of Civil Engineering, 16(6), 974-979.

[39] Park, W. (2013). Genetic-algorithm-based mix proportion design method for recycled aggregate concrete. Transactions of the Canadian Society for Mechanical Engineering, 37(3), 345-354.

[40] Cheng, M. Y., Prayogo, D., & Wu, Y. W. (2014). Novel genetic algorithm-based evolutionary support vector machine for optimizing high-performance concrete mixture. Journal of Computing in Civil Engineering, 28(4), 06014003.

[41] Dan, S., & Barai, S. V. (2014, August). Sustainable concrete mix—Design: Evolutionary algorithm approach. In 2014 International Conference on Data Science & Engineering (ICDSE) (pp. 94-99). IEEE.

[42] Golafshani, E. M., & Behnood, A. (2019). Estimating the optimal mix design of silica fume concrete using biogeography-based programming. Cement and Concrete Composites, 96, 95-105.

[43] Kwon, S. J., & Wang, X. Y. (2019). Optimization of the mixture design of low-CO2 high-strength concrete containing silica fume. Advances in Civil Engineering, 2019.

[44] Naseri, H. (2019). Cost optimization of no-slump concrete using genetic algorithm and particle swarm optimization. International Journal of Innovation, Management and Technology, 10(1), 33-37.

[45] Lee, H. S., Lim, S. M., & Wang, X. Y. (2019). Optimal Mixture Design of Low-CO 2 High-Volume Slag Concrete Considering Climate Change and CO 2 Uptake. International Journal of Concrete Structures and Materials, 13(1), 1-13.

[46] Zhang, J., Huang, Y., Wang, Y., & Ma, G. (2020). Multi-objective optimization of concrete mixture proportions using machine learning and metaheuristic algorithms. Construction and Building Materials, 253, 119208.

[47] Sadrossadat, E., Basarir, H., Karrech, A., & Elchalakani, M. (2021). Multi-objective mixture design and optimisation of steel fiber reinforced UHPC using machine learning algorithms and metaheuristics. Engineering with Computers, 1-14.

[48] Zhang, J., Huang, Y., Ma, G., & Nener, B. (2021). Mixture optimization for environmental, economical and mechanical objectives in silica fume concrete: A novel frame-work based on machine learning and a new meta-heuristic algorithm. Resources, Conservation and Recycling, 167, 105395.

[49] Shobeiri, V., Bennett, B., Xie, T., & Visintin, P. (2021). A comprehensive assessment of the global warming potential of geopolymer concrete. Journal of Cleaner Production, 297, 126669.

[50] The MathWorks, Inc. (2020a) Neural Network Toolbox, Natick, Massachusetts, United State

[51] Akpinar, P., & Uwanuakwa, F. I. D. (2016). Intelligent prediction of concrete carboration depth using neural networks. Bulletin of the Transilvania University of Brasov. Mathematics, Informatics, Physics. Series III, 9(2), 99.

[52] Naderpour, H., Rafiean, A. H., & Fakharian, P. (2018). Compressive strength prediction of environmentally friendly concrete using artificial neural networks. Journal of Building Engineering, 16, 213-219.

[53] Liu, Q. F., Iqbal, M. F., Yang, J., Lu, X. Y., Zhang, P., & Rauf, M. (2021). Prediction of chloride diffusivity in concrete using artificial neural network: Modelling and performance evaluation. Construction and Building Materials, 268, 121082.

[54] Xie, T., & Visintin, P. (2018). A unified approach for mix design of concrete containing supplementary cementitious materials based on reactivity moduli. Journal of Cleaner Production, 203, 68-82.

[55] UNESCO. Reinforced Concrete: An International Manual. London: Butterworths, 1971, p. 20.

[56] Wong, H. D. (2013). Cylinder Strength versus Cube Strength. In Standing Committee on Concrete Technology Annual Concrete Seminar, CEDD, Hong Kong.

[57] Chen, C., Habert, G., Bouzidi, Y., Jullien, A., & Ventura, A. (2010). LCA allocation procedure used as an incitative method for waste recycling: An application to mineral additions in concrete. Resources, Conservation and Recycling, 54(12), 1231-1240.

[58] Gursel, A.P. (2014). Life-cycle Assessment of Concrete: Decision-Support Tool and Case Study Application (UC Berkeley).

[59] Teh, S. H., Wiedmann, T., Castel, A., & de Burgh, J. (2017). Hybrid life cycle assessment of greenhouse gas emissions from cement, concrete and geopolymer concrete in Australia. Journal of Cleaner Production, 152, 312-320.

[60] Wang, X. Y. (2020). Optimal mix design of low-CO2 blended concrete with limestone powder. Construction and Building Materials, 263, 121006.

[61] Naseri, H., Jahanbakhsh, H., Hosseini, P., & Nejad, F. M. (2020). Designing sustainable concrete mixture by developing a new machine learning technique. Journal of Cleaner Production, 258, 120578.

[62] Yurdakul, E. (2010). Optimizing concrete mixtures with minimum cement content for performance and sustainability. Iowa State University.

[63] LeBow, C. (2018). Effect of cement content on concrete performance. University of Arkansas.

[64] Yu, J., Li, X., Fleming, D., Meng, Z., Wang, D., & Tahmasebi, A. (2012). Analysis on characteristics of fly ash from coal fired power stations. Energy Procedia, 17, 3-9.

[65] Ngu, L. N., Wu, H., & Zhang, D. K. (2007). Characterization of ash cenospheres in fly ash from Australian power stations. Energy & Fuels, 21(6), 3437-3445.

[66] Williams, R. P., & Van Riessen, A. (2010). Determination of the reactive component of fly ashes for geopolymer production using XRF and XRD. Fuel, 89(12), 3683-3692.

[67] Habert, G., De Lacaillerie, J. D. E., & Roussel, N. (2011). An environmental evaluation of geopolymer based concrete production: reviewing current research trends. Journal of cleaner production, 19(11), 1229-1238.

[68] Fly Ash Market, 2018. https://www.marketsandmarkets.com/Market-Reports/flyash-

market-76345803.html.

[69] Brinsmead, T.S., Hayward, J., Graham, P., 2014. Australian electricity market analysis report to 2020 and 2030, CSIRO report No. EP141067.

[70] Grand View Research, 2017. https://www.grandviewresearch.com/press-release/ global-steel-market

[71] LP Information (LPI), 2020. Global ground granulated blast-furnace slag (GGBFS) market growth, 2020e2025

[72] Guirguis, S. (1998). Cements: Properties and Characteristics. Cement and Concrete Association of Australia.

[73] Heaton, B. S., Down, F. W., & Emery, J. J. (1981). Properties of Ground Granulated Slags in Cement Blends. In The Second Australian Conference on Engineering Materials, held at Sydney, July 6-8, 1981.

[74] Phul, A. A., Memon, M. J., Shah, S. N. R., & Sandhu, A. R. (2019). GGBS and fly ash effects on compressive strength by partial replacement of cement concrete. Civil Engineering Journal, 5(4), 913-921.

[75] Shirdam, R., Amini, M., & Bakhshi, N. (2019). Investigating the Effects of Copper Slag and Silica Fume on Durability, Strength, and Workability of Concrete. International Journal of Environmental Research, 13(6), 909-924.

[76] Giergiczny, Z. (2019). Fly ash and slag. Cement and Concrete Research, 124, 105826.

[77] Benaicha, M., Jalbaud, O., Roguiez, X., Alaoui, A. H., & Burtschell, Y. (2015). Prediction of Self-Compacting Concrete homogeneity by ultrasonic velocity. Alexandria Engineering Journal, 54(4), 1181-1191.

[78] Ding, X., Ma, T., Zhang, W., Zhang, D., & Yin, T. (2018). Effects by property homogeneity of aggregate skeleton on creep performance of asphalt concrete. Construction and Building Materials, 171, 205-213.

[79] Olowofoyeku, A. M., Ofuyatan, O. M., Oluwafemi, J., & David, O. (2019, November). Effect of various types and sizes of aggregate on self-compacting concrete. In IOP Conference Series: Materials Science and Engineering (Vol. 640, No. 1, p. 012054). IOP Publishing.

[80] Oner, A. D. N. A. N., & Akyuz, S. (2007). An experimental study on optimum usage of GGBS for the compressive strength of concrete. Cement and concrete composites, 29(6), 505-514.

[81] Pillai, R. G., Gettu, R., & Santhanam, M. (2020). Use of supplementary cementitious materials (SCMs) in reinforced concrete systems–Benefits and limitations. Revista ALCONPAT, 10(2), 147-164.

[82] Brueggen, B., Kang, T. H., & Ramseyer, C. (2010). Experimental and SEM analyses of ground fly ash in concrete. International Journal of Concrete Structures and Materials, 4(1), 51-54.

[83] Uthaman, S., Vishwakarma, V., George, R. P., Ramachandran, D., Kumari, K., Preetha, R., ... & Amarendra, G. (2018). Enhancement of strength and durability of fly ash concrete in seawater environments: Synergistic effect of nanoparticles. Construction and Building Materials, 187, 448-459.

[84] Sethi, B., & Ahalawat, S. (2019). Fly Ash: A Potential By-Product Waste. In Zero Waste (pp. 301-315). CRC Press.

[85] Alsalman, A., Assi, L. N., Kareem, R. S., Carter, K., & Ziehl, P. (2021). Energy and CO2 emission assessments of alkali-activated concrete and Ordinary Portland Cement concrete: A comparative analysis of different grades of concrete. Cleaner Environmental Systems, 3, 100047.

[86] Gagné, R. (2016). Air entraining agents. In Science and Technology of Concrete Admixtures (pp. 379-391). Woodhead Publishing.

[87] Xie, T., & Visintin, P. (2018). A unified approach for mix design of concrete containing supplementary cementitious materials based on reactivity moduli. Journal of Cleaner Production, 203, 68-82.

[88] Oyebisi, S., Igba, T., Raheem, A., & Olutoge, F. (2020). Predicting the splitting tensile strength of concrete incorporating anacardium occidentale nut shell ash using reactivity index concepts and mix design proportions. Case Studies in Construction Materials, 13, e00393.

[89] Oyebisi, S., Ede, A., Olutoge, F., & Ogbiye, S. (2020). Evaluation of reactivity indexes and durability properties of slag-based geopolymer concrete incorporating corn cob ash. Construction and Building Materials, 258, 119604.

Supplementary Material A

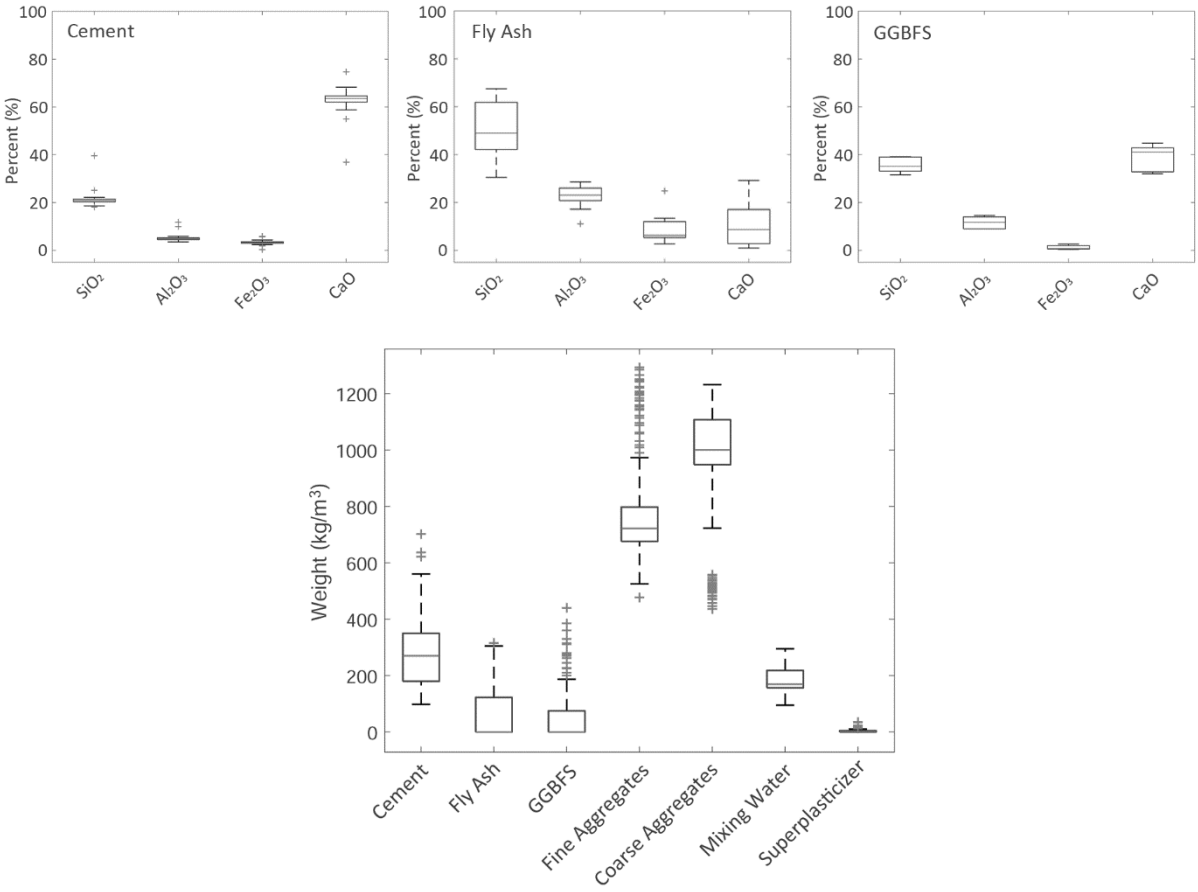

Fig. A-1 Distribution of SCMs concrete ingredients and chemical compositions of binders in the database.

Supplementary Material B

Table B-1 Transportation distance and mode of source materials for sensitivity analysis (adapted from Shobeiri et al. 2021).

Batching Plant	Case	GGBFS		FA	Quarry	Chemical Products	Cement
Melbourne		Port Kembla		Mt Piper Power Station	St Salmon	Melbourne-based provider	
		Road (km)		Road (km)	Road (km)	Road (km)	
	Min	845		835	2	41	
		Port Yokohama		Collie Power Station	Irymple	Perth-based provider	Waurn Ponds
		Water (km)		Road (km)	Road (km)	Road (km)	Road (km)
	Max	9088		3302	543	3420	90
Perth		Port Kembla		Collie Power Station	Strelley	Perth-based provider	
		Road (km)	Rail + road (km)	Road (km)	Road (km)	Road (km)	
	Min	3903	4441 + 21	219	13	10	

		Port Yokohama	Eraring Power Station	Gaskell Rd	Brisbane-based provider	Munster
		Water (km)	Road (km)	Road (km)	Road (km)	Road (km)
	Max	8317	3950	1647	4302	53

Supplementary Material C

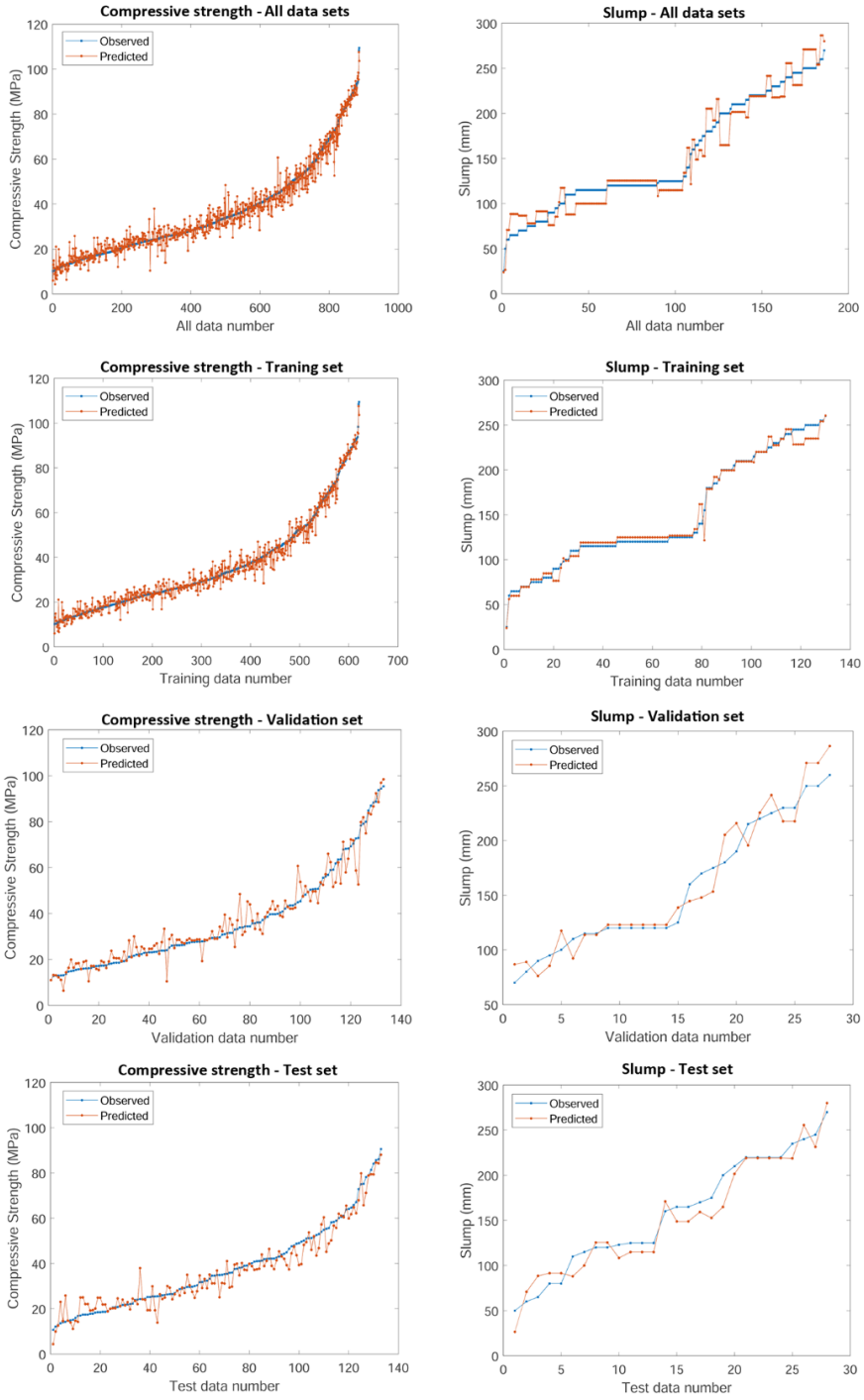

Fig. C-1 Prediction errors of compressive strength and slump for training set, test set, validation set and all-data sets

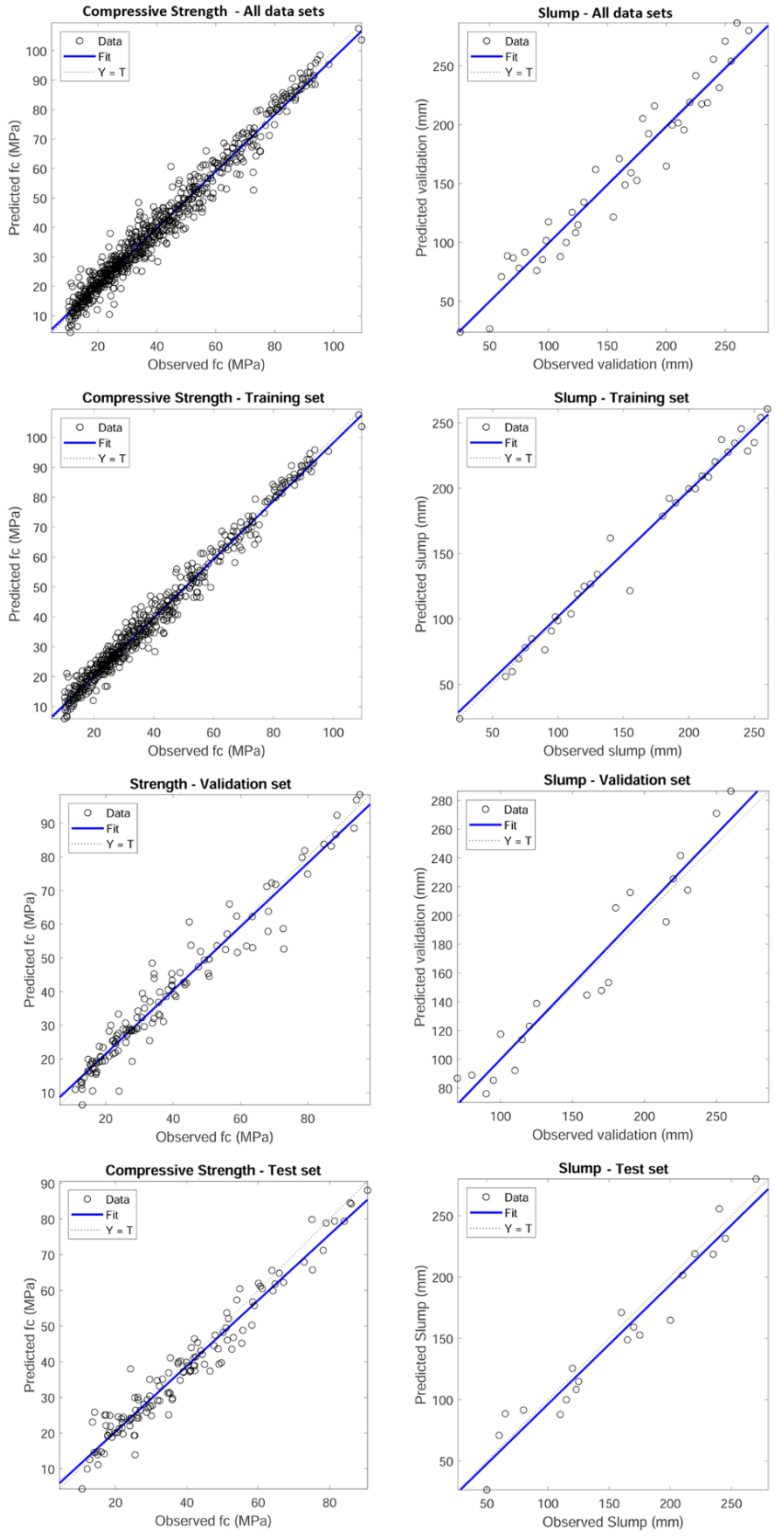

Fig. C-2 Correlation between the predicted compressive strength and slump for training set, test set, validation set and all-data sets

Supplementary Material D

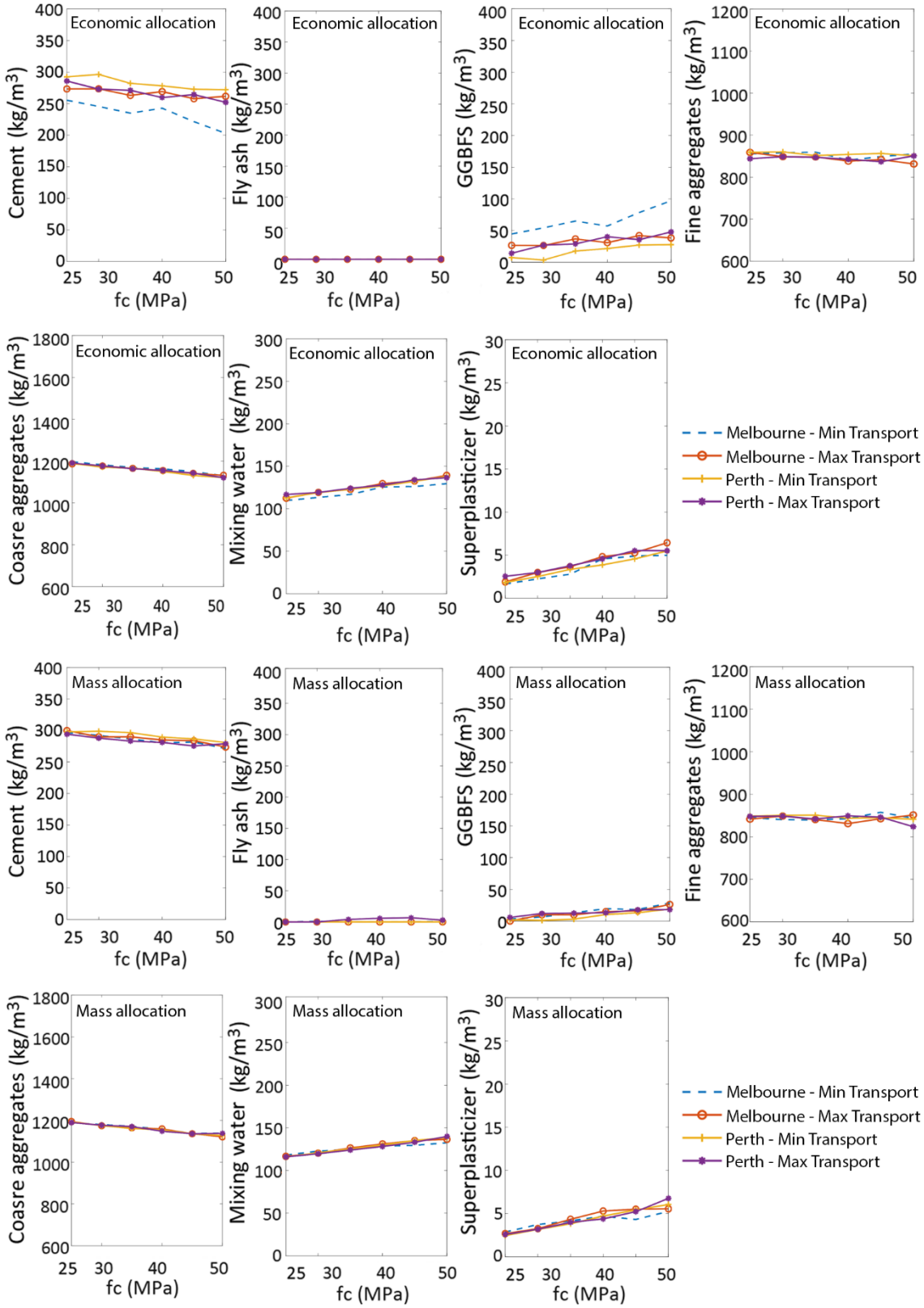

Fig. D-1 Optimal SCMs mixes with different allocation scenarios

Supplementary Material E

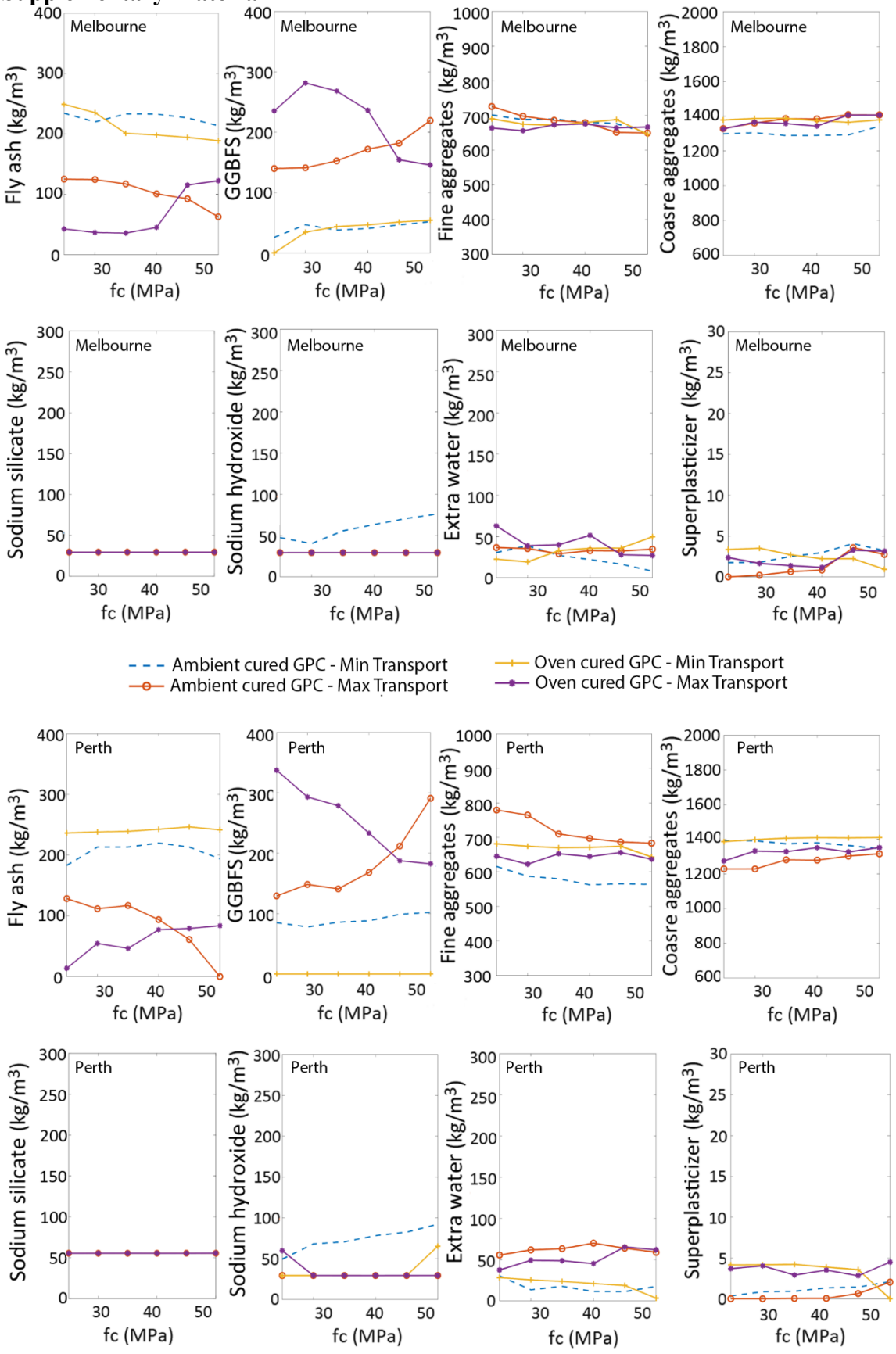

Fig. E-1 Optimal GPC mixes with no allocation scenario

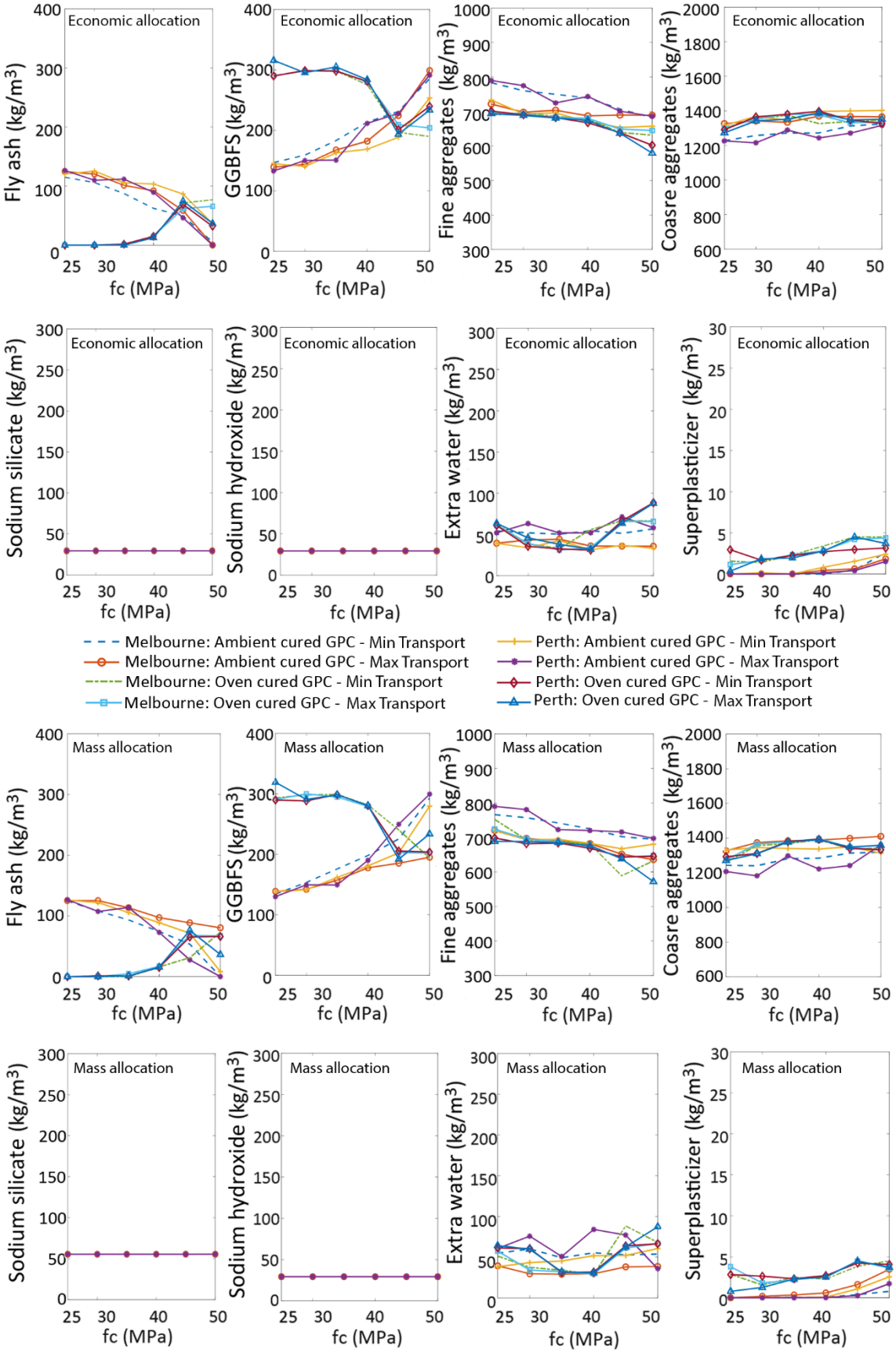

Fig. E-2 Optimal GPC mixes with different allocation scenarios

CHAPTER 3

Background

In this chapter, the developed generic mix design optimization framework is utilized to find optimum mixes of concrete with alternative fillers. Empirical models for mechanical properties of concrete with alternative fillers are also derived using a set of regression models.

The first publication *"A Comprehensive Data Driven Study of Mechanical Properties of Concrete with Waste-Based Aggregates: Plastic, Rubber, Slag, Glass and Concrete"* examines different fresh and hardened properties of concrete containing recycled plastic, rubber, slag, glass and concrete aggregates by analysing a large database of waste aggregate based concrete mixes. The influence of waste based aggregate type and replacement ratio on the concrete mechanical properties are investigated and the empirical models for mechanical properties of concrete with waste-based aggregates are developed and compared with existing models in the codes of practice.

The second publication *"Mix Design Optimization of Waste-based Aggregate Concrete for Natural Resource Utilization and Global Warming Potential"* first presents an ANN model to predict different properties of concrete with waste-based aggregates and then explores optimum mixes of concrete with different types of waste-based aggregates in terms of minimizing carbon dioxide emissions and natural resource utilization.

List of manuscripts

Shobeiri, V., Bennett, B., Xie, T., & Visintin, P. (2023). "Mix Design Optimization of Waste-based Aggregate Concrete for Natural Resource Utilization and Global Warming Potential". For Submission to *Journal of Cleaner Production*

Shobeiri, V., Bennett, B., Xie, T., & Visintin, P. (2023). "A Comprehensive Data Driven Study of Mechanical Properties of Concrete with Waste-Based Aggregates: Plastic, Rubber, Slag, Glass and Concrete". For Submission to *Journal of Sustainable Cement-Based Materials*

STATEMENT OF AUTHORSHIP

"A Comprehensive Data Driven Study of Mechanical Properties of Concrete with Waste-Based Aggregates: Plastic, Rubber, Slag, Glass and Concrete "
For Submission to *Journal of Sustainable Cement-Based Materials*

Shobeiri, V. (Candidate)

Prepared manuscript, performed all analyses, developed model and theory and acted as corresponding author (70%)

This paper reports on original research I conducted during the period of my Higher Degree by Research candidature and is not subject to any obligations or contractual agreements with a third party that would constrain its inclusion in this thesis. I am the primary author of this paper.

Signed… Date16/03/2023

Bennett, B.

Supervised and contributed to research (10%)

I certify that the candidate's stated contribution to the publication is accurate (as detailed above); permission is granted for the candidate in include the publication in the thesis; and the sum of all co-author contributions is equal to 100% less the candidate's stated contribution.

Signed… Date 17/04/2023

Xie, T.

Supervised and contributed to research (10%)

I certify that the candidate's stated contribution to the publication is accurate (as detailed above); permission is granted for the candidate in include the publication in the thesis; and the sum of all co-author contributions is equal to 100% less the candidate's stated contribution.

Signed… Date 17/04/2023

Visintin, P.

Supervised and contributed to research, and acted as corresponding author (10%)

I certify that the candidate's stated contribution to the publication is accurate (as detailed above); permission is granted for the candidate in include the publication in the thesis; and the sum of all co-author contributions is equal to 100% less the candidate's stated contribution.

Signed… Date 04/04/2023

A Comprehensive Data Driven Study of Mechanical Properties of Concrete with Waste-Based Aggregates: Plastic, Rubber, Slag, Glass and Concrete

Vahid Shobeiri, Bree Bennett, Tianyu Xie and Phillip Visintin

Abstract

In an attempt to reduce the environmental impact of concrete and reduce the consumption of natural resources, much research has focused on the development of mix designs that replace natural aggregates with waste materials. While this research has generally demonstrated feasibility, very limited research has aimed to compare the mechanical properties of these waste-based concretes to identify optimal usage. To this end, this paper investigates the properties (compressive strength, splitting tensile strength, flexural strength, elastic modulus, water absorption and slump) of concrete containing waste plastic, rubber, slag, glass and concrete aggregates by analysing a large database of 5321 waste aggregate based concrete mixes. The effects of waste-based aggregate type and the replacement ratio on the mechanical properties is discussed and the relationship between tensile strength, elastic modulus and compressive strength is quantified and compared to existing code approaches for natural aggregate concretes. Results show that the concrete mechanical properties are significantly affected by aggregate type. It is expected that the findings from this study can be helpful in identifying the optimum waste-based aggregate type based on intended use and that the databases compiled will assist in future data-driven modelling approaches.

Keywords: Waste-based aggregate concrete; waste aggregate type; mechanical properties, empirical models

Introduction

Preservation of natural resources and the reduction of Carbon Dioxide (CO_2) emissions are two of the great challenges society currently faces [1]. As one of the major contributors to CO_2 emissions and natural resource depletion, concrete accounts for the emission of nearly 8% of global greenhouse gas emissions and the consumption of 30% of non-renewable natural resources [2-3]. As a result, concrete production is credited as the sector that consumes the largest amount of natural resources [4]. For example, the global production of concrete consumes more than 4 billion tons of Ordinary Portland Cement (OPC), 8 billion tons of natural aggregates and 2 billion tons of freshwater annually [5-6]. This demand for concrete is expected to further rise as both population growth and an improved standard of living increase the demand for public infrastructure and high-density housing [7].

Aggregate is the primary ingredient of concrete by mass and accounts for approximately 75% of the total mass of concrete [8]. An effective approach for reducing the natural resource demand of concrete is to therefore replace natural aggregates with waste-based aggregates. Importantly from a supplier perspective, the incorporation of waste-based aggregates also has the potential to reduce the unit cost of concrete [9-12].

Waste-based concretes, and in particular those based on construction and demolition waste, have been predominately used in pavement design and have been incorporated into several national codes (e.g., European Cement Research Academy [13]). No waste-based concretes have however been widely utilized in structural concrete. To address this limitation, many studies have been conducted to develop structural grade concrete containing waste-based aggregates [14-16]. Due to variability in the characteristics of waste-based aggregates, concrete mechanical (e.g. slump, compressive and tensile strength and elastic modulus) and durability (e.g. water absorption) properties may vary significantly from identical mix designs containing only natural aggregates. This is important because it is these basic mechanical and durability

properties that are the basis for structural design [17].

A review of existing studies on the waste aggregate based concrete shows that while there are many studies in the literature that report experimental observations of changes to concrete compressive strength on the basis of the addition of varying proportions of a given type of waste-based aggregate; or that apply computational intelligence techniques (e.g., machine learning and artificial intelligence) to predict changes in compressive strength [18], there are a few studies dealing with the broader set of properties that are equally important for structural design [19]. This is important because the significant difference in the properties of natural and waste-based aggregates means that it is unlikely that the traditional approximations that may reliably be used to connect the compressive strength of concrete to its other mechanical properties will broadly apply to waste-based concrete.

The significant difference in the properties of various waste-based aggregates introduces the need for additional studies to investigate their mechanical properties in order to identify the optimum aggregate material based on the target mechanical properties, environmental considerations and the availability of waste materials. Moreover, because studies quantifying the performance of waste-based concretes are generally small and consider a limited parametric range, in order to apply computational intelligence methods to predict material performance, there is a need to aggregate the results from various studies to broaden the parametric variation.

In this study, we attempt to address these limitations by analysing a large database including 5321 concrete mixes containing different types of waste-based aggregates. As part of the study, the fresh and hardened properties of concretes with waste-based aggregates are studied and the interaction between conserving the natural resource by using waste-based aggregates and the resulting global warming potential (GWP) is investigated in terms of binder intensity. A series of regression analyses is also undertaken to identify models that link the broader mechanical properties of the concrete to the compressive strength.

Database description

To obtain a broad range of waste-based concrete mix designs, a database of 5321 mix designs were collected from 285 studies. The database includes: 1865 mixes with coarse recycled concrete aggregates, 1732 mixes with rubber aggregates, 213 mixes with fine and coarse plastic aggregates, 162 mixes with coarse steel slag aggregates, 153 mixes with fine glass aggregates and 1196 control mixes with only natural aggregates.

When considering plastic aggregates-based concrete, the database only includes mixes with polyethylene terephthalate (PET) and high-density polyethylene (HDPE) plastic aggregates because these make up the majority of all test data. Further, when considering concrete with rubber aggregates, the database includes those with rubber power, rubber crumb and rubber chips.

The resulting database contains 3728 measurements of 28-day compressive strength obtained from cubic samples ($f'_{c,cube}$), 1578 measurements of compressive strength obtained from cylindrical samples ($f'_{c,cylinder}$), 1181 measurements of elastic modulus (E_c), 2030 measurements of splitting tensile strength results (f_{st}), 1114 measurements of flexural strength results (f_r), 992 measurements of slump and 272 measurements of water absorption across all aggregate types. It should be noted that for rubber, concrete and plastic aggregate mix designs, the databases collated by Ref. [20-23] were reviewed and updated to include additional data and also to include information on water absorption, splitting tensile strength and flexural strength at different ages as well as binder chemical composition wherever possible.

The database provided in Supplementary Material A contains the following information

wherever reported:

- Concrete mix proportions including: mass of each binder material, natural and waste coarse and fine aggregates, water and superplasticizer; water-to-binder ratio, total aggregate-to-binder ratio (by weight) and waste aggregate replacement ratio (by weight).
- Chemical and physical characterizations of each concrete ingredient including: binder chemical composition, aggregate properties (specific gravity, fineness modulus, water absorption and maximum particle size of waste and natural aggregates).
- Concrete slump.
- Concrete curing conditions, size and shape of test specimens.
- Concrete mechanical properties at different ages including: compressive strength, elastic modulus, flexural strength, density and water absorption of concrete.

When collating the test database, to avoid the introduction of parameters with small test datasets only mixes under standard curing conditions were considered and supplementary cementitious materials (SCMs) were limited to fly ash, GGBFS, silica fume and kaolin.

The distributions of the most influential mix design parameters (i.e. water-to-binder (w/b) ratio, SCMs-to-binder ratio (s/b), binder-to-aggregate ratio (b/a) and fine-to-coarse aggregate ratio (fa/ca) and with the variations in the resulting mechanical properties is shown in Fig. 1 for each aggregate type. From Fig. 1 it can be observed that this database covers a broad range of cubic and cylindrical compressive strength (f_c'), elastic modulus (E_c), splitting tensile strength (f_{st}), flexural strength (f_r), slump, water absorption and waste aggregate replacement ratio (RR) for concrete with slag, concrete, glass, plastic and rubber aggregates. When interpreting Fig. 1, it should be noted that outliers have been evaluated based on the interquartile range (IQR) rule which identifies any point is an outlier if it is more 1.5 times of IQR.

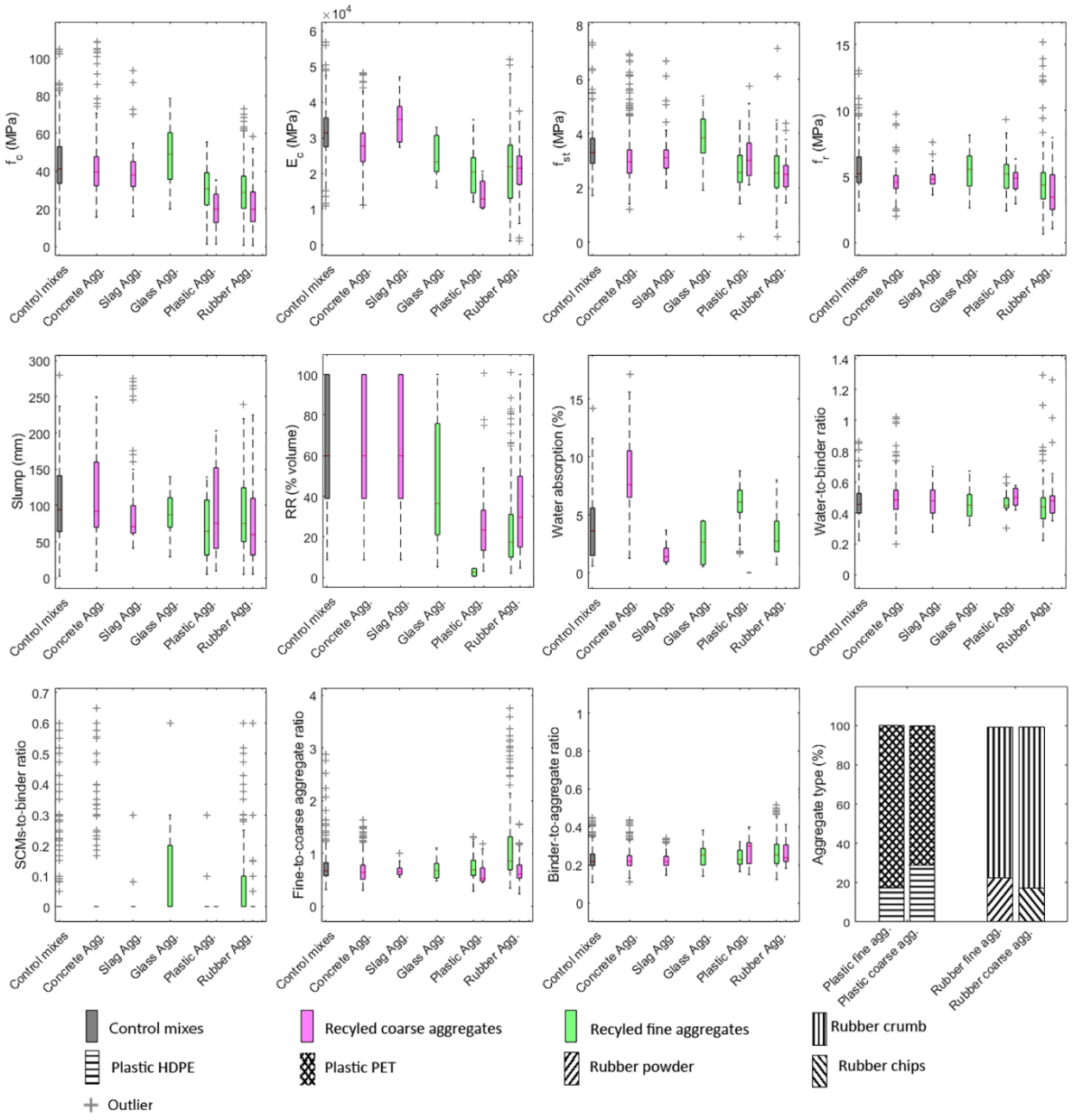

Fig. 1. Distribution of mechanical properties and other influential parameters in the waste aggregate based concrete database

Results and discussion

In this section the database is examined in more detail to identify the mechanisms that influence the behavior of the fresh and hardened properties for each type of waste aggregate-based concrete.

2.1 Fresh properties of concrete with waste-based

To better understand the effect of waste aggregate type on the concrete workability, in Fig. 2, the change of concrete slump with waste aggregate replacement ratio (*RR %*), water-to-binder ratio and superplasticizer content is shown separately for concrete containing each type of waste-based aggregate. To visualize these relationships, the ordinate reports slump, the abscissa reports the proportion by volume ratio of waste aggregate, the marker color is used to indicate water-to-binder ratio and the marker size is used to indicate superplasticizer content

(kg).

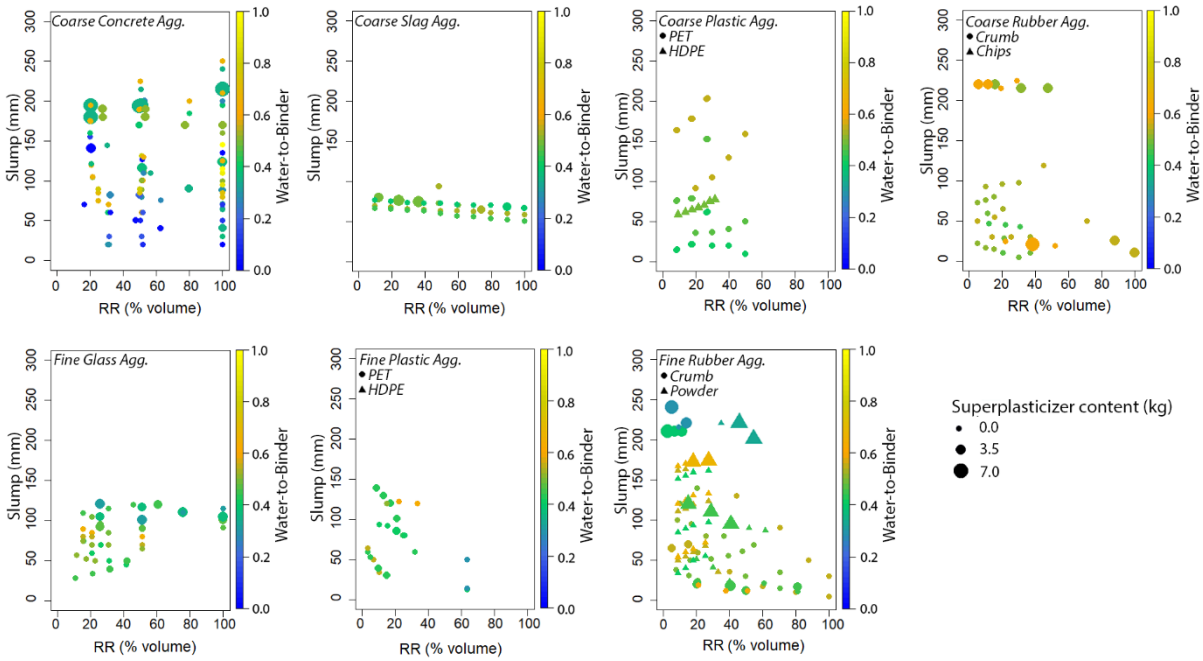

Fig. 2. Slump value of concrete with different types of waste aggregates

It can be seen from in Fig. 2, that as expected, the slump of all concretes with waste-based aggregates generally increases with an increase in the superplasticizer (SP) content, which is shown in Fig 2 as a function of marker size. The exception to this is concrete where crumb rubber aggregate replaces over 80% of the natural aggregates, at which point it appears that SP addition is no longer efficient. This change in behavior is attributed to the absorptive nature of the rubber aggregate, and also to their stiffness which causes them to deform, consuming kinetic energy and adversely affecting the flow of the concrete. This behavior is observed by other researchers [24-26] who report the need for increased SP dosages to maintain slump when replacing high volumes of natural aggregate with rubber aggregate.

Considering the marker size and color as the indicators of superplasticizer content and water-to-binder ratio respectively, it is seen from Fig. 2 for concrete with coarse concrete aggregates that mixes with similar maker size and color (similar superplasticizer content and water-to-binder ratio) and similar waste aggregate content (*RR* (%)) (see abscissa) can have substantially different slumps. For instance, it can be seen that for a 100% *RR*, the markers that represent the mixes with the smallest size (no superplasticizer) and similar color can have a slump value of between 120 mm to 250 mm. The reason for this can be attributed to several factors such as coarse-to-fine aggregate ratio and binder-to-total aggregate ratio as well as the initial moisture states of recycled concrete aggregates affecting the initial free water content of the mixture [27-31].

It is also clear that while the use of more coarse slag aggregates without admixture reduces the concrete slump generally, due to their rough surface and texture and absorptive capacity, higher percentages of fine glass aggregates may improve the concrete slump possibly due to their smooth impermeable surfaces [32-37]. Comparing across different aggregate types in Fig. 2 it can also be seen that regardless of type and size of rubber aggregates, concretes that contain rubber aggregates generally have limited workability when the waste aggregate content exceeds 40%, unless a higher water-to-binder ratio or superplasticizer content is used. The reason for this can be attributed to the water absorption capacity of rubber particles, their high

surface area, their soft nature, and the balling effects of rubber fibers, all of which negatively affect workability [38-40]. It can also be noted that in most cases for concrete containing coarse plastic aggregates with similar water-to-binder ratio and superplasticizer content, slump can slightly increase with an increase in *RR* (%). The reason for this may be attributed to the the relatively uniform size of manufactured aggregates, smoother surface and lower water absorption of plastic coarse aggregates as compared to natural coarse aggregates, leading to slightly better workability [41-44]. However, a reverse trend can be observed for the slump of concrete with small flaky plastic particles possibly due to their larger surface area and more angular shape compared to the rounded shape of natural sand particles [45-47].

2.2 Hardened properties of concrete with waste aggregates

There is little discussion in the literature that explicitly quantifies and compares the efficiency of concrete with different types of waste aggregates. To address this gap, and in order to allow for better identification of the optimal use of different waste aggregate types, this study utilizes a simplified index: the binder intensity (*BI*) [48]. The *BI* defined in Eq. 1 provides a measure of the concrete efficiency in terms of the total consumption of binder materials to deliver one unit of a given performance indicator.

$$BI = \frac{B}{P} \tag{1}$$

where in Eq. 1, B is the total amount of binders (kg/m^3) and P (MPa) is the performance requirement such as compressive strength, splitting tensile strength, flexural strength or elastic modulus at the concrete age of 28-days. It should be noted that this study utilizes the binder intensity as the performance indicator to quantify the interaction between minimizing natural resource utilization by using waste-based aggregates and the mechanical properties of concrete containing them. This is important because binder generally has a large impact on global warming potential (GWP) and the use of waste-based aggregate may influence the binder content. For instance, a higher w/b ratio or the use of an SCM may be used to compensate for the reduction in the properties of the concrete incorporating waste aggregates compared to those with only natural aggregate. Therefore, the analysis presented here gives the relationship between avoiding natural resource utilization (in terms of *RR (*%)) and GWP presented in terms of binder intensity.

Figures 3-6 show respectively the binder intensity of concrete mix designs for compressive strength, tensile strength, flexural strength and elastic modulus as a function of waste aggregate replacement ratio (*RR (*%)) for both control mixes with only natural aggregate (horizontal lines) and mixes with alternative fillers. To assist the comparison of binder intensity between different kinds of waste aggregates, Figs. 3-6 also include the best fit-curves for each type of waste aggregate. When interpreting the results shown in Figs. 3-6, it should be noted that each row of results represents a different aggregate type (e.g., waste concrete, slag, glass, plastic and rubber) and each panel within a row represents a different form and

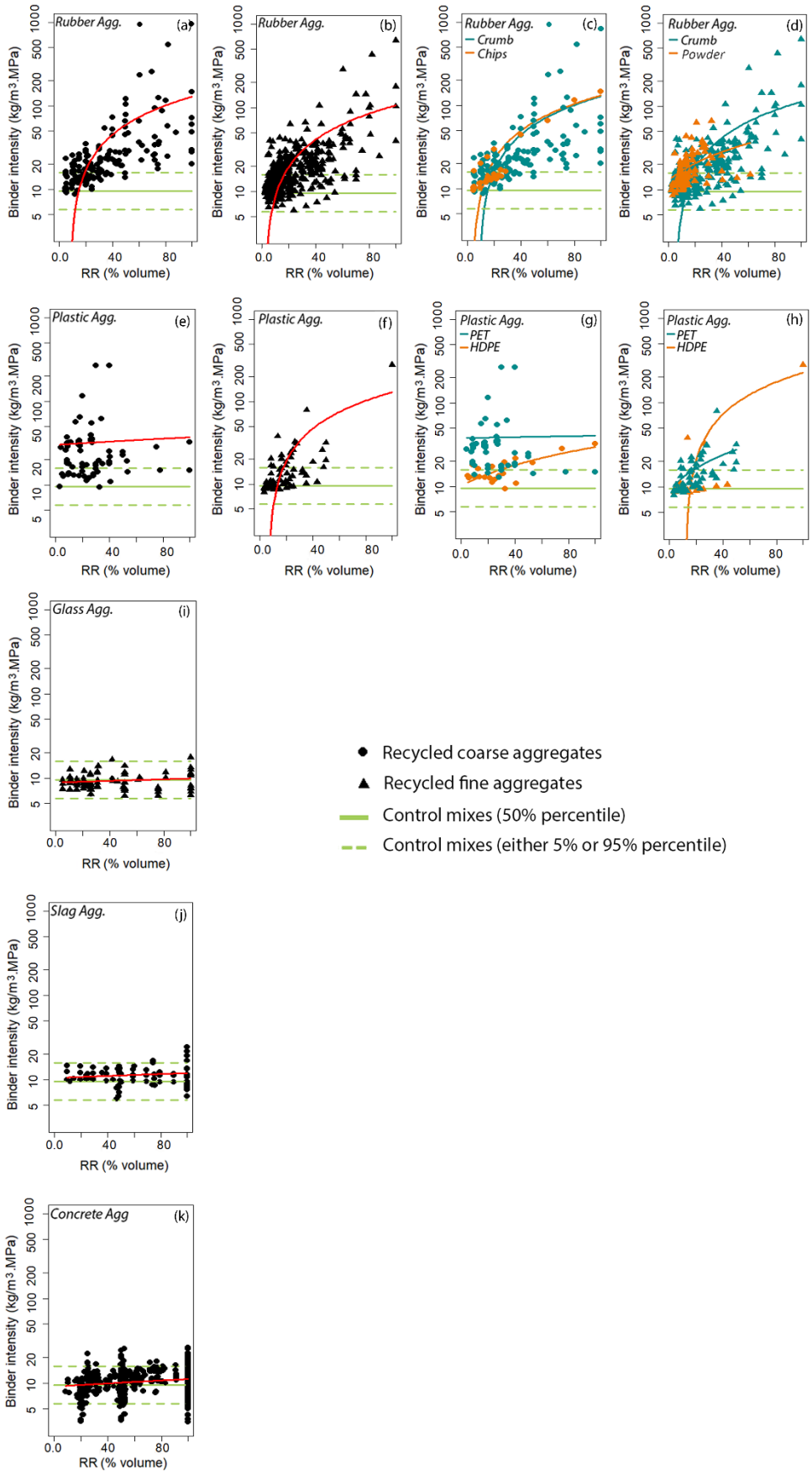

Fig. 3. Binder intensity of waste-based aggregate concrete for compressive strength

class of the same aggregate material type. For example, looking at the first row, subplot (a) in Figs. 3-6 shows coarse rubber aggregates, subplot (b) in Figs. 3-6 shows fine rubber aggregates, subplot (c) in Figs. 3-6 repeats the information in subplot (a) in Figs. 3-6 but now identifying the class of rubber coarse aggregates (crumb and chips) and subplot (d) repeats the information in subplot (b) in Figs. 3-6 but shows the class of rubber fine aggregates (crumb and powder). In the second row, subplots (e) and (f) in Figs. 3-6 respectively show the plastic coarse and fine aggregates and subplots (g) and (h) in Figs. 3-6 respectively show the class of plastic coarse and fine aggregates (PET and HDPE). It is worth mentioning that because there is a single class and size of concrete, glass and slag aggregates in the database, there is a single subplot in the third to fifth rows in Figs. 3-6 showing glass fine aggregate (subplot (i)), slag coarse aggregate (subplot (j)) and concrete coarse aggregate (subplot (k)) respectively. It can be seen from Fig. 3 that when considering compressive strength, the binder intensity generally increases as *RR* (%) increases regardless of the type of waste-based aggregate. This observation can be attributed to a combination of the poorer grading, lower strength and weaker interfacial transition zone between the waste-based aggregates and the concrete matrix, when compared to natural aggregates [49].

It is also clear from Fig. 3(i)-(k) that for waste concrete, glass and slag aggregates, for all values of *RR* (%), the binder intensity of concrete generally falls within the 90% confidence intervals for the binder intensity of the control mixes (*RR* = 0) which are shown as dashed horizontal lines. However, the binder intensity of concrete compressive strength with plastic and rubber aggregates (Fig. 3 (a)-(h)) significantly exceeds that of the control mixes, and although there is a trend for poorer performance at a higher *RR*, a significant number of mixes perform significantly poorer than the control mixes for all replacement ratios. For example, when considering mixes with waste concrete, glass and slag aggregates in Fig. 3 (i)-(k), more than 90% of binder intensity values lie within the 90% confidence intervals of the control mixes. Conversely, for mixes with rubber and plastic aggregates in Fig. 3(a)-(i), less than 30% of binder intensity of values are within the 90% confidence interval range of the control mixes. This behavior is a result of the coupled effects of several factors including: (i) the lower strength and specific gravity of plastic and rubber (ii) a smoother surface texture (iii) a flakey shape, and (iv) the less adhesive and more hydrophobic nature of plastic and rubber aggregates when compared to concrete and slag aggregates [50-52]. Although glass particles also generally have a smooth surface, which also negatively impacts the bond strength at the interfacial transition zone (ITZ) with cement paste, a similar reduction in performance is not observed because of their angular nature and pozzolanic properties [53-54].

In Fig. 3(i-k), because mix designs generally lie within the 90% confidence intervals of the natural aggregate concretes, it is suggested here that it is generally feasible to manufacture concrete with a high content of coarse slag aggregate, coarse concrete aggregate and fine glass aggregate replacement. However, for concrete with fine and coarse plastic and rubber aggregate replacement ratios of 30% and above, mix designs generally lie outside of the 90% confidence intervals of the natural aggregate control mixes and this suggests that aggregate replacement ratios above 30% are sub-optimal from the perspective of binder intensity. That is while there is a benefit from reducing the reliance on natural aggregates there is a cost associated with increased cement usage and therefore increased global warming potential. This can indicate the potential advantages of waste slag and concrete aggregates over rubber aggregates for higher aggregate replacement ratios even when optimal mix designs are used for rubber and plastic aggregates. This finding may not necessarily be generalized because durability characteristics of concrete with slag, concrete and rubber aggregates should also be

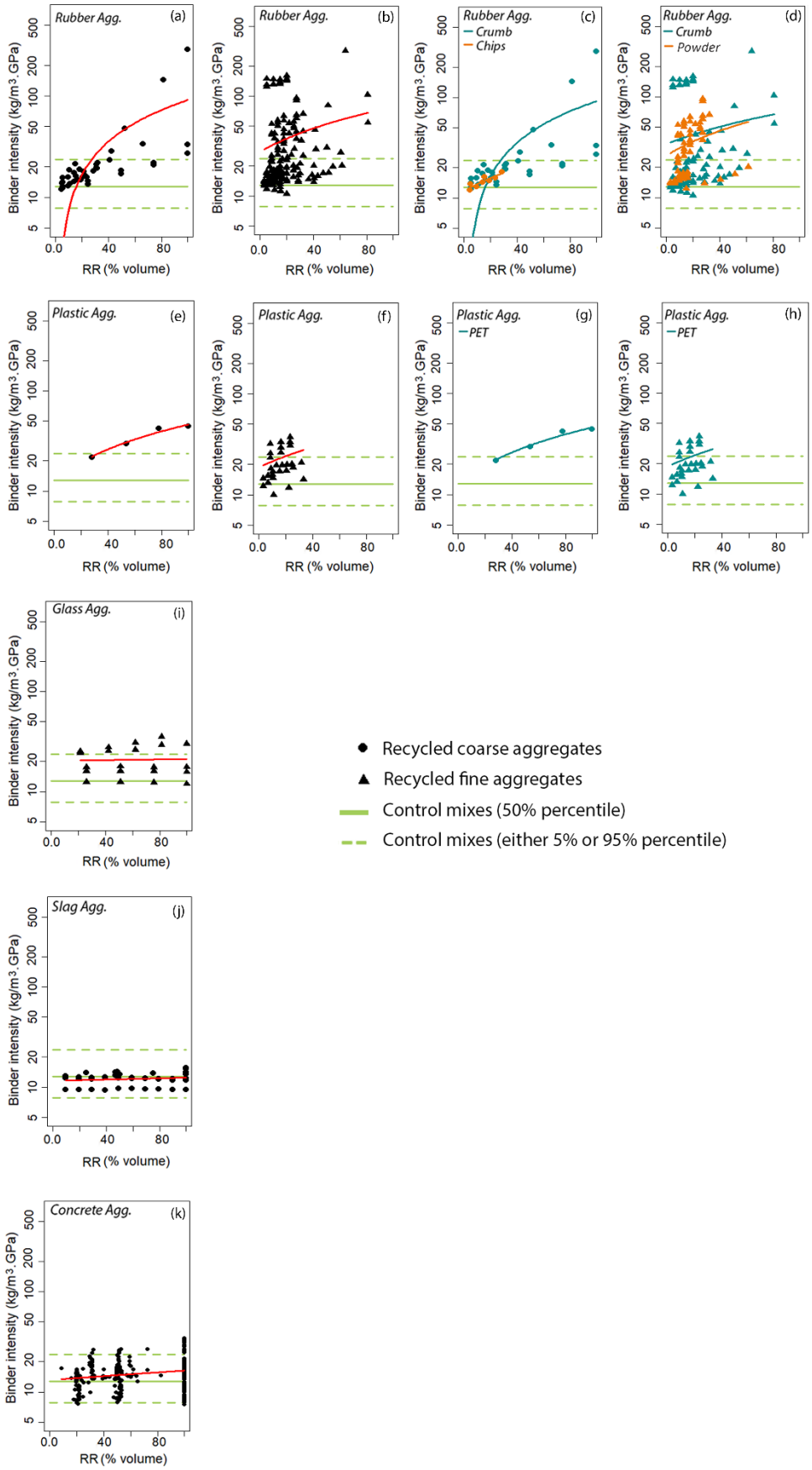

Fig. 4. Binder intensity of waste-based aggregate concrete for elastic modulus

considered for a more thorough assessment when sufficient experimental data are available. It is important to note that the effects of rubber and plastic aggregate's size and type (in terms of chips, crumb, PET, HDPE) on the concrete compressive strength have been widely reported in the literature [55-59]. However, it appears from Fig. 3(a-i) that the binder intensity can be affected more by the rubber and plastic content and possibly concrete mix design proportions than their size and type. For instance, it can be seen from Fig. 3(g) that it is feasible to manufacture HDPE and PET plastic aggregate concretes with similar waste aggregate replacement ratio and binder intensity when $RR < 30\%$ and binder intensity is smaller than 20 kg/m^3.MPa.

This finding is only valid from the perspective of concrete compressive strength, while for a more comprehensive assessment, the effect of reduction in water-to-binder ratio on the workability and durability of waste-based aggregate concrete should also be investigated.

The analysis shown in Fig. 3 is repeated in Figs. 4-6 but now defining the binder intensity in terms of elastic modulus (Fig. 4), flexural strength (Fig. 5) and splitting tensile strength (Fig. 6). It can be seen from Figs. 4-6 that an increase in binder intensity occurs for flexural strength, splitting tensile strength and elastic modulus as the quantity of waste-based aggregate incorporated into the mix increases. This is because the factors responsible for the reduction in the compressive strength of waste-based aggregate concrete in terms of surface roughness, fragility, porosity and other physical properties including density and elastic modulus are generally the same in decreasing splitting tensile strength, flexural strength and elastic modulus [60-64]. The exception to this is for slag aggregates, for which it appears that the best fit curve for binder intensity remains relatively constant and close to the 50^{th} percentile values of binder intensity of the control mixes for elastic modulus and splitting tensile strength, and slightly decrease in the case of flexural strength as the aggregate replacement ratio increases. The reason for this is likely the rougher surface texture, higher elastic modulus and hydraulic reactivity of steel slag aggregates compared to other waste-based aggregates, both of which may enhance the bond with the cement paste [65-66].

It appears from Fig. 4(j)-(k) that the binder intensity for elastic modulus of almost all mixes with slag and concrete aggregates remain within the 90 percentile range of binder intensity for control mixes for all aggregate replacement ratios. However, less than 50% of binder intensity for elastic modulus of mixes with glass, plastic fine aggregates and rubber fine and coarse aggregates are within the 90 percentile range of binder intensity for control mixes as shown in Fig. 4(a)-(h). This may indicate that the reduction in the binder intensity for elastic modulus of the concrete containing a higher dosage of slag or concrete aggregates is less prominent compared to the companion concrete with glass, plastic or rubber aggregates. The differences in density and elastic modulus of these waste aggregates may help to explain the differences in modulus of elasticity of concrete containing them [46]. It should be noted that compared to concrete containing plastic and rubber aggregates, the binder intensity for elastic modulus of concrete with glass aggregates was least affected with increasing *RR*. This is because of the higher density and lower water-to-binder ratio of glass aggregate concrete and the fact that concretes with rubber and plastic aggregates generally require more water to make them workable and therefore more binder is required to maintain the strength [61]. Similar to compressive strength and elastic modulus, it can be seen from Figs. 5-6(j-k) that concrete containing either slag and recycled concrete aggregates generally possess a lower binder intensity for flexural and splitting tensile strengths than concrete with plastic and rubber aggregates.

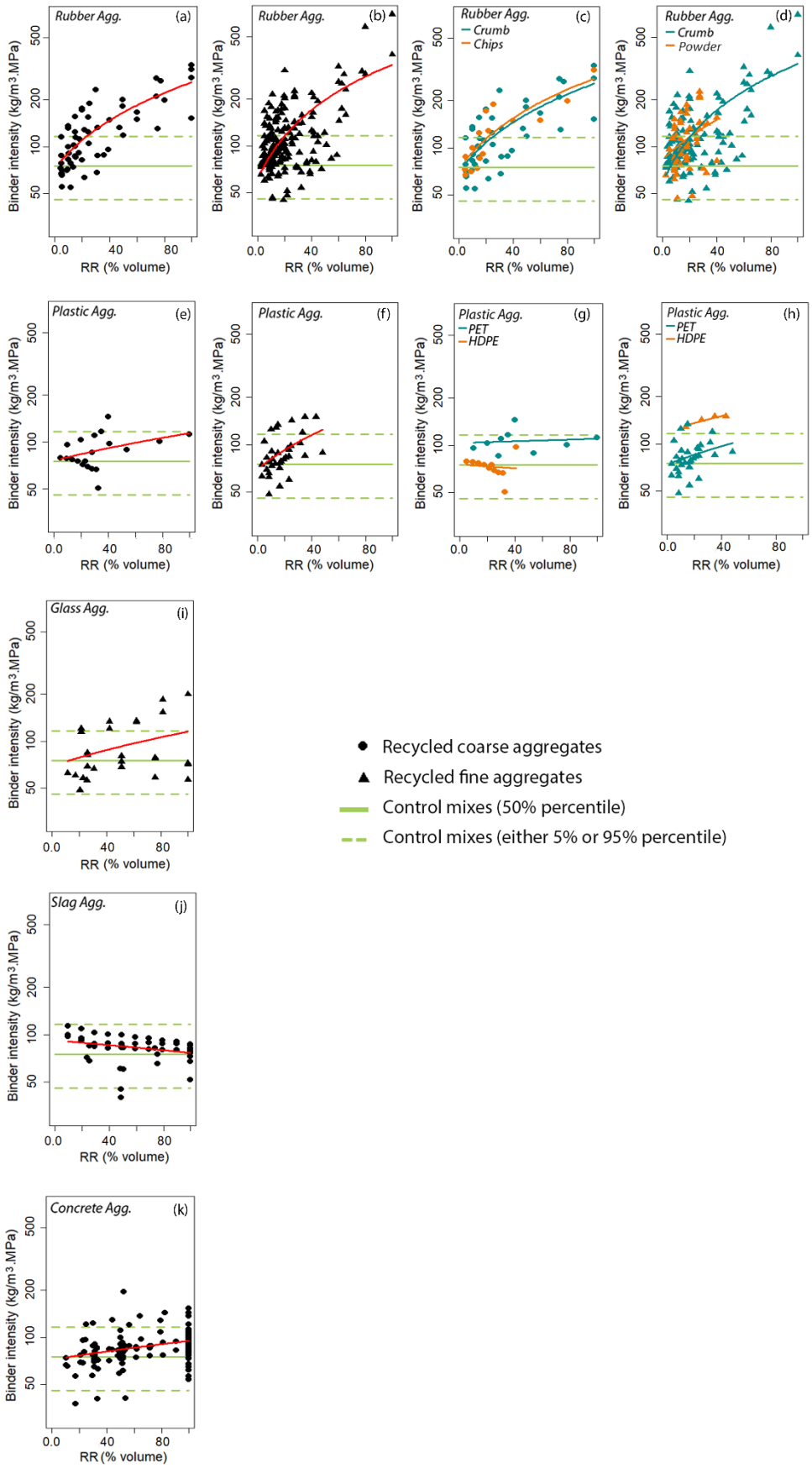

Fig. 5. Binder intensity of waste-based aggregate concrete for flexural strength

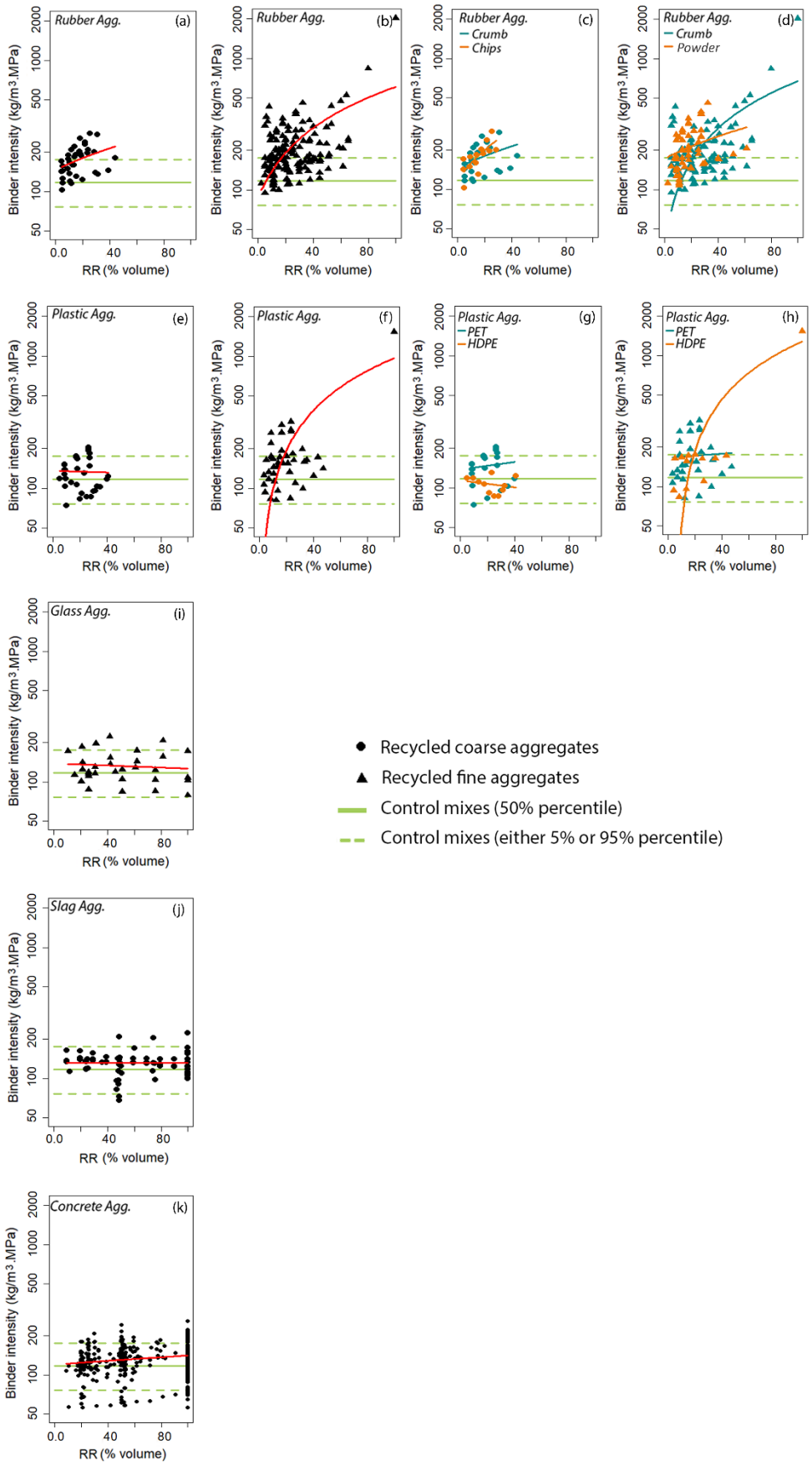

Fig. 6. Binder intensity of waste-based aggregate concrete for tensile strength

However, compared to the binder intensity derived for compressive strength, it can be seen from Figs. 5(i) that the binder intensity for flexural strength of glass aggregate based concrete increases more rapidly with an increase in the waste aggregate content, this occurs because the smooth surface of glass aggregates results in a weaker bond between glass particles and matrix when stress states change from compression to tension [68].

Given that very little research has been conducted to characterize the long-term durability of concretes with waste-based aggregates, here the water absorption of the concrete is used as a proxy for durability. In Fig. 7, the water absorption (%) is plotted as a function of the aggregate replacement ratio (%) and the concrete compressive strength (f_c) is expressed using a color ramp and each panel covers a different waste-based aggregate type and where possible the aggregate type is further broken down (e.g. based on the type of rubber).

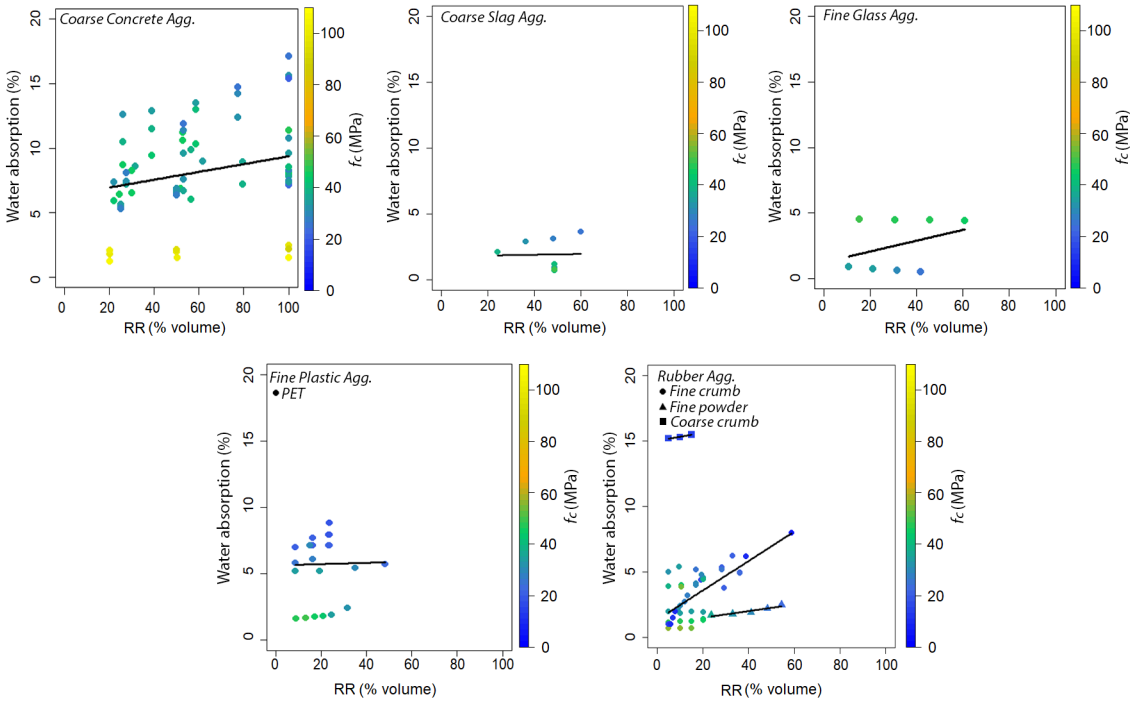

Fig. 7. Water absorption (%) of concrete with different types of waste aggregates

It can be seen from Fig. 7 that water absorption of concrete with different waste aggregate types generally increases with increases in the waste aggregate content and decreases with an increase in the compressive strength. This is because that the water-to-binder ratio (which is inversely related to compressive strength) and waste aggregate content generally influences the porosity of concrete and therefore the water absorption capacity of the concrete [69-70]. It also appears from Fig. 7 that water absorption capacity of concrete also depends on the texture and quality of waste aggregates [71]. For instance, waste aggregates such as concrete and slag aggregates which generally have a higher water absorption than natural aggregates generally produce concretes with higher water absorption [72-74]. Similarly, waste aggregates with low density, irregular shape and high specific surface such as small flaky plastic particles may negatively influence the absorption rate of concrete due to increase in the porosity of concrete structure [45,75-76]. It is also observed from Fig. 7 that water absorption of concrete increases with an increase in any type of rubber aggregate content likely due to high water retention and nonpolar nature of rubber which increases the air content and pore space in concrete [40,77]. A small number of studies have also reported that water absorption of concrete can slightly decrease with an increase in the glass particle content of up to 20%, this is likely due to a

combination of the lower permeability of glass particles compared to fine sand, the micro filler effect and the ability of glass to react with binder to form denser ITZs [33,78].

2.3 Empirical models for waste-based aggregate concrete

In the absence of specific design-oriented models to predict the mechanical properties of concrete with waste-based aggregates, codified models that have been developed for concrete with natural aggregate have been applied [79]. The application of models developed for concretes with only natural aggregates to predict the behavior of concretes with waste-based aggregates is problematic because, as shown above, the use of all waste-based aggregates influences mechanical properties because of a variety of factors [80-81]. To improve the ability to utilize concretes with waste-based aggregates in practice, it is therefore necessary to develop models that are specifically calibrated to each aggregate type and that can allow for a range of replacement ratios.

In this study, the waste-based aggregate concrete database described in Section 1 covering a wide variety of aggregate type, binders and mix designs are used to develop models to relate the mechanical properties (tensile strength and elastic modulus) to the concrete compressive strength (f_c) and aggregate replacement rate (%). Using the experimental observations contained in the database (Supplementary Material A), models to predict the elastic modulus (E_c) (Eq. 2), splitting tensile strength (f_{st}) (Eq. 3) and flexural tensile strength (f_r) (Eq. 4) have been calibrated, where the form of Eq. 2-4 was identified to be optimal as they provide a similar functional form to standard codified approaches as well as a good degree of accuracy.

$$E_c = \alpha_1 \times (f_c)^{\beta_1} + \gamma_1 \times (RA) \quad (2)$$

$$f_{st} = \alpha_2 \times (f_c)^{\beta_2} + \gamma_2 \times (RA) \quad (3)$$

$$f_r = \alpha_3 \times (f_c)^{\beta_3} + \gamma_3 \times (RA) \quad (4)$$

To find the coefficients of α, β and γ in the above equations, a series of regression analyses was undertaken on each concrete database with slag, concrete, glass, plastic and rubber aggregates. The results of analyses along with proposed relationships for natural aggregate concrete in international design codes including ACI 318-11 [82], AS3600-09 [83], NZS 3101 [84], CSA A23.3-04 [85], Eurocode 2-04 [86], JSCE-07 [87] and JCI-08 [88] are summarized in Tables 1-3 respectively for elastic modulus, splitting tensile strength and flexural strength. It should be noted that in order to have consistent empirical models for different types of waste aggregates when *RR* (%) is zero, control mixes are used to find α and β and waste aggregate mixes are used to find γ in the regression analyses.

It can be seen from Tables 1-3 that international design codes generally propose different relationships for the same empirical models yielding different predictions for the same grade of concrete. For instance, while for the empirical models for elastic modulus γ and β are considered to be respectively 9.50 and 0.33 in Eurocode 2-04, they are considered to be 3.32 and 0.50 (along with a constant coefficient of 6.90) for the same model in NZS 3101. Or for the splitting tensile strength models, γ and β can respectively range between [0.13-0.53] and [0.50-0.85] in different international design codes. The reason for this however may be attributed to the difference in the mix designs, local materials and testing methods leading to uncertainty in material property [89].

Given the insufficient data on the relationship between cubic and cylindrical compressive strength of concrete with waste-based aggregates is available (only 17 mix designs in Supplementary Material A have considered both cylinder and cube test results), the empirical models were calibrated using only the experimental observations obtained from cylindrical samples. This approach also allows for comparison to international design codes in Tables 1-3

which have also been developed from tests on cylindrical specimens.

1 Table 1. Proposed models in this study and codified models in international standards for elastic modulus

Outcome		Model coefficient								
		α_1	β_1	γ_1						Constant
				Waste aggregate type						
				Concrete	Slag	Glass	Fine Plastic	Coarse Plastic	Fine Rubber	Coarse Rubber	
E_c	Number of mixes	(220)		(160)	(11)	(0)	(4)	(4)	(85)	(26)	---
	f_c range (MPa)			[23-70]	[23-72]	---	[25-37]	[30-35]	[5-72]	[4-45]	
	RR (%) range			[9-100]	[47-100]	---	[10-26]	[25-100]	[1-65]	[11-100]	
	This study	5.24	0.49	-6.24	-1.53	---	-27.99	-20.30	-19.70	-8.90	---
	ACI 318-11 [82]	4.73	0.50	---	---	---	---	---	---	---	---
	CSA A23.3-04 [85]	4.50	0.50	---	---	---	---	---	---	---	---
	Eurocode 2-04 [86]	9.50	0.33	---	---	---	---	---	---	---	---
	JSCE-07 [87]	4.70	0.50	---	---	---	---	---	---	---	---
	JCI-08 [88]	6.30	0.45	---	---	---	---	---	---	---	---
	NZS 3101:2006 [84]	3.32	0.50	---	---	---	---	---	---	---	6.90

2

Table 2. Proposed models in this study and codified models in international standards for splitting tensile strength

Outcome		Model coefficient								
		α_2	β_2	γ_2						Constant
				Waste aggregate type						
				Concrete	Slag	Glass	Fine Plastic	Coarse Plastic	Fine Rubber	Coarse Rubber	
f_{st}	Number of mixes	(275)		(138)	(9)	(0)	(9)	(0)	(127)	(10)	---
	f_c range (MPa)			[20-68]	[32-73]	---	[8-44]	---	[5-63]	[16-39]	
	RR (%) range			[9-100]	[47-100]	---	[4-100]	---	[3-65]	[5-46]	
	This study	0.82	0.40	-0.74	0.54	---	-0.79	---	-1.37	-2.83	---
	AS 3600-09 [83]	0.40	0.50	---	---	---	---	---	---	---	---
	ACI 318-11 [82]	0.53	0.50	---	---	---	---	---	---	---	---
	Eurocode 2-04 [86]	0.30	0.67	---	---	---	---	---	---	---	---
	JSCE-07 [87]	0.44	0.50	---	---	---	---	---	---	---	---
	JCI-08 [88]	0.13	0.85	---	---	---	---	---	---	---	---
	NZS 3101:2006 [84]	0.44	0.50	---	---	---	---	---	---	---	---

Table 3. Proposed models in this study and codified models in international standards for flexural strength

Outcome		Model coefficient								
		α_3	β_3	γ_3						Constant
				Waste aggregate type						
				Concrete	Slag	Glass	Fine Plastic	Coarse Plastic	Fine Rubber	Coarse Rubber	
f_r	Number of mixes	(154)		(33)	(3)	(0)	(0)	(0)	(132)	(35)	---
	f_c range (MPa)			[22-63]	[23-36]	---	---	---	[4-63]	[3-45]	
	RR (%) range			[17-100]	[70-100]	---	---	---	[3-100]	[5-100]	
	This study	1.62	0.35	-1.13	0.22	---	---	---	-1.39	-2.83	---
	AS 3600-09 [83]	0.60	0.50	---	---	---	---	---	---	---	---
	ACI 318-11 [82]	0.62	0.50	---	---	---	---	---	---	---	---
	CSA A23.3-04 [85]	0.60	0.50	---	---	---	---	---	---	---	---
	Eurocode 2-04 [86]	0.43	0.67	---	---	---	---	---	---	---	---
	NZS 3101:2006 [84]	0.60	0.50	---	---	---	---	---	---	---	---

Table 4. Calculated statistical indicators for the proposed models in this study and codified models in international standards

		Aggregate type						
		Natural	Concrete	Slag	Fine Plastic	Coarse Plastic	Fine Rubber	Coarse Rubber

E_c																													
	This study	MPE (%)	MAE	COV	Mean	MPE (%)	MAE	COV	Mean	MPE (%)	MAE	COV	Mean	MPE (%)	MAE	COV	Mean	MPE (%)	MAE	COV	Mean	MPE (%)	MAE	COV	Mean	MPE (%)	MAE	COV	Mean
	ACI 318-11 [82]	15.63	4.34	32.36	1.04	14.33	3.92	26.14	1.06	15.82	4.45	31.86	1.04	15.64	4.33	32.71	1.04	16.39	4.39	34.96	1.05	22.94	4.38	53.25	1.11	18.75	4.19	48.71	1.08
	CSA A23.3-04 [85]	15.13	4.43	31.51	0.98	14.82	4.16	23.33	1.04	15.25	4.50	31.10	0.99	15.20	4.42	31.52	0.99	16.69	4.57	31.91	1.00	25.04	4.55	46.14	1.11	21.33	4.37	43.59	1.06
	Eurocode 2-04 [86]	15.77	4.83	29.98	0.94	13.98	4.10	22.19	0.99	15.71	4.84	29.58	0.94	15.72	4.80	29.98	0.94	17.14	4.95	30.36	0.95	24.36	4.75	43.89	1.05	21.22	4.68	41.47	1.01
	JSCE-07 [87]	17.04	4.45	22.76	1.08	18.39	4.76	16.77	1.13	16.99	4.49	22.41	1.08	17.35	4.51	22.75	1.09	19.04	4.66	23.02	1.10	33.71	5.24	34.62	1.26	29.02	4.81	32.51	1.21
	JCI-08 [88]	15.14	4.46	31.31	0.98	14.64	4.13	23.18	1.03	15.24	4.52	30.90	0.98	15.20	4.45	31.32	0.98	16.68	4.60	31.71	1.00	24.88	4.56	45.85	1.10	21.26	4.39	43.32	1.06
	NZS3101:2006 [84]	17.23	4.58	31.38	1.09	19.92	5.28	23.20	1.15	17.47	4.71	30.94	1.10	17.52	4.63	31.38	1.10	19.20	4.78	31.76	1.10	30.96	5.12	46.45	1.24	26.17	4.75	43.81	1.19
		17.24	5.33	22.12	0.93	14.52	4.31	16.37	0.97	16.89	5.24	21.83	0.93	17.19	5.29	22.12	0.93	18.63	5.44	22.40	0.95	28.59	5.32	32.38	1.08	26.18	5.27	30.60	1.04

f_{st}	This study	15.18	0.50	0.23	1.04	18.11	0.56	0.21	1.07	14.94	0.50	0.27	1.03	16.69	0.52	0.25	1.05	14.80	0.49	0.26	1.03	16.92	0.47	0.39	1.08	15.70	0.51	0.25	1.04
	AS 3600-09 [83]	28.28	1.04	0.20	0.73	25.31	0.92	0.17	0.78	28.46	1.06	0.24	0.72	28.63	1.03	0.22	0.73	29.19	1.05	0.24	0.72	26.59	0.91	0.30	0.76	28.06	1.02	0.21	0.73
	ACI 318-11 [82]	14.80	0.52	0.27	0.96	18.30	0.58	0.22	1.03	14.73	0.52	0.31	0.96	16.10	0.54	0.29	0.97	15.41	0.53	0.32	0.95	15.70	0.47	0.40	1.01	15.37	0.52	0.27	0.97
	Eurocode 2-04 [86]	16.44	0.57	0.38	0.99	20.76	0.65	0.31	1.07	16.03	0.56	0.45	0.99	17.44	0.58	0.40	0.99	17.54	0.59	0.44	0.97	16.60	0.51	0.54	1.02	16.98	0.57	0.39	1.00
	JSCE-07 [87]	22.39	0.83	0.22	0.80	21.09	0.75	0.18	0.86	22.55	0.84	0.26	0.80	23.09	0.83	0.24	0.81	23.32	0.84	0.26	0.79	21.06	0.71	0.33	0.84	22.32	0.81	0.23	0.81
	JCI-08 [88]	22.28	0.79	0.42	0.83	22.23	0.74	0.35	0.91	21.95	0.78	0.50	0.83	22.88	0.80	0.44	0.83	24.23	0.83	0.47	0.81	21.54	0.70	0.57	0.84	22.33	0.78	0.43	0.84
	NZS3101:2006 [84]	22.39	0.83	0.22	0.80	21.09	0.75	0.18	0.86	22.55	0.84	0.26	0.80	23.09	0.83	0.24	0.81	23.32	0.84	0.26	0.79	21.06	0.71	0.33	0.84	22.32	0.81	0.23	0.81
	This study	21.16	1.11	0.41	1.08	21.23	1.11	0.36	1.08	20.83	1.10	0.40	1.08	---	---	---	---	---	---	---	---	27.84	1.25	0.78	1.15	27.02	1.13	1.14	1.14

f_r	AS 3600-09 [83]	35.83	2.17	0.37	0.67	34.02	2.06	0.28	0.69	35.93	2.17	0.37	0.67	---	---	---	---	---	---	---	---	35.14	2.03	0.62	0.72	35.92	1.96	0.69	0.73
	ACI 318-11 [82]	35.83	2.17	0.37	0.67	34.02	2.06	0.28	0.69	35.93	2.17	0.37	0.67	---	---	---	---	---	---	---	---	35.14	2.03	0.62	0.72	35.92	1.96	0.69	0.73
	CSA A23.3-04 [85]	35.83	2.17	0.37	0.67	34.02	2.06	0.28	0.69	35.93	2.17	0.37	0.67	---	---	---	---	---	---	---	---	35.14	2.03	0.62	0.72	35.92	1.96	0.69	0.73
	Eurocode 2-04 [86]	23.56	1.38	0.68	0.88	23.50	1.36	0.51	0.90	23.58	1.38	0.67	0.88	---	---	---	---	---	---	---	---	26.36	1.40	1.08	0.93	27.70	1.33	1.18	0.94
	NZS3101:2006 [84]	35.83	2.17	0.37	0.67	34.02	2.06	0.28	0.69	35.93	2.17	0.37	0.67	---	---	---	---	---	---	---	---	35.14	2.03	0.62	0.72	35.92	1.96	0.69	0.73

In this study, the reliability of the relationships derived from the regression analysis are compared with that of empirical models in international design codes using several indices including mean absolute error (*MAE*), mean percentage error (*MPE %*), covariance (*COV*) and mean value (*MV*) as follows:

$$MAE = \frac{1}{n}\sum_{i=1}^{n}|O_i - P_i| \quad (5)$$

$$MPE = \frac{1}{n}\sum_{i=1}^{n}\left|\frac{O_i - P_i}{O_i}\right| \times 100 \quad (6)$$

$$COV = \frac{1}{n-1}\sum_{1=i}^{n}(O_i - \bar{O}_i) \times (P_i - \bar{P}_i) \quad (7)$$

$$MV = \frac{1}{n}\sum_{i=1}^{n}\left|\frac{O_i}{P_i}\right| \quad (8)$$

where O_i is the observed value, $\bar{O}_i$ is the mean of observed value, P_i is the predicted value, $\bar{P}_i$ is the mean of predicted value and n is the total number of observations in the regression analysis. It should be noted that when *MAE* and *MPE* are zero or *MV* is unity, the predicted and observed values from the regression equations are equal. These indices have been widely used by others to assess the goodness of fit of suggested regression models [90-93].

The above statistical indicators computed for natural aggregate concrete and concrete with different types of waste-based aggregates are shown in Table 4 for each of the mechanical properties. It can be seen from Table 4 that the proposed relationships in this study for elastic modulus of natural aggregate concrete can have a similar performance to those in ACI 318-11, CSA A23.3-04 and JSCE-07 based on the values of *MPE, MAE*, *COV* and *MV*. For instance, while the value of *MPE* for the proposed elastic modulus model in this study is similar to that for CSA A23.3-04 and ACI 318-11 and JSCE-07, it is generally smaller than that for other codified models shown in Table 4. Similarly, the values of *MPE* and *MAE* for the proposed splitting tensile strength models are respectively 7% and 35% smaller than those for the proposed models in JSCE-07, JCI-08 and NZS 3101. It should be noted that the proposed models in this study and Eurocode 2-04 for flexural strength fit to the mean data however other codified models fit more to the lower bound of data as shown in Table 4. It can be seen that while the values of *MPE*, *MAE*, *COV* and *MV* for the proposed model for flexural strength of natural aggregate concrete are 21.6%, 1.11, 0.41 and 1.08 respectively, these are 35.83%, 2.17, 0.37 and 0.67 respectively for ACI 318-11, AS3600-09, NZS 3101 and CSA A23.3-04 indicating a better prediction performance for the proposed empirical models.

In Table 4, it can also be seen that the models proposed in this study generally have a better prediction performance than codified models when applied to concretes with waste-based aggregates, and this is unsurprising given they have been calibrated to this dataset. In the case of empirical models for elastic modulus of concrete with slag and concrete aggregates, ACI 318-11, CSA A23.3-04 and JSCE-07 displayed similar performance to the models proposed in this study and they yield more accurate predictions than Eurocode 2-04, JCI-08 and NZS 3101.

It is worth noting that the equations proposed in this study for elastic modulus of rubber aggregate concrete are more accurate than those proposed by all codified models in international standards shown in Table 4. The reason for the poor fit of the codified models developed for natural aggregates is likely because of the significant change in the density of concrete containing rubber aggregates.

In terms of the regression models for splitting tensile strength of concrete with waste-based aggregate, it is seen in Table 4 that the accuracy of the proposed models has similar accuracy

to those presented in ACI 318-11 for natural aggregate concrete but the proposed models are a significant improvement compared to the other codified models for natural aggregates.

Conclusion

There is little discussion in the literature comparing the mechanical properties of concrete with different kinds of waste-based aggregates. This is important because the mechanical performance of concrete is greatly influenced by the type, properties and quality of aggregates. To address this limitation, this study compiles and analyses a large database of 5321 concrete mix designs that utilises waste-based aggregates to investigate the impact of using slag, glass, concrete, plastic and rubber aggregates.

A series of regression analyses is then undertaken on each waste concrete database and empirical models to link the elastic modulus, splitting tensile and flexural tensile strength to the compressive strength of the concrete are developed and compared with existing models in the codes of practice.

By comparing the performance of a very large number of concretes with different types of waste-based aggregates the following general conclusions can be made:

- The binder intensity of concrete with waste-based aggregates generally increases with an increase in the aggregate replacement ratio (*RR* %). However, the binder intensity of concrete with plastic and rubber aggregates increases more rapidly than that of concrete with slag, concrete and glass aggregates when increasing in *RR* (%). The reason for this can be attributed to several factors such as difference in strength and specific gravity, surface shape and adhesive and hydrophobic properties of plastic and rubber aggregates as compared to concrete and slag aggregates.
- While it is feasible to manufacture concrete with a high slag, concrete and glass aggregate content, concrete with a plastic and rubber aggregate content of 30% and above may display poor performance due to either weaker interfacial transition zone between binding materials and aggregates or suboptimal mix design.
- Workability of concrete with different types of waste aggregates can increase with an increase in superplasticizer content. However, concretes with a high crumb rubber aggregate content may not be workable, even if a high dose of superplasticizer is used, this is explained by the high surface area of the aggregate.
- While the slump of rubber aggregate concrete decreases more rapidly than that of slag and glass aggregate concrete with an increase in waste aggregate content, the slump of concrete with waste concrete aggregates is more dependent on the initial moisture states of concrete aggregates than waste aggregate content. It was observed that concretes with similar water-to-binder ratio and superplasticizer content but different waste concrete aggregate replacement can have similar slump values.
- The water absorption of concrete with different waste aggregate types increases with increases in waste aggregate content and decreases with an increase in compressive strength due to the important role water-to-binder ratio and waste aggregate content can play on the porosity of concrete. It was observed that concrete with slag and concrete aggregates, due to their high-water absorption capacity, and concrete with plastic and rubber aggregates due to their low density, irregular shape and high specific surface can result in higher water absorption capacity as compared to natural aggregate concrete.
- Based the error analyses, improved relationships for predicting the mechanical properties of natural aggregate concrete and waste-based aggregate concrete including

elastic modulus, splitting tensile strength and flexural strength were proposed as compared to several codified models in international standards.

Importantly, the collection of data has shown that while the production of concrete with waste-based aggregates has the benefit of minimizing natural resource utilization, care needs to be taken to ensure that they do not have a negative impact on global warming potential by poorly utilizing carbon intensive binders. It is expected that the very large dataset presented in this paper will benefit the research community in improving data-driven mix design approaches.

Acknowledgments

Vahid Shobeiri was supported by an Australian Government Research Training Program Scholarship.

References

[1] Smith, J. S., & Thomas, A. (2021). Integrated model and index for circular economy in the built environment in the Indian context. Construction Economics and Building, 21(3), 198-220.

[2] Verma, Abhishek, and Velaga Sarath Babu. "Influence of modified two-stage mixing approaches on recycled aggregate treated with a hybrid method of treatment." Australian Journal of Structural Engineering (2022): 1-24.

[3] Gholampour, A., Danish, A., Ozbakkaloglu, T., Yeon, J. H., & Gencel, O. (2022). Mechanical and durability properties of natural fiber-reinforced geopolymers containing lead smelter slag and waste glass sand. Construction and Building Materials, 352, 129043.

[4] Adesina, A. (2018). Use of Rice Husk in concrete: Review of mechanical properties. Monteiro, P. J., Miller, S. A., & Horvath, A. (2017). Towards sustainable concrete. Nature materials, 16(7), 698-699.

[5] Monteiro, P. J., Miller, S. A., & Horvath, A. (2017). Towards sustainable concrete. Nature materials, 16(7), 698-699.

[6] Mirza, J., Huseien, G. F., Shah, K. W., & KIRGIZ, M. S. (2020). Reduction in ecology, environment, economy and energy in concrete industry using waste materials. Journal of Advanced Composite Materials, Construction, Environment, and Nano Technology, (2).

[7] Hossain, M., Sultana, R., Patwary, M. M., Khunga, N., Sharma, P., & Shaker, S. J. (2022). Self-healing concrete for sustainable buildings. A review. Environmental Chemistry Letters, 1-9.

[8] Sivakumar, N., Muthukumar, S., Sivakumar, V., Gowtham, D., & Muthuraj, V. (2014). Experimental studies on high strength concrete by using recycled coarse aggregate. International Journal of Engineering and Science, 4(1), 27-36.

[9] Wang, X., Chin, C. S., & Xia, J. (2019). Material characterization for sustainable concrete paving blocks. Applied Sciences, 9(6), 1197.

[10] Zhang, Y., Gao, L., & Bian, W. (2020). Mechanical performance of concrete made with recycled aggregates from concrete pavements. Advances in Materials Science and Engineering, 2020.

[11] Contreras-Llanes, M., Romero, M., Gázquez, M. J., & Bolívar, J. P. (2021). Recycled Aggregates from Construction and Demolition Waste in the Manufacture of Urban Pavements. Materials, 14(21), 6605.

[12] Ozturk, O., Yildirim, H., Ozyurt, N., & Ozturan, T. (2022). Evaluation of mechanical

properties and structural behaviour of concrete pavements produced with virgin and recycled aggregates: an experimental and numerical study. International Journal of Pavement Engineering, 1-15.

[13] European Cement Research Academy, 2015. Closing the Loop: What Type of Concrete Re-use is the Most Sustainable Option? Report A-2015/1860, 41pp.

[14] Topcu, I. B., & Şengel, S. (2004). Properties of concretes produced with waste concrete aggregate. Cement and concrete research, 34(8), 1307-1312.

[15] Behera, M., Bhattacharyya, S. K., Minocha, A. K., Deoliya, R., & Maiti, S. (2014). Recycled aggregate from C&D waste & its use in concrete–A breakthrough towards sustainability in construction sector: A review. Construction and building materials, 68, 501-516.

[16] de Andrade Salgado, F., & de Andrade Silva, F. (2022). Recycled aggregates from construction and demolition waste towards an application on structural concrete: A review. Journal of Building Engineering, 52, 104452.

[17] Gholampour, A., Gandomi, A. H., & Ozbakkaloglu, T. (2017). New formulations for mechanical properties of recycled aggregate concrete using gene expression programming. Construction and Building Materials, 130, 122-145.

[18] Tam, V. W., Soomro, M., & Evangelista, A. C. J. (2018). A review of recycled aggregate in concrete applications (2000–2017). Construction and Building materials, 172, 272-292.

[19] Wang, B., Yan, L., Fu, Q., & Kasal, B. (2021). A comprehensive review on recycled aggregate and recycled aggregate concrete. Resources, Conservation and Recycling, 171, 105565.

[20] Xu et al. 2019 Parametric sensitivity analysis and modelling of mechanical properties of normal- and high-strength recycled aggregate concrete using grey theory, multiple nonlinear regression and artificial neural networks

[21] Xie et al. 2020 A unified model for predicting the compressive strength of recycled aggregate concrete containing supplementary cementitious materials

[22] Gravina et al 2021 HDPE and PET as Aggregate Replacement in Concrete: Life-cycle assessment, Material Development and a case study

[23] Gravina et al 2022 Toward the development of sustainable concrete with Crumb Rubber: Design-oriented Models, Life-Cycle-Assessment and a site application

[24] Chakradhara Rao, M., Bhattacharyya, S. K., & Barai, S. V. (2011). Influence of field recycled coarse aggregate on properties of concrete. Materials and structures, 44(1), 205-220.

[25] Dilbas, H., Şimşek, M., & Çakır, Ö. (2014). An investigation on mechanical and physical properties of recycled aggregate concrete (RAC) with and without silica fume. Construction and Building materials, 61, 50-59.

[26] Gayarre, F. L., Perez, C. L. C., Lopez, M. A. S., & Cabo, A. D. (2014). The effect of curing conditions on the compressive strength of recycled aggregate concrete. Construction and Building Materials, 53, 260-266.

[27] Poon, C. S., Shui, Z. H., Lam, L., Fok, H., & Kou, S. C. (2004). Influence of moisture states of natural and recycled aggregates on the slump and compressive strength of concrete. Cement and concrete research, 34(1), 31-36.

[28] Ferreira, L., De Brito, J., & Barra, M. (2011). Influence of the pre-saturation of recycled

coarse concrete aggregates on concrete properties. Magazine of Concrete Research, 63(8), 617-627.

[29] Kim, S. W., Yun, H. D., Park, W. S., & Jang, Y. I. (2015). Bond strength prediction for deformed steel rebar embedded in recycled coarse aggregate concrete. Materials & Design, 83, 257-269.

[30] Guerzou, T., Mebrouki, A., & Castro-Gomes, J. (2018). Study of concretes properties based on pre-saturated recycled aggregates. Journal of Materials and Engineering Structures «JMES», 5(3), 279-288.

[31] Zhang, H., Xu, X., Liu, W., Zhao, B., & Wang, Q. (2022). Influence of the moisture states of aggregate recycled from waste concrete on the performance of the prepared recycled aggregate concrete (RAC)–A review. Construction and Building Materials, 326, 126891.

[32] Terro, M. J. (2006). Properties of concrete made with recycled crushed glass at elevated temperatures. Building and environment, 41(5), 633-639.

[33] Malik, M. I., Bashir, M., Ahmad, S., Tariq, T., & Chowdhary, U. (2013). Study of concrete involving use of waste glass as partial replacement of fine aggregates. IOSR Journal of Engineering, 3(7), 08-13.

[34] Wright, J. R., Cartwright, C., Fura, D., & Rajabipour, F. (2014). Fresh and hardened properties of concrete incorporating recycled glass as 100% sand replacement. Journal of Materials in Civil Engineering, 26(10), 04014073.

[35] Zang, J., Li, W., & Shen, X. (2019). The influence of steel slag with variable particle size distribution on the workability and mechanical properties of concrete. Ceramics-Silikáty, 63(1), 67-75.

[36] Miah, M. J., Patoary, M. M. H., Paul, S. C., Babafemi, A. J., & Panda, B. (2020). Enhancement of mechanical properties and porosity of concrete using steel slag coarse aggregate. Materials, 13(12), 2865.

[37] Elgendy, G. M., Elagamy, A. H., Sherif, M. A., & EL-Badawy, S. M. (2021). Laboratory Evaluation of Green Concrete Mixes Containing High Percentages of Steel Slag Coarse Aggregate. MEJ. Mansoura Engineering Journal, 40(5), 29-37.

[38] Flores-Medina, D., Flores Medina, N., & Hernández-Olivares, F. (2014). Static mechanical properties of waste rests of recycled rubber and high quality recycled rubber from crumbed tyres used as aggregate in dry consistency concretes. Materials and structures, 47(7), 1185-1193.

[39] Akinyele, J. O., Salim, R. W., & Kupolati, W. K. (2016). Effect of rubber crumb on the microstructural properties of concrete. African Journal of Science, Technology, Innovation and Development, 8(5-6), 467-474.

[40] Bisht, K., & Ramana, P. V. (2017). Evaluation of mechanical and durability properties of crumb rubber concrete. Construction and building materials, 155, 811-817.

[41] Rahim, N. L., Sallehuddin, S., Ibrahim, N. M., Che Amat, R., & Ab Jalil, M. F. (2013). Use of plastic waste (high density polyethylene) in concrete mixture as aggregate replacement. In Advanced Materials Research (Vol. 701, pp. 265-269). Trans Tech Publications Ltd.

[42] Ramesan, A., Babu, S. S., & Lal, A. (2015). Performance of light-weight concrete with plastic aggregate. Int. J. Eng. Res. Appl, 5(8), 105-110.

[43] Alqahtani, F. K. (2022). Development of Composite PET Plastic-based Aggregate and its Utilization in Green Lightweight Concrete. Arabian Journal for Science and Engineering, 1-

10.

[44] Islam, M. (2022). Comparative Study of Concrete with Polypropylene and Polyethylene Terephthalate Waste Plastic as Partial Replacement of Coarse Aggregate. Advances in Civil Engineering, 2022.

[45] Dawood, A. O., Hayder, A. K., & Falih, R. S. (2021). Physical and mechanical properties of concrete containing PET wastes as a partial replacement for fine aggregates. Case Studies in Construction Materials, 14, e00482.

[46] Hama, S. M. (2022). Behavior of concrete incorporating waste plastic as fine aggregate subjected to compression, impact load and bond resistance. European Journal of Environmental and Civil Engineering, 26(8), 3372-3386.

[47] Harihanandh, M., & Karthik, P. (2022). Feasibility study of recycled plastic waste as fine aggregates in concrete. Materials Today: Proceedings, 52, 1807-1811.

[48] Damineli, B. L., Kemeid, F. M., Aguiar, P. S., & John, V. M. (2010). Measuring the eco-efficiency of cement use. Cement and Concrete Composites, 32(8), 555-562.

[49] Sharma, R., & Bansal, P. P. (2016). Use of different forms of waste plastic in concrete–a review. Journal of Cleaner Production, 112, 473-482.

[50] Andreu, G., & Miren, E. (2014). Experimental analysis of properties of high performance recycled aggregate concrete. Construction and Building Materials, 52, 227-235.

[51] Gesoglu, M., Güneyisi, E., Hansu, O., İpek, S., & Asaad, D. S. (2015). Influence of waste rubber utilization on the fracture and steel–concrete bond strength properties of concrete. Construction and Building Materials, 101, 1113-1121.

[52] Bamigboye, G. O., Tarverdi, K., Umoren, A., Bassey, D. E., Okorie, U., & Adediran, J. (2021). Evaluation of eco-friendly concrete having waste PET as fine aggregates. Cleaner Materials, 2, 100026.

[53] Metwally, I. M. (2007). Investigations on the performance of concrete made with blended finely milled waste glass. Advances in structural engineering, 10(1), 47-53.

[54] Ismail, Z. Z., & Al-Hashmi, E. A. (2009). Recycling of waste glass as a partial replacement for fine aggregate in concrete. Waste management, 29(2), 655-659.

[55] Topcu, I. B. (1995). The properties of rubberized concretes. Cement and concrete research, 25(2), 304-310.

[56] Khatib, Z. K., & Bayomy, F. M. (1999). Rubberized Portland cement concrete. Journal of materials in civil engineering, 11(3), 206-213.

[57] Ganjian, E., Khorami, M., & Maghsoudi, A. A. (2009). Scrap-tyre-rubber replacement for aggregate and filler in concrete. Construction and building materials, 23(5), 1828-1836.

[58] Tafheem, Z., Rakib, R. I., Esharuhullah, M. D., Alam, S. R., & Islam, M. M. (2018). Experimental investigation on the properties of concrete containing post-consumer plastic waste as coarse aggregate replacement. Journal of Materials and Engineering Structures «JMES», 5(1), 23-31.

[59] Belmokaddem, M., Mahi, A., Senhadji, Y., & Pekmezci, B. Y. (2020). Mechanical and physical properties and morphology of concrete containing plastic waste as aggregate. Construction and Building Materials, 257, 119559.

[60] Raj, B., Ganesan, N., & Shashikala, A. P. (2011). Engineering properties of self-compacting rubberized concrete. Journal of Reinforced Plastics and Composites, 30(23), 1923-

1930.

[61] Tan, K. H., & Du, H. (2013). Use of waste glass as sand in mortar: Part I–Fresh, mechanical and durability properties. Cement and Concrete Composites, 35(1), 109-117.

[62] Najim, K. B., & Hall, M. R. (2013). Workability and mechanical properties of crumb-rubber concrete. Proceedings of the Institution of Civil Engineers-Construction Materials, 166(1), 7-17.

[63] AL-Bawi, R. K., Kadhim, I. T., & AL-Kerttani, O. (2017). Strengths and failure characteristics of self-compacting concrete containing recycled waste glass aggregate. Advances in Materials Science and Engineering, 2017.

[64] Jirjees, F. F., Maruf, S. M., Rahman, A. R. A., & Younis, K. H. (2019). Behaviour of concrete incorporating tirederived crumb rubber aggregate. Int. J. Civ. Eng. Technol, 10(3), 3149-3157.

[65] Daoud, O., & Ibrahim, M. (2020). Utilization of Giad Steel Slag as Partial Replacement for Coarse Aggregates in Concrete. FES Journal of Engineering Sciences, 9(2), 53-57.

[66] Choudhary, S., Kishore, P. R., & Pachaiappan, S. (2022). Sustainable utilization of waste slag aggregates as replacement of coarse aggregates in concrete. Materials Today: Proceedings, 59, 240-247.

[67] Butler, L., West, J. S., & Tighe, S. L. (2013). Effect of recycled concrete coarse aggregate from multiple sources on the hardened properties of concrete with equivalent compressive strength. Construction and Building Materials, 47, 1292-1301.

[68] Serpa, D., De Brito, J., & Pontes, J. (2015). Concrete made with recycled glass aggregates: Mechanical performance. ACI Mater. J.[accepted for publication].

[69] Gupta, T., Chaudhary, S., & Sharma, R. K. (2014). Assessment of mechanical and durability properties of concrete containing waste rubber tire as fine aggregate. Construction and building Materials, 73, 562-574.

[70] Norhana, A. R., Kartini, K., & Hamidah, M. S. (2016, October). Recycled polyethylene terephthalate (PET) and rubber crumb as replacement to fine aggregate. In AIP Conference Proceedings (Vol. 1774, No. 1, p. 030025). AIP Publishing LLC.

[71] Malešev, M., Radonjanin, V., & Marinković, S. (2010). Recycled concrete as aggregate for structural concrete production. Sustainability, 2(5), 1204-1225.

[72] Belén, G. F., Fernando, M. A., Diego, C. L., & Sindy, S. P. (2011). Stress–strain relationship in axial compression for concrete using recycled saturated coarse aggregate. Construction and Building materials, 25(5), 2335-2342.

[73] Ahmed, S. (2013). Properties of concrete containing construction and demolition wastes and fly ash. Journal of materials in civil engineering, 25, 1864-1870.

[74] Çakır, Ö. (2014). Experimental analysis of properties of recycled coarse aggregate (RCA) concrete with mineral additives. Construction and Building Materials, 68, 17-25.

[75] Sadrmomtazi, A., Dolati-Milehsara, S., Lotfi-Omran, O., & Sadeghi-Nik, A. (2016). The combined effects of waste Polyethylene Terephthalate (PET) particles and pozzolanic materials on the properties of self-compacting concrete. Journal of Cleaner Production, 112, 2363-2373.

[76] Mousavimehr, M., & Nematzadeh, M. (2020). Post-heating flexural behavior and durability of hybrid PET–Rubber aggregate concrete. Construction and Building Materials, 265, 120359.

[77] Shah, S. F. A., Naseer, A., Shah, A. A., & Ashraf, M. (2014). Evaluation of thermal and structural behavior of concrete containing rubber aggregate. Arabian Journal for Science and Engineering, 39(10), 6919-6926.

[78] Mardani-Aghabaglou, A., Tuyan, M., & Ramyar, K. (2015). Mechanical and durability performance of concrete incorporating fine recycled concrete and glass aggregates. Materials and Structures, 48(8), 2629-2640

[79] Ghorbel, E., Wardeh, G., & Fares, H. (2019). Mechanical and fracture properties of recycled aggregate concrete in design codes and empirical models. Structural Concrete, 20(6), 2156-2170.

[80] Shaikh, F. U. A. (2018). Mechanical properties of concrete containing recycled coarse aggregate at and after exposure to elevated temperatures. Structural Concrete, 19(2), 400-410.

[81] Vakhshouri, B. (2018). Modulus of elasticity of concrete in design codes and empirical models: analytical study. Practice Periodical on Structural Design and Construction, 23(4), 04018022.

[82] ACI 318-11, Building Code Requirements for Structural Concrete and Commentary, PCA Notes on ACI 318-11: With Design Applications, ACI

[83] AS3600-2009, Australian Standard for Concrete Structures, 2009. S.A, North

Sydney.

[84] New Zealand Standard, Concrete Structures Standard. NZS 3101:2006. The Design of Concrete Structures, 2006. Wellington, New Zealand.

[85] International, Farmington Hills, Mich, 2011. Canadian Standard. C S A. A23.3-04, Design of Concrete Structures, Canadian

[86] Standard Association, 2004. British Standards Institution, Eurocode 2: Design of Concrete Structures: Part1-1: General Rules and Rules for Buildings, British Standards Institution,

2004.

[87] Japan Society of Civil Engineers, Standard Specification for Concrete Structure, JSCE, Tokyo, Japan, 2007.

[88] Japanese Civil Institute, Guidelines for Control of Cracking of Mass Concrete 2008, Japan Concrete Institute, 2008.

[89] Vongchavalitkul, S. (2014). Uncertainty Model of Concrete Elastic Modulus Effect to Critical Reinforced Concrete Buckling Load. In Advanced Materials Research (Vol. 931, pp. 525-528). Trans Tech Publications Ltd.

[90] Biondini, F., & Frangopol, D. M. (2008). Probabilistic limit analysis and lifetime prediction of concrete structures.

[91] Elsanadedy, H. M., Al-Salloum, Y. A., Abbas, H., & Alsayed, S. H. (2012). Prediction of strength parameters of FRP-confined concrete. Composites Part B: Engineering, 43(2), 228-239.

[92] Shah, A. A., Alsayed, S. H., Abbas, H., & Al-Salloum, Y. A. (2012). Predicting residual strength of non-linear ultrasonically evaluated damaged concrete using artificial neural network. Construction and Building Materials, 29, 42-50.

[93] Naseri, H., Jahanbakhsh, H., Moghadas Nejad, F., & Golroo, A. (2020). Developing a novel machine learning method to predict the compressive strength of fly ash concrete in

different ages. AUT Journal of Civil Engineering, 4(4), 3-3.

STATEMENT OF AUTHORSHIP

"Mix Design Optimization of Waste-based Aggregate Concrete for Natural Resource Utilization and Global Warming Potential"
For Submission to *Journal of Cleaner Production*

Shobeiri, V. (Candidate)

Prepared manuscript, performed all analyses, and developed model and theory (70%)

This paper reports on original research I conducted during the period of my Higher Degree by Research candidature and is not subject to any obligations or contractual agreements with a third party that would constrain its inclusion in this thesis. I am the primary author of this paper.

Signed… Date16/03/2023

Bennett, B.

Supervised and contributed to research (10%)

I certify that the candidate's stated contribution to the publication is accurate (as detailed above); permission is granted for the candidate in include the publication in the thesis; and the sum of all co-author contributions is equal to 100% less the candidate's stated contribution.

Signed… Date 17/04/2023

Xie, T.

Supervised and contributed to research (10%)

I certify that the candidate's stated contribution to the publication is accurate (as detailed above); permission is granted for the candidate in include the publication in the thesis; and the sum of all co-author contributions is equal to 100% less the candidate's stated contribution.

Signed… Date 17/04/2023

Visintin, P.

Supervised and contributed to research, and acted as corresponding author (10%)

I certify that the candidate's stated contribution to the publication is accurate (as detailed above); permission is granted for the candidate in include the publication in the thesis; and the sum of all co-author contributions is equal to 100% less the candidate's stated contribution.

Signed… Date 04/04/2023

Mix Design Optimization of Waste-based Aggregate Concrete for Natural Resource Utilization and Global Warming Potential

Vahid Shobeiri, Bree Bennett, Tianyu Xie and Phillip Visintin

Abstract

In this study, a mix design optimization framework based on genetic algorithms (GA), artificial neural networks (ANN) and a life-cycle assessment (LCA) with an emphasis on the global warming potential is developed to find optimal mixes of concrete with different types of waste aggregates including concrete, slag, glass, plastic and rubber. Integrating a large database containing 5321 waste-based aggregate mix designs, ANNs are used to predict different concrete slump, compressive strength, splitting tensile strength, flexural strength, elastic modulus and water absorption. Based on the ANN prediction model, two scenarios with the objective functions of minimizing natural resource utilization and minimizing carbon dioxide emissions of waste-based aggregate concretes are optimized using a genetic algorithm. When considering the impact of transport emissions, the interaction between the utilization of waste-based aggregates and the resulting carbon emissions are discussed. The results show that the developed ANN model is able to correctly predict different properties of waste-based aggregate concretes and the developed framework is capable of reducing carbon dioxide emissions by 50% as compared to similar mixes with an equivalent compressive strength in the database.

Keywords: Mix design optimization; waste-based aggregate concrete; natural resource utilization; carbon dioxide emissions

Introduction

Concrete is the most commonly used construction material, but its production contributes significantly to environmental degradation, including the depletion of natural resources and the emission of greenhouse gases. The production of concrete requires large amounts of natural resources, such as sand and gravel, which are becoming increasingly scarce (Han et al. 2021). Additionally, the production of cement, a key component of concrete, is a significant source of carbon dioxide equivalent ($CO_{2\text{-}wq}$) emissions, which contribute to global warming and climate change (Adesina 2020). In recent years, the use of waste-based aggregates in concrete production has been proposed as a potential solution to reduce the environmental impact of concrete, especially from the prospective of conserving natural resources. The waste-based aggregates that have been most commonly investigated are those derived from recycled concrete, which would otherwise generally end up in landfill (Nedeljković et al. 2021). The use of waste-based aggregates is therefore promoted on that basis that they conserve natural resources, and divert waste materials from landfills.

Many studies have explored the potential to use waste-based aggregates including fly ash (Usanova and Barabanshchikov 2020), slag (Dong et al. 2021), recycled concrete (Revilla-Cuesta et al. 2020), waste plastic (Basha et al. 2020), and rubber (Li et al. 2019). These studies have spanned the last three decades, and several detailed review papers (Li et al. 2020; Piccinali et al. 2022; Rashad 2022) have aimed to consolidate findings from across the field. Despite the significant research effort already expended, several challenges that prevent more widespread uptake still exist. For example:

1) The relationship between the properties of waste-based aggregates and the properties of the resulting concrete are complex and have not been well modelled.
2) Waste-based aggregates generally have highly variable physical and mechanical properties and may not always meet the minimum specifications required for use in concrete.
3) In most of the cases the mix designs for concrete containing waste-based aggregates are derived from the results of small-scaled experimental campaigns with limited variations in the key mixing factors.
4) The properties of different waste-based aggregate concretes have not compared or studied in detail to determine optimal conditions for their use.
5) The arguments for using different waste-based aggregates has generally be made without the use life-cycle assessment approaches, and few studies have compared the performance of different types of aggregates on the basis of a functional unit considering environmental impact and mechanical/durability performance.
6) Generic tools for mix design optimization of concretes with waste-based aggregates are needed, to have broad applicability, these should be verified using a large quantity of test data, and be capable of covering a wide variety of aggregate types and consider a broad range of mechanical properties required for real world application.

A review of existing literature on the waste aggregate based concrete also shows that while there are many studies in the literature that predict the compressive strength of concrete with recycled concrete aggregates (e.g., Yuan et al. 2022; Khan et al. 2022; Chen et al. 2022; Nguyen et al. 2023), there is no study for predicting a broader set of properties (e.g., slump, elastic modulus, splitting tensile strength, flexural strength and water absorption) of concrete with various types of waste aggregates (e.g., glass, slag, plastic and rubber aggregates). This is important because other properties of waste-based aggregate concretes are equally important for the structural performance of concrete containing waste aggregates. Moreover, while there are many studies dealing with mix design optimization of concrete with waste binder materials using soft computing methods (e.g., Cheng et al. 2014; Lee et al. 2019; Zhang et al. 2021; Shobeiri et al. 2023), there is no study investigating the mix design optimization of concrete with different types of waste aggregates due to the complexity of the design optimization as the properties of waste-based aggregate concrete significantly differ based on waste aggregate type (Belmokaddem et al. 2020).

To address these issues, this study proposes a large-scaled mix design optimization framework that integrates genetic algorithms, artificial neural networks, and a life-cycle assessment tool with a focus on global warming potential. The framework is developed to find optimal mixes of concrete using waste aggregates, including concrete, slag, glass, plastic, and rubber. A large database containing 5321 waste-based aggregate mix designs from 285 studies is used to train the artificial neural network to predict the properties of concrete with different types of waste aggregates including slump, compressive strength, splitting tensile strength, flexural strength, elastic modulus and water absorption.

The framework is then applied to optimize waste-based aggregate concrete mixes when the single objective is either minimizing natural resource utilization or minimizing carbon dioxide emissions. Furthermore, the effects of emissions generated during the transport of waste-based aggregates on the optimal concrete mix designs is also investigated. Overall, this study on waste aggregate-based concrete is focused on finding innovative and sustainable solutions to reduce the environmental impact of concrete production while improving its performance.

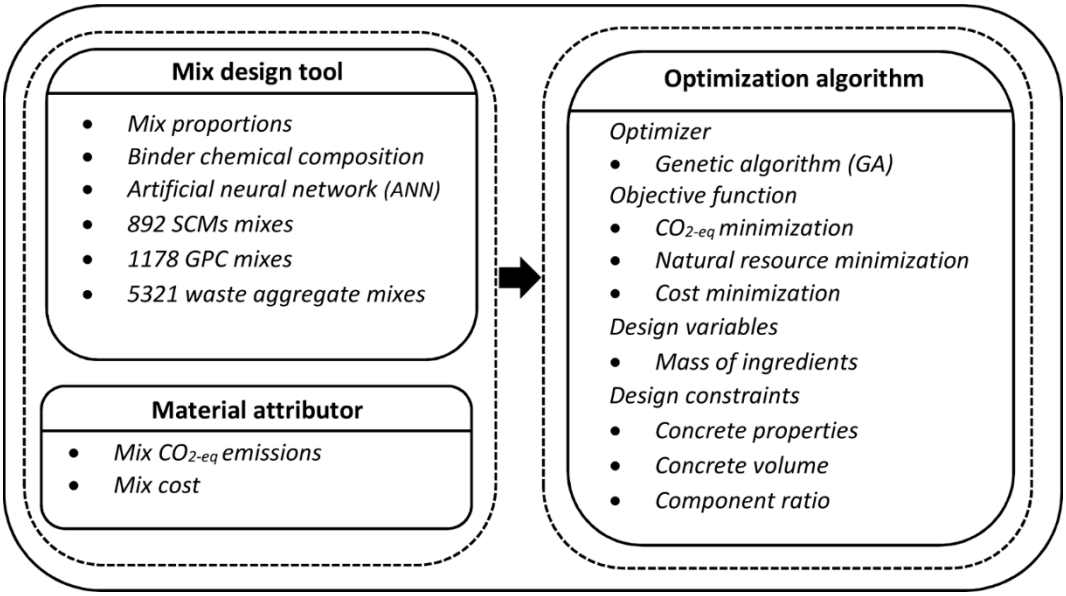

Fig. 1 The framework of concrete mix design optimization (extended from Shobeiri et al. 2022)

Mix design framework

This study utilizes a generic mix design optimization framework developed by Shobeiri et al. (2022) to investigate optimal waste-based aggregate concrete mixes in terms of minium global warming potential and natural resource utilization. As can be seen from Fig. 1, this framework relates (i) a mix design tool that predicts concrete material properties based on mix proportions and material characteristics to, (ii) a material attribute calculator that quantifies the cost and $CO_{2\text{-}eq}$ emissions of the concrete, (iii) to an optimization algorithm that identifies mixes based on a set of objective functions, constraints and design variables. These three components of mix design optimization framework are discussed in the following sections.

2.1 Mix design tool

In this study, a single hidden layer ANN in Matlab (MathWorks 2020) is used for the mix design optimization of waste-based aggregate concretes using a large database containing 5321 mix designs for concrete with various aggregates, including: recycled concrete aggregates (1865 mixes), rubber aggregates (1732 mixes), plastic aggregates (213 mixes), slag aggregates (162 mixes) and glass aggregates (153 mixes) ad natural aggregates (1196 mixes). This database which is a further development of the original databases collected by Xu et al. (2019), Xie et al. (2020), Gravina et al. (2021) and Gravina et al. (2022) covers a wide range of ingredients, waste aggregate contents, concrete properties and mix proportions (see Shobeiri et al. (2023) for more details on the database).

Since that the characteristics of aggregate are critical factors affect the mechanical properties of concrete, it is not rational to train a single ANN based on all 5321 mix designs using different types of aggregates, rather the ANN was trained independently for each type of aggregate. The ANN was trained to predict the slump, compressive strength, splitting tensile strength, flexural strength, elastic modulus and water absorption of concrete with each type of waste-based

aggregate based on the mass of constituent materials per cubic meter of concrete (cement, fly ash, granulated blast furnace slag (GGBFS), silica fume, water, fine and coarse natural aggregates, waste-based aggregates, superplasticizer) and the age of concrete at the time of testing for mechanical properties or at the time of mixing for the slump. It should be noted that the mass of ingredients are used to train ANN as weight ratio would be easier for LCA and critical transport distance analyses (see Sections 2.2 and 3.3). As opposed to previous applications of the framework that focused on optimization of concrete with different binders but only natural aggregates (Shobeiri et al. 2022 and 2023), in this study it was not possible to consider the chemical composition of the binders because this information has generally not been reported in studies focused on investigating waste-based aggregate concrete performance (less than 30% of mixes reported chemical composition of binders). It should be further noted that only fly ash, GGBFS and silica fume are considered in this study as they are the most commonly used SCMs in the database .

2.2. Material attribute tool

Although the generic framework above has previously been applied to calculate both the financial cost and CO2-eq emissions of $1m^3$ of concrete, in this study, given it was not possible to identify the cost of all waste-based aggregates only $CO_{2\text{-eq}}$ emissions have been considered (Adesina 2020). To calculate the $CO_{2\text{-eq}}$ emissions a detailed life-cycle assessment (LCA) with an emphasis on global warming potential (GWP) conducted by Shobeiri et al. (2021) and Gursel (2015) has been applied, and the reader is referred to these sources for full details. It should be noted that in the LCA, the emissions arisen from fuel pre-combustion, fuel combustion and electricity generations are calculated for GWP and the impact of allocating the emissions associated with alternative binders and the burden of recycling are ignored.

Based on the assumptions above, a Table 1 summarises the assumed $CO_{2\text{-eq}}$ emissions per kg of each material and the $CO_{2\text{-eq}}$ emissions per kg-km for different transportation modes (road, rail and sea), where the unit emissions from the production of cement, fly ash, GGBFS, silica fume, natural aggregates and superplasticizer are taken from Gursel (2015) and the unit emissions from the manufacture of different types of waste aggregates including concrete, slag, glass, plastic and rubber are taken from Roh et al. (2020), Javadabadi (2019) and Farina et al. (2017).

Table 1 Emissions factors for waste based aggregate concrete (see Gursel (2014), Roh et al. (2020), Javadabadi (2019) and Farina et al. (2017) for full details)

	Emissions factor		
Component	Manufacture (kg $CO_{2\text{-eq}}$/kg)	Transportation (kg $CO_{2\text{-eq}}$/kg-km)	
Cement	0.8966	Road	12.80×10^{-5}
Fly ash	0.0260	Rail	2.74×10^{-5}
GGBFS	0.0901	Sea	1.72×10^{-5}
Silica fume	0.0280		
Superplasticizer (liquid)	0.2290		
Water	0.0002		
Natural fine aggregate	0.0028		
Natural coarse aggregate	0.0039		
Concrete aggregate	0.0149		

Slag aggregate	0.0226		
Plastic aggregate	0.1360		
Rubber aggregate	0.2450		
Glass aggregate	0.2740		

2.3. Optimization tool

The optimization algorithm generates optimal mix designs according to the objective functions, constraints and the information provided by the mix design tool and the material attribute calculator. To complete the optimisation a genetic algorithm (GA) has been applied due to its capability in dealing with highly nonlinear models and a proven record of success in concrete mix design optimisation (Lee et al. 2019; Wang 2020; Naseri et al. 2020). The main GA components including objective functions, design variables and constraints are outlines in the following sections.

2.3.1 Objective function

Two different objective functions including (i) minimization of $CO_{2\text{-eq}}$ emissions (C_t) and (ii) minimization of natural resource utilization (N_u) are considered to investigate the interaction between global warming potential and natural resource utilization as follows:

$$C_t = \sum_i m_i (C_{prod_i} + C_{tran_i} \times d_i) \quad (1)$$

$$N_u = \frac{1}{RR} \quad (2)$$

where m_i and d_i are respectively the mass and transport distance of the concrete mix component *i*; C_{prod_i} and C_{tran_i} are respectively the production and transport emissions per kg of concrete component *i* (see Table 1); and *RR* is the waste-based aggregate replacement ratio which is defined as the volume of waste-based aggregates to the total volume of waste-based and natural aggregates of the same type. It should be noted that when the objective is to minimize the natural resource utilization, it is expected to contain more waste aggregates to conserve natural aggregate resources regardless of $CO_{2\text{-eq}}$ emissions.

2.3.2. Design variables

The design variables for the GA are taken to be the mass of concrete mix components including cement, fly ash, GGBFS, silica fume, natural fine and coarse aggregates, waste-based aggregates, water and superplasticizer. These design variables are provided to the optimiser along with the wet and hardened mechanical properties predicted by the ANN in the mix design tool described above.

2.3.4 Design constraints

To ensure the feasibility of optimal mix designs developed by GA, several constraints are applied as follows:

1- *Mechanical and workability constraints*: The mechanical properties (M) and workability (W) must remain within a desired tolerance (tol) of the target value as follows:

$$M_t - tol_M \leq M_p \leq M_t + tol_M \quad (3)$$

$$W_t - tol_W \leq W_p \leq W_t + tol_W \quad (4)$$

where subscripts t and p refer to the target and predicted values.

While any properties of concrete that can be predicted by the ANN can be used as the

targets, in this study, compressive strength and slump are identified by the mix design tool and used as constraints for GA as they are two commonly employed indicators to describe the fresh and hardened characteristics of concrete containing waste-based aggregates and have been the most widely reported in the database mix designs (Mirzahosseini et al. 2019; Silva et al. 2020).

2- *Concrete volume constraint:* The total volume of concrete mix ingredients minus the entrapped air must be constant.

3- *Concrete ingredient constraint:* The upper and lower bounds of mix ingredients must remain within their upper and lower bounds in the database. Moreover, the mixing factors (e.g., water-to-binder, binder-to-total aggregates and fine-to-coarse aggregate) must remain within the range available in the database.

Results and discussion

In this section the ability of the ANN to reliably predict the properties of waste-based aggregate concrete is first investigated and the interaction between carbon emissions minimization and natural resource usage minimization are then discussed through a transport sensitivity analysis. The environmental performance of optimal mixes considering both scenarios (minimization of $CO_{2\text{-eq}}$ emissions and natural resource usage) is finally compared with that of experimental mixes in the database.

3.1 ANN performance

Table 2 summarizes the predictive performance of ANN tool on training, validation and test sets for the properties of concrete with different types of waste aggregates based on root mean square error (RMSE), mean absolute error (MAE), coefficient of determination (R^2) and correlation coefficient (R). It should be noted that *RMSE*, *MAE*, *MAE*, R^2 and *R* are chosen to describe the predictive performance of ANN as they are the main performance indicators to quantify the goodness of fit of an ANN model (Chicco et al. 2021). It should also be noted that in the developed ANN model, the training (70%), testing (15%) and validation (15%) sets are randomly selected from the corresponding database. As can be seen from Table 2, a broader set of concrete properties including slump, compressive strength, splitting tensile strength, flexural strength, elastic modulus and water absorption is taken into account to have a better prediction of structural performance of waste-based aggregate concrete. It should be noted that since the performance of an ANN model is dependent of the size of database, the model presented here is more reliable than those reported in the literature (e.g., Turki et al. 2017; Hammoudi et al. 2019; Bawab et al. 2021). It can also be seen that for almost all types of waste-based aggregate concretes, ANN is trained with more number of mixes for other concrete properties than water absorption and slump due to less availability of water absorption and slump data for waste-based aggregate concretes in literature.. Considering the results shown in Table 2, it can be seen that the developed ANN model can be a reliable tool to predict the properties of concrete with different types of waste aggregates with R^2 larger than 65%, 72%, 67%, 44%, 57% and 80% respectively for slump, compressive strength, splitting tensile strength, flexural strength, elastic modulus and water absorption on validation and test sets.

For completeness, the correlation between the observed and predicted values for the properties of waste-based aggregate concrete is shown in Figs. S1-S3 in Supplementary Materials A. When interpreting the results in Figs. S1-S3, it should be noted that subplots (a), (b), (c), (d) and (e) in Figs. S1-S3 respectively show the correlation between the observed and predicted values for mixes with concrete, slag, plastic, rubber and glass aggregates on training, validation

and test sets; and these subplots are repeated in Figs. S1-S3 to show the correlation results for compressive strength and slump in Fig. S1, splitting tensile strength and flexural strength in Fig. S2 and elastic modulus and water absorption in Fig. S3. It can be seen from these figures that there is a good correlation between the observed and predicted values for the properties of concrete with different types of waste aggregates on different data sets.

Table 2 Statistical results for ANN model of waste-based aggregate concrete

Aggregate type	Data set	Output	*No of mixes*	*RMSE*	*MAE*	R^2	*R*
Concrete Agg.	Training	Slump	295	23.69	16.90	0.802	0.886
		Compressive strength	1737	6.72	5.08	0.819	0.903
		Tensile strength	781	0.30	0.22	0.911	0.955
		Flexural strength	168	0.45	0.33	0.834	0.895
		Elastic modulus	414	3.18	2.28	0.773	0.874
		Water absorption	89	0.72	0.52	0.950	0.942
	Validation	Slump	63	29.61	23.27	0.725	0.859
		Compressive strength	372	6.96	5.16	0.770	0.878
		Tensile strength	167	0.37	0.26	0.858	0.927
		Flexural strength	36	1.01	0.74	0.442	0.643
		Elastic modulus	89	3.53	2.42	0.628	0.800
		Water absorption	19	1.07	0.88	0.895	0.954
	Test	Slump	63	29.85	19.97	0.645	0.820
		Compressive strength	372	7.55	5.51	0.781	0.885
		Tensile strength	167	0.48	0.32	0.753	0.870
		Flexural strength	36	0.98	0.74	0.453	0.718
		Elastic modulus	89	4.04	2.86	0.569	0.772
		Water absorption	19	1.31	1.08	0.803	0.910
Slag Agg.	Training	Slump	59	2.97	2.04	0.998	0.997
		Compressive strength	150	1.64	1.25	0.990	0.988
		Tensile strength	97	0.30	0.21	0.896	0.942
		Flexural strength	64	0.13	0.07	0.988	0.991
		Elastic modulus	36	0.313	0.238	0.998	0.999
		Water absorption	17	0.30	0.24	0.789	0.962
	Validation	Slump	13	13.24	9.91	0.964	0.986
		Compressive strength	32	2.77	2.21	0.969	0.985
		Tensile strength	21	0.43	0.32	0.875	0.956
		Flexural strength	14	0.92	0.52	0.515	0.872
		Elastic modulus	8	0.87	0.77	0.979	0.997
		Water absorption	4	0.25	0.23	0.817	0.961
		Slump	13	15.61	11.77	0.928	0.972
		Compressive strength	32	3.27	2.63	0.910	0.955

	Test	Tensile strength	21	0.35	0.24	0.667	0.860
		Flexural strength	14	0.32	0.24	0.926	0.967
		Elastic modulus	8	2.57	1.39	0.870	0.943
		Water absorption	4	0.41	0.37	0.844	0.968
Glass Agg.	Training	Slump	42	2.89	1.88	0.988	0.998
		Compressive strength	120	1.77	1.08	0.990	0.996
		Tensile strength	32	0.09	0.05	0.993	0.997
		Flexural strength	32	0.35	0.25	0.926	0.964
		Elastic modulus	15	0.38	0.26	0.996	0.995
		Water absorption	11	0.13	0.11	0.995	0.997
	Validation	Slump	9	2.54	1.88	0.980	0.990
		Compressive strength	26	2.23	1.73	0.982	0.994
		Tensile strength	7	0.22	0.13	0.875	0.937
		Flexural strength	7	0.48	0.37	0.812	0.921
		Elastic modulus	3	0.76	0.58	0.955	0.984
		Water absorption	2	0.02	0.02	0.861	0.998
	Test	Slump	9	12.58	7.98	0.718	0.865
		Compressive strength	26	5.43	3.55	0.869	0.941
		Tensile strength	7	0.46	0.38	0.813	0.938
		Flexural strength	7	0.42	0.34	0.828	0.949
		Elastic modulus	3	1.39	0.99	0.915	0.958
		Water absorption	2	0.06	0.05	0.913	0.998
Plastic Agg.	Training	Slump	62	3.88	2.21	0.995	0.993
		Compressive strength	237	1.99	1.48	0.966	0.980
		Tensile strength	78	0.24	0.19	0.913	0.958
		Flexural strength	84	0.31	0.24	0.969	0.977
		Elastic modulus	31	0.19	0.11	0.998	0.999
		Water absorption	20	0.32	0.26	0.968	0.986
	Validation	Slump	13	16.03	11.60	0.900	0.952
		Compressive strength	51	4.11	3.01	0.798	0.893
		Tensile strength	17	0.49	0.32	0.736	0.874
		Flexural strength	18	0.63	0.44	0.889	0.947
		Elastic modulus	7	0.58	0.40	0.995	0.998
		Water absorption	4	0.50	0.45	0.923	0.994
	Test	Slump	13	25.68	13.34	0.737	0.873
		Compressive strength	51	3.61	2.64	0.892	0.945
		Tensile strength	17	0.42	0.31	0.800	0.902
		Flexural strength	18	1.02	0.72	0.805	0.941
		Elastic modulus	7	2.04	1.01	0.741	0.938
		Water absorption	4	0.30	0.25	0.981	0.991
		Slump	233	13.70	8.91	0.951	0.975

Rubber Agg.	Training	Compressive strength	1415	6.52	4.69	0.834	0.913
		Tensile strength	414	0.32	0.23	0.897	0.945
		Flexural strength	414	0.72	0.48	0.870	0.929
		Elastic modulus	328	5.45	3.69	0.782	0.850
		Water absorption	53	0.11	0.07	0.998	0.999
	Validation	Slump	50	32.51	22.42	0.753	0.874
		Compressive strength	303	6.96	5.23	0.828	0.911
		Tensile strength	89	0.38	0.29	0.822	0.908
		Flexural strength	89	1.11	0.75	0.581	0.778
		Elastic modulus	70	4.95	3.60	0.803	0.899
		Water absorption	11	0.63	0.41	0.972	0.997
	Test	Slump	50	33.40	24.02	0.757	0.873
		Compressive strength	303	8.53	6.24	0.721	0.857
		Tensile strength	89	0.48	0.37	0.803	0.896
		Flexural strength	89	1.44	0.90	0.511	0.784
		Elastic modulus	70	5.43	4.24	0.749	0.866
		Water absorption	11	0.70	0.44	0.967	0.989

3.2 Mix design optimization

It is well established (Medina et al. 2014; Bai et al. 2020) that the inclusion of waste-based aggregates without pretreating them generally results in reductions of the physical-, mechanical- and durability- properties of the concrete, and that these reduced properties are generally recovered through the use of additional binders which contribute heavily to $CO_{2\text{-eq}}$ emissions. To better understand the competing effects of conserving natural resources and reducing global warming potential, let us first investigate the mix design optimization of waste-based aggregate concretes when the single objective is to minimize (i) natural aggregate usage and (ii) to minimize $CO_{2\text{-eq}}$ emissions as has been commonly done in experimental research on both the development of waste-based aggregates and low emissions binders.

In this analysis, it is assumed that all concrete materials are provided locally and therefore no transportation for concrete materials is included in the analysis, the impact of transport will however be considered in a later case study. It should be noted that to assess the performance of the framework over a wide range of concretes, the target compressive strength is considered to be 30, 40 and 50 MPa (with a tolerance of 1 MPa) to account for concrete with different compressive strengths and the slump is fixed at 75 mm (with a tolerance of 5 mm) as this is the most common slump value in the database. It is also worth mentioning that the concrete volume constraint and the entrapped air are taken as 1 m3 and 2% respectively for the mix design optimization process.

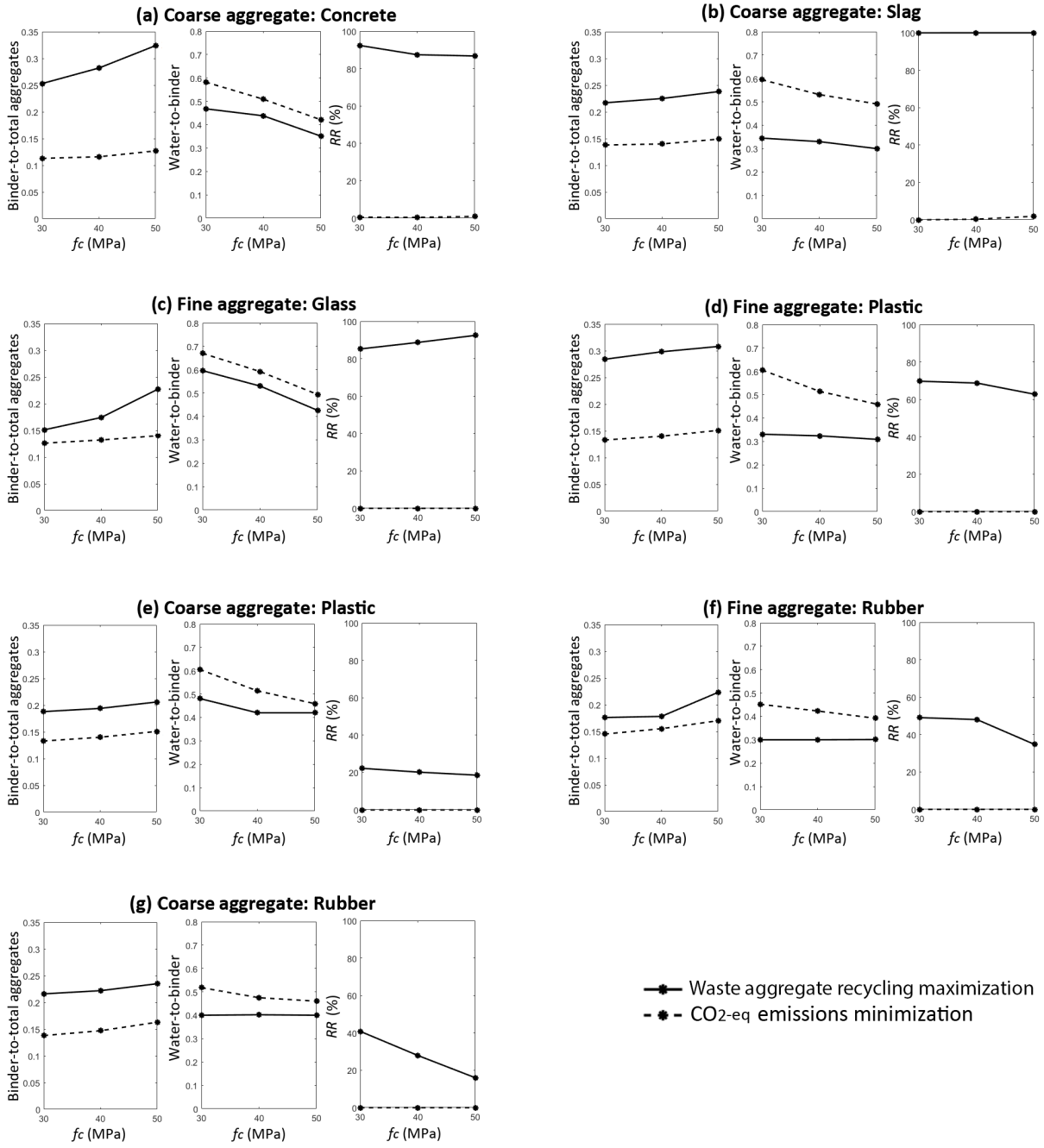

Fig. 2 Optimal waste-based aggregate mixes with waste aggregate recycling maximization and $CO_{2\text{-eq}}$ emissions minimization

Figure 2 shows the optimal concrete mixes for those containing different types of waste aggregates including (a) coarse concrete, (b) coarse slag, (c) fine glass, and (d) fine plastic, (e) coarse plastic, (f) fine rubber and (g) coarse rubber aggregates in terms of binder-to-total aggregate (w/a), water-to-binder (w/b) and waste aggregate replacement ratio (*RR* (%)). When interpreting the results shown in Fig. 2, it should be noted that the solid line represents optimal mixes when minimizing only natural resource utilization and the dashed line shows optimal mixes when minimizing only $CO_{2\text{-eq}}$ emissions.

It is clear from Fig. 2 that with the aim of only minimizing natural aggregate usage (solid line), *RR* (%) for optimal mixes is between 15% and 100% depending on the type of waste-based aggregate and target compressive strength. However, when the objective is to minimize $CO_{2\text{-}}$

$_{eq}$ emissions (dashed line), no waste aggregate is found to be applied in all the optimal mixes identified as the production of waste aggregates is more carbon intensive than the manufacture of natural aggregates as show in Table 1. It also appears that when the objective changes from carbon emissions minimization (dashed line) to waste aggregate recycling maximization (solid line), while binder-to-total aggregate increases, water-to-binder decreases for all optimal mixes with waste-based aggregates. This indicates that while there is a benefit from reducing the reliance on natural aggregates there is a cost associated with increased binder content to compensate the waste aggregate impact on the compressive strength of concrete.

It can also be seen from Fig. 2 that for both the minimization of natural resource usage and the minimization of $CO_{2\text{-}eq}$ emissions, for almost all concretes with waste-based aggregates, with an increase in compressive strength, a higher binder content is required, which is in agreement with that reported in literature (Piasta and Zarzycki 2017). It is also clear that for almost all optimal mixes, *RR* (%) decreases with an increase in compressive strength when the objective is to minimize natural resource utilization (solid line). This can be explained by the reduction in compressive strength that occurs when waste-based aggregates replace natural aggregates and therefore for higher-strength concrete there is a general tendency to reduce their volume (Daoud & Ibrahim 2020). The exception to this general trend is for optimal mixes with slag (Fig. 2(b)) and glass aggregates (Fig. 2(c)) where *RR* (%) is either constant at 100% for slag aggregates or slightly increases from 85% to 92% for glass aggregates as the compressive strength increases from 30 MPa to 50 MPa. This can be attributed to the angular nature and pozzolanic properties of fine glass aggregates, and high density and rough surface texture of coarse steel slag aggregates which can provide a better bond with cement paste compared to other types of waste aggregates (Metwally 2007; Ismail and Al-Hashmi 2009; Miah et al. 2020; Choudhary et al. 2022).

It is also clear that for waste aggregate recycling maximization (solid line), natural aggregates can be replaced with a higher proportion of recycled concrete, slag and glass aggregates than plastic and rubber aggregates while still meeting the same compressive strength requirements. For example, when considering the minimization of natural resources (solid line) for a 40 MPa concrete, the *RR* (%) for optimal mixes with recycled concrete, slag and glass aggregates (Fig. 2(a-c)) is more than 80%, while *RR* (%) is less than 70% for optimal mixes with plastic aggregates (Fig. 2(d-e)) and less than 50% for optimal mixes with rubber aggregates (Fig. 2(f-g)). The reason for this difference can be attributed to a range of factors such as lower strength and density, smoother surface texture and the less adhesive and more hydrophobic nature of plastic and rubber aggregates as compared to recycled concrete and slag aggregates resulting in a weaker bond strength at the interfacial transition zone (ITZ) with cement paste (Andreu and Miren 2014; Bamigboye et al. 2021). It should be noted that for waste aggregate recycling maximization (solid line), *RR* (%) for optimal mixes with fine plastic aggregates (Fig. 2(d)) is more than double than that for optimal mixes with coarse plastic aggregates (Fig. 2(e)) for all compressive strengths modelled.

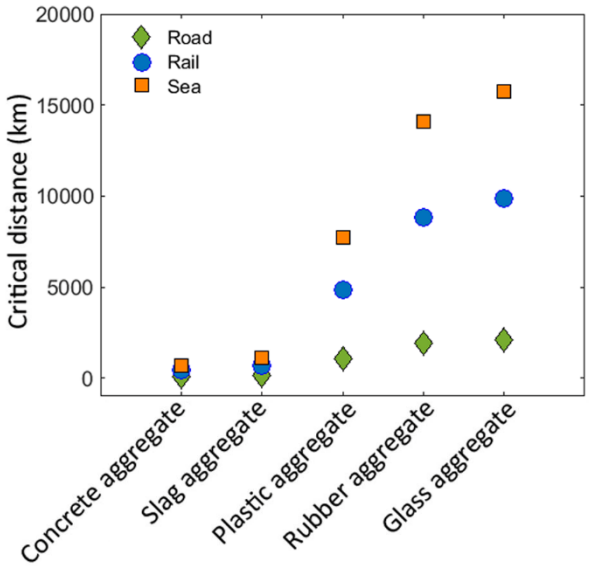

Fig. 3 Critical distances of natural aggregates compared to locally provided waste-based aggregates

3.3 Transport sensitivity analysis

A wide variety of waste aggregates have been used for concrete production to minimize virgin material usage and eliminate disposal related problems. However, the impact of waste aggregate utilization on global warming potential (GWP) should also be considered in terms of carbon emissions from their production and transportation. This is important because the production of waste aggregates (e.g., recycled concrete, slag, glass, plastic and rubber) are generally more energy intensive than the production natural aggregates (see Table 1) and some types of waste-based aggregates (e.g., slag) often need to be transported considerable distances (Crossin 2015). Therefore, to better understand the significant impact that the transport and production emissions of waste aggregates can have, let us now examine their performance in terms of the critical transport distance ($D_{critical}$), that is the distance that natural aggregate can be transported before it becomes more emissions intensive than the waste-based aggregate. That is:

$$D_{critical} = \frac{CO_{2-eq_{waste-agg}} - CO_{2-eq_{natural-agg}}}{CO_{2-eq_{transport}}} \quad (5)$$

where $CO_{2-eq_{waste-agg}}$ and $CO_{2-eq_{natural-agg}}$ are respectively the emissions associated with the production of waste and natural aggregates, and $CO_{2-eq_{transport}}$ is the emissions associated with transportation (road, rail and sea) of aggregates which are taken from Table 1. It should be noted that Eq. (1) only considers the emissions impact of aggregate and does not account for the functionality change of concrete due to waste aggregate utilization. In this analysis, it is assumed that the production of fine and coarse waste aggregate of the same type possess similar $CO_{2\text{-}eq}$ emissions and waste aggregates are provided locally.

Fig. 3 shows the critical distances of natural aggregates compared to waste-based aggregates with different transportation modes (road, rail and sea) where natural aggregates can be less emissions intensive than waste-based aggregates if they are provided from a quarry within the critical distance from the construction site. It can be seen that, as expected, the critical distances increase with a change in the transportation mode from road to rail and sea. However, this rise is less apparent for concrete and slag aggregates as their production emissions are much lower than those from other waste-based aggregates (see Table 1). In fact, the production emissions

of recycled concrete and slag aggregates are about 3 and 5 times more than that from natural aggregates (Roh et al. 2020; Park et al. 2019) leading to the critical distances of 95 km (road), 401 km (rail) and 703 km (sea) for concrete aggregates and 146 km (road), 683 km (rail) and 1088 km (sea) for slag aggregates. However, the production emissions of plastic, rubber and glass aggregates are respectively about 8, 15 and 17 times more than that from concrete aggregates (Bartolozzi et al. 2012; Tahanpour Javadabadi 2019). These high production emissions have resulted in the critical distances of 1040 km (road), 4861 km (rail) and 7745 km (sea) for plastic aggregates; 1892 km (road), 8840 km (rail) and 14080 km (sea) for rubber aggregates; and 2120 km (road), 9898 km (rail) and 15767 km (sea) for glass aggregates. It should be noted that the results presented here for critical distance of natural aggregates are the outcome of emissions factors of waste aggregates taken from Roh et al. (2020), Javadabadi (2019) and Farina et al. (2017) and may change with a change in the emissions factors of waste aggregates if the system boundary for the life-cycle assessment of waste aggregates changes or other technologies (materials' inventory that is available locally) are applied for the manufacture of waste aggregates. For these cases the absolute value of $D_{critical}$ should be applied for anlayzing.

The results of this analysis show that from the perspective of global warming potential (GWP), concrete aggregates can be a preferred substitute to natural aggregates over other waste-based aggregates including plastic, glass and rubber aggregates. However, as the critical distance of concrete aggregate and slag aggregate are relatively similar with that only a slightly longer distance is required to transport slag aggregate, this conclusion might not be generalized for slag aggregates because slag may not be generated locally and therefore a transport sensitivity analysis for slag aggregates might be required when the generation point of slag is known. It is important to note that the analysis presented here for critical distance of natural aggregates only considers GWP, and the environmental benefit of avoiding natural resource utilisation is a separate measure.

Having the critical distances for natural aggregates, let us now find optimal waste-based aggregate mixes for $CO_{2\text{-eq}}$ emissions minimization through a transport sensitivity analysis for natural aggregates. In this analysis, an average transport distance within Australia (Grant 2015) is applied for the transportation of concrete materials (62 km for cement and 200 km for SCMs and superplasticizer) and the transport distance of natural aggregates is considered to be 100 km, 1000 km, 2000 km and 10000 km (by road) to cover all the range of critical distances for natural aggregates. Fig. 4 shows the optimal concrete mixes with different types of waste aggregates for $CO_{2\text{-eq}}$ emissions minimization with a transport sensitivity analysis for natural aggregates. When interpreting the results shown in Fig. 4, subplots (a), (b), (c), (d), (e), (f) and (g) respectively show the optimal mixes with coarse concrete, coarse slag, fine glass, fine plastic, coarse plastic, fine rubber and coarse rubber aggregates in terms of binder-to-total aggregate (w/a), water-to-binder (w/b) and waste aggregate replacement ratio (*RR* %). Further, green, blue, yellow and orange dashed lines in Fig. 4 respectively show the transport distance of natural aggregates to be 100 km, 1000 km, 2000 km and 10000 km.

It appears from Fig. 4 that when the transport distance of natural aggregates is 100 km (green line), all optimal mixes are made with only natural aggregates (*RR* is almost zero) as the total emissions (production emissions plus transport emissions) from waste aggregates in this case are much higher than those from natural aggregates. For instance, when the transport distance of natural aggregates is 100 km, the total emissions from coarse concrete, coarse slag, coarse plastic and coarse rubber aggregates are respectively 1.3, 1.7, 8.5 and 15.1 times of that from natural coarse aggregates, and the total emissions from fine plastic, fine rubber and fine glass

aggregates are respectively 9.1, 16.1 and 18 times of that from natural fine aggregates.

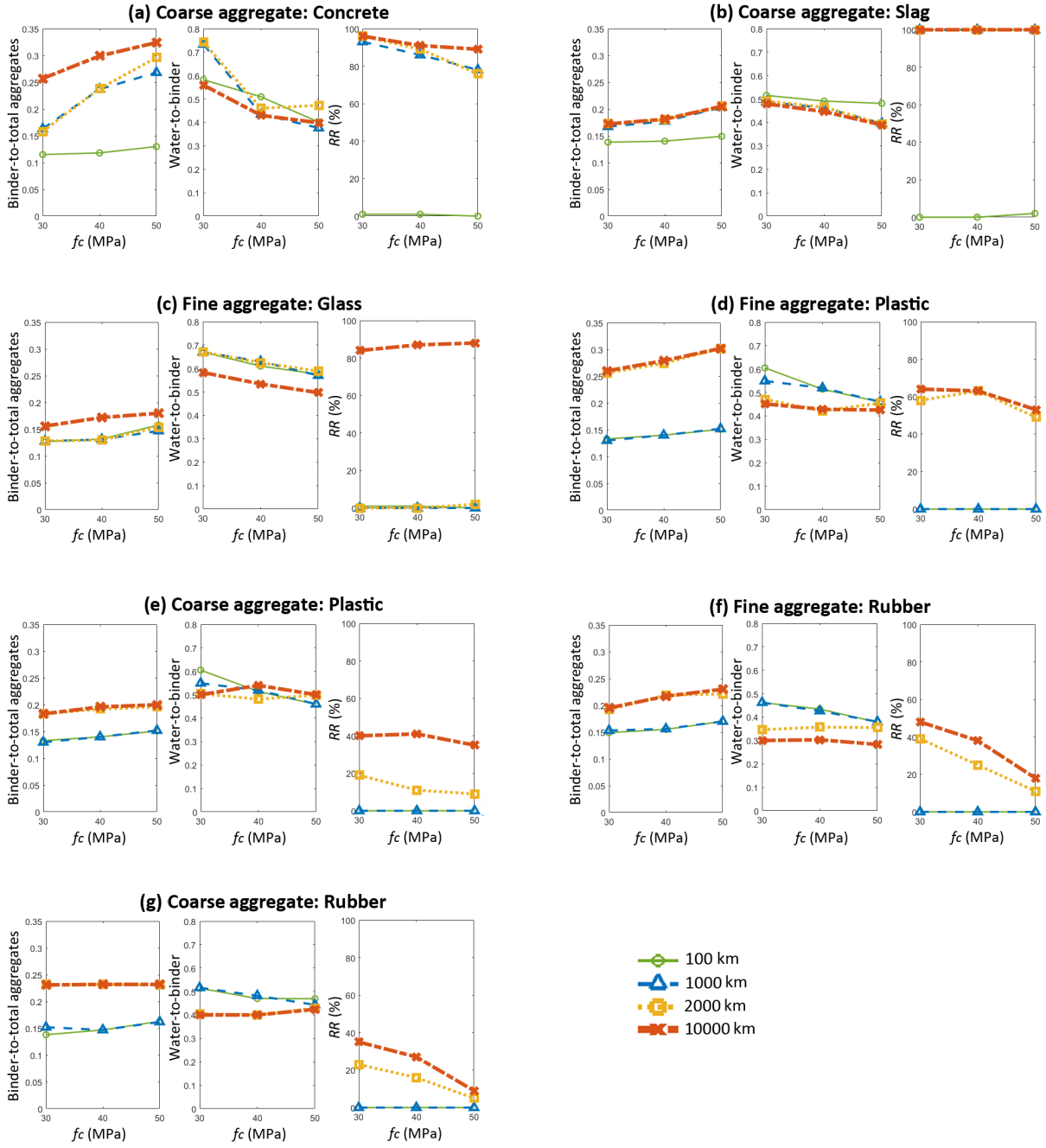

Fig. 4 Optimal waste-based aggregate mixes with $CO_{2\text{-eq}}$ emissions minimization and different road transport distances for natural aggregates

However, with an increase in the transport distance of natural aggregates from 100 km (green line) to 1000 km (blue line), *RR* (%) for the optimal mixes with coarse concrete and coarse slag aggregates increases from almost zero to more than 90%, and this change occurs because these waste-based aggregates now have lower total emissions than natural coarse aggregates, *RR* (%) for the optimal mixes with fine and coarse plastic and rubber aggregates, and fine glass aggregates still remains at zero as these waste aggregates still have higher total emissions than their corresponding natural aggregates. A similar switch to the replacement of natural aggregates with waste-based aggregates occurs for the remaining materials as their critical

transport distances are reached.

The results of analysis reveals that with an increase in the transport emission from natural aggregates, binder-to-total aggregate (b/a) and water-to-binder (w/b) respectively increases and decreases to account for the binder variation due to waste aggregate utilization (e.g., see green and orange lines in subplots for (b/a) and (w/b) in Fig. 4). It also shows that when the total emission from natural aggregates is higher than that from waste aggregates (e.g., when the transport distance of natural aggregates exceeds 10000 km), optimal mixes with different types of waste aggregates tend to reduce natural resource utilization and become similar to the mixes with the aim of natural resource usage minimization (see solid lines in Fig. 2) even if the objective is to minimize $CO_{2\text{-eq}}$ emissions. This is important as it shows the important role that the transport emissions of aggregates can play to make a trade-off between natural resource usage minimization and carbon emissions minimization.

3.4 Environmental efficiency

To investigate the interaction between the minimization of natural resource utilization and minimization of $CO_{2\text{-eq}}$ emissions, let us now examine the environmental performance of optimal waste-based aggregate mixes using an efficiency index, namely $CO_{2\text{-eq}}$ intensity (C_i) (Damineli et al. 2010):

$$C_i = \frac{CO_{2-eq_{concrete}}}{f_c} \tag{6}$$

where $CO_{2-eq_{concrete}}$ is the total $CO_{2\text{-eq}}$ emissions from the production 1 m^3 of concrete and f_c is the concrete compressive strength. It should be noted f_c is adopted in Eq. (6) as in most of the design oriented models, other concrete properties are considered as a function of compressive strength. The $CO_{2\text{-eq}}$ intensity (C_i) associated with optimal waste-based aggregate mixes with natural resource usage minimization and carbon emissions minimization and different transport cases for natural aggregates are shown in Fig. 5. To visualize the results shown in Fig. 5, the ordinate reports $CO_{2\text{-eq}}$ intensity (C_i), the abscissa reports compressive strength ($\boldsymbol{f_c}$) and the circle, square, upward-pointing triangle and diamond markers respectively show the transport distance of natural aggregates to be 100 km, 1000 km, 2000 km and 10000 km for $CO_{2\text{-eq}}$ emissions minimization. In Fig. 5, the environmental efficiency of optimal mixes with natural resource usage minimization is shown by downward-pointing triangle markers and the waste aggregate replacement ratio (RR (%)) for optimal mixes is demonstrated by the marker colour.

It is also seen that for all optimal mixes with a 100 km transport distance for natural aggregates, the $CO_{2\text{-eq}}$ intensity is higher for the natural resource usage minimization (downward-pointing triangle markers) than carbon emissions minimization (circle markers). However, when the transport distance of natural aggregates increases from 100 km to 10000 km, $CO_{2\text{-eq}}$ intensity of optimal mixes for carbon emissions minimization overtakes the $CO_{2\text{-eq}}$ intensity of the same mixes for natural resource usage minimization. The results of analysis in Fig. 5(d), for instance, show that for a 1000 km transport distance for natural aggregates, while the $CO_{2\text{-eq}}$ intensity of optimal mixes with fine plastic aggregates aiming at natural resource usage minimization (downward-pointing triangle markers in Fig. 5(d)) is higher than that of the same mixes for carbon emissions minimization (square markers in Fig. 5(d)), the $CO_{2\text{-eq}}$ intensities of fine plastic aggregate mixes with both natural resource usage minimization and carbon emissions minimization are similar when the transport distance of natural aggregates is 2000 km (see downward- and upward-pointing triangle markers in Fig. 5(d)).

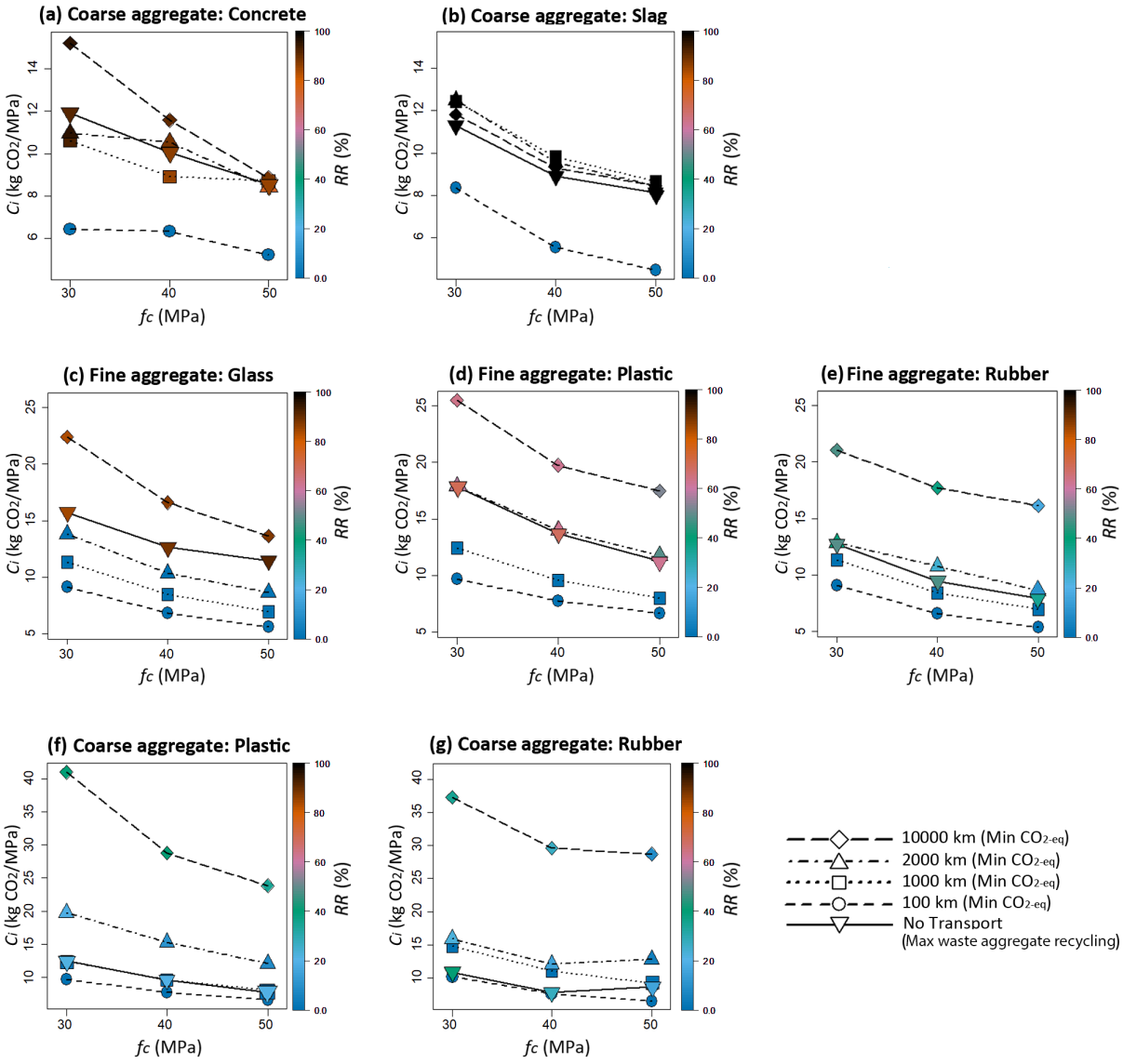

Fig. 5 $CO_{2\text{-eq}}$ intensity (*Ci*) of optimal waste-based aggregate mixes with carbon emissions minimization and natural resource usage minimization

Similarly, for a 2000 km transport distance for natural aggregates, while the $CO_{2\text{-eq}}$ intensity of optimal mixes with glass aggregates is higher for natural resource usage minimization than carbon emissions minimization (see downward- and upward-pointing triangle markers in Fig. 5(c)), the $CO_{2\text{-eq}}$ intensity of the same mixes is higher for carbon emissions minimization than natural resource usage minimization when the transport distance is 10000 km (see diamond and downward-pointing markers in Fig. 5(c)). It is worth mentioning that the $CO_{2\text{-eq}}$ intensity of all optimal mixes for carbon emissions minimization is higher than that for natural resource usage minimization when the transport distance of natural aggregates is 10000 km. This is however more apparent for optimal mixes with coarse plastic aggregates (Fig. 5(f)) and coarse rubber aggregates (Fig. 5(g)) than other types of waste aggregates as these mixes contain less waste aggregates and more natural aggregates to be transported longer distances.

Given that the transport emissions of natural aggregates have been shown to significantly influence the environmental impact of waste-based aggregate concretes in terms of natural resource utilization and $CO_{2\text{-eq}}$ emissions, let us finally consider a scenario in which the

environmental performance of optimal mixes is compared with that of experimental mixes in the database in terms of the $CO_{2\text{-eq}}$ intensity. In this analysis, the transport distance of natural aggregates is considered to be 100 km and 10000 km to capture the absolute minimum and absolute maximum of carbon dioxide emissions and waste aggregate utilization. The results of this analysis are shown in Fig. 6 in which grey circle markers and grey triangle markers show the experimental mixes in the database when the transport distance of natural aggregates is 100 km and 1000 km respectively; solid and dashed black lines represent the fitted curve for experimental mixes in the database when the transport distance of natural aggregates is 100 km and 1000 km respectively and the objective is to minimize carbon emissions; solid and dash orange lines show the same for optimal mixes; and solid green lines show the fitted curve for optimal mixes for natural resource usage minimization. It should be noted that in Fig. 6 the results of analysis are separately shown for concrete with different types of waste aggregates where subplots (a), (b), (c), (d), (e) and (f) represent the results for coarse concrete, coarse slag, fine glass, fine plastic, fine rubber and coarse rubber aggregates respectively.

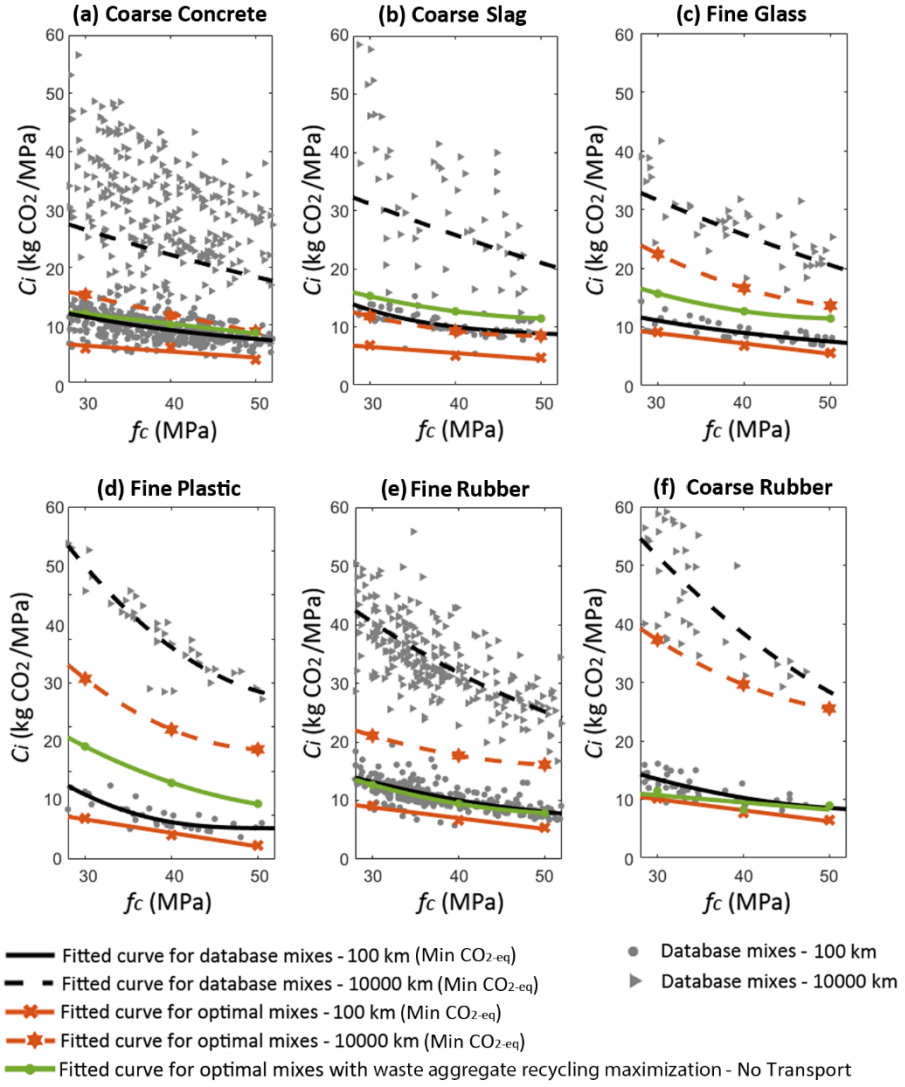

Fig. 6 Optimal and experimental mixes and their $CO_{2\text{-eq}}$ intensity (C_i) for carbon emissions minimization and natural resource usage minimization

It can be seen from Fig. 6 that all optimal mixes aiming at minimization of $CO_{2\text{-eq}}$ emissions (dashed and solid orange lines) have less $CO_{2\text{-eq}}$ intensity than database mixes with the same transport distance for natural aggregates (see dashed and solid black lines). For instance, optimal mixes with different types of waste aggregates have, on average, between 15%-50% (depending on the compressive strength and waste aggregate type) less $CO_{2\text{-eq}}$ intensity than database mixes when the transport distances of natural aggregates is 100 km and this is between 10%-65% less $CO_{2\text{-eq}}$ intensity when the transport distances of natural aggregates is 10000 km. This shows that the proposed optimization framework can generally develop optimal mixes with different types of waste aggregates offering lower $CO_{2\text{-eq}}$ emissions. Interestingly, when the objective changes from carbon emissions minimization (orange line) to natural resource usage minimization (green line), optimal mixes can either have similar $CO_{2\text{-eq}}$ intensity to database mixes or between 20%-50% more $CO_{2\text{-eq}}$ intensity than database mixes when the transport distance of natural aggregates for database mixes is 100 km (solid black lines). The reason for this is can be attributed to the distribution of mixes in the database used to train ANN encouraging optimal mixes to have more waste aggregates and possibly more binder content than database mixes of the same strength. However, with the same objective and a 10000 km transport for natural aggregates of database mixes, optimal mixes can have between 50%-85% less $CO_{2\text{-eq}}$ intensity than database mixes. This can be referred to the fact that the emissions arising from a 10000 km transport for natural aggregates of database mixes can outweigh the production emissions from waste-based aggregates and emissions associated with increased binder content for optimal mixes. This shows the importance of transport emissions from natural aggregate when it comes to the utilization of waste-based aggregate in concrete production.

Conclusion

In this study a generic framework for the mix design optimization of waste-based aggregate concretes is presented to reduce natural resource utilization and carbon dioxide emissions while keeping the concrete properties (compressive strength and slump) at desired levels. Utilising a large database of 5321 mix designs with concrete, slag, glass, plastic and rubber aggregates, an ANN was able to predict with good accuracy the properties of concrete with different types of waste aggregates. The results of analysis have shown the following findings:

- Ignoring the transport emissions (Section 3.2):
  (a) Optimal mixes contain higher volumes of waste-based aggregates when the objective is to minimize the natural resource utilization than when the objective is to minimize $CO_{2\text{-eq}}$ emissions. This is due to higher production emissions from waste aggregates than natural aggregates. However, optimal mixes with natural resource usage minimization contain more recycled concrete, slag and glass aggregates than plastic and rubber aggregates due to the difference in the physical properties of these waste-based aggregates (e.g., strength, density and surface texture).
  (b) When the objective changes from $CO_{2\text{-eq}}$ minimization to waste aggregate recycling maximization, the binder-to-total aggregate ratio increases, and the water-to-binder ratio decreases for all waste-based aggregate mixes. This shows that while there is a benefit to reducing natural aggregate utilization, there is a cost associated with increased binder content to compensate compressive strength loss.
  (c) When minimising $CO_{2\text{-eq}}$ emissions, regardless of compressive strength, all optimal mixes contain no waste aggregates, when minimising natural resource usage they can contain less waste aggregate when compressive strength increases and this is

because of unfavourable impact of waste aggregates on concrete compressive.

- Conducting a transport sensitivity analysis (Section 3.3 and 3.4):
  (a) All optimal mixes with carbon emissions minimization tend to utilize more waste aggregates when the transport distance of natural aggregates increases from 100 km to 10000 km. This results in an increase in binder-to-total aggregate and a decrease in water-to-binder ratio. This is, however, due to the increase in transport emissions from natural aggregates as compared to production emissions from waste aggregates and increased binder content when the transport distance of natural aggregates increases.
  (b) Depending on the transport distance of natural aggregates, the $CO_{2\text{-eq}}$ intensity of optimal mixes with either carbon emissions minimization or natural resource usage minimization can be lower. When the transport of natural aggregates is 100 km, the $CO_{2\text{-eq}}$ intensity of all optimal mixes with carbon emissions minimization is lower than that of the same mixes with waste aggregate recycling maximization and vice versa when the transport of natural aggregates is 10000 km.
  (c) The $CO_{2\text{-eq}}$ intensity of optimal mixes with carbon emissions minimization is lower than that of experimental mixes in the database for the same transport distances. However, the $CO_{2\text{-eq}}$ intensity of optimal mixes with natural resource usage minimization can either be lower or higher than that of database mixes depending on the transport emissions from database mixes. This is because optimal mixes with carbon emissions minimization make a trade-off between natural and waste aggregate content to minimize $CO_{2\text{-eq}}$ emissions. However, optimal mixes with waste aggregate recycling maximization tend to increase waste aggregate content regardless of carbon dioxide emissions.

Acknowledgments

Vahid Shobeiri was supported by an Australian Government Research Training Program Scholarship.

References

Metwally, I. M. (2007). Investigations on the performance of concrete made with blended finely milled waste glass. Advances in structural engineering, 10(1), 47-53.

Ismail, Z. Z., & Al-Hashmi, E. A. (2009). Recycling of waste glass as a partial replacement for fine aggregate in concrete. Waste management, 29(2), 655-659.

Miah, M. J., Patoary, M. M. H., Paul, S. C., Babafemi, A. J., & Panda, B. (2020). Enhancement of mechanical properties and porosity of concrete using steel slag coarse aggregate. Materials, 13(12), 2865.

Choudhary, S., Kishore, P. R., & Pachaiappan, S. (2022). Sustainable utilization of waste slag aggregates as replacement of coarse aggregates in concrete. Materials Today: Proceedings, 59, 240-247.

Daoud, O., & Ibrahim, M. (2020). Utilization of Giad Steel Slag as Partial Replacement for Coarse Aggregates in Concrete. FES Journal of Engineering Sciences, 9(2), 53-57.

Abusharar, S. W. (2015). Effect of particle sizes on mechanical properties of concrete containing crumb rubber. Innov. Syst. Des. Eng, 6, 114-125.

Andreu, G., & Miren, E. (2014). Experimental analysis of properties of high performance recycled aggregate concrete. Construction and Building Materials, 52, 227-235.

Bamigboye, G. O., Tarverdi, K., Umoren, A., Bassey, D. E., Okorie, U., & Adediran, J. (2021). Evaluation of eco-friendly concrete having waste PET as fine aggregates. Cleaner Materials, 2, 100026.

Guo, Y., Wu, J., Wang, C., & Zhang, F. (2020, March). Study on the influence of the shape and size of coarse aggregate on the strength of concrete. In IOP Conference Series: Materials Science and Engineering (Vol. 780, No. 4, p. 042008). IOP Publishing.

Bui, N. K., Satomi, T., & Takahashi, H. (2017). Improvement of mechanical properties of recycled aggregate concrete basing on a new combination method between recycled aggregate and natural aggregate. Construction and Building materials, 148, 376-385.

Zang, J., Li, W., & Shen, X. (2019). The influence of steel slag with variable particle size distribution on the workability and mechanical properties of concrete. Ceramics-Silikáty, 63(1), 67-75.

Elgendy, G. M., Elagamy, A. H., Sherif, M. A., & EL-Badawy, S. M. (2021). Laboratory Evaluation of Green Concrete Mixes Containing High Percentages of Steel Slag Coarse Aggregate. MEJ. Mansoura Engineering Journal, 40(5), 29-37.

Terro, M. J. (2006). Properties of concrete made with recycled crushed glass at elevated temperatures. Building and environment, 41(5), 633-639.

Malik, M. I., Bashir, M., Ahmad, S., Tariq, T., & Chowdhary, U. (2013). Study of concrete involving use of waste glass as partial replacement of fine aggregates. IOSR Journal of Engineering, 3(7), 08-13.

Wright, J. R., Cartwright, C., Fura, D., & Rajabipour, F. (2014). Fresh and hardened properties of concrete incorporating recycled glass as 100% sand replacement. Journal of Materials in Civil Engineering, 26(10), 04014073.

Zhang, H., Xu, X., Liu, W., Zhao, B., & Wang, Q. (2022). Influence of the moisture states of aggregate recycled from waste concrete on the performance of the prepared recycled aggregate concrete (RAC)–A review. Construction and Building Materials, 326, 126891.

Chakradhara Rao, M., Bhattacharyya, S. K., & Barai, S. V. (2011). Influence of field recycled coarse aggregate on properties of concrete. Materials and structures, 44(1), 205-220.

Gayarre, F. L., Perez, C. L. C., Lopez, M. A. S., & Cabo, A. D. (2014). The effect of curing conditions on the compressive strength of recycled aggregate concrete. Construction and Building Materials, 53, 260-266.

Crossin, E. (2015). The greenhouse gas implications of using ground granulated blast furnace slag as a cement substitute. Journal of Cleaner Production, 95, 101-108.

Grant, T.F., 2015. Life cycle inventory of cement & concrete produced in Australia. In:Life Cycle Strategies Pty Ltd. Australia, Melbourne.

Park, W. J., Kim, T., Roh, S., & Kim, R. (2019). Analysis of life cycle environmental impact of recycled aggregate. Applied Sciences, 9(5), 1021

Tahanpour Javadabadi, M. (2019). Comparative Life Cycle Assessment of Incorporating Recycled PET Aggregates into Concrete (Master's thesis, NTNU).

Bartolozzi, I., Antunes, I., & Rizzi, F. (2012, October). The environmental impact assessment of asphalt rubber: life cycle assessment. In Proceedings of the 5th Asphalt Rubber" Roads of the Future" International Conference, Munich, Germany (pp. 23-26).

Damineli, B.L., Kemeid, F.M., Aguiar, P.S., John, V.M., 2010. Measuring the eco-efficiency

of cement use. Cement Concr. Compos. 32 (8), 555e562.

Piasta, W., & Zarzycki, B. (2017). The effect of cement paste volume and w/c ratio on shrinkage strain, water absorption and compressive strength of high performance concrete. Construction and Building Materials, 140, 395-402.

Shobeiri, V., Bennett, B., Xie, T., & Visintin, P. (2022). A generic framework for augmented concrete mix design: Optimisation of geopolymer concrete considering environmental, financial and mechanical properties. Journal of Cleaner Production, 369, 133382.

Xu, J., Zhao, X., Yu, Y., Xie, T., Yang, G., & Xue, J. (2019). Parametric sensitivity analysis and modelling of mechanical properties of normal-and high-strength recycled aggregate concrete using grey theory, multiple nonlinear regression and artificial neural networks. Construction and Building Materials, 211, 479-491.

Xie, T., Yang, G., Zhao, X., Xu, J., & Fang, C. (2020). A unified model for predicting the compressive strength of recycled aggregate concrete containing supplementary cementitious materials. Journal of Cleaner Production, 251, 119752.

Gravina, R. J., Xie, T., Giustozzi, F., Zhao, X., & Visintin, P. (2021). Assessment of the variability and uncertainty of using post-customer plastics as natural aggregate replacement in concrete. Construction and Building Materials, 273, 121747.

Gravina, R. J., & Xie, T. (2022). Toward the development of sustainable concrete with Crumb Rubber: Design-oriented Models, Life-Cycle-Assessment and a site application. Construction and Building Materials, 315, 125565.

Gursel, A.P., 2014, Life-cycle Assessment of Concrete: Decision-Support Tool and Case Study Application (UC Berkeley).

V. Shobeiri, B. Bennett, T. Xie, P. Visintin, A comprehensive assessment of the global warming potential of geopolymer concrete, J. Clean. Prod. 297 (2021),

126669.

Farina, A., Zanetti, M. C., Santagata, E., & Blengini, G. A. (2017). Life cycle assessment applied to bituminous mixtures containing recycled materials: Crumb rubber and reclaimed asphalt pavement. Resources, Conservation and Recycling, 117, 204-212.

Roh, S., Kim, R., Park, W. J., & Ban, H. (2020). Environmental evaluation of concrete containing recycled and by-product aggregates based on life cycle assessment. Applied Sciences, 10(21), 7503.

H.S. Lee, S.M. Lim, X.Y. Wang, Optimal Mixture Design of Low-CO 2 High-Volume Slag Concrete Considering Climate Change and CO 2 Uptake, Int. J. Concr.

Struct. Mater. 13 (1) (2019) 1–13.

X.Y. Wang, Optimal mix design of low-CO2 blended concrete with limestone powder, Constr. Build. Mater. 263 (2020), 121006.

H. Naseri, H. Jahanbakhsh, P. Hosseini, F.M. Nejad, Designing sustainable concrete mixture by developing a new machine learning technique, J. Clean. Prod.258 (2020), 120578.

Mirzahosseini, M., Jiao, P., Barri, K., Riding, K. A., & Alavi, A. H. (2019). New machine learning prediction models for compressive strength of concrete modified with glass cullet. Engineering Computations, 36(3), 876-898.

Silva, P. F., Moita, G. F., & Arruda, V. F. (2020). Machine learning techniques to predict the compressive strength of concrete. Revista Internacional de Métodos Numéricos Para Cálculo

y Diseño En Ingeniería, 36(4).

Han, Y., Yang, Z., Ding, T., & Xiao, J. (2021). Environmental and economic assessment on 3D printed buildings with recycled concrete. Journal of Cleaner Production, 278, 123884.

Adesina, A. (2020). Recent advances in the concrete industry to reduce its carbon dioxide emissions. Environmental Challenges, 1, 100004.

Nedeljković, M., Visser, J., Šavija, B., Valcke, S., & Schlangen, E. (2021). Use of fine recycled concrete aggregates in concrete: A critical review. Journal of Building Engineering, 38, 102196.

Usanova, K., & Barabanshchikov, Y. (2020). Cold-bonded fly ash aggregate concrete. Magazine of Civil Engineering, (3 (95)), 104-118.

Dong, Q., Wang, G., Chen, X., Tan, J., & Gu, X. (2021). Recycling of steel slag aggregate in portland cement concrete: An overview. Journal of cleaner production, 282, 124447.

Revilla-Cuesta, V., Skaf, M., Faleschini, F., Manso, J. M., & Ortega-López, V. (2020). Self-compacting concrete manufactured with recycled concrete aggregate: An overview. Journal of Cleaner Production, 262, 121362.

Basha, S. I., Ali, M. R., Al-Dulaijan, S. U., & Maslehuddin, M. (2020). Mechanical and thermal properties of lightweight recycled plastic aggregate concrete. Journal of Building Engineering, 32, 101710.

Li, N., Long, G., Ma, C., Fu, Q., Zeng, X., Ma, K., ... & Luo, B. (2019). Properties of self-compacting concrete (SCC) with recycled tire rubber aggregate: A comprehensive study. Journal of Cleaner Production, 236, 117707.

Li, X., Ling, T. C., & Mo, K. H. (2020). Functions and impacts of plastic/rubber wastes as eco-friendly aggregate in concrete–A review. Construction and building materials, 240, 117869.

Piccinali, A., Diotti, A., Plizzari, G., & Sorlini, S. (2022). Impact of recycled aggregate on the mechanical and environmental properties of concrete: a review. Materials, 15(5), 1818.

Rashad, A. M. (2022). Behavior of steel slag aggregate in mortar and concrete-A comprehensive overview. Journal of Building Engineering, 53, 104536.

Yuan, X., Tian, Y., Ahmad, W., Ahmad, A., Usanova, K. I., Mohamed, A. M., & Khallaf, R. (2022). Machine Learning Prediction Models to Evaluate the Strength of Recycled Aggregate Concrete. Materials, 15(8), 2823.

Khan, K., Ahmad, W., Amin, M. N., Aslam, F., Ahmad, A., & Al-Faiad, M. A. (2022). Comparison of prediction models based on machine learning for the compressive strength estimation of recycled aggregate concrete. Materials, 15(10), 3430.

Chen, S., Wang, H., Guan, J., Yao, X., & Li, L. (2022). Determination method and prediction model of fracture and strength of recycled aggregate concrete at different curing ages. Construction and Building Materials, 343, 128070.

Nguyen, T. D., Cherif, R., Mahieux, P. Y., Lux, J., Aït-Mokhtar, A., & Bastidas-Arteaga, E. (2023). Artificial intelligence algorithms for prediction and sensitivity analysis of mechanical

Zhang, J., Huang, Y., Ma, G., & Nener, B. (2021). Mixture optimization for environmental, economical and mechanical objectives in silica fume concrete: A novel frame-work based on machine learning and a new meta-heuristic algorithm. Resources, Conservation and Recycling, 167, 105395.

Shobeiri, V., Bennett, B., Xie, T., & Visintin, P. (2022). A generic framework for augmented

concrete mix design: Optimisation of geopolymer concrete considering environmental, financial and mechanical properties. Journal of Cleaner Production, 369, 133382.

Lee, H. S., Lim, S. M., & Wang, X. Y. (2019). Optimal mixture design of low-CO2 high-volume slag concrete considering climate change and CO2 uptake. International Journal of Concrete Structures and Materials, 13(1), 1-13.

Cheng, M. Y., Prayogo, D., & Wu, Y. W. (2014). Novel genetic algorithm-based evolutionary support vector machine for optimizing high-performance concrete mixture. Journal of Computing in Civil Engineering, 28(4), 06014003.

Shobeiri, V., Bennett, B., Xie, T., & Visintin, P. (2023). Mix Design Optimization of Concrete Containing Fly Ash and Slag for Global Warming Potential and Cost Reduction. Case Studies in Construction Materials, e01832.

Belmokaddem, M., Mahi, A., Senhadji, Y., & Pekmezci, B. Y. (2020). Mechanical and physical properties and morphology of concrete containing plastic waste as aggregate. Construction and Building Materials, 257, 119559.

The MathWorks, Inc., 2020a, Neural Network Toolbox, Natick, Massachusetts, United State

Gursel, A.P., 2014, Life-cycle Assessment of Concrete: Decision-Support Tool and Case Study Application (UC Berkeley).

Adesina, A. (2020). Recent advances in the concrete industry to reduce its carbon dioxide emissions. Environmental Challenges, 1, 100004.

Medina, C., Zhu, W., Howind, T., de Rojas, M. I. S., & Frías, M. (2014). Influence of mixed recycled aggregate on the physical–mechanical properties of recycled concrete. Journal of cleaner production, 68, 216-225.

Bai, G., Zhu, C., Liu, C., & Liu, B. (2020). An evaluation of the recycled aggregate characteristics and the recycled aggregate concrete mechanical properties. Construction and building materials, 240, 117978.

Chicco, D., Warrens, M. J., & Jurman, G. (2021). The coefficient of determination R-squared is more informative than SMAPE, MAE, MAPE, MSE and RMSE in regression analysis evaluation. PeerJ Computer Science, 7, e623.

BKA, M. A. R., Ngamkhanong, C., Wu, Y., & Kaewunruen, S. (2021). Recycled aggregates concrete compressive strength prediction using artificial neural networks (ANNs). Infrastructures, 6(2), 17.

Hammoudi, A., Moussaceb, K., Belebchouche, C., & Dahmoune, F. (2019). Comparison of artificial neural network (ANN) and response surface methodology (RSM) prediction in compressive strength of recycled concrete aggregates. Construction and Building Materials, 209, 425-436.

Turki, M., Zarrad, I., Quéneudec, M., & Bouaziz, J. (2017). Prediction performance of compressive strength of cementitious materials containing rubber aggregates and filler using fuzzy logic method. Multidiscipline Modeling in Materials and Structures, 13(2), 284-296.

Bawab, J., Khatib, J., & Hwalla, J. Prediction Of The Compressive Strength Of Concrete Containing Waste Glass As A Replacement For Fine Aggregates Using Artificial Neural Networks.

Supplementary Material A

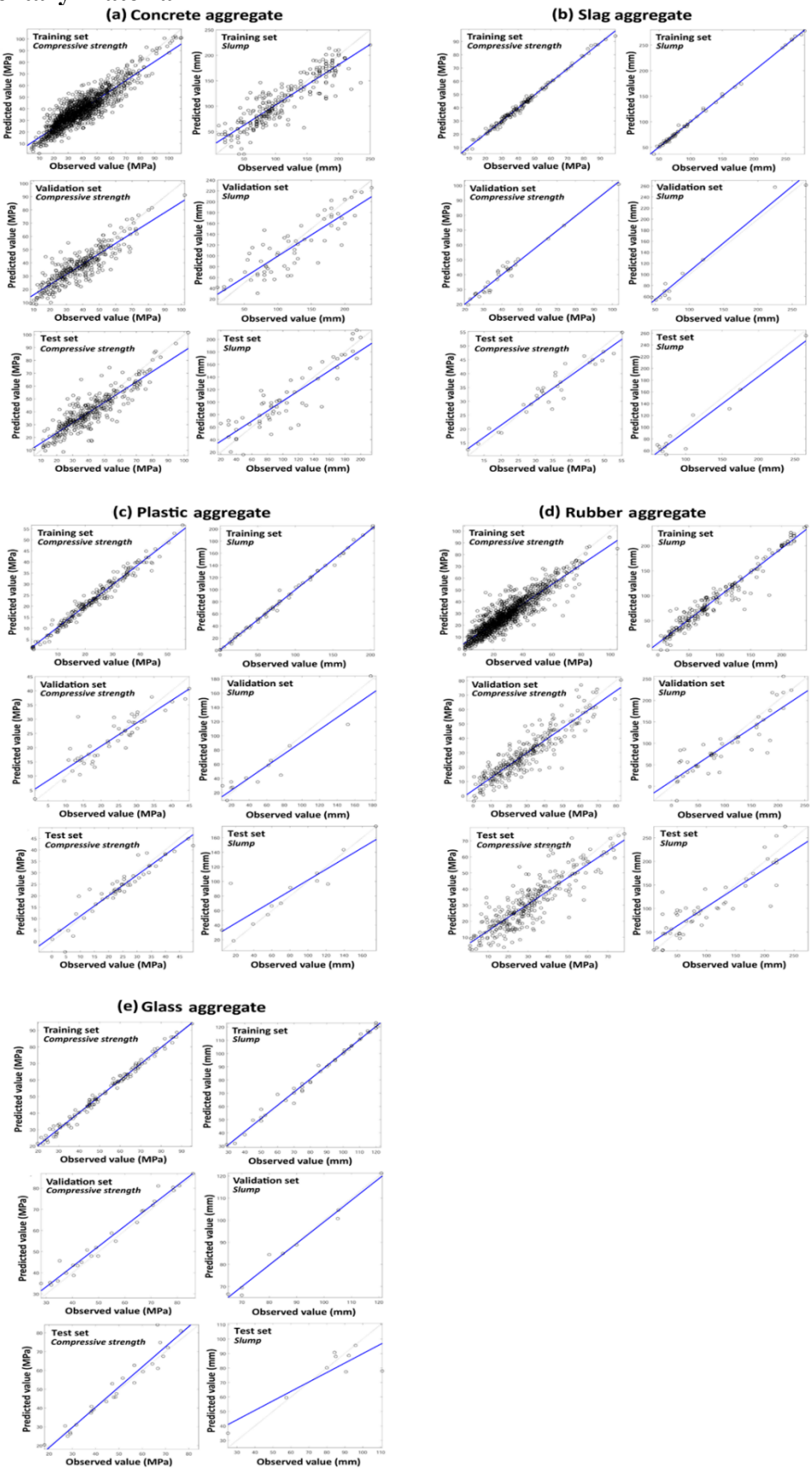

Fig. S1 Observed versus predicted compressive strength and slump for waste-based aggregate concrete

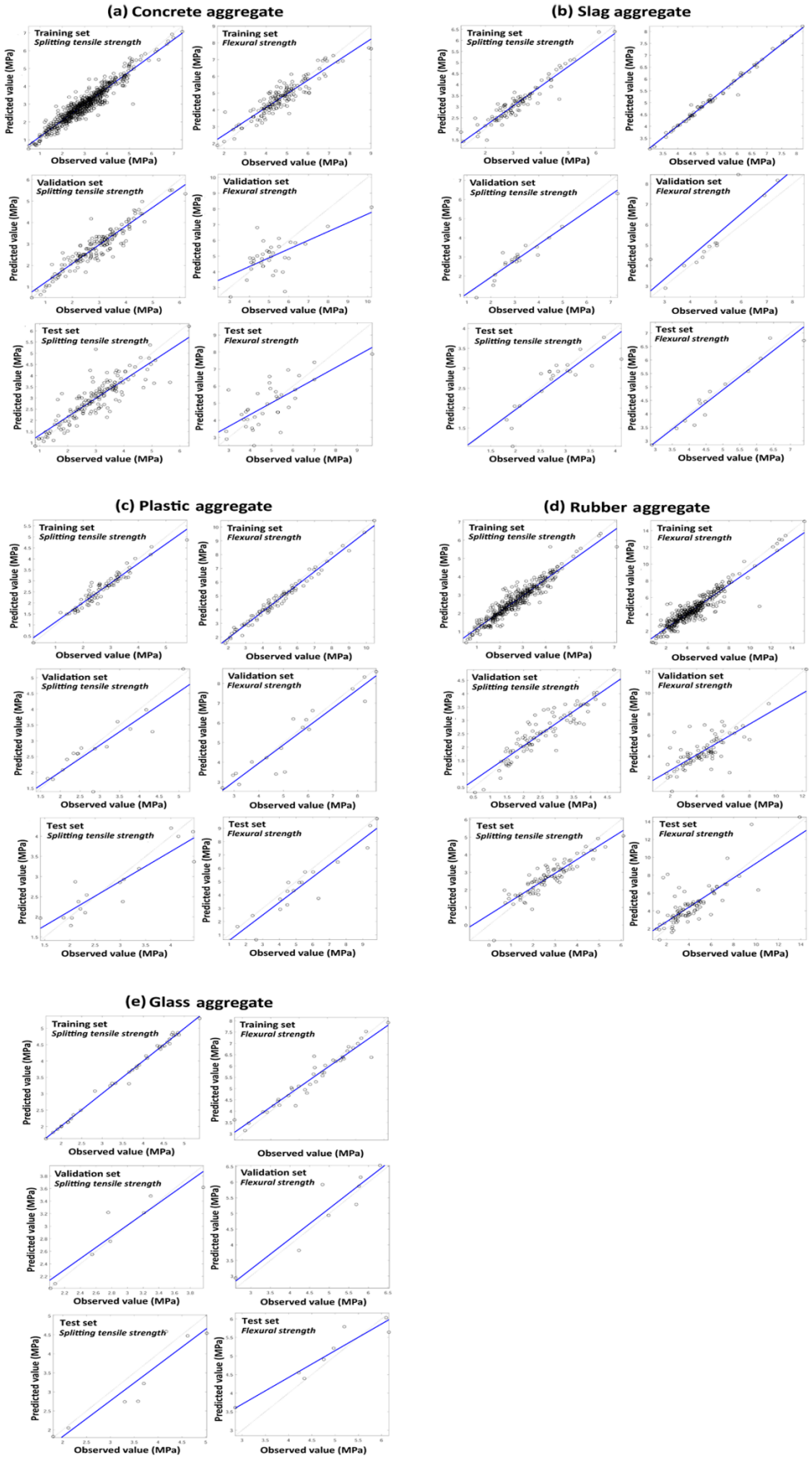

Fig. S2 Observed versus predicted splitting tensile strength and flexural strength for waste-based aggregate concrete

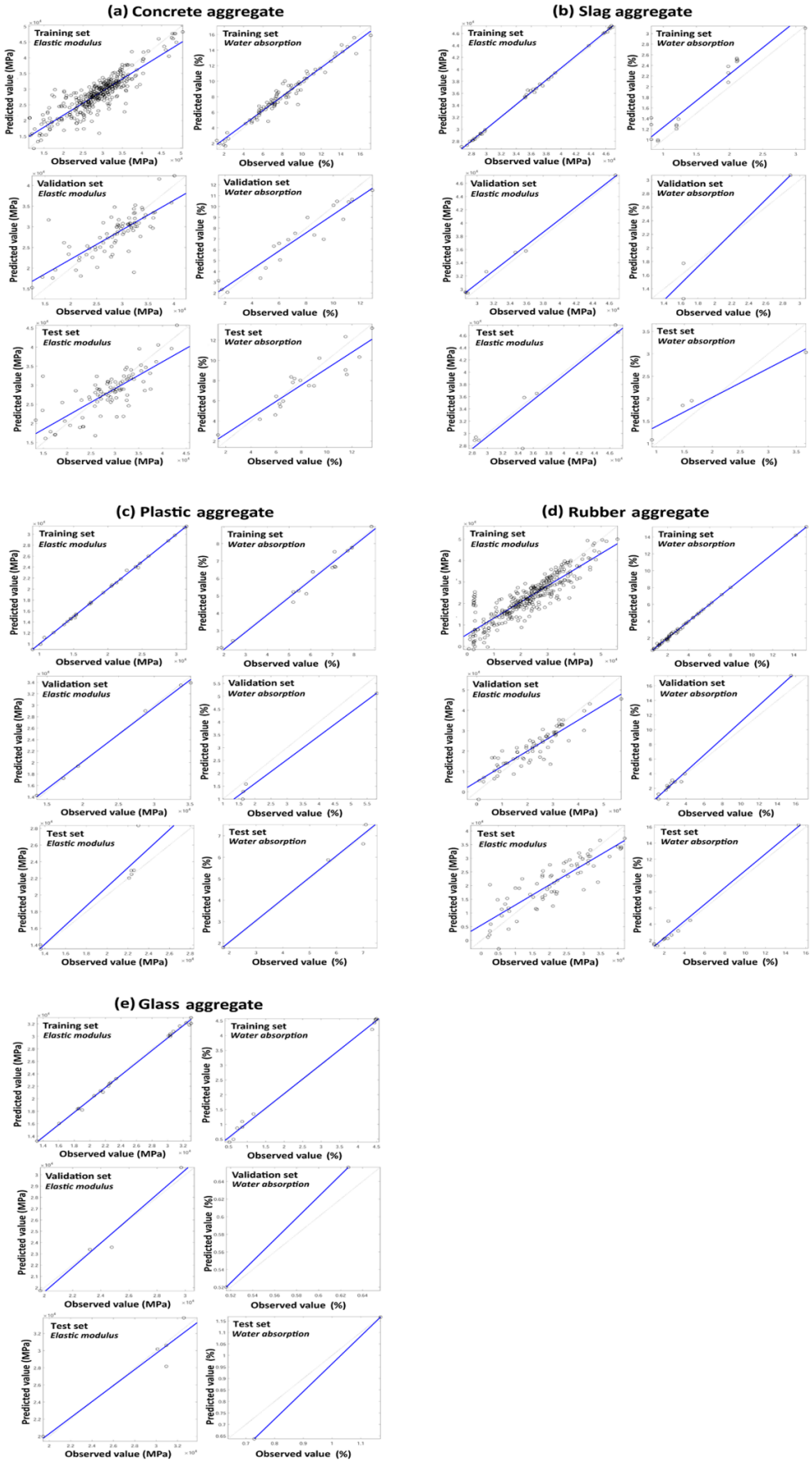

Fig. S3 Observed versus predicted elastic modulus and water absorption for waste-based aggregate concrete

CHAPTER 4

Concrete which is the most commonly used construction material on earth needs a large amount of cement and natural aggregates and approximately 0.85 to 0.92 tonne of carbon dioxide ($CO_{2\text{-}eq}$) are emitted for every tonne of cement produced. Therefore, to alleviate the effects of climate change we need sustainable solutions that can not only reduce greenhouse gas emissions from concrete but also introduce environmentally friendly alternative materials for conventional concrete materials. This thesis focused on overcoming this obstacle by integrating multi-objective optimization techniques into the comprehensive environmental life-cycle assessment tools with a focus on global warming potential (GWP) for optimization of concrete containing alternative waste materials for cement and natural aggregates. From this thesis, it is possible to find optimal mix designs of low emission waste-based concretes with desired mechanical properties based on the transport distance and mode of concrete materials, source of supplementary cementitious materials, and optimum type of waste-based aggregates which benefit not only environment but also help conserve natural resources.

Concluding Remarks

In this thesis, a generic concrete mix design optimization framework was presented to generate optimal mixes of a range of concrete types with alternative binders and alternative fillers in terms of minimizing carbon dioxide emissions, mix cost and natural resource utilization. The proposed framework develops optimum mixes with a set of desired properties (compressive strength and slump) based on the application of a detailed life-cycle assessment tool, artificial neural networks and multi-objective genetic algorithm optimization. The strength of developed framework lies in its accuracy, big calibration, efficiency and flexibility, and that it can be simply tailored to any local application via modification of the input parameters. This allows the user to make their own choice in relation to what local values are suited for their application for the purpose of reducing emissions, cost and natural resource utilization.

First the emissions factors form concrete ingredients used later in the thesis were obtained and the impacts of curing, energy grid sources, type of allocation scenario (no allocation, economic allocation and mass allocation) and material transport distances and mode (road, rail and sea) on the carbon dioxide emissions of geopolymer and traditional concretes were investigated. The critical transportation distances at which the manufacture of geopolymer concrete becomes more emissions intensive than conventional concrete of the same strength was also explored. It was shown that $CO_{2\text{-}eq}$ emissions from geopolymer concrete is less dependent to compressive strength than those of traditional concrete and that either geopolymer concrete or traditional concrete can have lower $CO_{2\text{-}eq}$ emissions depending on the allocation scenario, and transport distance, mode of concrete materials.

Optimal mixes were then investigated using the developed framework for geopolymer concrete considering environmental financial and mechanical properties. The effect of chemical makeup of binders and alkali activators as well as transportation distances of concrete ingredients on the optimal mixes were found to be significant. The developed framework was then validated by optimizing concrete mixes with supplementary cementitious materials (SCMs) where it was found that chemical makeup of cement, fly ash and slag, minimum cement content, transport allocation and emissions, and binder type were also significant when it comes to carbon dioxide emissions and cost of optimal mixes. It was shown that the use of an ANN to predict the compressive strength and slump of concrete can be improved significantly if the chemical

composition of materials is used in place of material types. It was also shown that the masses of binders in the optimal mix designs are a function of their chemical composition, transport distance and mode and allocation emissions and that there is a strong relationship between the mixture cost and $CO_{2\text{-eq}}$ emissions indicating that $CO_{2\text{-eq}}$ emissions increase with an increase in the mixture cost.

Different properties (compressive strength, splitting tensile strength, flexural strength, elastic modulus, water absorption and slump) of concrete with recycled plastic, rubber, slag, glass and concrete aggregates were investigated in terms of carbon intensity and aggregate replacement ratio by analysing a large database of waste aggregate-based concrete. This analysis aided to select optimum waste based aggregate type and replacement ratio based on the intended use of the concrete. Empirical models that link the elastic modulus, splitting tensile and flexural tensile strength to the compressive strength were derived for concrete with different types of waste-based aggregates which were than validated and compared to existing models in the codes of practice.

Different properties of concrete with various types of waste-based aggregates were then predicted using an ANN model and the versatility of the developed framework in this thesis was finally demonstrated through the mix design optimization of concrete with different types of waste-based aggregates in terms of minimizing carbon dioxide equivalent emissions and natural resource utilization. It was shown that the addition of waste-based aggregates leads to poorer mechanical performance which can be recovered via an increase in binder. However, the influence of waste-based aggregates on the concrete mechanical properties depends on the waste-based aggregate type and replacement ratio. It was also shown that improved relationships for predicting the mechanical properties of natural aggregate concrete and waste-based aggregate concrete can be achieved as compared to several codified models in international standards and that optimal mixes with waste-based aggregates can greatly change when the objective function changes from waste aggregate recycling maximization to $CO_{2\text{-eq}}$ emissions minimization.

Future Works

Possible extensions of this work include developing a generic framework considering a broader set of concrete properties (e.g., elastic modulus, splitting tensile strength, flexural strength and water absorption) as constraints for developing optimal mixes with minimized emissions, cost and natural resource utilization. This is important because all of these concrete properties are equally important for structural design. The developed framework in this work can consider different concrete properties as constraints however was limited in implementation because of data availability for some properties (e.g., water absorption). Another possible extension of this work is to develop a framework to reduce emissions and cost at the structural level. This can be done by developing structural optimization techniques to design material-efficient and carbon- and cost- effective structural frames (e.g., concrete, timber and steel frames) with optimal decking and foundation types at early-stage design decisions. This is important because developing novel structural systems using the structural optimization techniques can lead to large potential embodied cost and carbon savings which can help to meet the 2030 carbon targets for new buildings.